PROTEIN BIOSEPARATION USING SYNTHETIC MEMBRANES

PROTEIN BIOSEPARATION USING SYNTHETIC MEMBRANES: ENHANCEMENT OF SELECTIVITY AND THROUGHPUT

By

DHARMESHKUMAR M. KANANI, B.E., M. Sc. (Tech.)

A Thesis

Submitted to the School of Graduate Studies

in Partial Fulfillment of the Requirements

for the Degree

Doctor of Philosophy

McMaster University

DOCTOR OF PHILOSOPHY (2007) McMaster University

(Chemical Engineering) Hamilton, Ontario

TITLE: Protein Bioseparation using Synthetic Membranes: Enhancement of Selectivity and Throughput

AUTHOR: Dharmeshkumar M. Kanani, M. Sc. (Tech.) (Mumbai University)

SUPERVISOR: Professor Raja Ghosh

NUMBER OF PAGES: xxiv, 235

ABSTRACT

Cost-effective large-scale protein bioseparation will be the key issue for the biopharmaceutical industry in the coming years. Conventional protein purification techniques are severely limited in the sense that they give either good selectivity of separation at the cost of throughput or vice versa. Synthetic membrane based bioseparation techniques such as high-resolution ultrafiltration and membrane chromatography have the potential to combine high-throughput with high selectivity. This thesis focuses on approaches for obtaining both selectivity and throughput in membrane based protein bioseparation processes.

Obtaining high selectivity is one of the main objectives in high-resolution ultrafiltration. This thesis reports a novel approach for flexibly manipulating the selectivity of protein separation using a dual-facilitating agent. In this study it has been shown for the first time that the selectivity of separation can be altered as desired, i.e. if required, the selectivity can be reversed and thereby smaller proteins can be retained and larger proteins can be made to permeate by using a dual-facilitating agent. The results are explained in terms of protein-protein electrostatic interactions and Donnan effect. This novel approach is expected to significantly increase the flexibility of carrying out high-resolution ultrafiltration.

Membrane chromatography is based on the use of stacks of microporous synthetic membranes as chromatographic media. Due to lower binding capacities of commercial membranes in comparison to conventional beads for packed bed chromatography, the commercial success of membrane chromatography is largely limited to the flow-through applications. The study on membrane chromatography addresses the performances of new types of high-capacity macroporous gel-filled membranes for ion-exchange

chromatography of proteins. This work demonstrates the suitability of using one of these novel membranes for fractionation of plasma proteins.

Membrane fouling reduces product throughput and is considered a major problem in pressure driven membrane processes such as microfiltration and ultrafiltration. This thesis reports some significant contributions in the area of membrane fouling. A novel yet conceptually simple approach for modeling flux decline in constant pressure ultrafiltration, which takes into account the interplay between flux, concentration polarization and membrane fouling is discussed. Conventional fouling models account for the effects of concentration polarization and membrane fouling in a simple additive way. The basic hypothesis in the model discussed here is that flux decline in constant pressure ultrafiltration is self-attenuating in nature. This new approach is expected to be very useful in deciding the start-up conditions in membrane processes. Despite wide-spread use of in-line microfiltration for sterilization of therapeutic proteins prior to formulation, there has been no systematic study on fouling in such processes. Part of the fouling work in this thesis examines how resistance to filtration increases during in-line microfiltration of concentrated protein solution and the mechanism of protein fouling. It assesses the severity of fouling in terms of apparent reversible fouling and irreversible fouling. Traditional methods to measure the protein fouling resistances of membranes are time consuming and expensive. This thesis reports three protocols to compare the performance of microfiltration membranes for protein filtration. The first protocol, which is based on accelerated fouling in the dead end mode using pulsed injection technique is rapid, simple, and cost effective and gives valuable information about membrane performance. The remaining two protocols are based on the critical flux concept.

ACKNOWLEDGEMENTS

I take this opportunity to express my sincere gratitude to all those who have directly or indirectly contributed to this thesis.

First of all, I would like to thank my research supervisor, Dr. Raja Ghosh for his cheerful and masterly guidance as well as for the many opportunities I have been given to present my research work at several conferences over the last four years. His enthusiasm, research insight, patience and encouragement are truly unforgettable. I am finding difficult to imagine having a better learning experience and will certainly miss the supporting and enthusiastic environment Dr. Ghosh fosters. He is and will continue to be a source of motivation for my career development.

I would like to thank the members of my PhD committee, Dr. Carlos Filipe, Dr. Ron Childs and Dr. Ravi Selvaganapathy for their valuable advice and encouragement. Special mention must be made of Dr. Carlos Filipe for his willingness to always help and for the permission to use his lab equipments when needed.

I would also like to acknowledge a number of other colleagues at McMaster University for their kind help in the last four years. I thank two summer students, Tiffany Wong and Albert Chang for their hard work and the experiments they conducted. I am grateful to Paul Gatt (Chemical Engineering Department, McMaster University) for fabricating custom designed equipment pieces for my experimental work when needed and Marnie Timleck (Electron Microscopy Facility, McMaster Health Science) for her help in Confocal Microscopy. I thank Dr. A. Mika and Dr. E. Komkova for donating the high-capacity macroporous gel-filled membranes and Dr. Sriram for donating surface treated microfiltration membranes. I would also like to thank Ge Xin for his help with Gel Electrophoresis. My appreciation also goes to the Department Staff: Julie Birch,

Kathy Goodram, Lynn Falkiner, Andrea Vickers, Gord Slater, Doug Keller and Justina Derkach as well as Dr. Andrew Hrymak, the Head of Department, for their help and assistance when needed.

I thank my colleagues from Dr. Ghosh's research group, David, Lu, Dennis, Dr. Mohanty, Dr. Sun, Ray and graduate student friends from Chemical Engineering Department for their kind assistance and helpful discussions. I would also like to thank my friends at and around McMaster University for making my time in Hamilton amazingly fun and enriching on many levels. An exhaustive list is too big, but special mention must be made of my housemates Nilesh and Yuvraj along with Mallik, Binod, Sanjay, Girish, Prajyot and Kunal. I am also grateful to Mihir and his family, Mukeshbhai and his family, and my cousine Jayeshbhai for never letting me feel homesick.

I would like to express my wholehearted gratitude to my family for their constant encouragement, love, support and trust in my abilities. I am very fortunate to have two loving sisters, Asmita and Pushpa and a brother, Devendra. A special mention must be made of my parents for their unparalleled love and care. They are the greatest blessing in my life and all the credit goes to them for whatever I have achieved till the date.

Finally, I thank the Department of Chemical Engineering (McMaster University), 3M Canada, Shell Canada and Clifton W. Sherman for their financial support

To My Dear Parents

TABLE OF CONTENTS

Chapter 1 Introduction **1**

1.1 Protein bioseparation – A challenge facing the biopharmaceutical industry 1

1.2 Membrane based bioseparation techniques 4

1.2.1 Ultrafiltration 9

1.2.2 Membrane fouling 18

1.2.3 Membrane chromatography 22

1.3 References 27

Chapter 2 Research Objectives and Thesis Outline **38**

2.1 Background 38

2.2 Research objectives 40

2.2.1 High resolution UF 41

2.2.2 Membrane chromatography 42

2.2.3 Membrane fouling 42

2.3 Thesis outline 43

Chapter 3 A Novel Approach for High-Resolution Protein-Protein Separation by Ultrafiltration using a Dual-Facilitating Agent **47**

3.1 Abstract 47

3.2 Introduction 48

3.3 Experimental 50

3.3.1 Materials 50

3.3.2 Membrane filtration unit 50

3.3.3 Experimental set-up and methodology 51

3.3.4 Analysis of protein mixtures using membrane chromatography 51

3.3.5 Test for detection of BSA in permeate samples 52

3.4 Results and discussion 53

3.4.1 Ultrafiltration of lysozyme and myoglobin 53
3.4.2 Dual-facilitated separation of lysozyme and myoglobin using BSA 54
3.5 Conclusions 62
3.6 References 63

Chapter 4 A Constant Flux based Mathematical Model for Predicting Permeate Flux Decline in Constant Pressure Protein Ultrafiltration 65

4.1 Abstract 65
4.2 Introduction 66
4.3 Model Development 69
4.4 Experimental 76
4.4.1 Materials 76
4.4.2 Experimental Set-up and Methodology 76
4.5 Results and Discussion 79
4.6 Conclusion 93
4.7 References 93

Chapter 5 High-capacity Macroporous Gel-filled Membranes: Performance Evaluation for Ion-exchange Chromatography of Proteins 97

5.1 Abstract 97
5.2 Introduction 98
5.3 Experimental 104
5.3.1 Materials 104
5.3.2 Buffers and protein solutions 105
5.3.3 Experimental set-up and methodology 105
5.4 Results and discussion 109
5.4.1 Effect of pH 109

5.4.2 Effect of ionic strength 111
5.4.3 Effect of buffering ions 114
5.4.4 Effect of feed protein concentration 115
5.4.5 Effect of flow rate 117
5.4.6 HSA breakthrough experiments 122
5.4.7 Performance comparison of membrane modules 127
5.4.8 Dynamic adsorption isotherm 129
5.4.9 Non-specific binding 131
5.4.10 HSA-HIgG separation 132
5.5 Conclusions 136
5.6 References 137

Chapter 6 Membrane Fouling during In-line Protein Microfiltration Processes 140

6.1 Abstract 140
6.2 Introduction 142
6.3 Experimental 145
6.3.1 Materials 145
6.3.2 Protein microfiltration experiments 147
6.3.3 SEC analysis of protein samples 150
6.3.4 Confocal laser scanning microscopy 151
6.4 Results and discussion 152
6.5 Conclusion 190
6.6 References 191

Chapter 7 Membrane Fouling Assessment Techniques 194

7.1 Abstract 194
7.2 Introduction 195
7.3 Experimental 198
7.3.1 Materials 198

7.3.2 Buffer and protein solution preparation 198
7.3.3 Experimental set-up and methodology 199
7.4 Accelerated membrane fouling assessment in the dead-end mode using pulsed injection technique 205
7.5 Critical flux testing with syringe filter holder utilizing step input technique in the dead-end mode 210
7.6 Critical flux testing with stirred cell module in the pseudo steady-state mode 216
7.7 Summary 221
7.8 References 222

Chapter 8 Research Contributions and Recommendations for Future Work 226

8.1 Research contributions of thesis work 226
8.1.1 Protein bioseparation by ultrafiltration 227
8.1.2 Modeling of flux decline in ultrafiltration 228
8.1.3 Membrane chromatography 229
8.1.4 Protein fouling of MF membranes 230
8.1.5 Fouling assessment techniques 231
8.2 Recommendations for future research 232
8.2.1 Dual-facilitating agent in protein-protein separation 232
8.2.2 Ultrafiltration fouling 234
8.2.3 Microfiltration fouling 235

LIST OF TABLES

Table 3.1 Facilitated separation of myoglobin and lysozyme using BSA: effect of BSA concentration in the feed at two different permeate flux values 58

Table 4.1 Simulation constants for mathematical model 80

Table 4.2 Comparison of simulated osmotic pressure with experimental data at the end of constant pressure ultrafiltration 92

Table 4.3 Comparison of membrane fouling resistance at different TMP 92

Table 5.1: Commercial membrane adsorbers and their binding capacities 101

Table 5.2 Properties of the macroporous gel-filled membranes 106

Table 5.3 HSA binding capacities of the gel-filled membranes 124

Table 5.4 Performance comparison of custom designed membrane module with that of the conventional module 129

Table 5.5 Non-specific binding on gel-filled macroporous membranes 131

Table 6.1 Fouling rates during the three phases of TMP increase (BSA concentration: 10 kg/m^3; membrane: 0.45 micron cellulose acetate; flux: 8.49×10^{-4} m/s; volume of BSA solution filtered: 16 ml) 154

Table 6.2 Effect of protein filtration volume on the reversibility of fouling (BSA concentration: 10 kg/m^3; membrane: 0.45 micron cellulose acetate; flux: 8.49×10^{-4} m/s) 165

Table 6.3 Contribution of apparent reversible fouling towards total fouling during each phase of membrane fouling (BSA concentration: 10 kg/m^3; membrane: 0.45 micron cellulose acetate; flux: 8.49×10^{-4} m/s) 166

Table 6.4 Fouling resistance and membrane hydraulic resistance at the end of protein filtration at different fluxes (BSA concentration: 10 kg/m^3; 0.45 micron cellulose acetate membrane; volume of BSA solution: 24 ml) 177

Table 6.5 Total resistance and fouling resistance during the front wash steps 180

in experiment A and B (BSA concentration: 10 kg/m^3; 0.45 micron cellulose acetate membrane; Flux: 8.49×10^{-4} m/s; volume of BSA solution: 24 ml). Experiment A – First front wash at 2.12×10^{-4} m/s for 20 ml followed by second front wash at 8.49×10^{-4} m/s for 20 ml; Experiment B – First front wash at 8.49×10^{-4} m/s for 20 ml followed by second front wash at 2.12×10^{-4} m/s for 20 ml

Table 6.6 Fouling rates in two step intermittent protein filtration (BSA concentration: 10 kg/m^3; membrane: 0.45 micron cellulose acetate; flux: 8.49×10^{-4} m/s; total volume of BSA solution filtered: 8+32 ml) 184

Table 6.7 Fouling rates in four step intermittent protein filtration (BSA concentration: 10 kg/m^3; membrane: 0.45 micron cellulose acetate; flux: 8.49×10^{-4} m/s; total volume of BSA solution filtered: 4+4+4+4 ml) 186

Table 7.1 Membrane performance comparison via a newly defined parameter termed as 'Performance Factor' using the first protocol 209

Table 7.2 Slope of TMP vs. permeate volume data at different fluxes for all the membranes tested in the second protocol 215

Table 7.3 Slope of TMP vs. permeate volume data at different fluxes for all the membranes tested in the third protocol 219

LIST OF FIGURES

Figure 1.1 Different types of membrane structures 5

Figure 1.2 Block diagram illustrating typical positions of MF, UF and membrane chromatography in the downstream processing of protein based biopharmaceuticals 7

Figure 1.3 Schematic diagrams of (a) dead-end filtration and (b) cross-flow filtration 9

Figure 1.4 Concentration polarization 14

Figure 1.5 Loss of productivity due to membrane fouling in (a) constant pressure ultrafiltration and (b) constant flux ultrafiltration 19

Figure 1.6 Mechanisms of membrane fouling: (a) external fouling and (b) internal fouling 20

Figure 1.7 Transport phenomena in packed bed chromatography and membrane chromatography 24

Figure 1.8 Commonly used membrane module configurations in membrane chromatography 26

Figure 3.1 Effect of permeate flux on the separation of lysozyme and myoglobin using 30 kDa MWCO PES membrane 54

Figure 3.2 Chromatograms of permeate samples obtained by ultrafiltration with and without BSA at two different permeate fluxes. (A) Flux = 3.394×10^{-6} m/s, without BSA; (B) Flux = 3.394×10^{-6} m/s, with BSA; (C) Flux = 1.697×10^{-6} m/s, without BSA; (D) Flux = 1.697×10^{-6} m/s, with BSA; 1^{st} peak = myoglobin; 2^{nd} peak = lysozyme 56

Figure 3.3 Effect of (BSA/myoglobin) molar ratio on the separation of lysozyme and myoglobin using 30 kDa MWCO PES membrane; Permeate flux = 3.394×10^{-6} m/s 60

Figure 3.4 Effect of (BSA/myoglobin) molar ratio on the separation of lysozyme and myoglobin using 30 kDa MWCO PES membrane. Permeate 61

flux = 1.697×10^{-5} m/s

Figure 4.1 Pressure profile in constant flux ultrafiltration obtained using the pulsed sample injection technique 71

Figure 4.2 General approach for predicting flux decline in constant pressure ultrafiltration 72

Figure 4.3 Detailed scheme for predicting permeate flux decline including working equations 75

Figure 4.4 Schematic diagram of set-up used for constant flux ultrafiltration experiments 78

Figure 4.5 Schematic diagram of set-up used for constant pressure ultrafiltration experiments 78

Figure 4.6 TMP - time profiles obtained from five different constant flux HSA ultrafiltration experiments 81

Figure 4.7 Flux decline at 7.4 kPa TMP: (a) Simulated osmotic pressure and wall concentration, (b) Simulated membrane fouling resistance, and (c) Comparison of simulated and experimental permeate flux 83

Figure 4.8 Flux decline at 27.8 kPa TMP: (a) Simulated osmotic pressure and wall concentration, (b) Simulated membrane fouling resistance, and (c) Comparison of simulated and experimental permeate flux 86

Figure 4.9 Flux decline at 37.4 kPa TMP: (a) Simulated osmotic pressure and wall concentration, (b) Simulated membrane fouling resistance, and (c) Comparison of simulated and experimental permeate flux 89

Figure 5.1 Sketch showing the structure of macroporous gel filled membranes (Note: Convective transport occurs through the pores in the soft structured gel) 103

Figure 5.2 ESEM image of Q type 2 macroporous gel-filled membrane 103

Figure 5.3 Effect of pH on relative HSA binding on Q type 1 membrane 110

Figure 5.4 Effect of pH on relative HSA binding on Q type 2 membrane 111

Figure 5.5 Effect of ionic strength on HSA binding on Q type 1 membrane 113

Figure 5.6 Effect of ionic strength on HSA binding on Q type 2 membrane 113

Figure 5.7 Effect of buffering ions on HSA binding on Q type 1 and 2 membranes 115

Figure 5.8 Effect of feed concentration on HSA binding on Q type 1 membrane 116

Figure 5.9 Effect of feed concentration on HSA binding on Q type 2 membrane 117

Figure 5.10 Effect of feed flow rate on HSA binding on Q type 1 membrane 118

Figure 5.11 Effect of feed flow rate on HSA binding on Q type 2 membrane 119

Figure 5.12 HSA breakthrough on Q type 1 membrane 123

Figure 5.13 HSA breakthrough on Q type 2 membrane 124

Figure 5.14 Comparison of protein binding on conventional rigid porous membrane with that on the macroporous gel-filled membrane 126

Figure 5.15 HSA breakthroughs on Q type 1 membrane with custom designed membrane module and the conventional module 128

Figure 5.16 Double reciprocal plot of bound concentration versus feed concentration under saturating conditions. This plot demonstrates that HSA binding on the Q type 2 membrane follows Langmuir adsorption isotherm 130

Figure 5.17 Separation of HSA and HIgG using Q type 2 membrane (flow rate: 7 ml/min; diameter of membrane disc: 42 mm; number of discs: 1; feed: 10.12 kg/m^3 HSA + 2.63 kg/m^3 HIgG; binding buffer: 10 mM sodium phosphate; pH5.5; eluting buffer: 1 M NaCl) 133

Figure 5.18 Affinity chromatograms obtained with feed, flow-through and eluted peak samples from HSA/HIgG separation using Q type 2 membrane (peak 1: HSA and peak 2: HIgG) 135

Figure 5.19 Non-reducing SDS-PAGE (10%) obtained with feed, flow through and purified HSA samples 136

Figure 6.1 Schematic diagram of experimental set-up 148

Figure 6.2 TMP as a function of permeate volume (BSA concentration: 10 kg/m^3; 0.45 micron cellulose acetate membrane; Flux: 8.49×10^{-4} m/s; volume of BSA solution: 16 ml); P – Protein filtration, B – Buffer filtration 153

Figure 6.3 Complete pore blockage, intermediate pore blockage and pore constriction law analysis of BSA microfiltration in terms of their linearized form (BSA concentration: 10 kg/m^3; membrane: 0.45 micron cellulose acetate; flux: 8.49×10^{-4} m/s; volume of BSA solution filtered: 16 ml) 155

Figure 6.4 UV absorbance of permeate during BSA microfiltration (BSA concentration: 10 kg/m^3; 0.45 micron cellulose acetate membrane; Flux: 8.49×10^{-4} m/s; volume of BSA solution: 16 ml); P – Protein filtration, B – Buffer filtration 158

Figure 6.5 Chromatogram of front-wash sample obtained with high performance gel filtration column, Superdex 200 10/300 GL (flow rate: 0.2 ml/min) 159

Figure 6.6 Chromatograms of feed and permeate samples obtained with high performance gel filtration column, Superdex 200 10/300 GL (flow rate: 0.2 ml/min) 161

Figure 6.7 TMP profiles of two MF membranes housed in separate filtration module connected in series (BSA concentration: 10 kg/m^3; membrane: 0.45 micron cellulose acetate; flux: 8.49×10^{-4} m/s; volume of BSA solution filtered: 16 ml); P – Protein filtration, B – Buffer filtration 162

Figure 6.8 Effect of protein filtration volume on the reversibility of membrane fouling (BSA concentration: 10 kg/m^3; 0.45 micron cellulose acetate membrane; Flux: 8.49×10^{-4} m/s; volume of BSA solution filtered: 4, 6, 8 and 16 ml) 164

Figure 6.9 fluorescent images of membrane cross-sections super-imposed on their reflection images showing protein deposition at the end of (a) phase I, (b) phase II and (c) phase III (BSA concentration: 10 kg/m^3 + 0.005 kg/m^3 Alexa Fluor labeled BSA; membrane: 0.45 micron cellulose acetate; flux: 8.49×10^{-4} m/s) 168

Figure 6.10 fluorescent images of z-projection of membranes fouled with 16 ml of protein (a) before front washing and (b) after front washing (BSA concentration: 10 kg/m^3 + 0.005 kg/m^{3}l Alexa Fluor labeled BSA; membrane: 0.45 micron cellulose acetate; flux: 8.49×10^{-4} m/s) 169

Figure 6.11 Effect of prior protein adsorption in static condition on protein deposition during protein filtration (BSA concentration: 10 kg/m^3; 0.45 micron cellulose acetate membrane; Flux: 8.49×10^{-4} m/s; volume of BSA solution: 24 ml); P – Protein filtration, B – Buffer filtration 171

Figure 6.12 TMP vs. permeate volume profiles at different feed protein concentration (0.45 micron cellulose acetate membrane; Flux: 8.49×10^{-4} m/s; volume of BSA solution: 24 ml); P – Protein filtration, B – Buffer filtration 172

Figure 6.13 TMP vs. protein mass profiles at different feed protein concentration (0.45 micron cellulose acetate membrane; Flux: 8.49×10^{-4} m/s; volume of BSA solution: 24 ml); P – Protein filtration 173

Figure 6.14 TMP vs. permeate volume profiles at different flux during protein filtration (BSA concentration: 10 kg/m^3; 0.45 micron cellulose acetate membrane; volume of BSA solution: 24 ml); P – Protein filtration, B – Buffer filtration 175

Figure 6.15 Effect of front washing flow rate on the reversibility of membrane fouling (BSA concentration: 10 kg/m^3; 0.45 micron cellulose acetate membrane; Flux: 8.49×10^{-4} m/s; volume of BSA solution: 24 ml); P – Protein filtration, B – Buffer filtration 179

Figure 6.16 TMP profiles of 0.45 and 0.2 micron pore size cellulose acetate membranes (BSA concentration: 10 kg/m^3; Flux: 4.24×10^{-4} m/s; volume of BSA solution: 24 ml); P – Protein filtration, B – Buffer filtration 181

Figure 6.17 TMP profiles of 0.2 micron pore size cellulose acetate and 0.22 micron pore size PVDF membranes (BSA concentration: 10 kg/m^3; Flux: 4.24×10^{-4} m/s; volume of BSA solution: 24 ml); P – Protein filtration, B – Buffer filtration 182

Figure 6.18 TMP as a function of permeate volume in two step protein filtration separated by buffer filtration (BSA concentration: 10 kg/m^3; 0.45 micron cellulose acetate membrane; flux: 8.49×10^{-4} m/s; volume of BSA solution: 8+32 ml); P – Protein filtration, B – Buffer filtration 183

Figure 6.19 TMP as a function of permeate volume in four step protein filtration, each separated by 20 ml of buffer filtration (BSA concentration: 10 kg/m^3; 0.45 micron cellulose acetate membrane; flux: 8.49×10^{-4} m/s; volume of BSA solution: 4+4+4+4 ml); P – Protein filtration, B – Buffer filtration 185

Figure 6.20 Continuous protein filtration vs intermittent protein filtration (BSA concentration: 10 kg/m^3; 0.45 micron cellulose acetate membrane; flux: 8.49×10^{-4} m/s; total volume of BSA solution: 8 ml) 188

Figure 6.21 Continuous protein filtration vs intermittent protein filtration 189

(BSA concentration: 10 kg/m^3; 0.45 micron cellulose acetate membrane; flux: 8.49×10^{-4} m/s; total volume of BSA solution: 16 ml)

Figure 7.1 Experimental set-up for accelerated membrane fouling assessment in the dead-end mode 200

Figure 7.2 Experimental set-up for critical flux testing with syringe filter holder 202

Figure 7.3 Experimental set-up for the stirred cell based protocol 204

Figure 7.4 TMP vs. time profiles for six different MF membranes in the first protocol (BSA concentration: 60 kg/m^3; flux: 8.49×10^{-4} m/s and; pulse volume: 5 ml) 206

Figure 7.5 Critical flux study of different membranes in dead end mode: TMP and flux at different permeate volumes (BSA concentration: 10 kg/m^3; step size: 4 ml) 212

Figure 7.6 Critical flux of PVDF membrane (BSA concentration: 10 kg/m^3; step size: 4 ml) 213

Figure 7.7 Critical flux of surface treated membranes (BSA concentration: 10 kg/m^3; step size: 4 ml) 214

Figure 7.8 Critical flux of different MF membranes with the stirred cell protocol (BSA concentration: 10 kg/m^3; cross flowrate: 32.5 ml/min; stirring speed: 950±50 rpm; step size: 10 ml) 217

Nomenclature

AUC_b	area under the curve of bound peak (AU-m^3)
AUC_u	area under the curve of unbound peak (AU-m^3)
BSA	bovine serum albumin
C	protein concentration (kg/m^3)
C_b	protein concentration in bulk feed (kg/m^3)
C_f	protein feed concentration (kg/m^3)
C_g	protein gelation concentration (kg/m^3)
C_p	protein concentration in permeate(kg/m^3)
C_w	protein wall concentration (kg/m^3)
CA	cellulose acetate
d_p	average pore diameter (m)
D	diffusion coefficient (m^2/s)
HSA	human serum albumin
HIgG	human immunoglobulin G
J_v	volumetric permeate flux (m/s)
J_v^0	water flux (m/s)
k	mass transfer coefficient (m/s)
l_p	length of pore (m)
m	slope of the linear portion of TMP-time profile in constant flux ultrafiltration (kPa/s)
M_b	mass bound to membrane (kg)
M_i	mass injected (kg)
MF	microfiltration
MWCO	molecular weight cut off
PES	polyethersulfone
PVDF	polyvinylidenefluoride
ΔP	transmembrane pressure (kPa)

P_1	transmembrane pressure corresponding to buffer filtration through new membrane disc (kPa)
P_2	maximum transmembrane pressure during protein filtration or the test (kPa)
P_3	transmembrane pressure corresponding to buffer filtration through fouled membrane disc (kPa)
P_f	pressure of feed stream (kPa)
P_p	pressure of permeate stream (kPa)
P_r	pressure of retentate stream (kPa)
q	mass of protein bound per unit volume of membrane (kg/m^3)
r	impeller diameter (m)
rpm	revolution per minute
R_{CP}	hydraulic resistance of concentration polarization layer (kPa s/m)
Re_{pore}	pore Reynolds number
R_f	fouling resistance (kPa s/m)
R_g	gel layer resistance (kPa s/m)
R_m	total membrane resistance (kPa s/m)
R_m^0	membrane hydraulic resistance (kPa s/m)
R_m^*	initial rapid fouling constant (kPa s/m)
S_a	apparent sieving coefficient
S_i	intrinsic sieving coefficient
SEC	size exclusion chromatography
t	time (s)
Δt	small time increment (s)
t_R	duration of initial rapid fouling phase (s)
TMP	transmembrane pressure (kPa)
u_s	superficial liquid velocity (m/s)
UF	ultrafiltration

y	distance from the edge of concentration polarization layer toward membrane (m)

Greek Symbols

α	fouling rate constant (kPa/m)
δ	boundary layer thickness (m)
δ_m	membrane thickness (m)
ε	porosity
θ_c	centerline residence time (s)
θ_D	diffusion time (s)
μ	viscosity (kg/ms)
υ	kinematic viscosity (m^2/s)
ξ_1	permeability of new membrane disc (m/kPas)
ξ_2	permeability of fouled membrane disc (m/kPas)
$\Delta\pi$	osmotic pressure (kPa)
τ	tortuosity
ϖ	stirring speed (s^{-1})
ψ	selectivity
ψ^{-1}	reversed selectivity
Z	performance factor (m/kPa^2s)

Preface

This PhD thesis is organized in a sandwich style based on the following published and preparatory articles:

1. D.M. Kanani, X. Sun, R. Ghosh, Reversible and irreversible membrane fouling during in-line microfiltration of concentrated protein solution (Communicated to Journal of Membrane Science).

2. D.M. Kanani, R. Ghosh, Fouling assessment techniques, 3M Canada, June 2006.

3. D.M. Kanani, E. Komkova, T. Wong, A. Mika, R.F. Childs, R. Ghosh, Separation of human plasma proteins HSA and HIgG using high-capacity macroporous gel-filled membranes, Biochem. Eng. J. 35 (2007) 295-300.

4. D.M. Kanani, R. Ghosh, A constant flux based mathematical model for predicting permeate flux decline in constant pressure protein ultrafiltration, J. Membr. Sci. 290 (2007) 207-215.

5. D.M. Kanani, R. Ghosh, CDM Filipe, A novel approach for high-resolution protein-protein separation by ultrafiltration using a dual-facilitating agent, J. Membr. Sci. 243 (2004) 223-228.

These articles were prepared by Dharmeshkumar M. Kanani. Dr. C.D.M. Filipe, Dr. R.F. Childs and Dr. R. Ghosh provided guidance with research focus and idea development and reviewed the draft of manuscripts. Dr. E. Komkova and Dr. A. Mika prepared the high-capacity macroporous gel-filled membranes and gave some useful suggestions about the use of these membranes. They also provided the ESEM image of these membranes along with the membrane properties such as nominal pore size and porosity of the membranes. Dr. X. Sun helped with the SEC analysis of protein samples for the presence of BSA dimers and aggregates for MF fouling study. Ms. T. Wong and Mr. A. Chang worked in our laboratories and helped run experiments under the supervision of Dharmeshkumar M. Kanani in the summer 2004 and 2005 respectively. The work reported in this thesis was undertaken between September 2003 and September 2007.

Chapter 1

Introduction

1.1 Protein bioseparation – A challenge facing the biopharmaceutical industry

Advances in life sciences and molecular biology have led to identification of several proteins of significant therapeutic potential. The development of genetic engineering and hybridoma technology in the 1970s made commercial scale production of these proteins possible. More than 100 protein based biopharmaceuticals were approved and marketed in USA and in the EU by mid-2002 [1-2]. These included monoclonal antibodies, vaccines, hormones and several blood proteins. Their collective global market was worth more than $10 billion in 2002 [1-2]. Today, biotech is one of the most research-intensive industries and is seen worthy of investment, including venture funding [3]. Aging baby boomer population and rising wish to eradicate leading death

causing diseases such as cancer and diabetes are providing a huge potential to market biopharmaceuticals. Currently, several protein biopharmaceuticals are being evaluated in clinical trials.

New innovations and technologies in upstream processing have significantly increased expression levels of proteins in bioreactors. However, large-scale protein purification which is referred to as protein bioseparation continues to be a major challenge [4-6]. Proteins are very complex macromolecules and needed to be processed at mild operating conditions due to their fragile three dimensional structures. Biological feed streams are generally very dilute with respect to the target proteins and contain many impurities. Several of these impurities have similar physicochemical properties as the target protein. Conventional protein purification techniques are severely limited in the sense that they either give good separation at the cost of productivity or vice versa. Therefore traditionally, protein bioseparation is carried out according to the so called RIPP scheme [7-10], which stands for Recovery, Isolation, Purification and Polishing. In this scheme, feed streams are first treated with high-productivity, low-resolution techniques to reduce the material volume and to increase the product concentration. This is followed by high-resolution, low-productivity techniques to get the pure target protein. Due to the large number of steps involved in the downstream processing of protein biopharmaceuticals using the RIPP scheme, the overall yield can be very low and this contributes to the high cost of such products.

Cost effectiveness of a protein bioseparation process is critical since it typically accounts for 50-80% of the total production cost [10]. Up to now, the industry hasn't bothered too much about bioprocessing cost, primarily due to the significantly inflated product prices made possible by patent protection. However, a large number of blockbuster protein biopharmaceuticals will off-patent by the end of the decade and pricing will have to become more competitive. The generic biopharmaceutical product market will therefore become much bigger than now and biopharmaceutical companies will have to seriously think about cost-effective manufacturing. Moreover, rising drug costs is putting an increased public pressure on the biopharmaceutical industry to pay more attention to the economic aspects of bio-manufacturing.

The most significant limitation of protein bioseparation is problems related to scale-up, i.e. development of commercial scale processes from laboratory scale processes. A good bioseparation process must ideally combine high productivity with high resolution. Currently used bioseparation techniques are focused entirely around resolution at the expense of productivity. The generic biopharmaceutical industry is increasingly facing a shortage of manufacturing capacity due to increased sales of approved protein biopharmaceuticals. In order to sustain the growth of the biopharmaceutical industry there is a strong need for the development of new bioseparation technologies both for generic and niche applications which not only give good separation but also high productivity. This will help in increasing the production capacity of proteins and also help in bringing down the overall cost.

1.2 Membrane based bioseparation techniques

The term 'filtration' is normally used for separation of solids from fluid. In membrane separation processes, one goes a step further to separate dissolved solutes in a solution from one another as well as from solvent, using thin semi-permeable barriers called membranes. A membrane separates different components of a solution by the combination of sieving, hindered transport through the narrow membrane pores and other specific interactions between the solution components and membrane material (such as hydrophilic, hydrophobic and electrical interactions). A membrane can be made from either organic polymers such as cellulose, cellulose acetate, polysulfone, polyethersufone, polyvinylidine fluoride and polyamide or inorganic materials such as ceramics, glass or metals. From a structure point of view, there are two types of membranes: 1) symmetric or isotropic and 2) asymmetric or anisotropic. A symmetric membrane is characterized by uniform structural composition and morphology at all positions within it while, an asymmetric membrane has two or more structural planes of different morphology or composition (See Figure 1.1). A membrane can be either porous or dense based on its morphology. Porous membranes have either tiny pores (also known as track-etch membranes) or network of interconnected pores while dense membranes do not have any pores and transport of material takes place mainly by a partition-diffusion mechanism.

Dense membrane

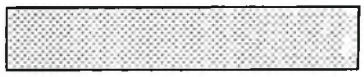

Porous membrane

(a) Symmetric membranes

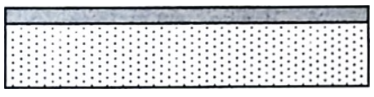

Dense membrane fused on macroporous support

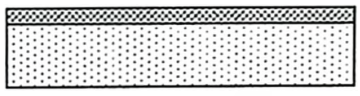

Porous membrane fused on macroporous support

(b) Asymmetric membranes

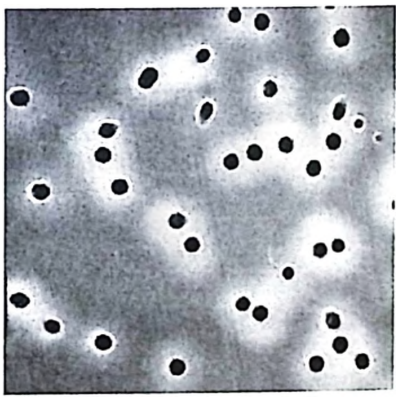

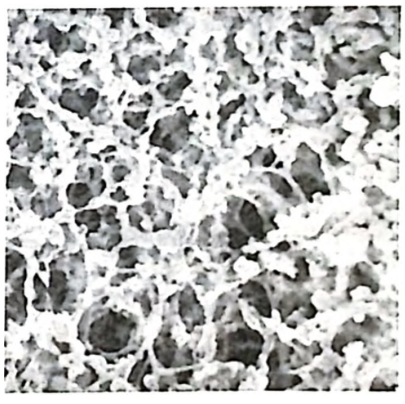

(c) Porous membranes [10]

Figure 1.1 Different types of membrane structures

Among different kinds of membrane processes, microfiltration (MF), ultrafiltration (UF) and membrane chromatography have found many applications in bioseparation of protein based products [11]. MF and UF are considered as pressure-driven non-adsorptive membrane processes while membrane chromatography is regarded as an adsorptive technique. They all employ porous membranes to carry out the required separation. Due to convective transport of material through the pores of membranes in all three techniques, they give much faster separation in comparison to other competing techniques and can easily handle the large volume of liquid. MF membranes have pore sizes in the range of 0.05 to 10 μm. They are typically used for clarification and sterile filtration type of applications to separate cells or cellular particles from the liquid media. UF membranes have pore sizes between 1 and 20 nm and are widely used for separation of macromolecules from solvent or small molecules e.g. protein concentration, buffer exchange and desalting. Membrane chromatography is relatively a new technique introduced to overcome some of the limitations associated with packed bed chromatography and employs microfiltration (or larger pore sizes) membranes. It is used for certain niche applications in the biopharmaceutical industry such as removal of small amount of impurities from the large volume of feed. All these membrane processes are normally operated around ambient temperature and hence provide maximum assurance of protein stability. Figure 1.2 shows a block diagram illustrating typical positions of MF, UF and membrane chromatography in the downstream processing of protein based biopharmaceuticals.

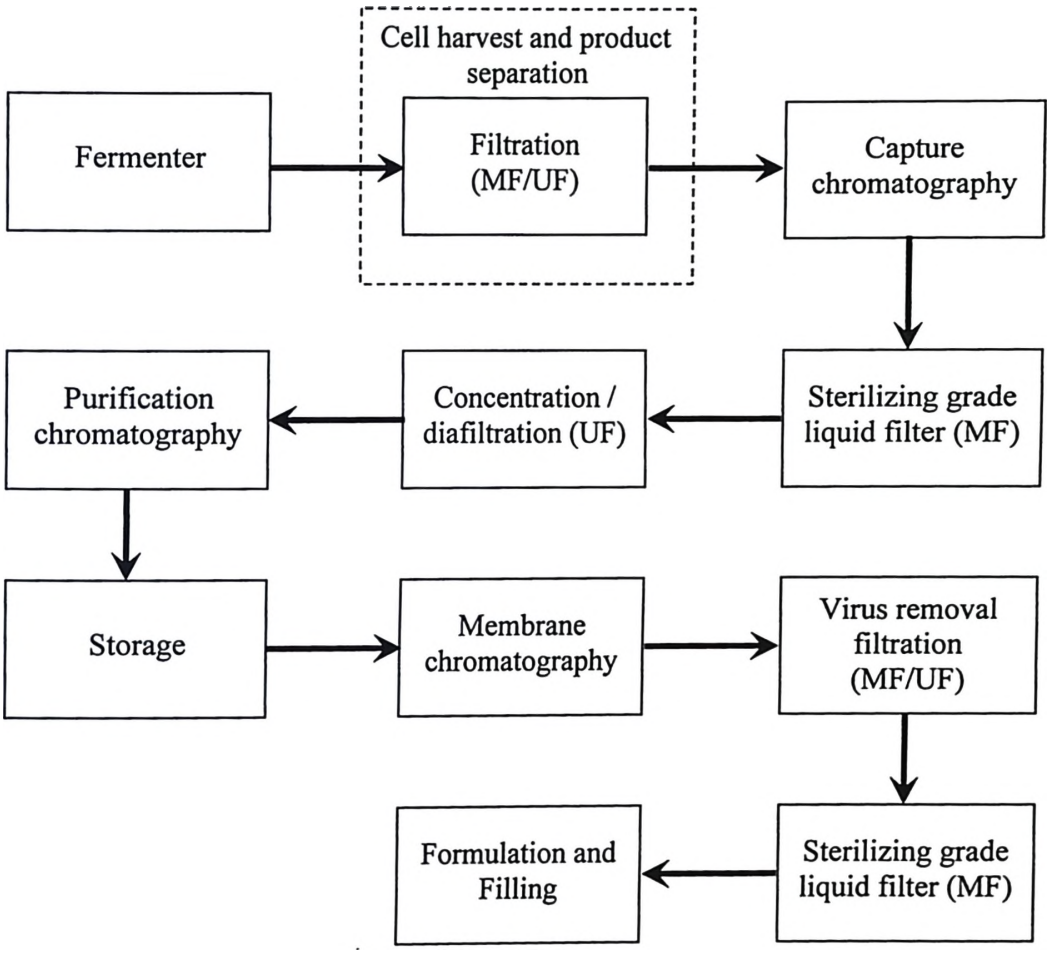

Figure 1.2 Block diagram illustrating typical positions of MF, UF and membrane chromatography in the downstream processing of protein based biopharmaceuticals

Normally, MF and UF are operated in two distinctly different modes depending on their applications: 1) dead-end filtration (or normal flow filtration) and 2) cross-flow

filtration (or tangential flow filtration). Figure 1.3 shows schematic diagrams of typical dead-end filtration and cross-flow filtration processes. In both modes, fluid flows across the membrane through the pores due to applied pressure difference called transmembrane pressure. The process stream which passed through the membrane is termed as permeate or filtrate. When the amount of particulate matter in the feed is very low and solute transmission through the membrane is nearly 100%, dead-end mode is preferred over cross-flow mode. In dead-end mode, fluid flows only perpendicular to the membrane. In cross-flow mode, fluid flows parallel to the membrane surface in addition to the normal flow across the membrane. Cross-flow or tangential flow parallel to the membrane surface helps in removing the particulate matter or solute molecules retained by the membrane, which otherwise can put an added resistance or decrease the effective transmembrane pressure across the membrane through osmotic pressure. The process stream which flows parallel to the membrane surface in cross flow mode and leaves the module at other end is termed as retentate. The transmembrane pressure across the membrane in cross-flow mode is defined as:

$$\Delta P = \frac{P_f + P_r}{2} - P_p \tag{1.1}$$

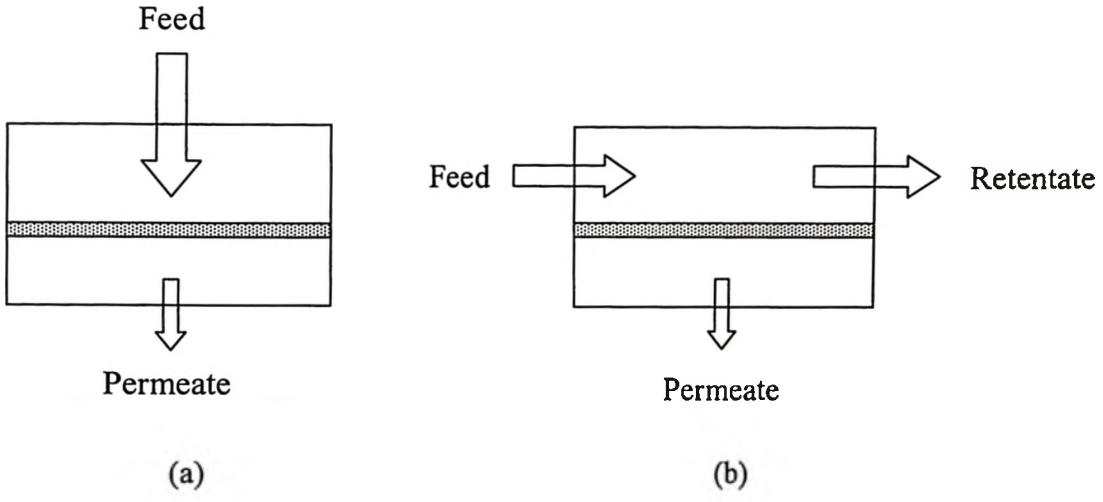

Figure 1.3 Schematic diagrams of (a) dead-end filtration and (b) cross-flow filtration

1.2.1 Ultrafiltration

Ultrafiltration is typically considered as a sized based separation technique and is widely used throughout the downstream processing of protein based products due to high throughput, low process cost and ease of scale-up [12-13]. The pore size or separation characteristics of UF membrane is usually expressed in terms of the molecular weight cut-off (MWCO). The MWCO of a membrane is defined as the molecular weight of a polymer such as dextrans or PEGs which can be retained by the membrane for more than 90%. Normally, UF is used to carry out the separation of proteins in the molecular weight range of 5-500 kDa. UF membranes are asymmetric in nature, with a thin skin layer (approximately 5-10 μm thick) supported by a macroporous substructure. The skin layer is responsible for the selectivity of UF membrane while the macroporous substructure

provides mechanical strength. Such types of asymmetric UF membranes give higher filtration rate than symmetric membranes since the resistance provided by the macroporous substructure is negligible in comparison to the skin layer which is only few micrometers thin. This will cut down the process time and required membrane area. UF membranes can be cast from variety of polymers such as cellulose (regenerated), cellulose acetate, cellulose triacetate, polysulfone, polyethersulfone, polyamide, polyimide, polyvinyl alcohol and polyacrylonitrile with a range of pore size. Among these, polysulfone, polyethersulfone and cellulose (regenerated) are quite widely used in the biopharmaceutical industry.

1.2.1.1 Performance and engineering models

The performance of UF process is normally evaluated from the three parameters:

1. apparent sieving coefficient
2. selectivity and
3. flux

Apparent sieving coefficient (S_a) is defined as the ratio of concentration of solute in the permeate to that in the bulk feed. It gives idea about the transmission of solute through the membrane and hence the separation achieved. For fully transmittable solutes, S_a would be one while for completely rejected solutes S_a would be zero. It depends on the protein-solvent system, the membrane, physicochemical conditions and the permeate flux [14]. For partially transmittable solutes, it also depends on the system hydrodynamics.

Since partially transmittable solutes can accumulate near the membrane surface, S_a would be different than the actual sieving coefficient of membrane, which is termed as intrinsic sieving coefficient (S_i). Intrinsic sieving coefficient is defined as the ratio of concentration of solute in the permeate to the wall concentration (concentration of solute in the solution adjacent to the membrane surface on the feed side).

$$S_a = \frac{C_p}{C_b} \tag{1.2}$$

$$S_i = \frac{C_p}{C_w} \tag{1.3}$$

Another important parameter, selectivity (ψ) assesses the efficiency of binary protein fractionation in UF in one stage. It is defined as:

$$\Psi = \frac{S_{a1}}{S_{a2}} \tag{1.4}$$

Here, subscript 1 stands for the preferentially transmitted protein while 2 stands for the preferentially retained protein.

The flux (J_v) is defined as the volumetric flow rate of permeate/filtrate per unit membrane surface area. It characterizes the throughput of UF process: higher the flux,

better the throughput. The flux in UF process depends on the membrane properties, solvent properties, trans-membrane pressure, solute concentration and system hydrodynamics. For pure solvent or a very dilute solution the flux can be calculated using the pore flow model [15]:

$$J_v = \frac{\varepsilon d_p^{\,2} \Delta P}{32 \mu l_p} \tag{1.5}$$

The pore flow model assumes the membrane made of straight cylindrical pores. According to this model, flux is a very strong function of membrane pore diameter. Since most of the UF membranes can not be visualized as having straight cylindrical pores, another model called 'membrane hydraulic resistance model' is frequently used to calculate the flux [14]:

$$J_v = \frac{\Delta P}{R_m^{\,o}} \tag{1.6}$$

Here, $R_m^{\,o}$ represents membrane hydraulic resistance, which basically combines all the parameters characterizing the membrane and solvent properties in the 'pore flow model' in to one parameter. Equation 1.6 is valid only for the filtration of a very dilute solution. If a protein is partially retained by the membrane, the flux decreases significantly even for the moderately dilute solution due to the phenomenon called concentration

polarization. Concentration polarization is the build up of retained protein molecules in the solution near the membrane surface. The build up of retained protein molecules near the membrane surface not only presents the extra hydraulic resistance to flow but also reduces the effective trans-membrane pressure by offering osmotic pressure. The permeate flux in UF process with partial or complete rejection of proteins can be calculated from the modified form of the 'membrane hydraulic resistance' model [14]:

$$J_v = \frac{\Delta P - \Delta \Pi}{R_m{}^o + R_{cp}} \tag{1.7}$$

This model takes into consideration both the contribution of osmotic pressure and the hydraulic resistance provided by concentration polarization layer in protein UF. If the permeate flux or the bulk protein concentration is too high, a gel layer can be formed on top of the membrane due to the extensive protein build up. In such situation, Equation 1.7 needs to be modified to include the extra resistance provided by the gel layer [14]:

$$J_v = \frac{\Delta P - \Delta \Pi}{R_m{}^o + R_{cp} + R_g} \tag{1.8}$$

If existence of a hydrodynamic boundary layer next to the membrane is assumed, which is parallel to the membrane surface, then concentration polarization layer is nothing but the concentration gradient of retained protein molecules in this hydrodynamic boundary layer. The transport of protein molecules into the boundary layer towards the membrane

takes place by convection while their back-transport away from the boundary layer towards the bulk feed takes place by diffusion [see Figure 1.4]. At steady state, the solution of material balance of proteins in a control volume within the concentration polarization layer gives the following equation known as 'concentration polarization model' [16]:

$$J_v = k \ln\left(\frac{C_w - C_p}{C_b - C_p}\right) \tag{1.9}$$

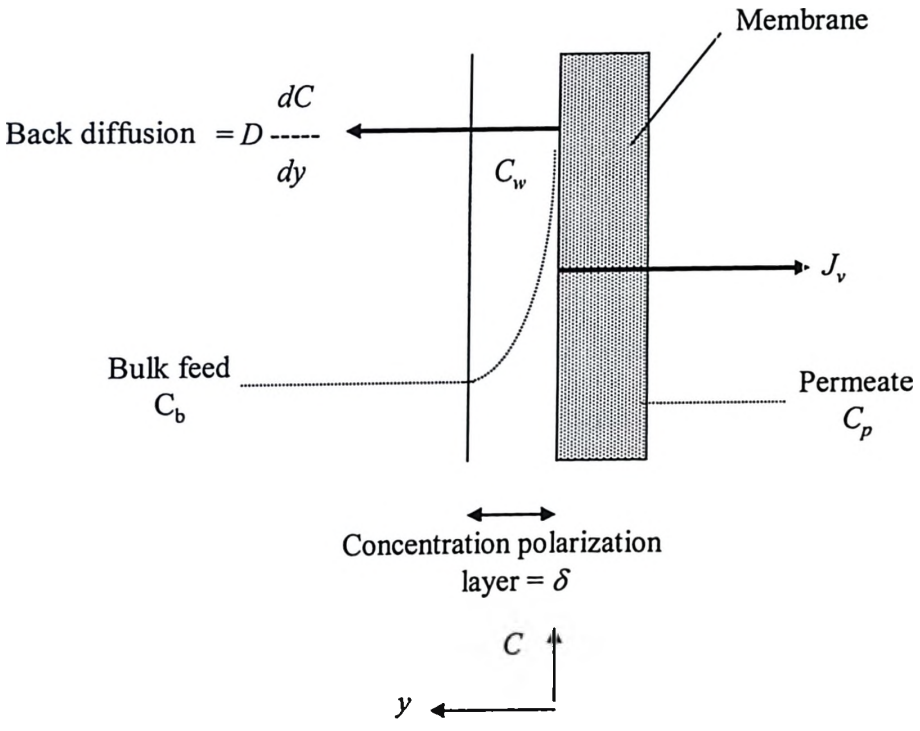

Figure 1.4 Concentration polarization

According to concentration polarization model, flux in protein UF process can be improved by increasing the mass transfer coefficient in the module. The mass transfer coefficient is a measure of diffusive back-transport of the protein and depends on the system hydrodynamics of the UF module and diffusivity of the protein. For complete protein rejection, Equation 1.9 becomes:

$$J_v = k \ln(\frac{C_w}{C_b}) \tag{1.10}$$

When protein wall concentration C_w reaches the gelation concentration of protein, there would be no further increase in C_w. In this situation, Equation 1.10 would become:

$$J_v = k \ln(\frac{C_g}{C_b}) \tag{1.11}$$

Equation 1.11 is known as 'gel polarization equation'. With the formation of gel layer on the membrane surface, flux becomes independent of the trans-membrane pressure. In this pressure independent region, the flux depends only on the system hydrodynamics or the mass transfer coefficient for the given feed solution. At fixed mass transfer coefficient, this plateau flux is termed as the limiting flux.

1.2.1.3 Protein fractionation

Traditionally, UF is considered as a low-resolution technique with high-throughput. It is generally thought to be a sized based technique and used to carry out the separation of molecules differing more than 10 fold in size. This somewhat limited selectivity of UF has been attributed to the broad pore size distribution in membrane, concentration polarization, membrane fouling and protein-protein interactions [14, 17]. Research in the last decade has shown that UF can be used to achieve more fine separations such as protein-protein separations by proper choice of membrane, buffer conditions and operating parameters [14, 17-19]. Selection of UF membrane with proper pore size and surface properties such as charge and hydrophilicity is a key factor in protein fractionation [20-24]. Buffer conditions such as pH and salt concentration can be optimized to exploit the differences in hydrodynamic volumes of proteins due to differences in their charges [25-49]. Operating parameters such as permeate flux and system hydrodynamics can be used to exploit the predominant mode of protein transport (for example diffusive or convective) through the membrane and concentration polarization to affect the protein fractionation by UF membrane [25-45, 50-53]. A book chapter by Ghosh [14] and review paper by Wan et al [17] have comprehensively summarized the work done by various researchers in the area of protein fractionation by UF. Based on research findings by the various researchers, Ghosh [14] has suggested following thumb rules for protein fractionation:

1. Transmission of protein through UF membrane is highest at its isoelectric point due to its lower hydrodynamic volume.

2. Protein transmission is relatively insensitive to the solution pH at high salt concentration.
3. Oppositely charge proteins can interact to form complexes in solution resulting in the lower transmission of both proteins.
4. The transmission behavior of protein depends on the presence of other proteins in the solution.
5. High salt concentration can be used to reduce the protein-protein interactions
6. Similar charge on the protein and membrane can hinder the transmission of protein.
7. pH and ionic strength of the solution can be manipulated to obtain the so called 'reverse selectivity', a situation where the larger protein is preferentially transmitted through the membrane compared to the smaller one.
8. The permeate flux and system hydrodynamics should be optimized to achieve optimum selectivity and protein transmission.
9. Adsorption of protein on membrane can change the flux and transmission properties of a membrane.

Since, protein fractionation by UF can not be achieved based on solely size difference, a lot of process optimization is needed to fine-tune the different operating and physicochemical parameters. This demands an extensive amount of experimental work which is both time consuming and expensive. Development of new techniques such as pulsed sample injection [31, 54] and parameter scanning ultrafiltration [55-56] is

expected to boost the exploration of UF for the fractionation of real protein mixtures by enabling the rapid and inexpensive process optimization. Protein fractionation by ultrafiltration can now become the reality thanks to the novel modes of operation such as carrier phase ultrafiltration [31] and high performance tangential flow filtration [18, 57]. These novel modes of operation give better control of the process over conventional modes such as dead-end and cross-flow.

1.2.2 Membrane fouling

Membrane fouling offers the biggest challenge for membrane technologist. Membrane fouling refers to the adsorption and deposition of protein molecules on or inside the membrane [58]. It increases membrane resistance during a process. In constant pressure membrane process, flux decreases with time due to fouling while in constant flux membrane process, fouling reflects in increased TMP in order to sustain a particular flux through the membrane (see Figure 1.5). Fouling not only reduces the throughput in the membrane process by reducing the flux but also changes membrane's separation characteristics. Protein adsorption in static conditions normally results in the monolayer of proteins on membrane while membrane fouling often results in the deposition of multilayered proteins which is relatively more compact than protein adsorption in static conditions. Therefore protein adsorption in static conditions gives only marginal increase in flow resistance without affecting the separation characteristics significantly, but protein deposition in dynamic filtration conditions offers significantly more flow resistance with altered separation characteristics [59-60].

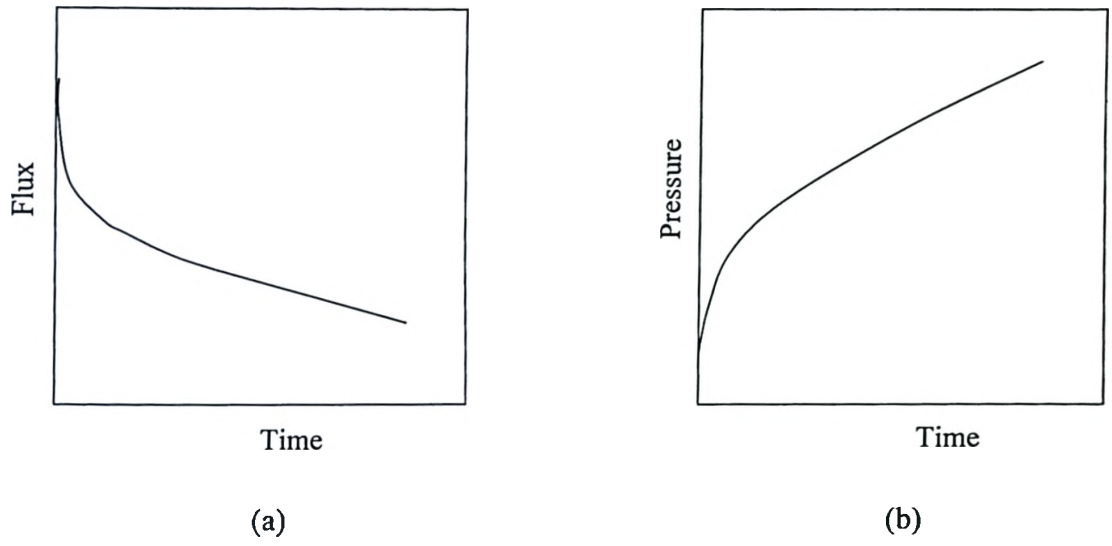

Figure 1.5 Loss of productivity due to membrane fouling in (a) constant pressure ultrafiltration and (b) constant flux ultrafiltration

Figure 1.6 shows the different fouling mechanisms which can be classified into two categories: 1) internal fouling and 2) external fouling. Internal fouling refers to the adsorption or deposition of proteins within the pores of the membrane. The three possible mechanisms by which membrane can be fouled internally are direct interception, inertial impaction and diffusional transport of proteins to the pore walls [14]. External membrane fouling refers to the adsorption/deposition of proteins on the external membrane surface. External fouling hinders the transmission of proteins by either increasing the effective membrane thickness or completely and/or partially blocking the pore entrance. In external fouling, protein molecules are transported to the membrane surface for adsorption/deposition either by diffusion or convection and sieving. The extent and

nature of membrane fouling depend on the properties of membrane and protein; physicochemical properties of the solution such as pH and salt concentration; and operating parameters, e.g. TMP, flux and system hydrodynamics. Among these, system hydrodynamics play major role in deciding the efficiency of membrane processes. Marshall et al [58] has quite extensively reviewed the literature until 1993 for protein fouling of MF and UF membrane. After 1993, several researchers have reported the studies on the structure of protein deposits; fouling mechanisms; role of protein-protein and protein-membrane interactions in membrane fouling; and effects of different operating parameters on protein denaturation and its subsequent consequences on membrane fouling [61-71].

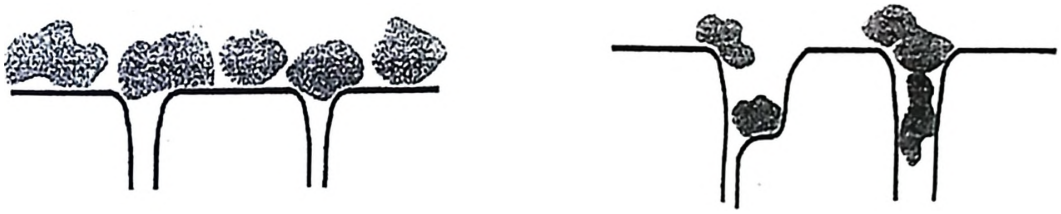

(a) (b)

Figure 1.6 Mechanisms of membrane fouling: (a) external fouling and (b) internal fouling

In protein UF, flux decreases with time due to both concentration polarization and membrane fouling. At high transmembrane pressure, concentration polarization is quite

severe particularly at the start of UF, but its contribution in flux decline becomes negligible towards the end of process [72-74]. Concentration polarization is different than membrane fouling that it refers to the protein molecules accumulated in the solution near the membrane surface. While membrane fouling refers to the protein molecules accumulated on/inside the membrane. In fact, gel layer formation can be said one form of fouling. Concentration polarization influences the membrane fouling, the more severe concentration polarization, the higher amount of membrane fouling is. Proteins also foul the microfiltration membranes even though the pore sizes of membranes are at least 10 fold higher than the sizes of proteins. Many researchers have studied protein fouling in both microfiltration and ultrafiltration and modeled their experimental data using one or combination of different blocking laws [75-85].

Membrane fouling is nearly unavoidable phenomenon and almost all the solute molecules foul the membrane more or less. Flux loss and the original separation characteristics of the membrane can be restored partially by cleaning the membrane by either physical methods such as backwashing or chemical methods which include the rinsing of membrane with alkaline, acidic or surfactants solution. With each cleaning cycle with chemical agents, the membrane life decreases and since the cost of membrane is still substantial, control of membrane fouling is essential.

1.2.3 Membrane chromatography

Adsorptive chromatography is the most widely used technique for high resolution separation and analysis of proteins in the biopharmaceutical industry. It is traditionally carried out using packed bed as a stationary phase which has some significant drawbacks. The pressure drop in a packed bed is normally high and may increase during a process due to bed consolidation and column blinding (by accumulated colloidal material). A major disadvantage of packed-beds particularly those using soft chromatographic media, is the diffusion limited transport of solute molecules from mobile phase (bulk solution) to their binding sites during adsorption and from there back to mobile phase during desorption (see Figure 1.7). This increases both process time and process liquid volume, which in turn affect the economy of packed bed chromatography heavily both in terms of labor cost and buffer cost. The complicated transport phenomena of diffusion limited separations in packed beds also make scale-up very difficult. By using mono-dispersed, non-porous, rigid chromatographic media some of these drawbacks can be overcome [86-87]. However, they suffer from low binding capacities and are generally expensive. Also the problem of high pressure drop still remains with these media.

The use of microfiltration (or larger) pore size membranes as chromatographic media can alleviate some of the problems linked with packed beds [88]. In membrane chromatographic processes, solute transport to their binding sites takes place predominantly by convection (see Figure 1.7). Convective transport reduces mass transfer resistance significantly which leads towards binding kinetics dominant adsorption

process. Generally speaking, binding kinetics is much faster in comparison to diffusion limited mass transfer. This makes membrane chromatography much faster in comparison to packed bed chromatography. This not only saves time but also reduces buffer consumption. Buffer cost alone accounts for 70-75% of the total cost of packed-bed chromatography while it contributes only 7-8% of the total cost of membrane chromatography. Labor cost accounts for around 15% of the total cost of packed-bed chromatography while it contributes only 7-8% of the total cost of membrane chromatography. Though membranes cost is almost double when compared to packed beds, the lower buffer and labor cost make membrane chromatography cheaper by a factor of 2-4 [89].

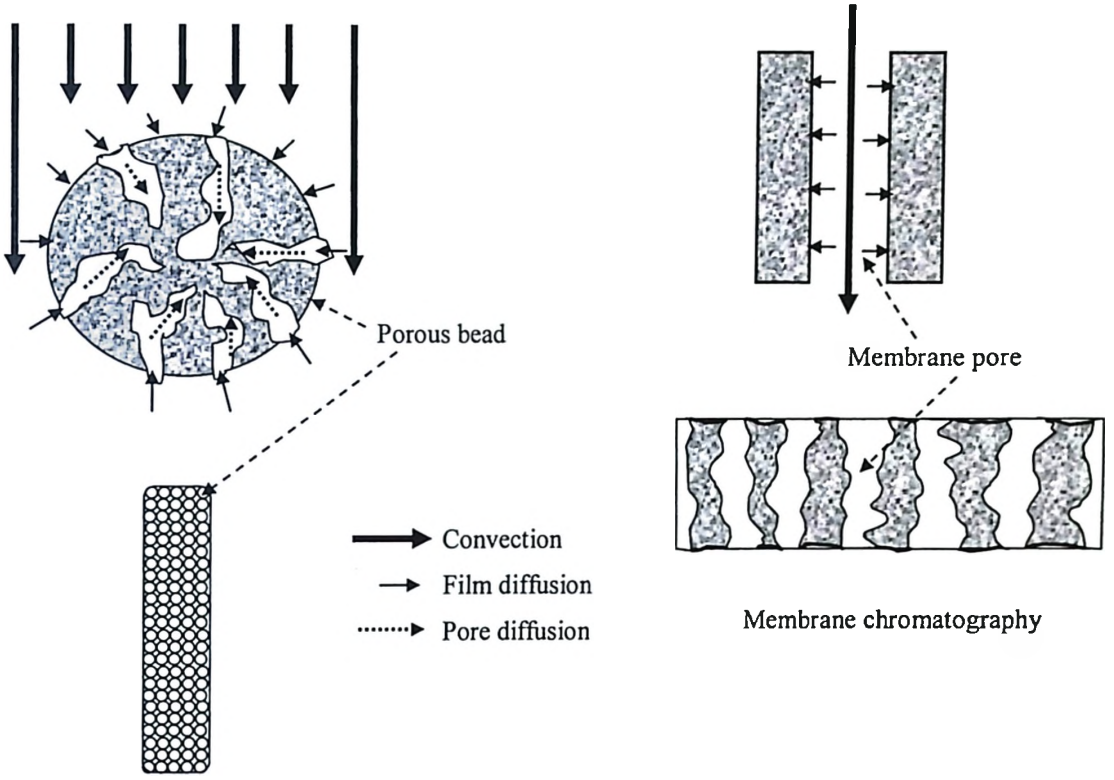

Figure 1.7 Transport phenomena in packed bed chromatography and membrane chromatography

In the context of mass transfer, hydrodynamics, binding capacity, and available surface area, membranes behave in the same way as packed-beds of small non-porous particles [90]. The real benefit of a membrane is the continuity of the solid phase. In practice, it is difficult to make a very short adsorptive bed having a large cross-sectional

area using loose particles but this is achievable with membranes. Due to shorter bed heights with membranes, pressure drop tends to be low in membrane adsorbers compared to packed beds. Due to recent developments in membrane manufacturing technology, membrane chromatographic devices are now easier and cheaper to mass-produce. This makes it possible to have disposable membrane adsorbers, which eliminates the requirement for cleaning and equipment re-validation. Another major advantage of membrane adsorbers is the relative ease of scale-up compare to packed-beds. Membrane chromatography is particularly suitable for larger proteins, which rarely enter in the pores of porous chromatographic media and only bind on the external surface of such media.

The chromatographic interactions in the macroporous membranes are identical to those in the packed columns. These include: 1) affinity 2) ion-exchange and 3) hydrophobic. Among these, affinity interactions are very popular in the literature mainly due to the relative ease in attaching different ligands on the membranes [91]. Ion-exchange membranes are the second major segment of media used in membrane chromatography. Different charged groups such as sulfonic acid (S), sulfopropyl (SP), diethylaminoethyl (DEAE), and quaternary ammonium (Q) were used as ligands to obtain high protein binding membranes. Two types of membrane modules are commonly used for membrane chromatography. The design of the flat sheet type membrane module (see Figure 1.8) is based on that of an in-line syringe type filter holder. This type is suitable for small-scale biomanufacturing. The radial flow type membrane module (see Figure 1.8) is better suited for large-scale biopharmaceutical production. There are

several review papers which describe collectively preparation of adsorptive membranes, fundamental mechanisms, operation and applications of membrane chromatography along with opportunities and challenges in membrane chromatography [90-94]. Several examples have already demonstrated the viability of using membrane adsorbers for fast and efficient capture of biomolecules. These include the preparative purification of human serum albumin from human plasma [95], large-scale purification of oligonucleotides [96], ion-exchange chromatography of monoclonal antibodies [97], and virus purification [98].

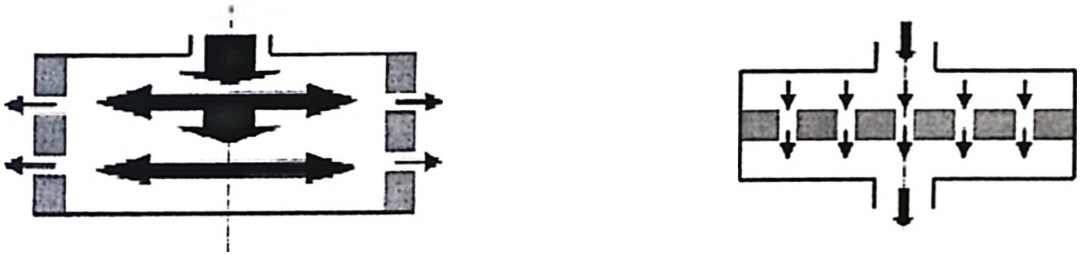

Radial flow

Flat sheet

Figure 1.8 Commonly used membrane module configurations in membrane chromatography

Membrane chromatography is increasingly gaining acceptance in the biopharmaceutical industry [11, 99]. The factors driving this are lower operating cost, speed, higher productivity, linear scalability and disposable nature. Sartorious was one of

the first companies to introduce membrane chromatography devices in the market. Other membrane companies such as Pall and Millipore have subsequently introduced chromatography products for a range of different application.

1.3 References

1. G. Walsh, Biopharmaceuticals: biochemistry and biotechnology, John Wiley & Sons, West Sussex, 2004.
2. R.J.Y. Ho, M. Gibaldi, Biotechnology and biopharmaceuticals: transforming proteins and genes into drugs, John Wiley & Sons, Hoboken, New Jersey 2003.
3. D. Strickland, The guide to biotechnology, Biotechnology Industry Organization (BIO), Washington D.C., 2007.
4. E.N. Lightfoot, J.S. Moscariello, Bioseparations, Biotechnol. Bioeng., 87 (2004) 259.
5. T.M. Przybycien, N.S. Pujar, L.M. Steele, Alternative bioseparation operations: life beyond packed-bed chromatography, Curr. Opin. Biotechnol., 15 (2004) 469.
6. A.A. Shukla, M.R. Etzel, S. Gadam, Process scale bioseparations for the biopharmaceutical industry, Taylor & Francis, Boca Raton, Florida, 2007.
7. P.A. Belter, E.L. Cussler, W.-S. Hu, Bioseparations: downstream processing for biotechnology, John Wiley & Sons, New York, 1988.
8. S. Ahuja, Handbook of bioseparations, Academic Press, San Diego, CA, 2000.
9. M.R. Ladisch, Bioseparations engineering: principles, practice, and economics, John Wiley & Sons, New York, 2001.

10. R. Ghosh, Principles of bioseparations engineering, World Scientific, Singapore, 2006.
11. R.V. Reis, A. Zydney, Bioprocess membrane technology, J. Membr. Sci., 297 (2007) 16.
12. L.J. Zeman and A.L. Zydney, Microfiltration and Ultrafiltration Principles and Applications, Marcel Dekker, New York, 1996.
13. M. Cheryan, Ultrafiltration and Microfiltration Handbook, Technomic, Lancaster, 1998.
14. R. Ghosh, Protein bioseparation using ultrafiltration: theory, applications and new developments, Imperial College Press, London, 2003.
15. E. Flaschel, C. Wandrey, M.R. Kula, Ultrafiltration for the separation of biocatalysts, in A. Fiechter (Ed.), Advances in biochemical engineering/biotechnology, Vol. 26, Springer Verlag, Berlin, 1983, pp. 73.
16. W.F. Blatt, Principles and practice of ultrafiltration, in P. Meares (Ed.), Membrane separation processes, Elsevier Science, Amsterdam, 1976, pp. 81.
17. Y. Wan, R. Ghosh, Z. Cui, Fractionation of proteins using ultrafiltration: developments and challenges, Dev. Chem. Eng. Mineral Process., 13 (2005) 1.
18. R.V. Reis, A. Zydney, Membrane separations in biotechnology, Curr. Opin. Biotechnol., 12 (2001) 208.
19. R.V. Reis, A. Zydney, Protein ultrafiltration, in M.C. Flickinger, S.W. Drew (Ed.), Encyclopedia of bioprocess technology: fermentation, biocatalysis and bioseparation, John Wiley & Sons, New York, 1999, pp. 2197.

20. R. Schnabel, P. Langer, S. Breitenbach, Separation of protein mixtures by Bioran porous glass membranes, J. Membr. Sci., 36 (1988) 55.

21. M.D. Goncalves, F. Galenbeck, Serum protein fractionation by membrane processes – centrifugal ultrafiltration, osmosedimentation and multistage ultrafiltration, Sep. Sci. Technol., 24 (1989) 303.

22. R. Audionos, J.L. Branger, Ultrafiltration concentration of enzyme hydrolysates, J. Membr. Sci., 68 (1992) 195.

23. W.D. Deeslie, M. Cheryan, Fractionation of soy protein hydrolysates using ultrafiltration membranes, J. Membr. Sci., 57 (1992) 411.

24. O. Lebere, G. Daufin, Fouling and selectivity of membranes during separation of beta-casein, J. Membr. Sci., 88 (1994) 263.

25. S. Saksena, A.L. Zydney, Effect of solution pH and ionic strength on the separation of albumin from immunoglobulins (IgG) by selective filtration, Biotechnol. Bioeng., 43 (1994) 960.

26. Q.Y. Li, Z.F. Cui, D.S. Pepper, Fractionation of HSA/IgG by gas sparged ultrafiltration, J. Membr. Sci., 136 (1997) 181.

27. Q.Y. Li, R. Ghosh, S.R. Bellara, Z.F. Cui, D.S. Pepper, Enhancement of ultrafiltration by gas sparging with flat sheet membrane modules, Sep. Purif. Technol., 14 (1998) 79.

28. M. Balakrishnan, G.P. Agarwal, Protein filtration in a vortex flow filter. II: separation of simulated mixtures, J. Membr. Sci., 112 (1996) 75.

29. S. Nakatsuka, A.S. Michaels, Transport and separation of proteins by ultrafiltration through sorptive and non-sorptive membranes, J. Membr. Sci., 69 (1992) 189.

30. M. Nystrom, P. Aimar, S. Luque, M. Kulovaara, S. Metsamuuronen, Fractionation of model proteins using their physicochemical properties, Colloids Surf., A, 138 (1998) 185.

31. R. Ghosh, Fractionation of biological macromolecules using carrier phase ultrafiltration, Biotechnol. Bioeng. 74 (2001) 1.

32. L. Zhang, H.G. Spencer, Selective separation of proteins by microfiltration with formed in-place membranes, Desalination, 90 (1993) 137.

33. K.C. Ingam, T.F. Busby, Y. Sahlestrom, F. Castino, Separation of macromolecules by ultrafiltration: influence of protein adsorption, protein-protein interactions and concentration polarization, in A.R. Cooper (Ed.), Polymer science and technology: ultrafiltration membranes and applications, Vol. 13, Plenum Press, New York, 1980, pp. 141.

34. E. Iritani, Y. Mukai, T. Murase, Upward dead-end ulftrafiltration of binary protein mixtures, Sep. Sci. Technol., 30 (1995) 369.

35. L. Millesime, J. Dulieu, B. Chaufer, Fractionation of proteins with modified membranes, Bioseparation, 6 (1996) 135.

36. R.G. Nel, S.F. Oppennheim, V.G.J. Rodgers, Effect of solution properties on solute permeate flux in bovine serum albumin - IgG ultrafiltration, Biotechnol. Prog. 19 (1994) 960.

37. S. Nakao, H. Osada, H. Kurata, S. Kimura, Separation of proteins by charged ultrafiltration membranes, Desalination, 70 (1988) 191.

38. R. Ghosh, S.S. Silva, Z.F. Cui, Lysozyme separation by hollow fiber ultrafiltration, Biochem. Eng. J., 6 (2000) 19.

39. R.H.C.M. van Eijndhoven, S. Saksena, A.L. Zydney, Protein fractionation using electrostatic interactions in membrane filtration, Biotechnol. Bioeng., 48 (1995) 406.

40. R. Shukla, M. Balakrishnan, G.P. Agarwal, Bovine serum albumin-hemoglobin fractionation: significance of ultrafiltration system and feed solution characteristics, Bioseparation, 9 (2000)7.

41. F. Sannier, C. Lecoeur, Q. Zhao, I. Garreau, J.M. Piot, Separation of hemoglobin and myoglobin from yellowfin tuna red muscle by ultrafiltration: effect of pH and ionic strength, Biotechnol. Bioeng., 52 (1996) 501.

42. R. Ghosh, Z.F. Cui, Protein purification by ultrafiltration with pre-treated membrane, J. Membr. Sci., 167 (2000) 47.

43. R. Ghosh, Z.F. Cui, Purification of lysozyme using ultrafiltration, Biotechnol. Bioeng., 68 (2000) 191.

44. R.K. Mehra, W.J. Donnelly, Fractionation of whey-protein components through a large pore-size, hydrophilic, cellulosic membrane, J. Dairy Res., 60 (1993) 89.

45. N. Ehsani, S. Parkkinen, M. Nystrom, Fractionation of natural and model egg white protein solutions with modified and unmodified polysulfone UF membranes, J. Membr. Sci., 13 (1997) 105.

46. N.N. Sudareva, O.I. Kurenbin, B.G. Belenkii, Increase in the efficiency of membrane fractionation, J. Membr. Sci., 68 (1992) 263.

47. N. Ehsani, M. Nystrom, H. Ojamo, M. Siikaaho, Separation of enzymes produced by Trichoderma reesei with hydrophobic ultrafiltration membranes, Process Biochem., 31 (1996) 253.

48. R. Ghosh, Z.F. Cui, Fractionation of BSA and lysozyme using ultrafiltration: effect of pH and membrane pretreatment, J. Membr. Sci., 139 (1998) 17.

49. A. Higuchi, S. Mishima, T. Nakagawa, Separation of proteins by surface modified polysulfone membranes, J. Membr. Sci. 57 (1991) 175.

50. R. Ghosh, Q.Y. Li, Z.F. Cui, Fractionation of BSA and lysozyme using ultrafiltration: Effect of gas sparging. AIChE J. 44 (1998) 61.

51. C.S. Slater, T.G. Jr Huggins, C.A. III Brooks, H.C. Hollein, Purification of alkaline phosphatase in ultrafiltration in a stirred cell batch cell, Sep. Sci. Technol., 21 (1986) 575.

52. H.C. Chen, R.R. Zall, Concentration and fractionation of clam viscera proteinases by ultrafiltration, Process. Biochem., 20 (1985), 46.

53. C. Charcosset. M.Y. Jaffrin, L.-H. Ding, Effect of permeate to feed ratio on protein recovery in membrane plasma fractionation, J. Membr. Sci., 60 (1991) 87.

54. R. Ghosh, Y.H. Wan, Z.F. Cui, G. Hale, Parameter scanning ultrafiltration: rapid optimization of protein separation, Biotechnol. Bioeng., 81 (2003) 673.

55. R. Ghosh, Z.F. Cui, Analysis of protein transport and polarization through membranes using pulsed sample injection technique. J. Membr. Sci. 175 (2000) 75.

56. Y.H. Wan, R. Ghosh, Z.F. Cui, High-resolution plasma protein fractionation using ultrafiltration, Desalination, 144 (2002) 301.

57. R.V. Reis, S. Gadam, L.N. Frautschy, S. Orlando, E.M. Goodrich, S. Saksena, R. Kuriyel, C.M. Simpson, S. Pearl, A.L. Zydney, High performance tangential flow filtration, Biotechnol. Bioeng., 56 (1997) 71.

58. A.D. Marshall, P.A. Munro and G. Tragardh, The effect of protein fouling in microfiltration and ultrafiltration on permeate flux, protein retention and selectivity: A literature review, Desalination 91 (1993) 65.

59. W.R. Bowen, Q. Gan, Properties of microfiltration membranes: Flux loss during constant pressure permeation of bovine serum albumin, Biotechnol. Bioeng. 38 (1991) 688.

60. R.F. Boyd and A.L. Zydney, Analysis of protein fouling during ultrafiltration using a two-layer membrane model, Biotechnol. Bioeng., 59 (1998) 451.

61. M. Meireles, P. Aimar, V. Sanchez, Albumin denaturation during ultrafiltration: effects of operating conditions and consequences on membrane fouling, Biotechnol. Bioeng., 38 (1991) 528.

62. E. Iritani, Y. Mukai, T. Murase, Properties of filter cake in dead-end ultrafiltration of binary protein mixtures with retentive membranes, Chem. Eng. Res. Des., 73 (1995) 551.

63. V. Chen, Performance of partially permeable microfiltration membranes under low fouling conditions, J. Membr. Sci., 147 (1998) 265.

64. K.J. Kim, V. Chen, A.G. Fane, Some factors determining protein aggregation during ultrafiltration, Biotechnol. Bioeng., 42 (1993) 260.

65. I.H. Huisman, P. Pradanos, A. Hernandez, The effect of protein-protein and protein-membrane interactions on membrane fouling in ultrafiltration, J. Membr. Sci., 179 (2000) 79.

66. K.J. Kim, A.G. Fane, C.J.D. Fell, D.C. Joy, Fouling mechanisms of membranes during protein ultrafiltration, J. Membr. Sci., 68 (1992) 79.

67. P. Bacchin, P. Aimar, V. Sanchez, Model for colloidal fouling of membranes, AIChE J., 41 (1995) 368.

68. P. Harmant, P. Aimar, Coagulation of colloids retained by porous wall, AIChE J., 42 (1996) 3523.

69. S.F. Oppenheim, C.B. Phillips, V.G. Rodgers, Analysis of initial protein surface coverage on fouled ultrafiltration membranes, J. Colloid Interface Sci., 184 (1996) 639.

70. M.K. Ko, J.J. Pellegrino, R. Nassimbene, P. Marko, Characterization of the adsorption-fouling layer using globular proteins on ultrafiltration membranes, J. Membr. Sci., 76 (1993) 101.

71. S.T. Kelly, W.S. Opong, A.L. Zydney, The influence of protein aggregates on the fouling of microfiltration membranes during stirred cell filtration, J. Membr. Sci. 80 (1993) 175.

72. M.K. Ko, J.J. Pellegrino, Determination of osmotic pressure and fouling resistances and their effects on performance of ultrafiltration membranes, J. Membr. Sci., 74 (1992) 141.

73. V. Gekas, P. Aimar, J.P. Lafaille and V. Sanchez, A simulation study of the adsorption - concentration polarization interplay in protein ultrafiltration, Chem. Eng. Sci., 48 (1993) 2753.

74. F.R. Bevia, V.G. Yagues, J.F. Sempere, M.J.F. Torres, An improved model with time-dependent adsorption for simulating protein ultrafiltration, Chem. Eng. Sci., 52 (1997) 2343.

75. E.M. Tracey, R.H. Davis, Protein fouling of track-etched polycarbonate microfiltration membranes, J Colloid Interface Sci. 167 (1994) 104.

76. C.C. Ho, A.L. Zydney, A combined pore blockage and cake filtration model for protein fouling during microfiltration, J. Colloid Interface Sci. 232 (2000) 389.

77. M. Hlavacek, F. Bouchet, Constant flowrate blocking laws and an example of their application to dead-end microfiltration of protein solutions, J. Membr. Sci. 82 (1993) 285.

78. W.R. Bowen, J.I. Calvo, A. Hernandez, Steps of membrane blocking in flux decline during protein microfiltration, J. Membr. Sci. 101 (1995) 153.

79. C.C. Ho, A.L. Zydney, Transmembrane pressure profiles during constant flux microfiltration of bovine serum albumin, J. Membr. Sci. 209 (2002) 363.

80. S.T. Kelly, A.L. Zydney, Mechanisms for BSA fouling during microfiltration, J. Membr. Sci. 107 (1995) 115.

81. S. Kosvintsev, R.G. Holdich, I.W. Cumming, V.M. Starov, Modelling of dead-end microfiltration with pore blocking and cake formation, J. Membr. Sci. 208 (2002) 181.

82. E. Iritani, Y. Mukai, Y. Tanaka, T. Murase, Flux decline behavior in dead-end microfiltration of protein solutions, J. Membr. Sci. 103 (1995) 181.

83. J.S. Shiau, C.H. Tang, T.Y. Lin, D.M. Wang, A model for resistance growth during protein microfiltration, Sep. Sci. Technol. 38 (2003) 917.

84. G. Bolton, D. LaCasse, R. Kuriyel, Combined models of membrane fouling: Development and application to microfiltration and ultrafiltration of biological fluids, J. Membr. Sci. 277 (2006) 75.

85. C.D. Orsello, W. Li, C.C. Ho, A three mechanism model to describe fouling of microfiltration membranes, J. Membr. Sci. 280 (2006) 856.

86. K. Kalghatgi, Cs. Horvath, Rapid analysis of proteins and peptides by reversed-phase chromatography, J. Chromatogr., A 398 (1987) 335.

87. T. Hashimoto, Non-porous hydrophilic resin-based packings for the separation of biopolymers, J. Chromatogr., A 544 (1991) 257.

88. S. Brandt, R.A. Goffe, S.B. Kessler, J.L. O'Connor, S.E. Zale, Membrane-based affinity technology for commercial scale purifications, BioTechnology 6 (1988) 779.

89. T.N. Warner, S. Nochumson, Re-thinking the economics of chromatography – new technologies and hidden costs, Biopharm Int. 16 (2003) 58.

90. D. Roper, E. Lightfoot, Separation of biomolecules using adsorptive membrane, J. Chromatogr., 702 (1995) 3.

91. R. Ghosh, Protein separation using membrane chromatography: opportunities and challenges, J. Chromatogr. A 952 (2002) 13.

92. C. Charcosset, Purification of proteins by membrane chromatography, J. Chem. Technol. Biotechnol., 71 (1998) 95.

93. X. Zeng, E. Ruckenstein, Membrane chromatography: Preparation and applications to protein separation, Biotechnol. Prog., 15 (1999) 1003.

94. J. Thommes, M.R. Kula, Membrane chromatography-An integrative concept in the downstream processing of proteins, Biotechnol. Prog., 11 (1995) 357.

95. K.H. Gebauer, J. Thommes, M.R. Kula, Plasma protein fractionation with advanced membrane adsorbents, Biotech. Bioeng., 54 (1997) 181.

96. R.R. Deshmukh, T.N. Warner, F. Hutchison, M. Murphy, W.E. Leitch, D.L. Patricia, G.S. Srivatsa, D.L. Cole, Y.S. Sanghvi, Large-scale purification of antisense oligonucleotides by high-performance membrane adsorber chromatography, J. Chromatogr., A 890 (2000) 179.

97. H.L. Knudsen, R.L. Fahrner, Y. Xu, L.A. Norling, G.S. Blank, Membrane ion-exchange chromatography for process-scale antibody purification, J. Chromatogr., A 907 (2001) 145.

98. A. Karger, B. Bettin, H. Granzow, T.C. Mettenleiter, Simple and rapid purification of alphaherpesviruses by chromatography on a cation exchange membrane, J. Virological Methods, 70 (1998) 219.

99. C. Boi, Membrane adsorbers as purification tools for monoclonal antibody purification, J. Chromatogr., B 848 (2007) 19.

Chapter 2

Research Objectives and Thesis Outline

2.1 Background

Bioseparation is a difficult and critical step in the manufacturing process for protein based biopharmaceuticals. Proteins are considered labile macromolecules due to their three-dimensional structures and needed to be processed at mild operating conditions. They are generally produced at very low concentrations with many impurities having quite similar physicochemical and biological properties as target proteins and at the same time, the purity requirements are usually very high. They also need to be processed in aseptic conditions due to the fear of contamination. All these necessitate a gentle separation and purification technique with high throughput and selectivity for the product. Conventional bioseparation techniques are severely limited in the sense that they either give good separation with limited throughput or can handle large volume of feed

but with poor selectivity. This necessitates large number of steps in the downstream processing of protein based biopharmaceuticals and reduces the overall yield. Protein bioseparation accounts for the major fraction of the manufacturing cost and presents the main obstacle in the scale up. This is mainly due to the dominance of techniques such as packed bed chromatography which give high resolution but at the cost of low product throughput. For purification of products such as monoclonal antibodies and plasma proteins, there is a significant amount of interest in alternatives to packed bed chromatography.

Synthetic membrane based processes such as ultrafiltration, microfiltration and membrane chromatography are promising bioseparation techniques that are being examined in industry and academia. Being modular in nature, these techniques are easy to scale up. Membrane based processes employ mild processing conditions and avoid the extreme pH or temperature conditions. The inherent high-throughput characteristic of porous membranes results in shorter process time and hence higher recoveries and product purities due to lesser protein degradation during processing. Ultrafiltration is considered a high throughput technique having potential for use in high resolution purification processes. Ultrafiltration has largely replaced gel permeation chromatography for concentration and diafiltration type of applications. Research in the last decade has shown that the resolution power of ultrafiltration could be increased dramatically while maintaining its inherent high-throughput characteristic. The promising protein fractionation ability of ultrafiltration has potential to challenge the position of

packed bed chromatography in bioprocessing. Microfiltration has found increasingly greater use in the biopharmaceutical industry for sterilization of therapeutic proteins prior to formulation due to some apparent advantages over other competing techniques. It is widely used for the initial harvest of therapeutic proteins from mammalian, yeast and bacterial cell cultures over other competing processes such as centrifugation, and expanded bed chromatography. Despite several obvious advantages offered by both ultrafiltration and microfiltration, their commercial scale usage is challenged by membrane fouling. Membrane fouling is very complex in nature due to its dependence on a large number of parameters. Fouling results not only in the loss of productivity but also changes the separation characteristic of membrane over a period of time. It demands frequent chemical cleaning of the membrane which in turn shortens the life of a membrane. Another membrane based process, membrane chromatography is becoming quite popular in the biopharmaceutical industry due to faster separation on account of convective driven transport. Membrane chromatographic devices are now easier and cheaper to mass produce due to recent advances in membrane manufacturing technology. This eliminates the requirements for equipment cleaning and re-validation. Membrane chromatography is cheaper by factor of 2-4 compared to packed bed chromatography due to reduced mobile phase and labor cost.

2.2 Research objectives

With this background, the primary objectives of this thesis are three fold:

1. High resolution UF
2. Membrane chromatography
3. Membrane fouling

2.2.1 High resolution UF

Recently, UF has drawn considerable attention for protein fractionation application. Selectivity of UF membrane can be changed quite dramatically by exploiting the electrostatic interaction between membrane and proteins in addition to the differences in protein sizes. Protein-protein interactions, protein-membrane interactions, the extent of concentration polarization and the predominant mode of protein transport through the membrane (i.e. diffusion and convection) are all considered key factors which affect protein-protein separation by ultrafiltration. The effective size of protein molecule in the context of membrane separation can be manipulated as desired by manipulating the size of diffuse ion cloud. This can be done by carefully choosing the pH and ionic strength of the solution. Earlier work has exploited the protein-membrane electrostatic interactions with controlled concentration polarization and membrane fouling to alter the selectivity of UF. But there is very little work done to exploit protein-protein interactions (or solute-solute interactions in general) which has potential to play significant role in altering the selectivity of UF. Generally, it is believed that protein-protein interactions in UF decrease the transmission of both proteins. Within this context the fundamental objective of my thesis in this area is to explore protein-protein interactions to enhance/alter the selectivity of the UF process.

2.2.2 Membrane chromatography

Despite several clear advantages over packed bed chromatography, the use of membrane chromatography in protein bioprocessing is still restricted to certain niche applications such as processing of large volumes of liquid containing low concentration of target proteins or removal of specific impurities such as endotoxins. This is mainly due to the relatively lower binding capacities of commercial membranes. Commercial membranes are rigid in nature in the sense binding takes place only on the pore walls and external surfaces. The poor module design with inadequate inlet flow distribution and outlet flow collection further reduces the effective utilization of intrinsic binding capacities of the membranes. With this background, the primary objectives of this thesis in this area are two fold: 1) to test the performance of new type of high-capacity macroporous gel-filled ion-exchange membranes and 2) to demonstrate the suitability of these membranes for the separation of major proteins from the feed solution such as separation of human plasma proteins HSA & HIgG.

2.2.3 Membrane fouling

Membrane fouling is a major problem in realizing the full potential of membrane based separation techniques such as ultrafiltration and microfiltration. There is still a lack of agreement over both the mechanism and rate of fouling in the literature. In UF, where protein transmission is either partial or zero, concentration polarization makes membrane

fouling more complex to understand and predict. Particularly in constant pressure UF, it is extremely difficult to predict the flux decline due to interplay among the membrane fouling, concentration polarization and flux. In MF process, membrane gets fouled by proteins even though the pore size of membrane is an order of magnitude larger than the size of protein. Due to the complex nature of membrane fouling, there are no standard, industry-wide accepted protocols for measuring membrane fouling. Within this context, my fundamental objectives in this area are three fold:

1. To develop a mathematical model which is conceptually simpler, easy to use and can serve as a tool to predict the permeate flux decline in constant pressure protein ultrafiltration
2. To study membrane fouling during in-line protein microfiltration processes and
3. To develop rapid, reliable and cost-effective protein fouling assessment techniques both in the dead-end and cross-flow mode.

2.3 Thesis outline

This thesis contains in total eight chapters. Chapter 1 presents the introduction to protein bioseparation and different membrane processes namely ultrafiltration, membrane chromatography and microfiltration. Chapter 2 provides the research objectives and thesis outline. The eighth chapter concludes the significant research contributions with some recommendations for future work.

Chapter 3 was published by Journal of Membrane Science in 2004 (D.M. Kanani, R. Ghosh and CDM Filipe, J. Membr. Sci. 243 (2004) 223-228). It reports a novel approach for high-resolution protein-protein separation by ultrafiltration using a dual-facilitating agent. In this work, we have shown for the first time that the selectivity of UF can be manipulated as desired by simultaneously increasing the transmission of one protein and decreasing the transmission of another protein using a dual-facilitating agent. In this work, a reversed selectivity was reported for the UF of mixture of two model proteins myoglobin and lysozyme using BSA as a dual-facilitating agent. This dual-facilitating agent based novel approach is expected to significantly increase the flexibility of carrying out protein fractionation using UF.

Chapter 4 was also published by Journal of Membrane Science in 2007 (D.M. Kanani and R. Ghosh, J. Membr. Sci. 290 (2007) 207-215). It reports a constant flux based mathematical model for predicting permeate flux decline in constant pressure ultrafiltration. This model is conceptually simpler and easy to implement compared to other available models. It considers the interplay between permeate flux, concentration polarization and membrane fouling in constant pressure UF which is dynamic in nature. This model is expected to serve as a useful predictive tool to decide the start-up conditions in ultrafiltration process which are very critical in pressure driven membrane processes.

Chapter 5 is based on the work on membrane chromatography. It includes the characterization of two novel high-capacity macroporous gel-filled membranes for ion-exchange chromatography of proteins. In this work, effects of different parameters such as pH, buffer ions, salt concentration, feed protein concentration and superficial velocity on HSA binding on both the membranes were studied. One of the membranes (having much higher protein binding capacity than that of the commercial membranes) was subsequently used to separate the simulated feed solution consisting of HSA and HIgG to demonstrate its suitability for the plasma protein fractionation. Part of this work was published by Biochemical Engineering Journal in 2007 (D.M. Kanani, E. Komkova, T. Wong, A. Mika, R.F. Childs and R. Ghosh, Biochem. Eng. J., 35 (2007) 295-300). Remaining work was presented in two parts at two separate conferences: AIChE 2004 at Austin, USA and Seventh CSChE Ontario-Quebec Biotechnology meeting at Kingston, Canada.

Chapter 6 is based on the work on membrane fouling during in-line protein microfiltration processes. Part of this work is submitted to Journal of Membrane Science for publication. This study looks at increase in filtration resistance during in-line protein microfiltration and the mechanism of protein fouling of MF membranes. It assesses the severity of fouling in terms of apparent reversible fouling and irreversible fouling during the course of filtration. It also looks at the effects of front washing and intermittent protein filtration on membrane performance.

Chapter 7 is based on the report submitted to 3M Canada. It describes three fouling assessment techniques for microfiltration membranes and their applications in comparing the fouling propensity of different surface treated microfiltration membranes developed at McMaster University with commercial membranes. The first technique is based on accelerated fouling and rapidly gives information about the membrane permeability, propensity of fouling and loss of membrane permeability due to both reversible and irreversible fouling. Apart from being robust, reproducible and cost-effective, it is quite rapid and simple. The second and third techniques are based on critical flux concept.

Chapter 3

A Novel Approach for High-Resolution Protein-Protein Separation by Ultrafiltration Using a Dual-Facilitating Agent

This chapter is organized based on a paper published in Journal of Membrane Science, 243 (2004) 223-228 by Dharmesh M. Kanani, Raja Ghosh and Carlos D.M. Filipe.

3.1 Abstract

This paper discusses a novel approach based on the use of the protein BSA as a dual-facilitating agent for manipulating the separation of two model proteins having comparable molecular weights. When a binary mixture of lysozyme and myoglobin alone was ultrafiltered lysozyme was transmitted through the membrane to a substantially

greater extent than myoglobin. However, when BSA was added to the feed solution, lysozyme was largely retained by the same membrane while the transmission of myoglobin was significantly increased leading to reversal of selectivity of separation. The decrease in lysozyme transmission was due to electrostatic BSA-lysozyme interaction, while the simultaneous increase in myoglobin transmission was due to Donnan effect. Thus, using a dual-facilitating agent the transmissions of lysozyme and myoglobin though a membrane could be manipulated as desired. This novel approach of using a dual-facilitating agent can be expected to significantly increase the flexibility of carrying out high-resolution protein-protein separation using ultrafiltration.

3.2 Introduction

High-resolution protein-protein separation using ultrafiltration is feasible only at highly optimised conditions e.g. [1 - 4]. Parameters that need to be optimised include pH, salt concentration, feed concentration, permeate flux and membrane module hydrodynamics. The transmission of a transmittable protein through an ultrafiltration membrane could be reduced due to the presence of significantly retained proteins in the feed stream [5, 6]. However, as described in this paper a retained protein could actually increase the transmission of a transmittable protein through a membrane. This paper discusses a novel approach based on the use of a dual-facilitating agent (BSA in this case) for flexible manipulation of the separation of two model proteins lysozyme and myoglobin having comparable molecular weights (i.e. 14 kDa and 17 kDa respectively).

When a binary mixture of lysozyme and myoglobin was ultrafiltered using a 30 kDa MWCO polyethersulfone membrane, lysozyme was transmitted to a substantially greater extent than myoglobin at all the operating conditions examined. However, when BSA was added to the feed solution, lysozyme was largely retained by the same membrane while the transmission of myoglobin was significantly increased. The decrease in lysozyme transmission was due to electrostatic BSA-lysozyme interaction, while the simultaneous increase in myoglobin transmission was due to Donnan effect. Thus, using BSA as dual-facilitating agent, the protein transmission profile though the membrane could be manipulated as desired. In this case, the selectivity of separation was flipped around and "reversed selectivity" thus obtained whereby the "larger" protein in the mixture to be fractionated i.e. myoglobin, was selectively transmitted through the membrane while the "smaller" protein i.e. lysozyme was retained. This approach of using a dual-facilitating agent can be expected to significantly increase the flexibility of carrying out high-resolution protein-protein separation using ultrafiltration.

In this fractionation study involving model proteins BSA was used as a dual-facilitating agent on account of its molecular size which ensured its total retention, and its charge (at the operating conditions used) which ensured the dual-facilitated effect. The objective of this study was primarily to establish "proof of concept" of dual-facilitated separation. Indeed, any other macromolecule having the appropriate molecular size and charge could have been used.

3.3 Experimental

3.3.1 Materials

Lysozyme (catalogue # L-7651), myoglobin (catalogue # M-0630) and BSA (catalogue # A-7906) were purchased from Sigma Chemical Company. Lysozyme has a molecular weight of 14 kDa and a p*I* of 11.0; myoglobin has a molecular weight of 17 kDa and a p*I* of 7.0; BSA has a molecular weight of 67 kDa and a p*I* of 4.9. Polyethersulfone ultrafiltration membranes (Omega, 30 kDa MWCO) were donated by Pall Corporation. PVDF microfiltration membranes (syringe type, 0.2 micron pore diameter) used for membrane chromatographic analysis were purchased from Whatman. The carrier phase (or buffer) used in the ultrafiltration experiments was 20 mM Tris, pH 9.0. All solutions were prepared using 18.2 MΩ-cm water obtained from a Simplicity^{TM} (Millipore) ultrapure water purification unit.

3.3.2 Membrane filtration unit

A stirred cell ultrafiltration module (having a working volume of 20 ml) was used in the experiments. The module could be fitted with membrane discs, which were cut out from flat sheets. The effective diameter of the membrane within the module was 24 mm. The impeller diameter was 20 mm and this impeller was driven by a magnetic stirrer (VWR). The same stirring speed (~ 400 rpm) was used in all the experiments. This gave a modified Reynolds number ($\varpi r^2/\nu$) of ~700 at the ambient conditions.

3.3.3 Experimental set-up and methodology

The separation of lysozyme and myoglobin was investigated using pulsed sample injection ultrafiltration [7]. This technique allows rapid determination of protein sieving coefficient and selectivity data and can be carried out using very small amounts of test substances. A stirred cell ultrafiltration unit was integrated with an AKTAPrime chromatographic system (Amersham Biosciences). The configuration was similar to that discussed by Ghosh and Cui [7]. The positive displacement pump of the AKTAPrime system ensured constant permeate flux through the membrane. The proteins to be separated i.e. myoglobin and lysozyme were injected into the membrane module in the pulse mode and protein-protein separation was assessed by analysing permeate and retentate sample sets collected at around the same time. The protein mixture injected had 5 kg/m^3 each of lysozyme and myoglobin. In experiments involving BSA as dual-facilitating agent, solutions of this protein (concentration = 20 kg/m^3) were also injected into the membrane module in the pulse mode. Different sized sample loops were used for injecting protein solutions into the module. All experiments were carried out in duplicate and averaged values of results were reported. The results were found to be reproducible.

3.3.4 Analysis of protein mixtures using membrane chromatography

The protein compositions in the retentate and permeate samples obtained were analysed by cation-exchange membrane chromatography using 0.2 micron PVDF membranes. This method is based on the lysozyme separation technique reported by

Ghosh [8] using the same membrane. The mobile phase used for these experiments was 20 mM Tris, pH 8.0 and the flow rate used was 3 ml/min. At the test conditions this media specifically bound lysozyme while allowing myoglobin to pass through. The bound lysozyme was eluted using high salt concentration (i.e. 1 M NaCl). A 100 µl sample loop was used for injecting protein samples. The effluent stream was monitored at 280 nm and calibration curves (i.e. area under the curve versus concentration) were used to determine the protein composition of the samples.

3.3.5 Test for detection of BSA in permeate samples

The ultrafiltration membrane used in the experiments i.e. 30 kDa MWCO polyethersulfone would normally be expected to totally retain BSA. In order to verify this pulsed injection ultrafiltration experiments with BSA alone were carried out at different permeate fluxes at which lysozyme-myoglobin separation was examined. The lack of UV absorbance of the permeate streams indicated absence of BSA. Random permeate samples collected from the facilitated lysozyme-myoglobin separation experiments were analysed for presence of BSA using size exclusion chromatography. A 60 cm long K 9/60 column (Amersham Biosciences) packed with Sephacryl S-200 (Amersham Biosciences) was used for this analysis. The mobile phase (50 mM NaCl) flow rate used for these experiments was 0.8 ml/min and a 100 µl loop was used for sample injection. No BSA could be detected in these samples.

3.4 Results and discussion

3.4.1 Ultrafiltration of lysozyme and myoglobin

Figure 3.1 shows the effect of permeate flux on the apparent sieving coefficients of lysozyme and myoglobin. The apparent sieving coefficient (S_a) is defined as:

$$S_a = \left(C_p / C_b \right) \tag{3.1}$$

The figure also shows the selectivity at the different permeate flux values examined. Selectivity (ψ) is defined as:

$$\psi = \left(\frac{S_{a\ Lysozyme}}{S_{a\ Myoglobin}} \right) \tag{3.2}$$

The apparent sieving coefficient of lysozyme decreased as the permeate flux was increased whereas the apparent sieving coefficient of myoglobin increased. The net result of this was a decrease in selectivity with increase in permeate flux. The apparent sieving coefficient of lysozyme was significantly higher than that of myoglobin at all the permeate flux values examined. These experimental results can be explained based on theory discussed by earlier workers [1-4]. Figure 3.2 shows chromatograms obtained with permeate samples collected at two different permeate flux values (see chromatograms A and C). The decrease in selectivity with increase in permeate flux is clearly evident from these.

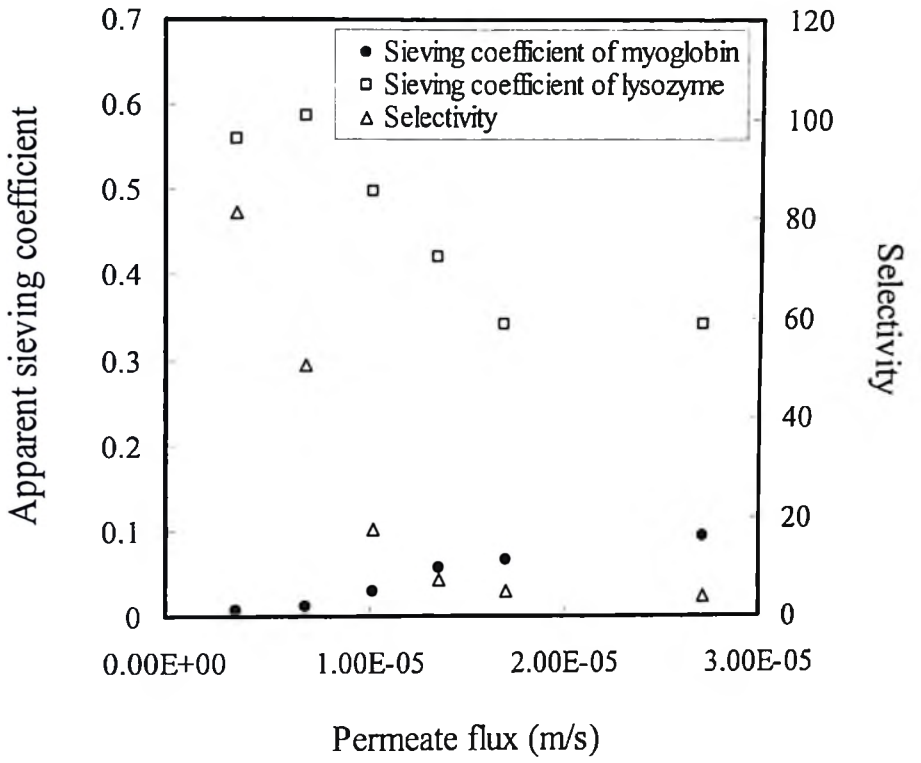

Figure 3.1 Effect of permeate flux on the separation of lysozyme and myoglobin using 30 kDa MWCO PES membrane

3.4.2 Dual-facilitated separation of lysozyme and myoglobin using BSA

Table 3.1 shows the results obtained from the dual-facilitated lysozyme-myoglobin separation experiments carried out using various BSA concentrations. BSA was selected as a dual facilitating agent since it had the desirable physicochemical

properties, i.e. molecular weight of 67 kDa which ensured its total retention by the 30 kDa MWCO membrane and a p*I* of 4.9 which made it negatively charged at the operating pH (i.e. 9.0). These experiments were carried out at two different permeate flux values (i.e. 3.394×10^{-6} m/s and. 1.697×10^{-5} m/s). The lysozyme to myoglobin mass ratio in the pulsed feed was kept fixed at 1:1 in all the experiments. In a pulsed ultrafiltration experiment, the concentration of any transmitted protein within the stirred cell would decrease with time, the rate of decrease depending on the magnitude of transmission. Table 3.1 lists the initial effective concentrations of the various proteins in the feed, these being determined by dividing the amount of each protein injected by the volume of the stirred cell. In these experiments the lysozyme-myoglobin mixture was first pulsed followed immediately by the BSA pulse. Figure 3.2 shows chromatograms obtained with permeate samples collected at two different permeate flux values (see chromatograms B and D). The reversal of selectivity, i.e. higher transmission of myoglobin in comparison to lysozyme is clearly evident from these. By comparing chromatogram A with chromatogram B it can be seen that the protein composition of the permeate could be almost totally reversed by use of BSA as dual-facilitating agent.

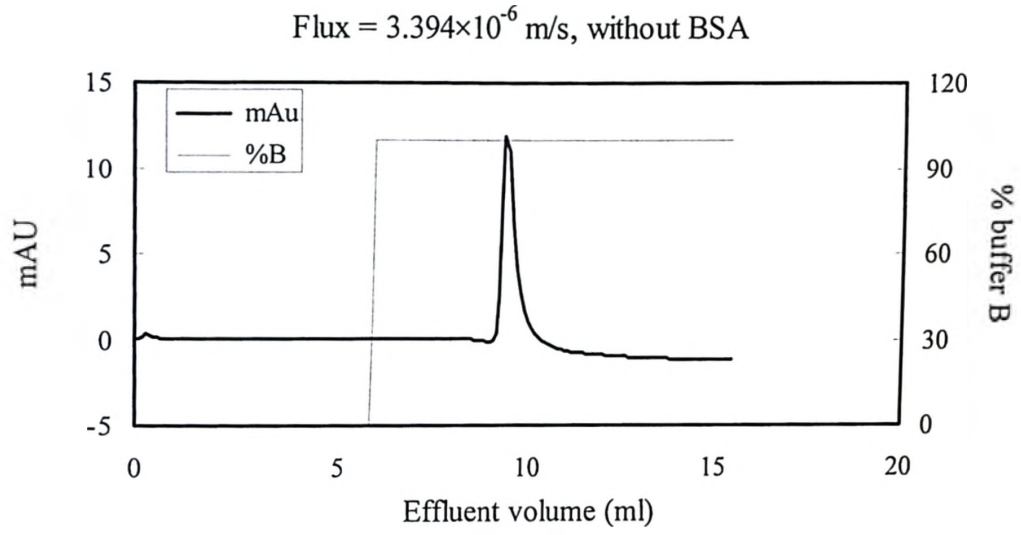
Flux = 3.394×10-6 m/s, without BSA
mAu
%B
mAU
% buffer B
Effluent volume (ml)
15
10
5
0
-5
120
90
60
30
0
0
5
10
15
20

(A)

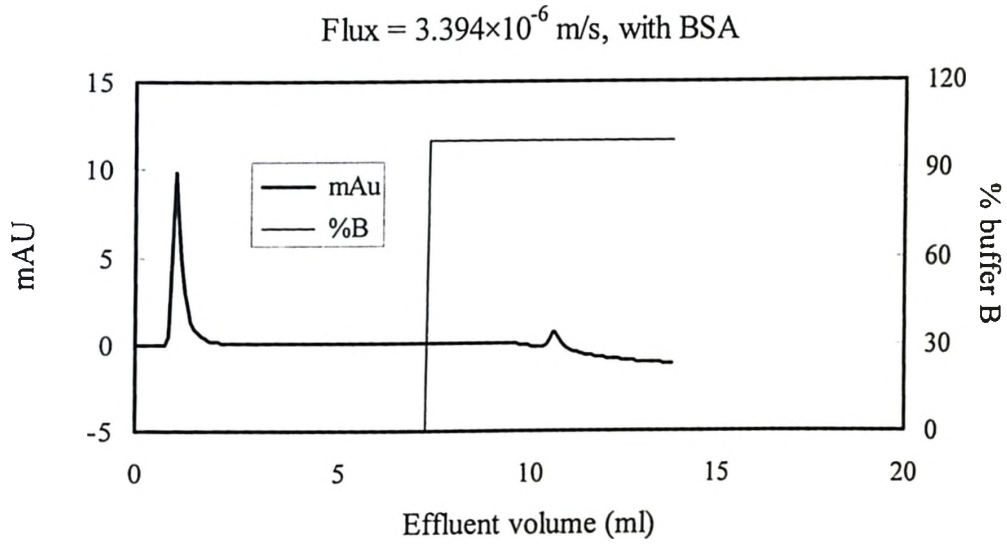
Flux = 3.394×10-6 m/s, with BSA
mAu
%B
mAU
% buffer B
Effluent volume (ml)
15
10
5
0
-5
120
90
60
30
0
0
5
10
15
20

(B)

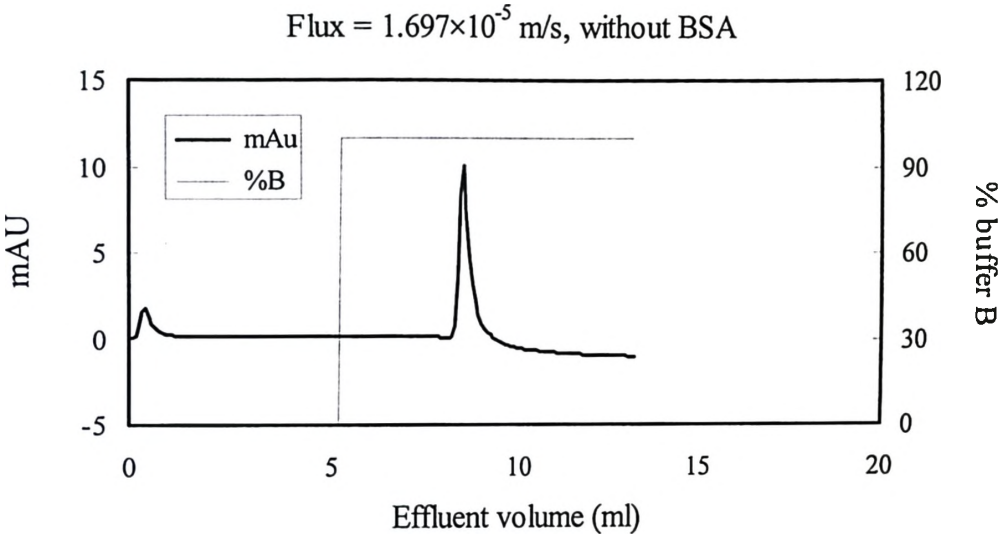

(C)

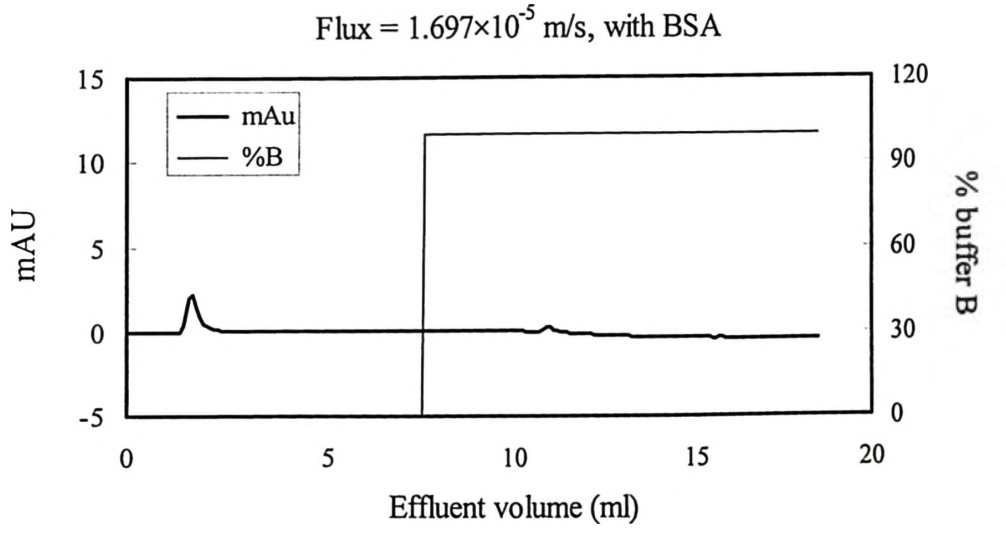

(D)

Figure 3.2 Chromatograms of permeate samples obtained by ultrafiltration with and without BSA at two different permeate fluxes. 1st peak = myoglobin; 2nd peak = lysozyme

Table 3.1 also lists the apparent sieving coefficients of myoglobin and lysozyme obtained. These values were obtained by dividing the protein concentrations in the permeate samples collected early on in each experiment by their corresponding initial effective feed concentrations. There is a degree of approximation involved in this calculation due to slight off-set between the feed and permeate. However, given the rate at which material permeate an ultrafiltration membrane coupled with the fact that these permeate samples were collected within the first few minutes of operation, it is unlikely that the feed concentration would have changed significantly. In all the lysozyme-myoglobin separation experiments carried out using BSA as dual-facilitating agent, the transmission of myoglobin was significantly higher than that of lysozyme.

Table 3.1 Facilitated separation of myoglobin and lysozyme using BSA: effect of BSA concentration in the feed at two different permeate flux values

Permeate flux (m/s)	Initial effective feed concentration (kg/m^3)			Apparent sieving coefficient	
	Lysozyme	Myoglobin	BSA	Lysozyme	Myoglobin
3.394×10^{-6}	0.125	0.125	0.500	0.02	0.13
3.394×10^{-6}	0.125	0.125	1.000	0.03	0.29
3.394×10^{-6}	0.125	0.125	2.000	0.02	0.31
3.394×10^{-6}	0.500	0.500	0.500	0.03	0.06
1.697×10^{-5}	0.125	0.125	0.500	0.01	0.05
1.697×10^{-5}	0.125	0.125	1.000	0.01	0.10
1.697×10^{-5}	0.125	0.125	2.000	0.01	0.16

From data shown in Figure 3.1 and Table 3.1, it is evident that presence of BSA caused a significant drop in lysozyme transmission. At the operating pH (i.e. 9.0) BSA would be negatively charged while lysozyme would be positively charged. Hence, these proteins would interact by electrostatic attraction. The decrease in lysozyme transmission due to presence of BSA in the feed has been reported by Ingham et al. [5].

Comparison of data shown in Figure 3.1 and Table 3.1 also shows that the presence of BSA had a significant effect on the myoglobin transmission. The role of BSA in increasing myoglobin transmission can be explained in terms of Donnan effect. Donnan effect has been used by earlier workers to explain negative rejection of salts by polyelectrolytes [9] and proteins [10]. However, there are no reports on such effects of one protein on another or indeed on the use of this effect for selective protein-protein separation. At the operating pH (i.e. 9.0) both myoglobin and BSA were negatively charged. Among the two, BSA was quantitatively retained by the membrane while myoglobin was potentially transmittable. The presence of the retained negatively charged BSA within the module resulted in the negatively charged myoglobin molecules being pushed through the membrane in order to restore the charge balance. The magnitude of enhancement in myoglobin transmission was found to depend on the amount of BSA present within the membrane module: the greater the BSA concentration the higher was the enhancement. This clearly suggests that Donnan effect was indeed the cause for increase in myoglobin transmission. Figures 3.3 and 3.4 show the effect of

(BSA/myoglobin) molar ratio in the feed on the separation of myoglobin and lysozyme. The reversed selectivity (ψ^{-1}) is defined as:

$$\psi^{-1} = \left(\frac{S_{a\ Myoglobin}}{S_{a\ Lysozyme}} \right) \tag{3.3}$$

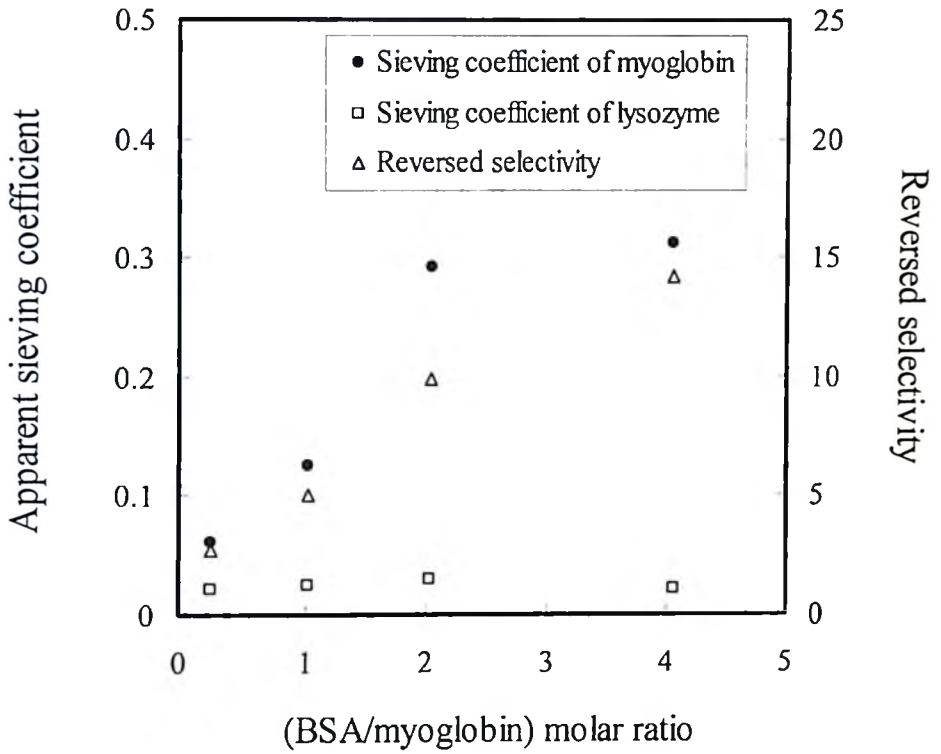

Figure 3.3 Effect of (BSA/myoglobin) molar ratio on the separation of lysozyme and myoglobin using 30 kDa MWCO PES membrane. Permeate flux = 3.394×10^{-6} m/s

The reversed selectivity increased as the (BSA/myoglobin) molar ratio was increased. This was due to the increase in myoglobin transmission since the lysozyme transmission

remained largely constant and low. Table 3.1 shows that the enhancement in myoglobin transmission by BSA was greater at the lower permeate flux value. This also indicates the role of the Donnan effect in increasing myoglobin transmission. The Donnan effect is likely to be more significant at lower permeate flux values, i.e. when convective transport of protein is lower. At higher fluxes, the convective protein transport would dominate over the Donnan effect and hence relatively lower enhancement in myoglobin transmission would be expected.

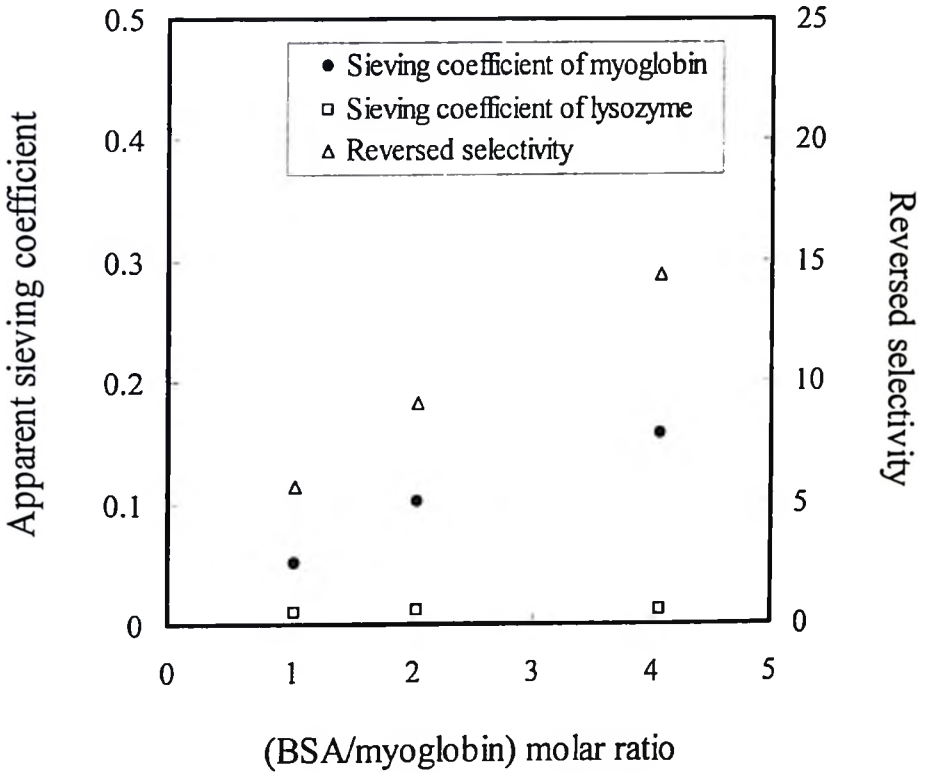

Figure 3.4 Effect of (BSA/myoglobin) molar ratio on the separation of lysozyme and myoglobin using 30 kDa MWCO PES membrane. Permeate flux = 1.697×10^{-5} m/s

In the experiments discussed in this paper BSA was used for the dual-facilitated separation of model proteins since it had the desirable physicochemical properties. However, in the case of a real bioseparation, BSA might not be the most appropriate dual-facilitated separating agent. Other appropriately sized and charged macromolecules such as charged dextrans could be used in such cases. Another thing to be noted is that the reversed selectivity demonstrated in this paper is not the only manner in which selectivity of separation could have been altered. Indeed, using a quantitatively retained positively charged dual-facilitating agent in the same model protein separation the normal selectivity could possibly have been increased, i.e. by increase in lysozyme transmission via Donnan effect and simultaneous decrease in myoglobin transmission by electrostatic myoglobin-dual-facilitating agent interaction.

3.5 Conclusions

The experimental results discussed in this paper clearly show that BSA could indeed be used as a dual-facilitating agent for manipulating the separation of lysozyme and myoglobin by ultrafiltration. In the absence of BSA, lysozyme was transmitted to a significantly greater extent than myoglobin. However, the presence of BSA in the feed totally changed the protein profile in the permeate, i.e. myoglobin was transmitted to a significantly greater extent than lysozyme. The decrease in lysozyme transmission resulted from electrostatic interaction between lysozyme and BSA while the increase in myoglobin transmission was driven by Donnan effect. The effect of BSA concentration

on myoglobin transmission suggests the role of Donnan effect. The fact that the increase in myoglobin transmission was greater at lower permeate fluxes further establishes this point. This approach of using a dual-facilitating agent can be expected to significantly increase the flexibility of carrying out high-resolution protein-protein separation using ultrafiltration.

3.6 References

1. A. Higuchi, S. Mishima, T. Nakagawa, Separation of proteins by surface modified polysulfone membranes, J. Membr. Sci., 57 (1991) 175.
2. S. Saksena, A.L. Zydney, Effect of solution pH and ionic strength on the separation of albumin and immunoglobulin (IgG) by selective filtration, Biotechnol. Bioeng., 43 (1994) 960.
3. M. Nystrom, P. Aimar, S. Luque, M. Kulovaara, S. Metsamuuronen, Fractionation of model proteins using their physiochemical properties, Colloid. Surface. A., 138 (1998) 185.
4. R. Ghosh, Q.Y. Li, Z.F. Cui, Fractionation of BSA and lysozyme using ultrafiltration: Effect of gas sparging, AIChE J., 44 (1998) 61.
5. K.C. Ingham, T.F. Busby, Y. Sahlestrom, F. Castino, Separation of macromolecules by ultrafiltration, in A.R. Cooper (Ed.), Polymer Science and Technology: Ultrafiltration Membranes and Applications, Planum, New York, 1980, Vol. 13, pp. 141.

6. N.N. Sudareva, O.I. Kurenbin, B.G. Belenkii, Increase in efficiency of membrane fractionation, J. Membr. Sci., 68 (1992) 263.
7. R. Ghosh, Z.F. Cui, Analysis of protein transport and polarization through membranes using pulsed sample injection technique, J. Membr. Sci., 175 (2000) 75.
8. R. Ghosh, Purification of lysozyme by microporous PVDF membrane based chromatographic process, Biochem. Eng. J., 14 (2003) 109.
9. J. Gilron, N. Gara, O. Kedem, Experimental analysis of negative salt rejection in nanofiltration membranes, J. Membr. Sci., 185 (2001) 223.
10. T. Croguennec, F. Nau, G. Brule, Lysozyme effect on ion transmission through an ultrafiltration membrane, Eur. Food Res. Technol., 211 (2000) 349.

Chapter 4

A Constant Flux based Mathematical Model for Predicting Permeate Flux Decline in Constant Pressure Protein Ultrafiltration

This chapter is organized based on a paper published in Journal of Membrane Science, 290 (2007) 207-215 by Dharmesh M. Kanani and Raja Ghosh.

4.1 Abstract

This paper discusses a novel approach for predicting permeate flux decline in constant pressure ultrafiltration of protein solutions. A constant pressure process is assumed to be made up of a large number of small, sequential, constant flux ultrafiltration steps: the flux decreasing due to fouling and other related factors at the end of each step. The advantage of this approach is that constant flux ultrafiltration is easier to study,

characterize and model than constant pressure ultrafiltration. Consequently model parameters can be obtained in reliable and reproducible manner. Constant pressure ultrafiltration is dynamic in nature since both the magnitude of osmotic back-pressure and the extent of membrane fouling decrease as the permeate flux decreases with time. The proposed model takes into consideration the interplay between permeate flux, concentration polarization and membrane fouling. The model demonstrates that the initial rapid flux decline is due to a combination of concentration polarization and membrane fouling while during the remaining part of the process, the effect of concentration polarization becomes negligible. The model also shows that concentration polarization affects the initial flux decline only at higher transmembrane pressures. This model which was validated using experimental data is conceptually simpler than other available models and easy to use. In addition to its value as a predictive tool it would particularly be useful for deciding appropriate start-up conditions in ultrafiltration processes.

4.2 Introduction

Ultrafiltration is widely used for protein bioseparation. Fouling and concentration polarization have long been recognized as major problems in protein ultrafiltration [1-4]. Conventional ultrafiltration is carried out at a constant transmembrane pressure and the effects of fouling and concentration polarization are observed in the form of permeate flux decline with time. The decrease in permeate flux with time in constant pressure ultrafiltration is difficult to model due to its dynamic nature resulting from the constantly

changing convective transport of protein towards the membrane: a factor that could potentially affect the extents of both concentration polarization and membrane fouling. Most of the earlier work on modelling flux decline in ultrafiltration processes is based on the film theory. These models assume that the concentration polarization layer builds up very rapidly at the start of the process and remains more or less constant after that [5-7]. The initial rapid decline in flux is attributed to concentration polarization with negligible contributions from membrane fouling. The more gradual decline in flux (following the initial rapid decline) is attributed to membrane fouling at constant concentration polarization conditions. This approach therefore accounts for the effects of concentration polarization and membrane fouling in a simple additive way. However, most experiments suggest that the flux can only be recovered after substantial membrane cleaning, clearly suggesting the significantly greater role of membrane fouling in flux decline.

Earlier Gekas *et al.* [8] have studied the interplay between adsorption and concentration polarization in protein ultrafiltration to predict the flux decline in constant pressure mode. Their approach is based on a generalized diffusion equation for the polarized boundary layer with a source term for adsorption. Several other studies have clearly differentiated between static protein adsorption on the membrane and dynamic protein deposition during membrane fouling [9-10]. Protein adsorption is an equilibrium process in which the solute molecules get partitioned between the solution and the membrane. In adsorption, the protein molecules are in direct contact with the membrane and hence limited to a monolayer. During ultrafiltration protein molecules can also be

sequestered near the membrane by protein-protein interactions [9]. Several researchers have found significant increase in membrane associated protein due to convective deposition [11-12]. Boyd and Zydney [13] have reported the formation of more tightly packed dynamic protein layer during ultrafiltration than that formed by static adsorption. All of these would indicate that increase in membrane resistance would be much higher than due to static protein adsorption.

Several researchers have studied membrane fouling in the constant flux membrane filtration processes [14-17]. In constant flux ultrafiltration the convective flow of material towards the membrane remains constant. As a result the magnitude of concentration polarization is also likely to remain constant. In a study of membrane fouling by BSA in a constant flux mode Ghosh [17] found that the rate of membrane fouling remained constant at a given flux, this rate increasing with increase in flux. A simple mathematical model for increase in transmembrane pressure during constant flux ultrafiltration which took into consideration the contributions of concentration polarization, rapid initial fouling and long-term fouling was discussed in this paper. The model discussed in the current paper is a modified transposed form of that discussed by Ghosh [17]. In constant pressure ultrafiltration flux decreases continuously and hence it may be hypothesized that so would the osmotic pressure and rate of membrane fouling. In the proposed model, a constant pressure ultrafiltration process is assumed to be made up of a large number of small constant flux steps. A series of constant flux experiments were first carried out with human serum albumin as model foulant and 30 kDa

polyethersulfone (PES) as model retentive membrane to obtain information about osmotic pressure and fouling rates. The decrease in flux with time in human serum albumin ultrafiltration with the same membrane was then calculated by applying a transposed from of the model discussed by Ghosh [17] to each of the discrete constant flux steps comprising the constant pressure process. The proposed model and the results obtained are discussed.

4.3 Model Development

In an earlier study, the fouling of ultrafiltration membranes by BSA in the constant flux mode using a novel pulsed injection technique has been discussed [17]. The test membrane was housed in a stirred cell membrane module which provided the desired hydrodynamic conditions by a magnetically driven impeller. Buffer was pumped through the membrane module using a high performance pump and the pressure was continuously recorded. A pulse of test foulant was then introduced into the membrane module and the fouling was observed in terms of the increase in transmembrane pressure. At a certain stage in the experiment, the foulant was removed from the stirred cell and the pressure due to buffer filtration through the fouled membrane was recorded. In constant flux ultrafiltration the transmembrane pressure (TMP) increases due to concentration polarization and membrane fouling. Two distinct phases of pressure increase were identified: an initial rapid increase, followed by a more gradual linear increase (see Figure 4.1). The initial rapid non-linear increase in TMP is attributed to concentration

polarization and rapid initial membrane fouling, while the linear gradual increase in TMP is due to slow long-term membrane fouling. The increase in TMP with time was described by the model shown below which is a modified form of the osmotic pressure – resistance model:

$$\Delta P = \Delta\pi + J_v\left(R_m^0 + R_m^* + \alpha t\right) \qquad (4.1)$$

$R_m{}^0$ is a property of the membrane while $R_m{}^*$ depends on the membrane-foulant system. α and $\Delta\pi$ depend on the permeate flux, both increasing with increase in the value of J_v. All these values can be experimentally determined as indicated in Figure 4.1.

The current model attempts to describe the decrease in permeate flux in constant pressure ultrafiltration by considering such a process to be made up of a large number of small constant flux steps. The rational behind this approach is the attenuating nature of the permeate flux decline in a constant pressure process, i.e. the rate of decrease in permeate flux diminishes with the decrease in the magnitude of permeate flux. In an earlier paper [17] it was experimentally demonstrated using constant flux experiments that osmotic pressure ($\Delta\pi$) and rate constant for membrane fouling (α) were strong functions of permeate flux (J_v), both increasing with increase in flux. The general approach used in the current work is shown in Figure 4.2. A series of constant flux experiments were carried out with a particular membrane-foulant system to obtain the osmotic pressure and fouling rate constants. The decrease in permeate flux with time for

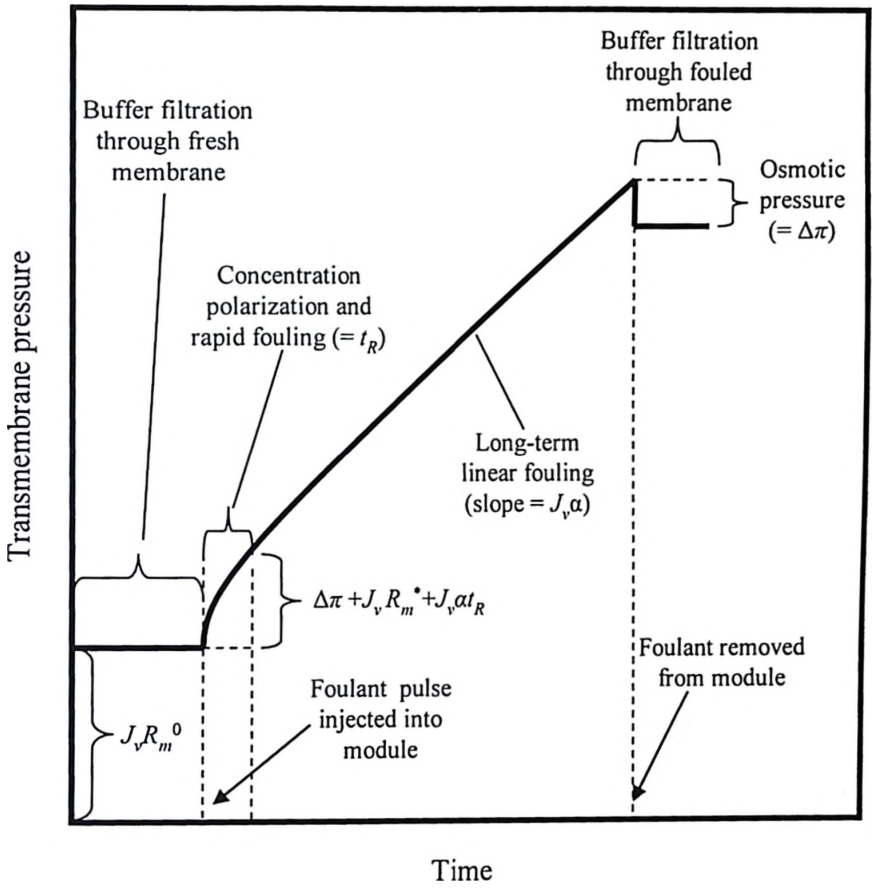

Figure 4.1 Pressure profile in constant flux ultrafiltration obtained using the pulsed sample injection technique (adapted from Ref. 17)

the same membrane-foulant system in the constant pressure mode is then predicted using the information obtained from the constant flux experiments. In the proposed model, it is assumed that the initial flux in constant pressure ultrafiltration would correspond to pure water (or buffer) flux of a fresh membrane at the operating pressure. Therefore the first constant flux step in the model corresponded to this. In all subsequent steps, the osmotic

pressure at that instant and the cumulative increase in resistance due to membrane fouling were taken into account to calculate the permeate flux. In this scheme, the interplay between the three major components, i.e. permeate flux, resistance due to membrane fouling and osmotic pressure (due to concentration polarization) were taken into account.

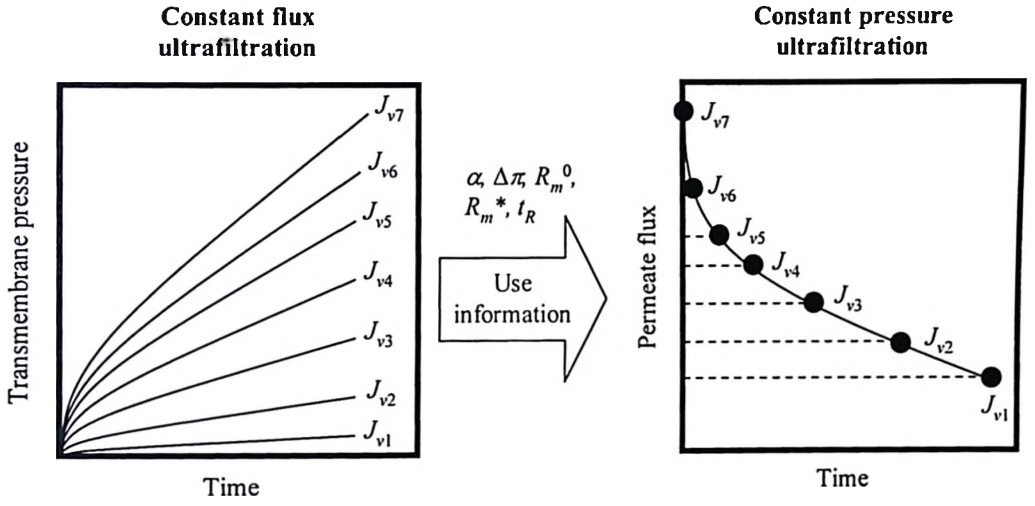

Figure 4.2 General approach for predicting flux decline in constant pressure ultrafiltration

The concentration polarization layer of the foulant takes a certain amount of time to build up. The foulant mass balance equation for the concentration polarization layer, assuming that diffusion and convection of the foulant within this layer takes place predominantly perpendicular to the membrane surface is given below [8]:

$$\frac{\partial C}{\partial t} + J_v \frac{\partial C}{\partial y} = D \frac{\partial^2 C}{\partial y^2} \qquad (4.2)$$

The diffusion coefficient is assumed to be foulant concentration independent. Equation (4.2) is an unsteady state initial value problem. The permeate flux can be expressed using the osmotic pressure model:

$$J_v = \frac{\Delta P - \Delta \pi}{R_m} \tag{4.3}$$

R_m can be expressed as the sum of R_m^0 (the resistance of the unfouled membrane) and R_f (the resistance due to fouling). R_f changes with time due to the deposition and adsorption of foulant. R_f in constant flux ultrafiltration is expressed as [17]:

$$R_f = R_m^* + \alpha t \tag{4.4}$$

Where $\alpha = \frac{m}{J_v}$

It was found that R^*_m was independent of the flux while m did depend on the permeate flux.

Figure 4.3 shows the scheme used in the current model for predicting the flux in constant pressure ultrafiltration using the data extracted from constant flux ultrafiltration. The current approach is based on transposing equation (4.1) to the form shown below which is proposed for modeling permeate flux decline in constant pressure ultrafiltration:

$$J_{v,i} = \frac{\Delta P - \Delta \pi_{i-1}}{R_{m_{i-1}} + \frac{R_m^* \Delta t}{t_R} + \frac{m_{i-1} \Delta t}{J_{v,i-1}}} \tag{4.5}$$

Here, $R_{m_{i-1}}$ is the cumulative resistance at time t_{i-1}. It is assumed that R^{*}_{m} is linearly distributed over the time period t_R which is the duration of the initial rapid fouling phase. Matthisson [18] has shown that adsorption of BSA on an ultrafiltration membrane occurs in two steps, rapidly at first and more gradually later. This is consistent with the finding discussed in [17]. m_{i-1} is the slope of linear region of TMP-time profile in constant flux ultrafiltration experiment at flux $J_{v,i-1}$. Δt is the time step of the ultrafiltration process during which the permeate flux is assumed to be constant. Equation (4.5) is used to calculate the permeate flux until $t = t_R$, after which the following equation is used:

$$J_{v,i} = \frac{\Delta P - \Delta \pi_{i-1}}{R_{m_{i-1}} + \dfrac{m_{i-1}\Delta t}{J_{v,i-1}}} \tag{4.6}$$

Equation (4.2) which has J_v as a variable can be solved numerically in conjunction with equations (4.5) and (4.6) using a tridiagonal matrix algorithm [19] with the following set of conditions:

The initial condition is

$$C(y,0) = C_b \text{ at } t = 0 \tag{4.7}$$

and the boundary conditions are

a) for $y = 0$, $C(0,t) = C_b$ (4.8)

b) for $y = \delta$, $J_v C(\delta,t) = D\dfrac{\partial C(\delta,t)}{\partial y}$ (4.9)

Equations (4.2), (4.5)-(4.9) were made dimensionless before solving by numerical methods using the same procedure used by Gekas et al [8].

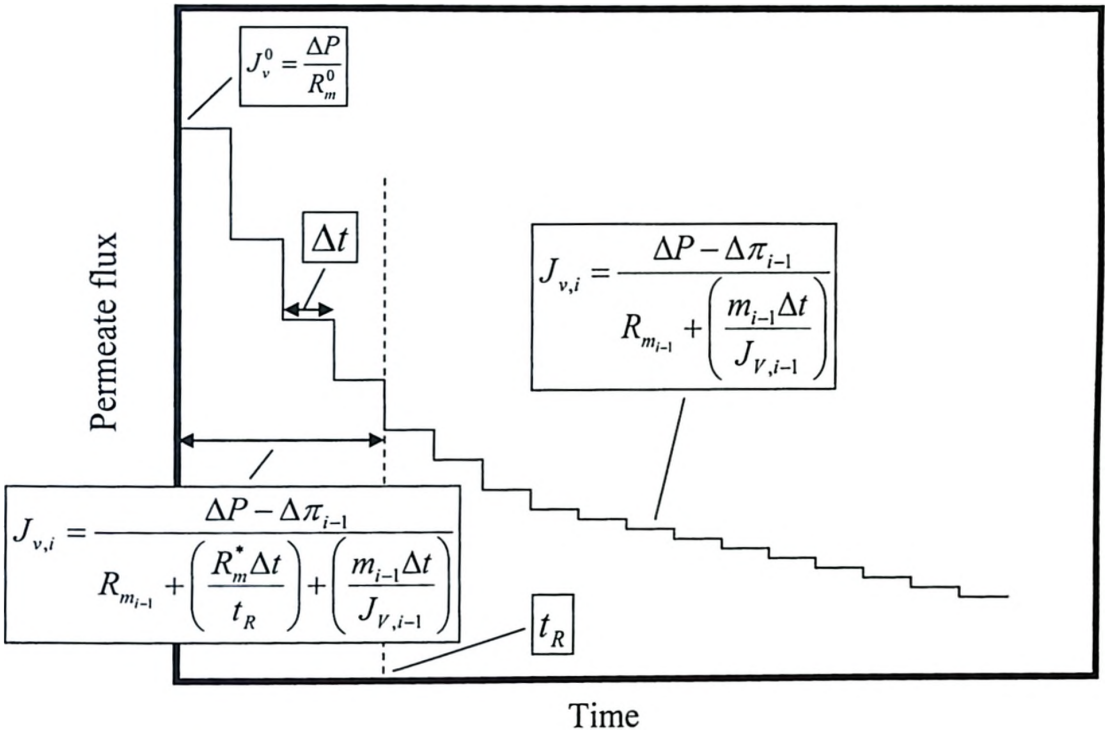

Figure 4.3 Detailed scheme for predicting permeate flux decline including working equations

4.4 Experimental

4.4.1 Materials

Purified Human Serum Albumin (HSA, 200 g/l) was kindly donated by the Scottish Blood Transfusion Services, Edinburgh, UK. HSA has a molecular weight of 69 kDa and pI of 4.9. Polyethersulfone (PES) ultrafiltration membranes (product # OM030076, 30 kDa MWCO) were purchased from Pall Corporation. Sodium phosphate buffer (50 mM, pH 4.8) was used as carrier phase in all the experiments. The buffer and all other solutions used in the experiments were prepared using the water (18.2 MΩ cm) obtained from NANOpure Diamond Life Science (UV/UF) Ultrapure water purification system (Barnstead). All solutions were microfiltered using cellulose acetate membrane (0.45 micron, Nalgene Nunc International, Product # DS0210-4045) before use.

4.4.2 Experimental Set-up and Methodology

All membrane fouling experiments were carried out using the pulsed injection technique [20]. Figure 4.4 shows the schematic diagram of the experimental set-up used for the fouling experiments in the constant flux mode. The stirred cell module had working volume of 15.5 ml, and housed a membrane disc having effective diameter of 24 mm. The suspended bar impeller (diameter = 18.7 mm) inside the module was magnetically driven. In all the experiments, the stirring speed was maintained at approximately 950±50 rpm (determined using a digital tachometer). A positive displacement pump (Amersham Biosciences; HiLoad Pump P-50) was used to drive the

buffer through the ultrafiltration membrane at constant flow rate. 200 g/l HSA solution was injected into the ultrafiltration module in the form of pulse using a V-7 sample injector (Amersham Biosciences) fitted with a 25 µl sample loop. This gave a bulk protein concentration of 0.32 g/l within the module. The purpose of injecting a small amount of highly concentrated protein solution was to make sure the injection time had minimal effect on the kinetics of concentration polarization. TMP across the membrane was continuously monitored using a pressure sensor (GBS-BTA, Vernier Software & Technology) connected to a computer through an interface. In constant pressure experiments, the pump was removed from the set-up and the buffer reservoir was pressurized using compressed air (see Figure 4.5). The permeate mass was continuously monitored using an analytical balance (Mettler Toledo AB204-S) which was connected to a computer through an interface for data logging. The permeate flux was calculated from the permeate mass versus time data by appropriate differentiation.

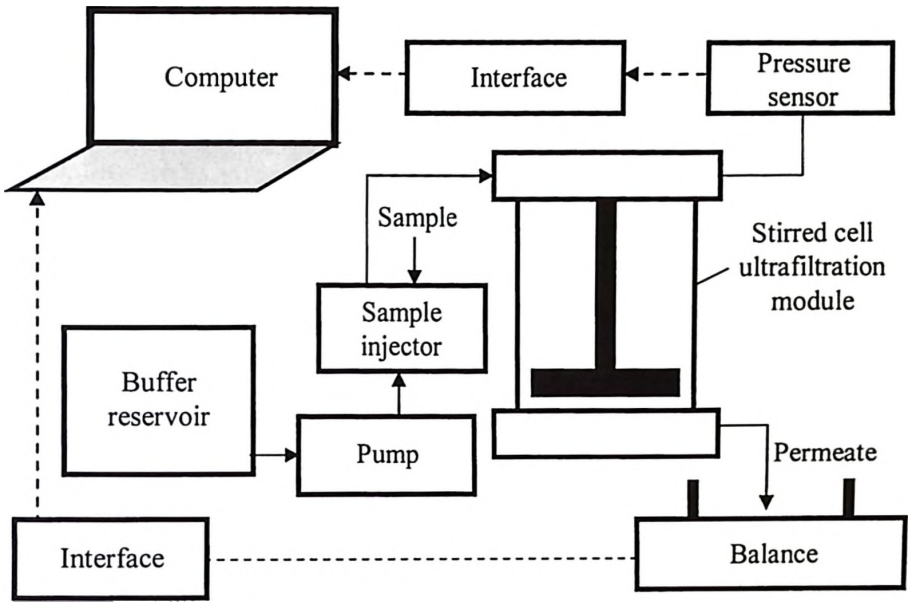

Figure 4.4 Schematic diagram of set-up used for constant flux ultrafiltration experiments

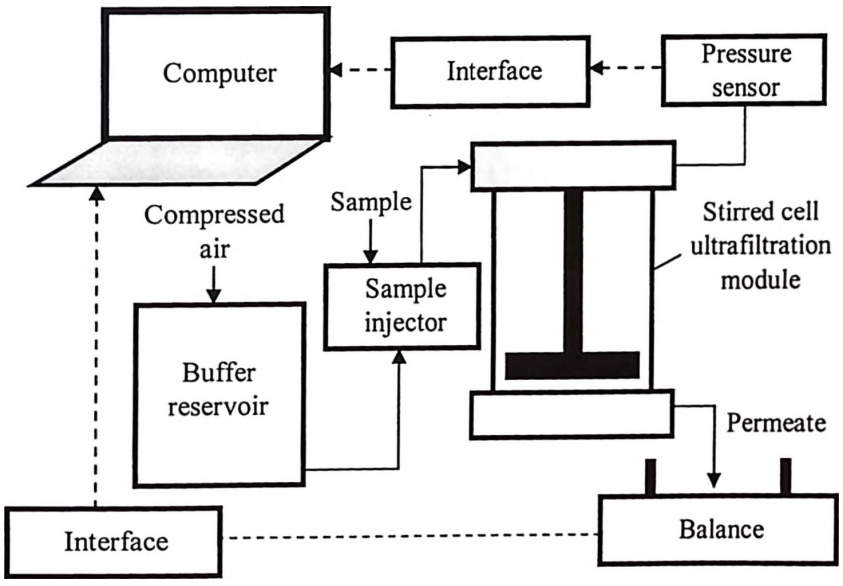

Figure 4.5 Schematic diagram of set-up used for constant pressure ultrafiltration experiments

Each fouling experiment was carried out with a fresh membrane disc. In constant flux ultrafiltration experiments, the protein sample was injected into the stirred cell module after 30 minutes of constant flux buffer flow through the membrane. This ensured complete removal of additives like glycerin (humectant) and sodium azide (bacteriostat) from the membrane pores. The steady TMP value thus obtained was used to determine the hydraulic permeability of each new membrane disc. Similarly, in constant pressure ultrafiltration experiment, the protein sample was injected after 30 minutes of buffer flow through the membrane. In this case the constant flux of buffer through the membrane was used to determine the hydraulic permeability. Each constant flux ultrafiltration experiment was carried out for 75 minutes at the end of which the protein solution was removed from the module and the membrane disc was thoroughly rinsed with water (18.2 MΩ cm). Then permeability of the fouled membrane disc was determined by buffer filtration in a manner similar to that before protein ultrafiltration. All experiments reported in this paper were carried out at ambient temperature conditions (24 Celsius).

4.5 Results and Discussion

Figure 4.6 shows the TMP profiles a five different constant fluxes. The steady TMP before protein injection in all the experiments confirm the absence of any other foulant in buffer. After the injection of the protein sample the TMP increased very rapidly initially followed by slow but linear increase over the remaining period of experiment. This is consistent with that reported in an earlier paper [17]. The data shown

in Figure 4.6 was used to calculate the values for m and $\Delta\pi$ at the different fluxes as discussed in [17]. The dependence of $\Delta\pi$ on wall concentration of human serum albumin was determined from a best fit curve obtained with data reported in the literature [21]. The boundary layer thickness at the stirring speed used in the fouling experiments i.e. 950±50 rpm was determined as described by [20]. All the empirical correlations along with the different simulation constants used in the mathematical model are shown in Table 4.1.

Table 4.1 Simulation constants for mathematical model

$D = 6.1\times10^{-11}$ m^2/s		Ref [22]
$k = 7.78\times10^{-6}$ m/s		
$\delta = 7.837\times10^{-6}$ m		
$C_b = 0.32$ kg/m^3		
$R_m^* = 4.16782\times10^5$ kPa s/m		
$t_R = 1500$ s		
R_m^0	12.247357×10^5 kPa s/m (for TMP = 7.4 kPa)	
	12.576164×10^5 kPa s/m (for TMP = 27.8 kPa)	
	9.668005×10^5 kPa s/m (for TMP = 37.4 kPa)	
$\Delta\pi = (0.0001C_w^2) + (0.0209C_w)$		Ref [21]
$m = 6.4067\times10^{-5}\exp(249950J_v)$		

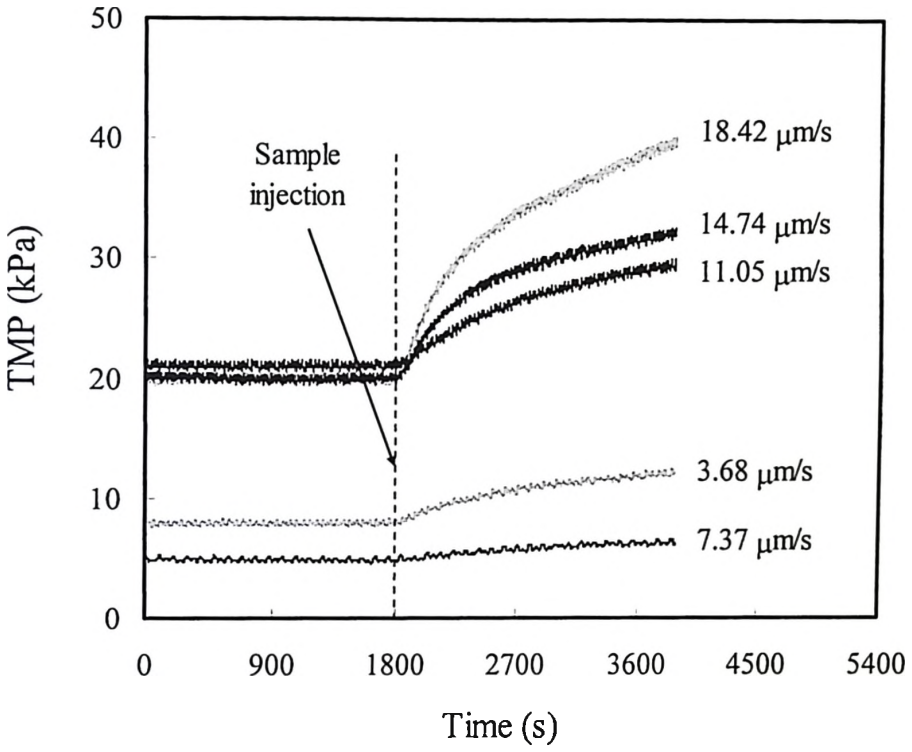

Figure 4.6 TMP - time profiles obtained from five different constant flux HSA ultrafiltration experiments

Figure 4.7(a) shows the simulation results for the wall protein concentration and osmotic pressure in an ultrafiltration experiment carried out at 7.4 kPa TMP. Both increased very rapidly during the initial few seconds of ultrafiltration indicating that the build up of concentration polarization is very fast. This increase was too rapid to be observed in a plot such as that shown in Figure 4.7 (a). The osmotic pressure and wall protein concentration then decreased with time, more rapidly during the first 1800 s and

more gradually after that. This is due to the attenuating nature of the permeate flux in constant pressure ultrafiltration which in turn decreases the convective transport of protein molecules towards the membrane. Figure 4.7 (b) shows that the simulated fouling resistance increased with time in the same constant pressure ultrafiltration experiment. The resistance increased at a faster rate during the first few minutes of ultrafiltration due to the initial rapid fouling. After this, the increase in fouling resistance was more gradual with the rate of increase diminishing with time. This can be explained in terms of the dependence of fouling rate on flux as discussed in [17], i.e. the rate of fouling decreases with decrease in permeate flux. Figure 4.7(c) shows the simulated and experimental permeate flux data for ultrafiltration carried out at 7.4 kPa TMP. At this transmembrane pressure, the osmotic backpressure was negligible compared to the transmembrane pressure. The decrease in flux with time was almost entirely due to membrane fouling. Therefore it may be concluded that at low transmembrane pressures, concentration polarization has virtually no effect on the permeate flux. The simulated data and experimental data trend are in reasonably good agreement. The experimental permeate flux data shows a bit of scatter. This is due to the fact that the permeate was collected in a drop-wise manner in the beaker placed on the electronic balance. When each drop fell into the beaker the impact caused the permeate mass data to scatter a bit. This effect was further magnified when the permeate flux data was calculated by the differentiation method.

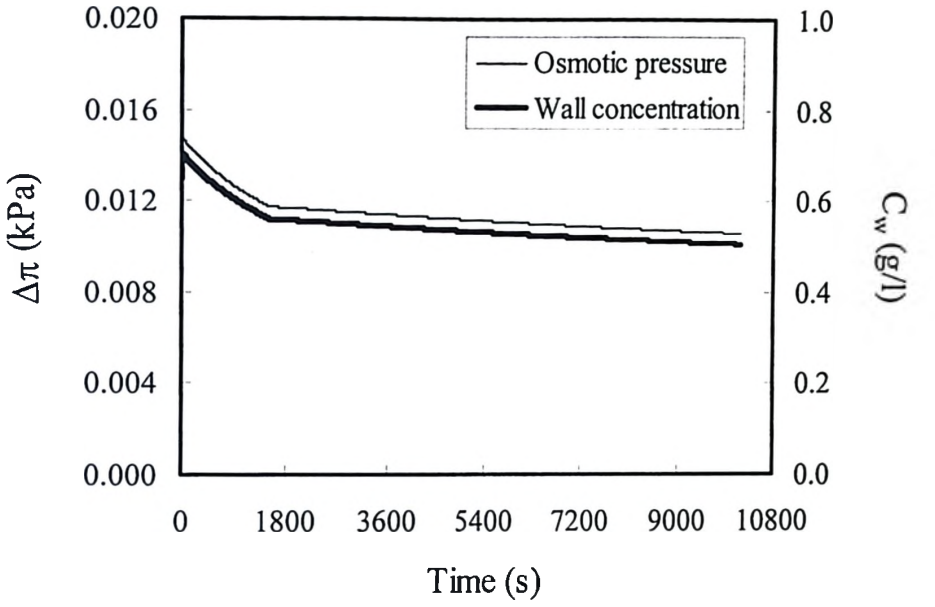
0.020
0.016
0.012
0.008
0.004
0.000
Δπ (kPa)
1.0
0.8
0.6
0.4
0.2
0.0
C_w (g/l)
Osmotic pressure
Wall concentration
0
1800
3600
5400
7200
9000
10800
Time (s)

(a)

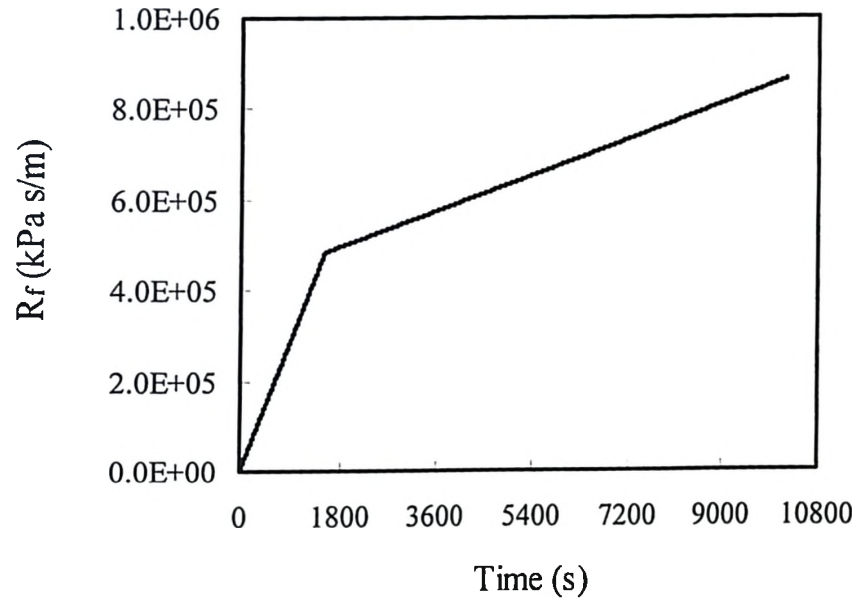
1.0E+06
8.0E+05
6.0E+05
4.0E+05
2.0E+05
0.0E+00
Rf (kPa s/m)
0
1800
3600
5400
7200
9000
10800
Time (s)

(b)

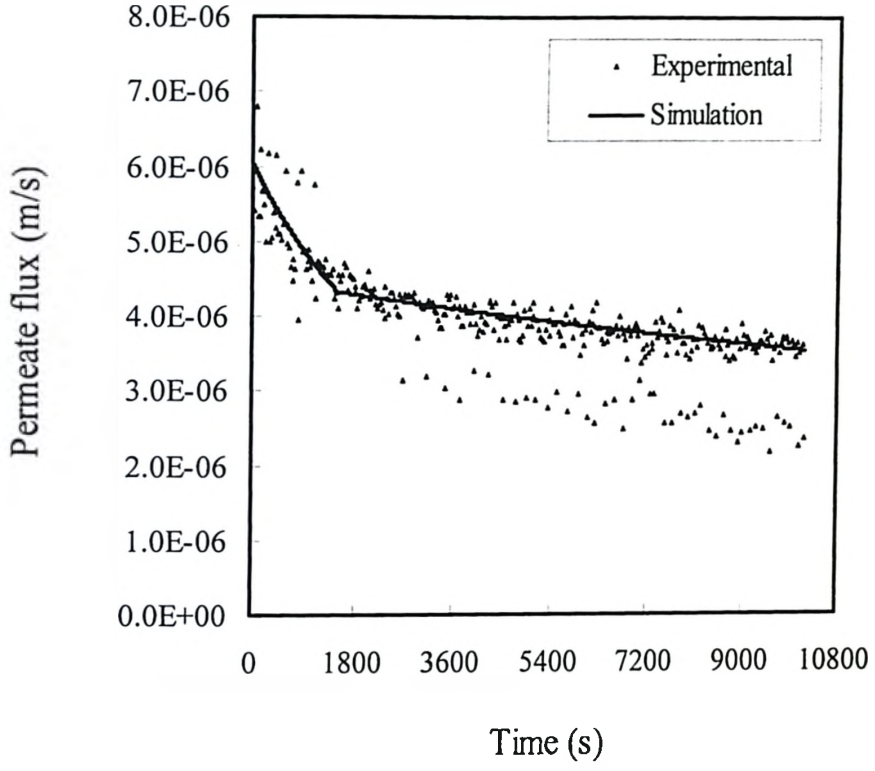

(c)

Figure 4.7 Flux decline at 7.4 kPa TMP: (a) Simulated osmotic pressure and wall concentration, (b) Simulated membrane fouling resistance, and (c) Comparison of simulated and experimental permeate flux

Figure 4.8(a) shows the simulation values of the wall protein concentration and osmotic pressure in an experiment carried out at 27.8 kPa TMP. As observed at 7.4 kPa TMP, the wall concentration and osmotic pressure increased to their maximum values during the initial few seconds of ultrafiltration. However, the magnitude of maximum

osmotic pressure and maximum wall concentration were both significantly higher than that observed at 7.4 kPa TMP. Also the subsequent decrease in osmotic pressure and wall protein concentration with time were more rapid. Figure 4.8(b) shows the simulated fouling resistance profile over the course of time in the same experiment. At this TMP too the fouling resistance was the main reason for the decrease in permeate flux. The magnitude of osmotic pressure was significant only during the first few hundred seconds. Beyond this point, this had virtually no effect on the permeate flux. Figure 4.8(c) shows the comparison of simulated permeate flux at 27.8 kPa TMP with the experimental data. Here again, the simulation results are in excellent agreement with experimental data. The scatter of experimental data was less than that observed at 7.4 kPa TMP. This is due to the fact that at 27.8 kPa TMP, the frequency of permeate drop was significantly greater. Also the permeate mass data had a greater magnitude and hence the impact of the drops was less significant.

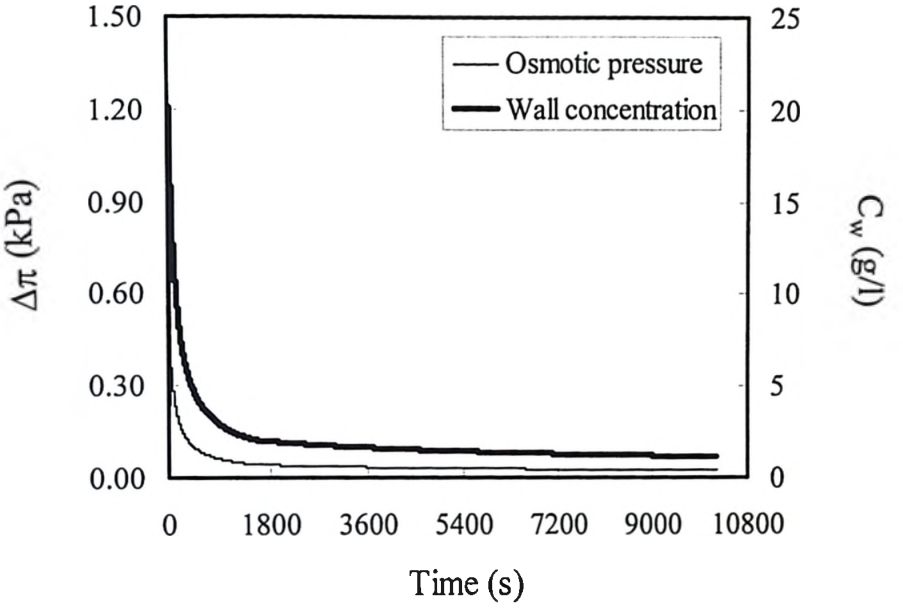
1.50
1.20
0.90
0.60
0.30
0.00
Δπ (kPa)
25
20
15
10
5
0
C_w (g/l)
Osmotic pressure
Wall concentration
0
1800
3600
5400
7200
9000
10800
Time (s)

(a)

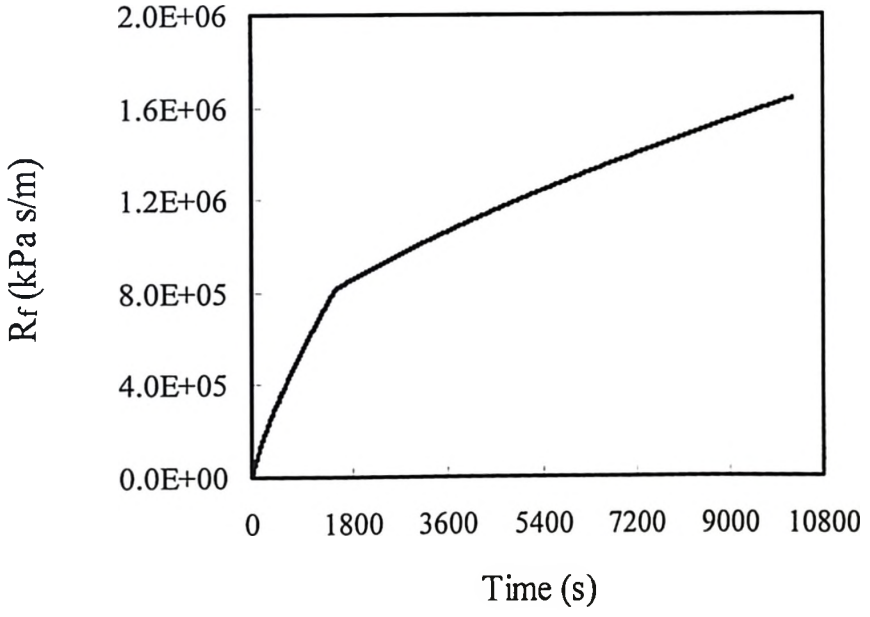
2.0E+06
1.6E+06
1.2E+06
8.0E+05
4.0E+05
0.0E+00
R_f (kPa s/m)
0
1800
3600
5400
7200
9000
10800
Time (s)

(b)

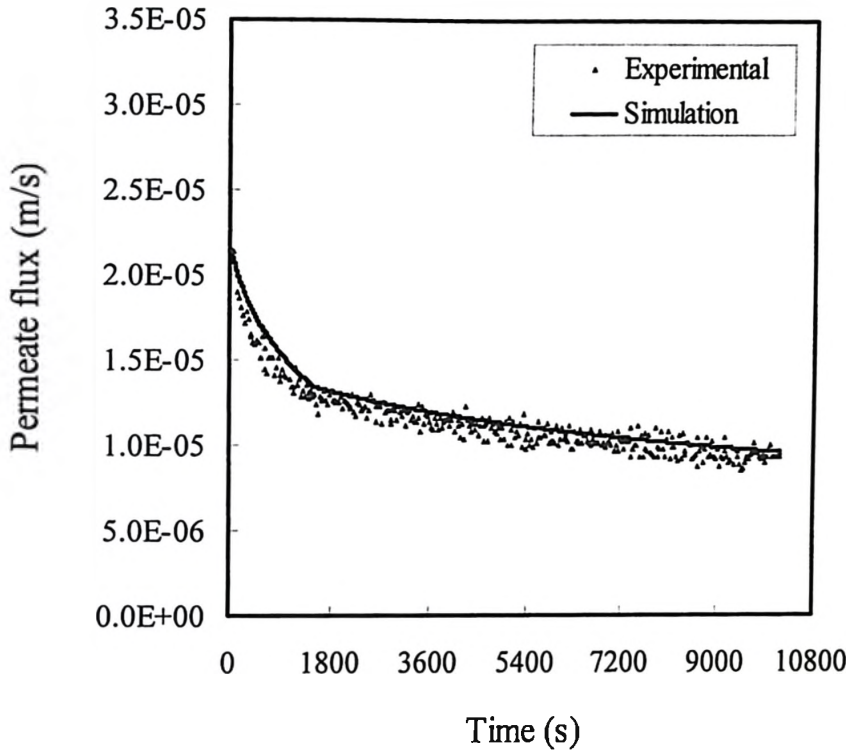

(c)

Figure 4.8 Flux decline at 27.8 kPa TMP: (a) Simulated osmotic pressure and wall concentration, (b) Simulated membrane fouling resistance, and (c) Comparison of simulated and experimental permeate flux

Figures 4.9(a) and 4.9(b) show the simulated protein wall concentration and osmotic pressure, and the membrane fouling resistance during ultrafiltration carried out at 37.4 kPa TMP. As expected, the wall concentration and osmotic pressure were significantly higher than at 27.8 kPa TMP. At this TMP, the effect of osmotic on

permeate flux was quite significant at the start of the process However, the osmotic pressure decreased rapidly and after about 1500 s, it became inconsequential. Figure 4.9(c) shows the simulated and experimental permeate flux data for this TMP. The model over predicts the decrease in permeate flux during the very early stages of ultrafiltration. This is due to the very high values of osmotic pressure predicted by the model. However, as the fouling resistance term becomes significant, the model self-corrects and the simulated data after about 1000 s are in reasonably good agreement with the experimental data.

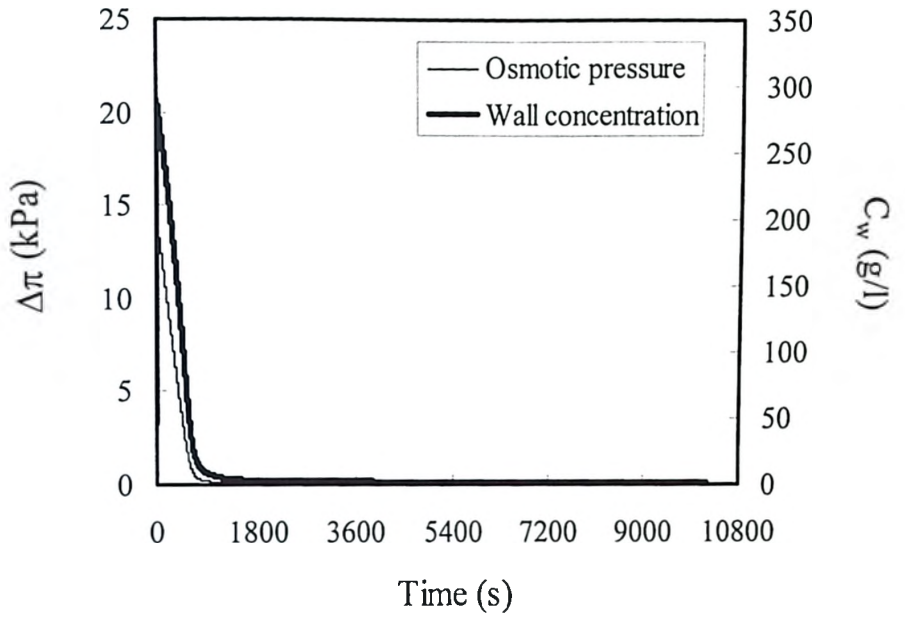
Osmotic pressure
Wall concentration
Δπ (kPa)
C_w (g/l)
Time (s)
0
5
10
15
20
25
50
100
150
200
250
300
350
0
1800
3600
5400
7200
9000
10800

(a)

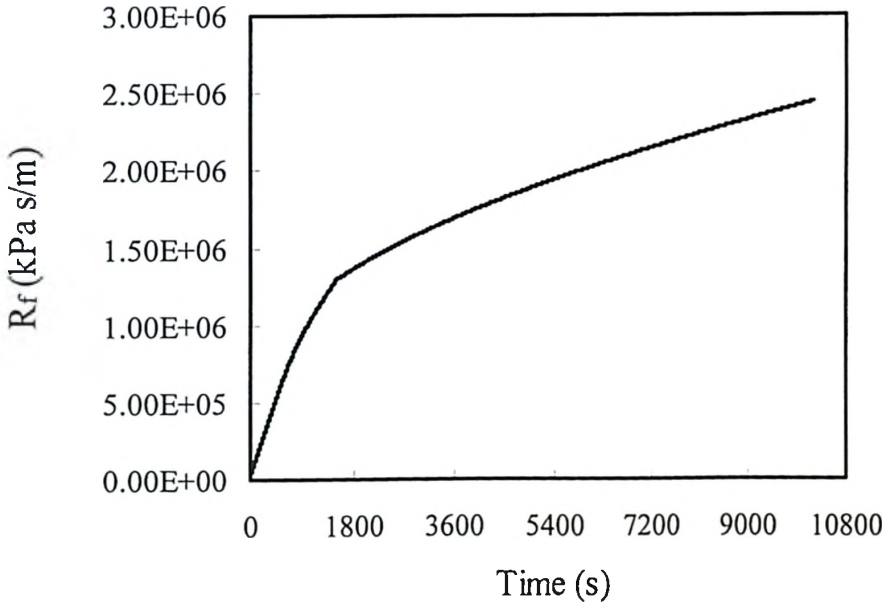
R_f (kPa s/m)
Time (s)
0.00E+00
5.00E+05
1.00E+06
1.50E+06
2.00E+06
2.50E+06
3.00E+06
0
1800
3600
5400
7200
9000
10800

(b)

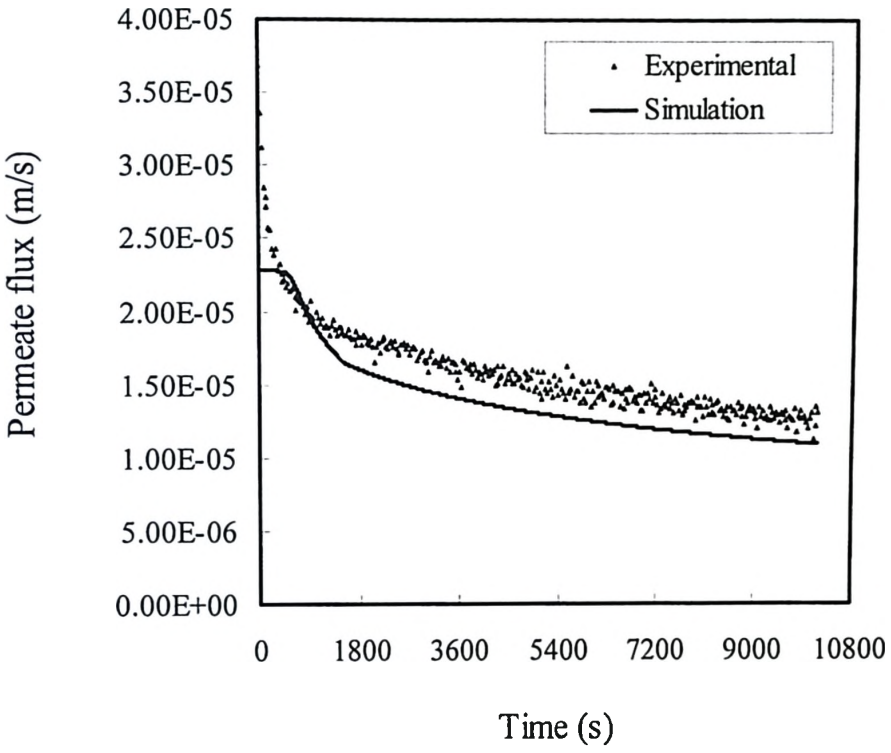

(c)

Figure 4.9 Flux decline at 37.4 kPa TMP: (a) Simulated osmotic pressure and wall concentration, (b) Simulated membrane fouling resistance, and (c) Comparison of simulated and experimental permeate flux

The model clearly suggests that fouling plays a far more significant role than concentration polarization in reducing permeate flux in constant pressure ultrafiltration. Table 4.2 shows the simulated and experimental osmotic pressure values after 170 minutes in constant pressure ultrafiltration. Quite clearly the osmotic pressure did not have much role in permeate flux decline in the TMP range examined. The model also suggests that the rate of fouling would be highest at the start of the process due to the combination of the rapid initial fouling and the higher value of the long term fouling rate constant at higher fluxes. As the permeate flux decreases, the rate constant for long term fouling decreases and this reduces the rate of increase in fouling resistance. Chudacek and Fane [23] and Opong and Zydney [24] have reported that protein layers which are initially deposited on a membrane during a membrane filtration process are much more closely packed than in later stages. It should be noted that in our model the effect for flux history on membrane fouling has been neglected. An earlier study has shown that flux history could potentially affect membrane fouling in step up and step down constant flux experiments [17]. The proposed model could serve as a useful tool for optimizing the operating TMP. Table 4.3 compares the simulated membrane fouling resistance at the three different TMPs for two different cumulative permeate volumes. The extents of membrane fouling are similar at 7.4 and 27.8 kPa but significantly higher at 37.4 kPa. Such information would be useful in identifying the trade-off between productivity and membrane working life, something that is very important in membrane process designing.

Table 4.2 Comparison of simulated osmotic pressure with experimental data at the end of constant pressure ultrafiltration

TMP (kPa)	Simulated $\Delta\pi$ (kPa)	Experimental $\Delta\pi$ (kPa)
7.4	0.011	~ 0
27.8	0.024	~ 0
37.4	0.030	~ 0

Table 4.3 Comparison of membrane fouling resistance at different TMP

Permeate volume collected (m^3/m^2)	TMP (kPa)	Membrane fouling resistance, R_f ($\times 10^5$ kPa s/m)	Time (s)	Average permeate flux ($\times 10^{-6}$ m/s)
0.03063	7.4	7.32780	7200	4.25
	27.8	8.73441	1952	15.69
	37.4	12.97981	1504	20.36
0.04159	7.4	8.63913	10200	4.08
	27.8	9.77709	2814	14.78
	37.4	14.47043	2192	18.98

4.6 Conclusion

A novel mathematical modeling approach for predicting the permeate flux decline in constant pressure ultrafiltration using the data extracted from constant flux ultrafiltration experiments is discussed in this paper. Constant pressure ultrafiltration is assumed to be made up of a large number of sequential constant flux steps. The proposed model not only predicts the permeate flux decline in constant pressure ultrafiltration but also explains the interplay between flux, concentration polarization and membrane fouling. According to the model, fouling is the major contributory factor in permeate flux decline over the range of transmembrane pressures examined. The effect of osmotic pressure is significant only in the early part of constant pressure ultrafiltration carried out at higher transmembrane pressures. The rate of increase in membrane fouling resistance decreases with time on account of the steady decrease in permeate flux. The simulated permeate flux data obtained using the proposed model is in good agreement with experimental data. This model can be used to optimize the operating transmembrane pressure and to identify the trade off between productivity and working life of an ultrafiltration membrane.

4.7 References

1. A.G. Fane, Ultrafiltration: Factors influencing flux and rejection, in R.J. Wakeman (Ed.), Progress in filtration and separation, Volume 4, Elsevier, Amsterdam, 1986, pp. 102-179.

2. L.J. Zeman and A.L. Zydney, Microfiltration and ultrafiltration: Principles and applications, Marcel Dekker, New York, 1996.
3. M. Cheryan, Ultrafiltration and microfiltration handbook, Technomic, Lancaster, 1998
4. R. Ghosh, Protein bioseparation using ultrafiltration: Theory, applications and new developments, Imperial College Press, London, 2003
5. P. Aimar, C. Taddei, J.P. Lafaille and V. Sanchez, Mass transfer limitations during ultrafiltration of cheese whey with inorganic membranes, J. Membr. Sci., 38 (1988) 203.
6. A.G. Fane, Factors affecting flux and rejection in ultrafiltration, J. Sep. Proc. Technol., 4 (1983) 15.
7. A. Suki, A.G. Fane and C.J.D. Fell, Flux decline in protein ultrafiltration, J. Membr. Sci., 21 (1984) 269.
8. V. Gekas, P. Aimar, J.P. Lafaille and V. Sanchez, A simulation study of the adsorption—concentration polarization interplay in protein ultrafiltration, Chem. Eng. Sci., 48 (1993) 2753.
9. A.D. Marshall, P.A. Munro and G. Tragardh, The effect of protein fouling in microfiltration and ultrafiltration on permeate flux, protein retention and selectivity: A literature review, Desalination, 91 (1993) 65.
10. M.K. Ko, J.J. Pellegrino, R. Nassimbene and P. Marko, Characterization of the adsorption-fouling layer using globular proteins on ultrafiltration membranes, J. Membr. Sci., 76 (1993) 101.

11. M. Turker and J. Hubble, Membrane fouling in a constant-flux ultrafiltration cell, J. Membr. Sci., 34 (1987) 267.

12. W.R. Bowen and D.T. Hughes, Properties of microfiltration membranes. Part 2. Adsorption of bovine serum albumin at aluminum oxide membranes, J. Membr. Sci., 51 (1990) 189.

13. R.F. Boyd and A.L. Zydney, Analysis of protein fouling during ultrafiltration using a two-layer membrane model, Biotechnol. Bioeng., 59 (1998) 451.

14. S. Chang, A.G. Fane, T.D. Waite, Analysis of constant permeate flow filtration using dead-end hollow fiber membranes, J. Membr. Sci., 268 (2006) 132.

15. O. LeBerre, G. Daufin, Skimmilk crossflow microfiltration performance versus permeation flux to wall shear stress ratio, J. Membr. Sci., 117 (1996) 261.

16. A. D. Marshall, P.A. Munro, G. Tragradh, Influence of permeate flux on fouling during the microfiltration of beta-lactoglobulin solutions under cross-flow conditions, J. Membr. Sci., 130 (1997) 23.

17. R. Ghosh, Study of membrane fouling by BSA using pulsed injection technique, J. Membr. Sci., 195 (2002) 115.

18. E. Matthiasson, The role of macromolecular adsorption in fouling of ultrafiltration membranes, J. Membr. Sci., 16 (1983) 23.

19. R. Richtmeyer and K.W. Morton, Difference methods for initial-value problems, Interscience, New York, 1967.

20. R. Ghosh and Z.F. Cui, Analysis of protein transport and polarization through membranes using pulsed sample injection technique, J. Membr. Sci., 175 (2000) 75.

21. J. Rescic, V. Vlachy, A. Jamnik and O. Glatter, Osmotic pressure, small-angle X-ray, and dynamic light scattering studies of human serum albumin in aqueous solutions, J. Colloid Interface Sci., 239 (2001) 49.

22. D.E. Raymond, A. Manz and H.M. Widmer, Continuous separation of high molecular weight compounds using a microlitre volume free-flow electrophoresis microstructure, Anal. Chem., 68 (1996) 2515.

23. M.W. Chudacek and A.G. Fane, The dynamics of polarization in unstirred and stirred ultrafiltration, J. Membr. Sci., 21 (1984) 145.

24. W.S. Opong and A.L. Zydney, Hydraulic permeability of protein layers deposited during ultrafiltration, J. Colloid Interface Sci., 142 (1991) 41.

Chapter 5

High-capacity Macroporous Gel-filled Membranes: Performance Evaluation for Ion-exchange Chromatography of Proteins

This chapter is organized based on a paper published in Biochemical Engineering Journal, 35 (2007) 295-300 by Dharmesh M. Kanani, Elena Komkova, Tiffany Wong, Alicja Mika, Ronald F. Childs and Raja Ghosh.

5.1 Abstract

One of the main limitations of using membranes as chromatographic media is the generally lower solute binding capacities when compared with particulate media. Hence their use is largely restricted to flow through applications for the removal of small

amounts of target proteins or impurities from large volume of feed. This chapter discusses the use of two novel macroporous gel-filled membranes for ion-exchange chromatography of proteins. These membranes, which displayed anion-exchange behavior, were prepared by anchoring quaternary ammonium salt gels within the pores of a non-woven, polypropylene fabric. The morphology of these membranes ensured that they had all the positive attributes of chromatographic membranes resulting from the predominance of convective solute transport, in addition to having significantly higher protein binding capacities compared to rigid membranes. In this work, HSA binding on both the membranes were studied at different operating parameters such as pH, buffer ions, salt concentration, feed protein concentration and superficial velocity and the potential operating conditions from the context of human plasma protein fractionation were identified. At an optimized condition, the HSA binding capacities of these two novel membranes, Q type 1 and Q type 2 under saturating conditions were determined to be 113 mg/ml and 299 mg/ml respectively. The suitability of using Q type 2 membrane for plasma fractionation was demonstrated by the separation of a simulated feed solution consisting of HSA and HIgG.

5.2 Introduction

Membrane chromatography is increasingly being used for protein bioseparation [1-4]. It is significantly faster than packed bed (or column) chromatography and requires less mobile phase to operate. Mobile phase cost is about 70-75% of the total processing

cost in packed bed chromatography of proteins while it only accounts for 7-8% of the cost with membrane chromatography [5]. This coupled with lower labor cost make membrane chromatography cheaper by a factor of 2-4 [5]. A shorter process time also increases product recovery due to lower protein degradation. Membrane chromatography seems to be particularly promising for separation of larger proteins, which find it difficult to enter into the pores of particulate chromatographic media and consequently bind only on the external surface of such media [6]. Due to new developments in membrane manufacturing technology, membrane chromatographic devices are now easier and cheaper to mass produce and the use of cheap disposable devices eliminates the requirements for equipment cleaning and re-validation. Membrane chromatography being modular in nature is relatively easier to scale-up.

The main challenge with membrane chromatography is the generally lower protein binding capacity when compared with gel-based media [6]. The problem of low intrinsic binding capacity of membranes is further aggravated by poor module designs, particularly by inadequate inlet flow distribution and outlet flow collection. Hence, the current usage of membrane chromatography is restricted to niche applications such as the processing of large volumes of dilute feed streams and the removal of small amounts of specific impurities such as endotoxins. The binding capacity of rigid polymeric membranes commonly used in membrane chromatography for protein binding is low since this is limited to the pore walls and external surfaces only. Table 5.1 lists some of the commercially available membrane adsorbers with their approximate protein binding

capacities. These were calculated from the data supplied in product manuals. A two-pronged approach is essential to improve membrane chromatography: a) development of membranes with higher binding capacities, and b) development of better designed membrane modules [6]. In a recent patent application a new membrane module design was disclosed by Ghosh using which membrane binding capacity utilization could be significantly improved [7,8]. Attempts to improve the binding capacity have been based around the creation of 3-dimensional binding domains within the membranes. The grafting of polymers onto membranes for reducing steric hindrance associated with binding of large molecules on rigid surfaces has been reported by Koguma et al. [9]. Tomomi et al. [10] and Ulbricht and Yang [11] have reported the use of polymer brush based binding domains for increasing protein binding capacity. The approach described in this chapter is based on the creation of a macroporous gel based 3-dimensional binding domain within an appropriate porous supporting material.

Table 5.1: Commercial membrane adsorbers and their binding capacities

Product Name	Manufacturer	Approx. protein* binding capacity (mg/ml)
Sartobind MA15 and MA100 (S, C, Q and D type•)	Sartorious	22-29
Sartobind Factor-two family	Sartorious	28-30
Vivapure centrifugal ion exchangers	Vivascience	22-30
Mustang Q	Pall	70

* In most of the instances, protein binding capacities for anion exchange membranes were reported with serum albumin and for cation exchange membranes with lysozyme.

• S ≅ Sulfonic acid (strongly acidic cation exchanger)

C ≅ Carboxyl groups (weakly acidic cation exchanger)

Q ≅ Quaternary ammonium (strongly basic anion exchanger)

D ≅ Diethylamine (weakly basic anion exchanger)

This chapter examines the protein binding performance of a new type of high-capacity anion-exchange membranes [12] developed at McMaster University and their possible application in plasma protein fractionation. These membranes consisted of

quaternary ammonium salt gels anchored within macroporous, non-woven, polypropylene fabric. A sketch showing the structure of these Q type membranes and an ESEM image of one of the membranes are shown in Figures 5.1 and 5.2 respectively. With this new type of membranes, binding took place within the three dimensional gel network formed inside the macropores and hence the binding capacity was higher. At the same time, the flow of feed solution through the gel network being convective in nature and hence the solute transport mechanisms were similar to those with rigid membranes. In this work, the bioseparation of human serum albumin (HSA) using two different Q type macroporous gel membranes is studied first. The effects of operating parameters such as pH, buffer substance, salt concentration, feed protein concentration and superficial velocity on human serum albumin (HSA) binding on the macroporous gel-filled membranes were first examined. The dynamic protein binding capacities of the membranes at selected conditions were then determined by carrying out a series of breakthrough experiments. The feasibility of using one of these membranes for plasma fractionation was then demonstrated by separating HSA, the most abundant protein present in human plasma from HIgG, the second most abundant plasma protein. Almost 70% of total plasma protein is HSA while HIgG accounts for another 17-20%. These being the two main plasma proteins, these are fractionated in large quantities for biopharmaceutical uses.

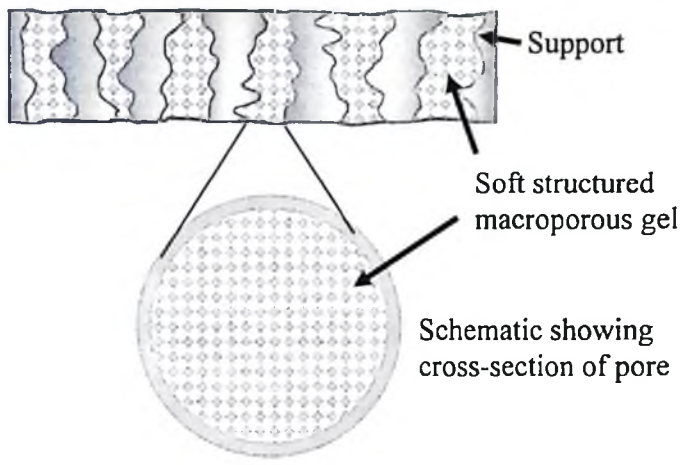

Figure 5.1 Sketch showing the structure of macroporous gel filled membranes (Note: Convective transport occurs through the pores in the soft structured gel)

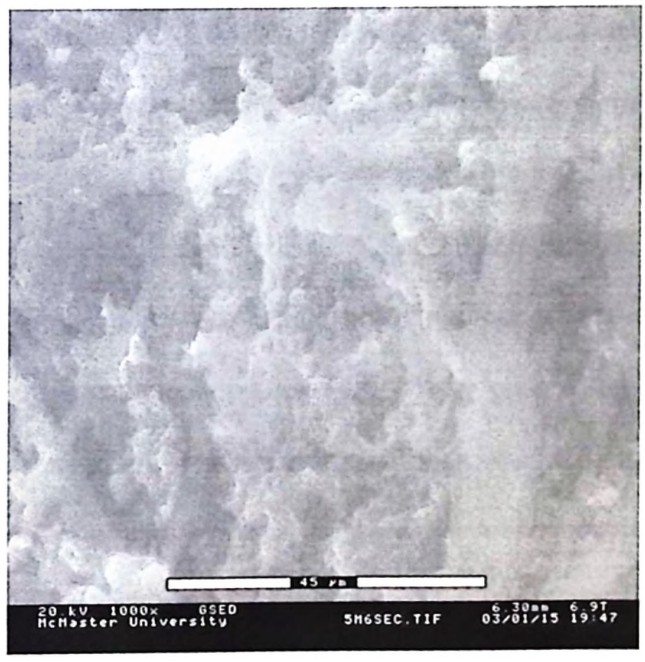

Figure 5.2 ESEM image of Q type 2 macroporous gel-filled membrane

5.3 Experimental

5.3.1 Materials

Purified HSA and HIgG were kindly donated by the Scottish Blood Transfusion Services, Edinburgh, UK. The molecular weights of HSA and HIgG are 69 kDa and 155 kDa respectively while their isoelectric points are 4.7 and 7.0 respectively. Two different types of macroporous gel-filled anion-exchange (or Q type) membranes were prepared in the laboratory by anchoring a quaternary ammonium salt macroporous gel within the pores of a non-woven, polypropylene fabric as described by Childs et al. [12]. In these membranes, convective transport of solute occurs through the pores in the structured gels and not through the pores of the support. The non-woven polypropylene support was supplied by Hollingsworth and Vose Company and had pore diameter in the range of 6.5 to 15.0 μm. The macroporous gel forming material was polymerized in-situ and was firmly held in place within the non-woven polypropylene support matrix. Initial tests showed that the macroporous gel did not leak out of the support even when high pressure differentials were applied across the membrane. Initial tests also revealed that Q type 2 membrane increased in volume by as much as 40% by gel-swelling following wetting. The non-woven polypropylene material used as support was flexible in nature and could accommodate the gel-swelling. A custom designed membrane module was used for most of the membrane chromatography experiments [7]. The glass fiber prefilter discs (catalogue # AP2504200) between which the membrane discs were stacked within the membrane module were purchased from Millipore. The adsorption isotherm was studied

using a syringe filter holder (Whatman, stainless steel, 13 mm diameter) within which a single membrane disc having an effective diameter of 10 mm was housed. All laboratory chemicals were purchased from Sigma.

5.3.2 Buffers and protein solutions

All buffers and solutions were prepared using water obtained from a NANOpure Diamond Life Science (UV/UF) ultrapure water system. These were micro-filtered and degassed prior to use. The protein solutions were prepared in appropriate buffers followed by pH adjustment using 0.1 M HCl and centrifugation at 10,000 rpm for 20 minutes for removal of particulate matter. Total protein concentration of feed solutions was measured using the Bradford assay method [13].

5.3.3 Experimental set-up and methodology

The porosity (or voidage fraction) of the membranes were measured based on water uptake by dry membranes. The nominal pore sizes of the membranes were determined from water flux data using the porosity data. The properties of both the membranes, Q type 1 and Q type 2 are shown in Table 5.2. The pore sizes reported in Table 5.2 are those of the structured gels and not those of the macroporous supports. Before their first use, membranes were conditioned by alternately passing 10 mM sodium phosphate buffer (pH 7.0) and 1 M NaCl solution through them several times. The membrane chromatographic experiments were carried out using an AKTA^{TM} prime liquid

chromatographic system (Amersham Biosciences). The chromatographic column normally used in such a system was replaced by a custom designed membrane module which was of the same type as discussed in [7]. Within this module a stack of flat sheet membrane discs supported in between three glass fiber prefilter discs on both side could be housed, the effective diameter of the membrane discs being 42 mm. The membrane discs of both membrane types had the same dry thickness of approximately 250 microns each. In experiments using the Q type 1 membrane, stack of four flat sheet discs having total thickness around 1000 microns was used while with the Q type 2 membrane only one disc was used. Preliminary experiments showed that the Q type 2 membrane had a significantly higher HSA binding capacity. A 50 ml superloop was used for injecting protein samples. Before injecting protein solutions into the membrane module, the appropriate binding buffer was passed through the membrane till stable readings were obtained. The flow of binding buffer through the membrane was continued after injecting the protein sample till all the unbound proteins were washed away from the membrane module. The bound protein was eluted using 1 M NaCl prepared using the corresponding binding buffer.

Table 5.2 Properties of the macroporous gel-filled membranes

Membrane	Q type 1	Q type 2
Nominal pore size (microns)	0.30-0.40	0.15 – 0.20
Porosity (-)	0.60-0.65	0.5-0.55
Dry thickness (microns)	250	250
Wet thickness (microns)	-	350

The performance of the macroporous gel-filled membranes was investigated first in the pulse input mode and later in the step input mode. The UV absorbance of the effluent stream from the membrane module was continuously monitored at 280 nm in both modes to keep the track of HSA concentration. The pulse input mode was used for studying the effects of different physicochemical and operating parameters such as pH, buffer species, ionic strength, feed concentration and flow rate on the relative binding capacities of the membranes. In these experiments the amount of protein sample injected in a pulse was significantly in excess of the binding capacity, the purpose of which being to obtain two peaks: one due to excess unbound protein and the other due to the eluted bound protein. By comparing the areas under the curve of the bound and unbound peaks, the effects of physicochemical and operating parameters on relative amount of protein bound could be observed with a high degree of sensitivity. The amount of HSA bound to the membrane was determined from the bound and unbound peak areas using the equation shown below:

$$M_b = M_i\left(\frac{AUC_b}{AUC_b + AUC_u}\right) \tag{5.1}$$

The relative amount of protein bound was obtained by dividing the amount bound at an experimental condition by the maximum amount bound in the respective experimental range.

The step input mode experiments were carried out to obtain HSA breakthrough curves. From these curves the absolute HSA binding capacities of the two membrane types were determined. A literature survey has shown that the definition of the point of breakthrough is highly subjective and user dependent. This has variously been defined as the point at which the effluent concentration reaches 1%, 5%, 10% or even 20% of the feed concentration or simply the point at which the solute is first observed in the effluent. The analytical system used in our studies allowed accurate determination of the incipient breakthrough i.e. when the HSA first appeared in the effluent. In this paper binding capacities of the gel-filled membranes are reported based on three breakthrough point designations: a) the incipient breakthrough, b) 1% breakthrough, and c) saturation.

The feed solution for HSA/HIgG separation was prepared by mixing stock solutions of pure HSA and pure HIgG in the binding buffer followed by pH adjustment. Quantitative analysis of HSA/HIgG mixtures (i.e. feed, flow-through and purified HSA samples) was carried out by affinity chromatography using a HiTrap r-Protein-A FF column (1 ml, Amersham Bioscience) using the AKTA^{TM} prime system. This column selectively bound HIgG from 20 mM sodium phosphate (pH 7.0) as mobile phase while the bound antibody was eluted using 0.1 M sodium citrate buffer (pH 3.0). The HSA/HIgG mixtures were also analyzed by 10% SDS-PAGE under non-reducing condition using a Hoefer miniVE electrophoresis unit. The protein bands were visualized using Coomassie brilliant blue R-250 dye.

5.4 Results and discussion

5.4.1 Effect of pH

The effect of pH on HSA binding was studied using 10 mM sodium phosphate buffer of appropriate pH. The HSA feed solutions (concentration = 20 kg/m^3) were prepared in the appropriate binding buffer. The Q type 1 membrane was tested using a pulse volume of 10.5 ml while the Q type 2 membrane was tested using a pulse volume of 5.0 ml. These tests were carried out at a fixed flow rate of 7 ml/min that gave a membrane bed residence time of 11.9 seconds for the Q type 1 membrane and 3.0 seconds for the Q type 2 membrane. Figure 5.3 shows the relative amounts of HSA bound at different pH values on the Q type 1 membrane. In the pH range studied (i.e. 5.5-7.5) the binding increased with increase in pH. Based on the results of earlier experiments (not reported in this chapter) the adsorptive gel material used to prepare the Q type 1 membrane would be expected to be positively charged to similar extents at the three pH values examined. Hence the increase in HSA binding capacity with pH was due to the effect of pH on net negative charge on HSA, i.e. the pI of HSA being 4.9, increase in pH resulted in higher negative charge on this protein. Higher pH values were not examined since these were not much practical interest from HSA bioseparation point of view. The next most abundant plasma protein from which HSA is required to be separated is human immunoglobulin G (HIgG) which has a pI of 7.0. Therefore at pH values greater than 7.0, both HSA and HIgG would be negatively charged and would bind to the membrane. In plasma protein fractionation the major goal is HSA/HIgG separation. The strategy for

separating these two proteins using an anion-exchange membrane would be to operate at a pH value at which only HSA is bound to the membrane.

Fig 5.4 shows the relative amounts of HSA bound at different pH values on the Q type 2 membrane. Between pH 6.0 and 7.0 the HSA binding increased with pH but did not increase any further when the pH was increased to 8.0. As with the Q type 1 membrane, the adsorptive gel material used to prepare the Q type 2 membrane was positively charged to similar extents at the different pH values examined. Hence the increase in HSA binding capacity with pH (between pH 6.0 and 7.0) was due to the effect of pH on net negative charge on HSA.

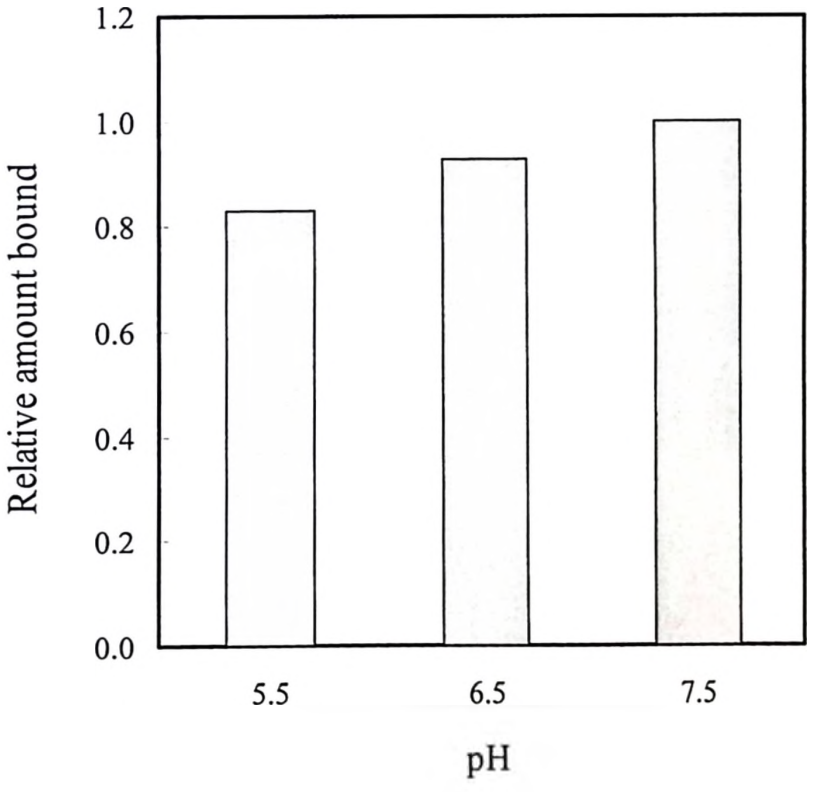

Figure 5.3 Effect of pH on relative HSA binding on Q type 1 membrane

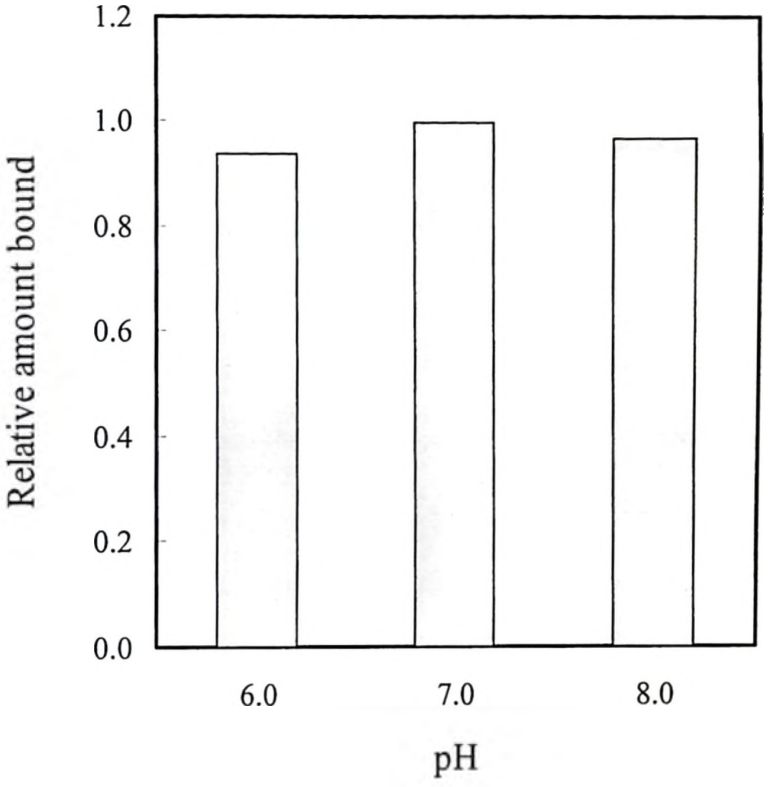

Figure 5.4 Effect of pH on relative HSA binding on Q type 2 membrane

5.4.2 Effect of ionic strength

Figures 5.5 and 5.6 show the effect of the ionic strength of the binding buffer on the relative HSA binding on Q type 1 and Q type 2 membranes respectively. All these experiments were carried out using a fixed flow rate of 7 ml/min. The HSA feed solutions (concentration = 20 kg/m^3) were prepared using the appropriate binding buffer. With both membrane types pulse volume of 5 ml was used. From Figures 5.5 and 5.6, it is evident that as ionic strength of the buffer was increased, the amount of HSA bound decreased.

Ionic strength of the binding buffer would be expected to affect protein binding in two ways. The negatively charged ionic species in the buffer would compete with the negatively charged HSA for binding sites on the membrane. The ionic species present in the buffer also have the capability to shield electrostatic interaction between the membrane and the protein, the rule of thumb being: the higher the ionic strength, the greater would the shielding be. However, at the relatively low ionic strength values examined here, the first mechanism would be expected to predominate as charge shielding usually takes place at very high ionic strengths. The results shown in Figures 5.5 and 5.6 could therefore be explained in terms of the increased competition for charged sites on the membrane at higher ionic strengths and the consequent lowering in protein binding capacity. Hence, 10 mM phosphate buffer was chosen as binding buffer for the subsequent experiments.

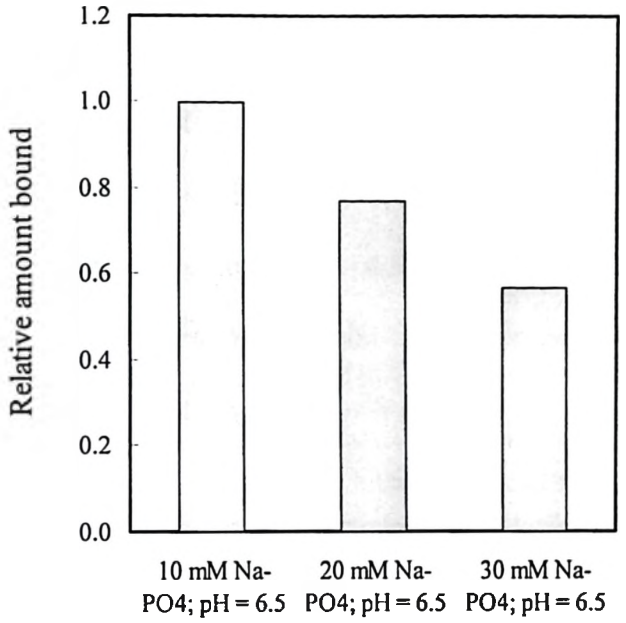

Figure 5.5 Effect of ionic strength on HSA binding on Q type 1 membrane

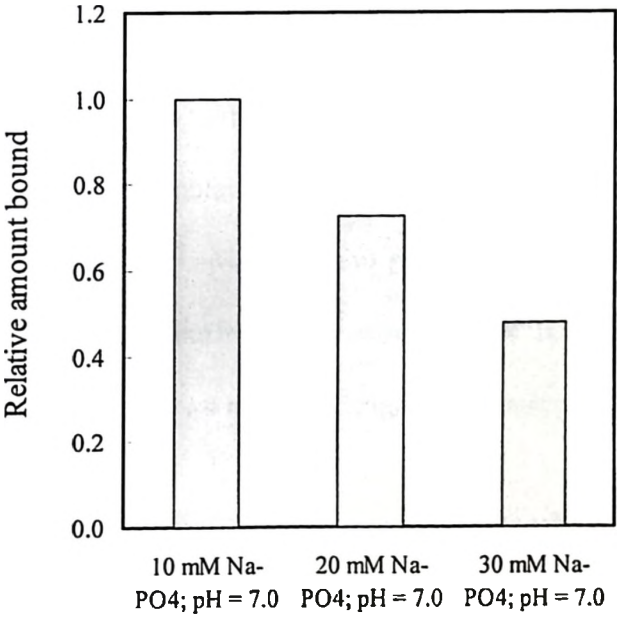

Figure 5.6 Effect of ionic strength on HSA binding on Q type 2 membrane

5.4.3 Effect of buffering ions

Figure 5.7 shows the effect of buffering ions (Phosphate and Tris) in the binding buffer on the relative amount of HSA binding on Q type 1 and Q type 2 membranes. Again, all the experiments were performed at pH 6.5 using a fixed flow rate of 7 ml/min. The HSA feed solutions (concentration = 20 kg/m^3) were prepared using the appropriate binding buffer. Both Q type 1 and Q type 2 membranes showed higher amount of HSA binding with tris buffer compared to phosphate buffer. This can be explained again with the help of charge on buffering ions. Tris ions carry the same positive charge as the quarternary ammonium ions on the gel matrices in the membrane while phosphate ions are negatively charged. Since phosphate ion carry a charge opposite to that of the functional groups of the gel matrices, they would compete with the negatively charged HSA for binding sites on the membrane. Hence, HSA binding would be lower with phosphate buffer compared to tris buffer. Even though tris buffer gave higher amount of HSA binding with both the membranes, phosphate buffer was chosen for subsequent separation experiments mainly because of natural presence of phosphate ions in human plasma. The use of phosphate buffer in the separation of HSA from HIgG would eliminate buffer exchange step before anion exchange membrane chromatography.

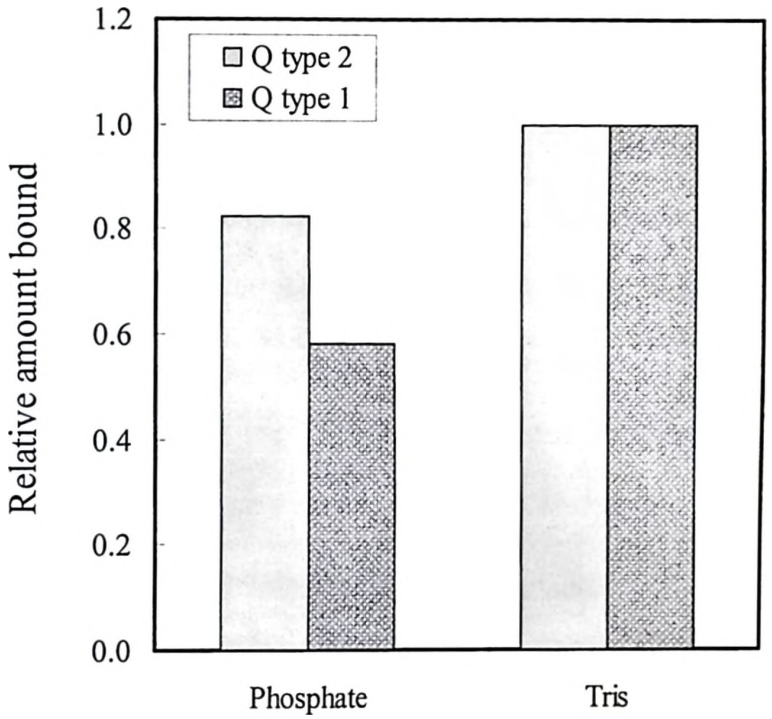

Figure 5.7 Effect of buffering ions on HSA binding on Q type 1 and 2 membranes

5.4.4 Effect of feed protein concentration

The effect of feed protein concentration on the relative amounts of HSA bound on the Q type 1 and Q type 2 membranes was examined by challenging the membranes with pulses of protein solutions of different concentrations. The sample volume of the pulse was varied in such a way so as to keep the total mass of protein injected in each experiment nearly constant (i.e. around 210 mg). This was achieved by timed sample injection from a 50 ml Superloop (Amersham Biosciences). Figure 5.8 shows the relative

amounts of protein bound on the Q type 1 membrane at different applied HSA concentrations. The HSA binding was found to be nearly the same at all the applied concentrations examined. These results indicate that in the concentration range examined, the amount of protein bound was independent of the protein concentration in the feed and dependent only on the amount of protein used to challenge the membrane. This is an attribute particularly useful for process design purposes. Figure 5.9 shows the relative amounts of protein bound on the Q type 2 membrane at different applied HSA concentrations. As with the Q type 1 membrane the HSA binding was found to be nearly the same at all the applied concentrations examined.

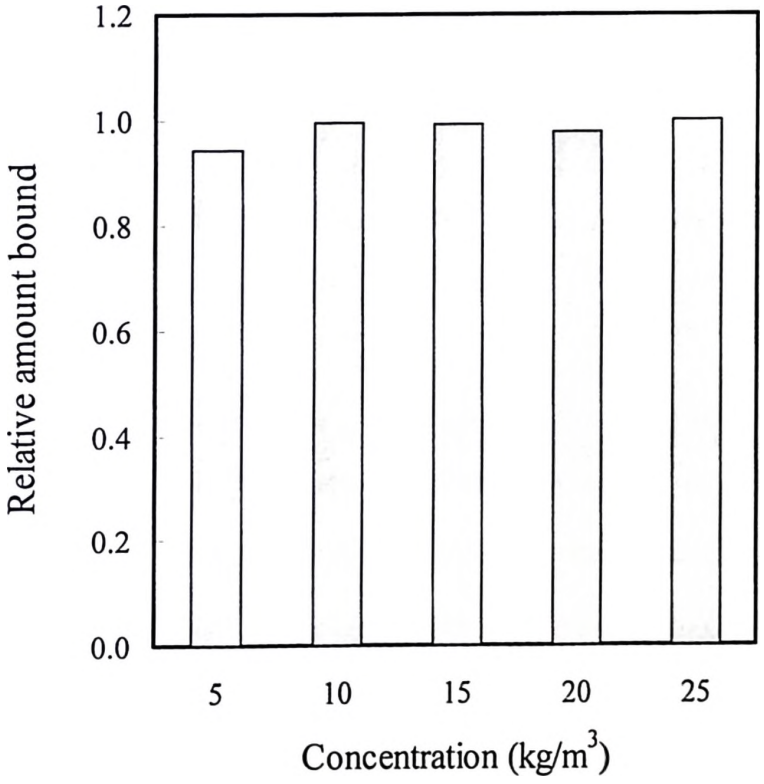

Figure 5.8 Effect of feed concentration on HSA binding on Q type 1 membrane

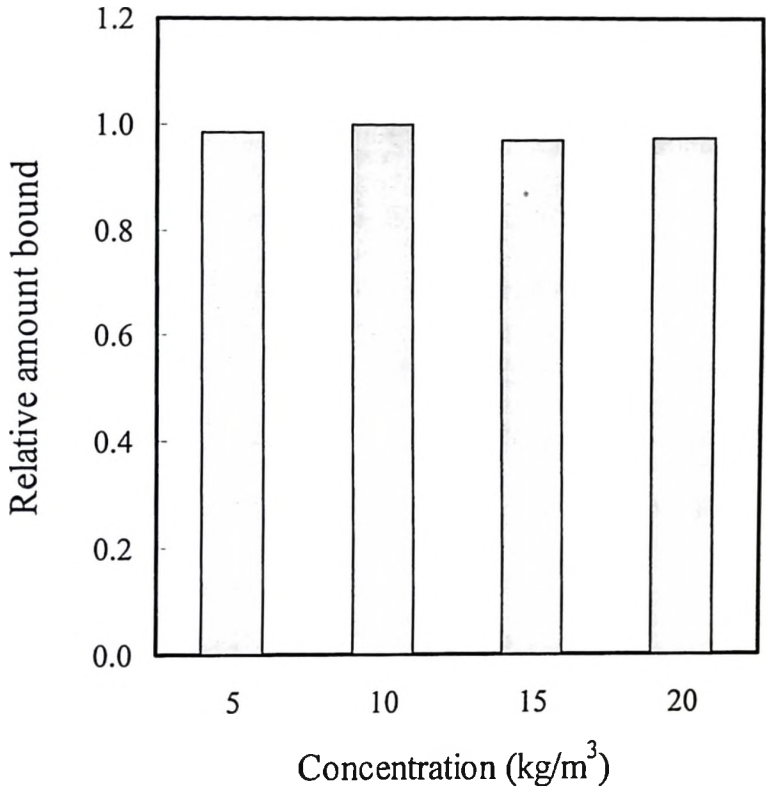

Figure 5.9 Effect of feed concentration on HSA binding on Q type 2 membrane

5.4.5 Effect of flow rate

High flow rate is one of the attractive features of membrane chromatography. This is particularly important from a productivity point of view. The effect of flow rate through the membrane stack on the relative amount of HSA bound was studied in the 3-11 ml/min range. For the Q type 1 membrane this flow rate range resulted in a bed residence time range of 7. 6 to 27.7 seconds while for the Q type 2 membrane which had a smaller bed volume, the corresponding range was 1.9 to 6.9 seconds. The HSA feed

solution (concentration = 20 kg/m^3) used in these experiments was prepared using 10 mM sodium phosphate buffer (pH 6.5). With Q type 1 membrane the pulse volume was 10.5 ml while with the Q type 2 membrane the pulse volume was 5 ml. Figures 5.10 and 5.11 show the relative amounts bound at different bed residence times on Q type 1 and Q type 2 membranes respectively. For the experimental ranges examined, the binding on both membranes were found to be independent of the bed residence time. Independence of the binding capacity on the flow rate meant that even at the lowest bed residence times examined in each case, a protein molecule in the feed would have the opportunity to reach a binding site during its sojourn in the membrane.

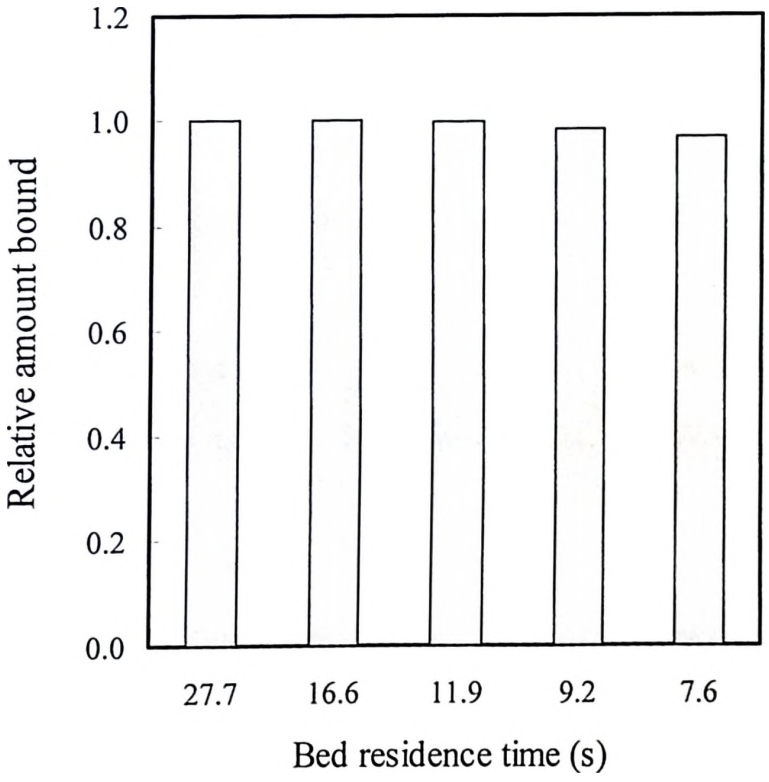

Figure 5.10 Effect of feed flow rate on HSA binding on Q type 1 membrane

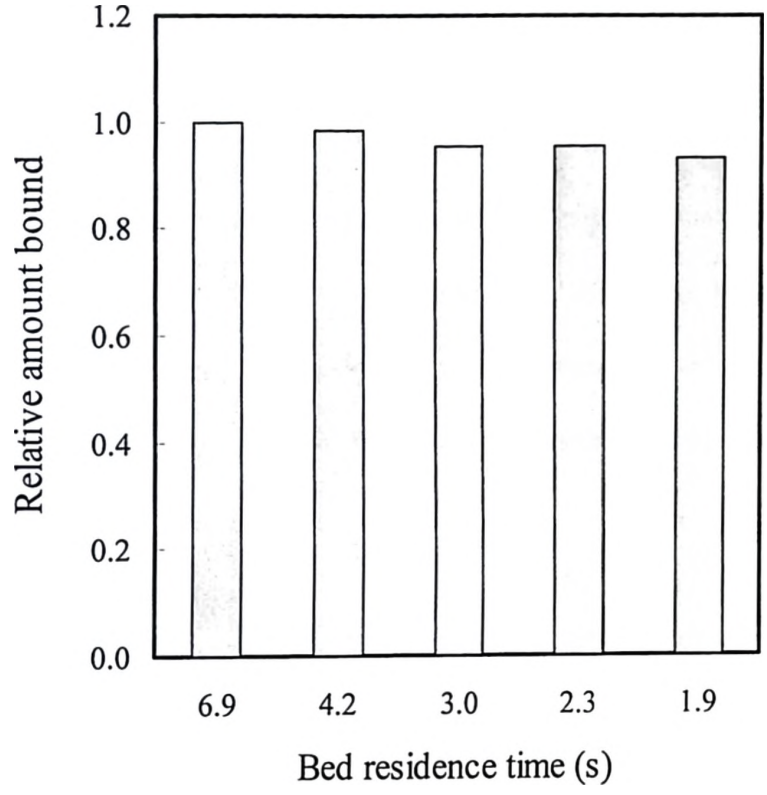

Figure 5.11 Effect of feed flow rate on HSA binding on Q type 2 membrane

The transport of a molecule across the chromatographic membrane is largely convective in nature. The average Reynolds number of the fluid flowing through the pores of membrane is given by:

$$\mathrm{Re}_{pore} = \left(\frac{u_s d_p}{\upsilon \varepsilon}\right) \tag{5.2}$$

The average pore diameter of the Q type 1 membrane was in the 0.3-0.4 micron range while that of the Q type 2 membrane was in the 0.15-0.20 micron range. The porosities of

Q type 1 and Q type 2 membranes were in the range of 0.60-0.65 and 0.5-0.55 respectively. For the flow rate range examined, the pore Reynolds number for both membranes were found to be very small i.e. in the $9.8\times10^{-6} - 8.8\times10^{-5}$ range. Therefore at all the flow rates examined in this study, the fluid flow through the membranes was laminar. In the laminar flow regime the pore centerline velocity is twice that of the average velocity of fluid in the pores. Based on this a characteristic convection time which is a measure of the minimum residence time of a molecule within a membrane disc can be obtained:

$$\theta_C = \frac{\delta_m \tau \varepsilon}{2u_s} \tag{5.3}$$

The average tortuosity of the membranes under consideration would be hard to estimate. However, even making the most conservative estimate for tortuosity, i.e. for $\tau = 1$, the characteristic convection times at a flow rate of 11 ml/min (which was the highest flow rate examined) was 2.27 s for Q type 1 membrane and 0.47 s for Q type 2 membrane.

In order for molecules to bind on a membrane these have to be transported from the fluid flowing through the membrane to the binding sites present on the membrane material. In the laminar flow regime, this transport which is radial relative to the pore is largely expected to be diffusive. Based on membrane and solute properties, a characteristic diffusion time, which is a measure of the maximum time it would take for a

molecule to diffuse from the pore centerline to the binding site on the pore wall can be defined:

$$\theta_D = \frac{d^2_{pore}}{4D} \tag{5.4}$$

If we assume the diffusivity of HSA to be around 6.1×10^{-11} m^2/s [14], then the θ_D value for the Q type 1 and Q type 2 membranes were 6.56×10^{-4} s and 1.64×10^{-4} s respectively. Thus even at the highest flow rate examined in this study, the protein molecules traveling through the pores of both types of membranes had sufficient time to reach the binding sites during their transit through the membrane. This explained why the HSA binding on both membranes were unresponsive to the flow rates through them.

The preceding analysis is best used for rigid membranes with well defined pores. For the gel-filled membranes discussed in this paper the actual values of the characteristic convection and diffusion times would be expected to be different from those mentioned in the previous paragraphs. However, given the huge difference between the characteristic convection and diffusion times for each membrane, the justification provided to the unresponsiveness of the HSA binding capacities towards flow rate would still be valid.

5.4.6 HSA breakthrough experiments

The dynamic HSA binding on the Q type 1 and 2 membranes were studied in the step input mode with 10 mM sodium phosphate buffer having pH 6.5 as a binding buffer at 7 ml/min flow rate. The objective of these experiments was to obtain HSA breakthrough curves with both membranes to determine the binding capacities of the membranes. These experiments were carried out using a custom designed 42 mm diameter module [7]. In the breakthrough experiments using both types of membrane the feed solution was 20 kg/m^3 HSA prepared in 10 mM sodium phosphate buffer (pH 6.5).

In the breakthrough experiments, the protein solutions were injected using a 50 ml Superloop (Amersham Biosciences). The UV absorbance of the effluent was continuously measured and from the data obtained, effluent concentration-effluent volume profiles (or breakthrough curves) were created using appropriate absorbance-concentration calibration for HSA. Figure 5.12 shows the breakthrough curve obtained with the Q type 1 membrane while Figure 5.13 shows the breakthrough curve obtained with the Q type 2 membrane. The cumulative amount of HSA bound on the membrane in each case was calculated from the breakthrough curve using material balance. A hydraulic correction factor was applied to correct for the void volume of the system. Table 5.3 shows the incipient, and 1% breakthrough binding capacities of the gel-filled membranes along with their saturation binding capacities. The incipient breakthrough binding capacity corresponded to when the HSA first appeared in the effluent while the 1% value corresponded to when the effluent protein concentration was 1% of the feed

concentration. The saturation binding capacity was determined from the area under the curve of the eluted HSA peak based on appropriate calibration for this protein. These binding capacities were calculated based on the dry thickness of these membranes. The Q type 1 membrane did not swell appreciably in the wet state and hence the dry and wet basis binding capacities for this membrane would be similar. However the Q type 2 membrane swelled quite significantly and hence for calculating the effective binding capacity on the wet basis the 40% increase in membrane volume should be taken into account.

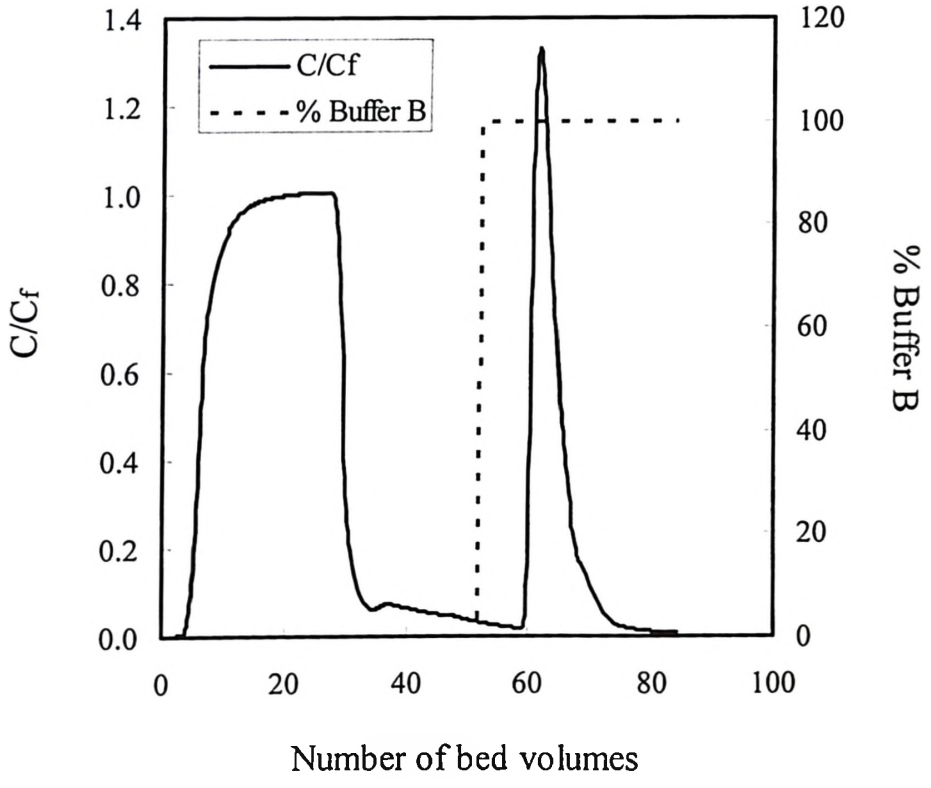

Figure 5.12 HSA breakthrough on Q type 1 membrane

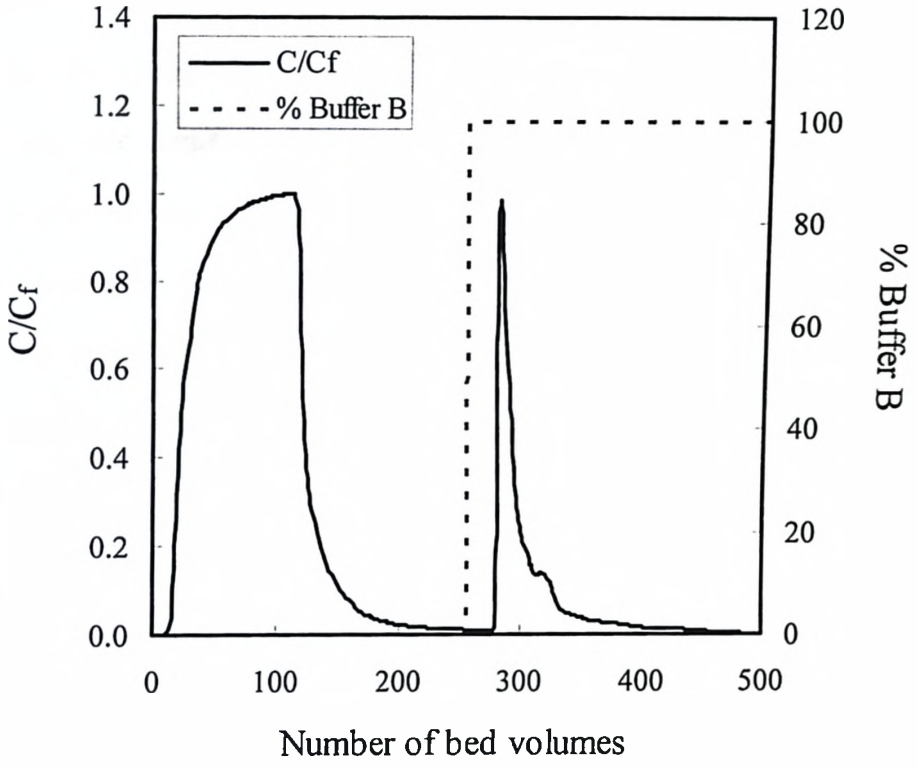

Figure 5.13 HSA breakthrough on Q type 2 membrane

Table 5.3 HSA binding capacities of the gel-filled membranes

Membrane	Binding capacity (mg/ml)		
	Incipient breakthrough	1% breakthrough	Saturation
Q type 1	66.7	78.3	113
Q type 2	223.0	260.3	299.8

From a comparison of these binding capacities with data shown in Table 5.1, it is evident that the Q type 1 and 2 membranes bound considerably more protein than currently available commercial membranes. Gebauer et al. [15] have reported a human serum albumin binding capacity in the range of 31 mg/ml using a DEAE/CM ion-exchange membrane. Branovic et al. [16] have reported an HSA binding value of 32 mg/ml on a disc shaped QA monolith column. With currently available particulate chromatographic media the HSA binding capacity is in the range of 120 mg/ml [17]. As shown in Figure 5.14, the macroporous gel within the Q type 2 membrane almost entirely occupied the flow space within the support material generating a very high density of binding sites. With rigid membranes, the binding is limited to the surface of the pores and a significant amount of the flow space has no role in the binding process (also see Figure 5.14). Another factor which could potentially explain the increase in binding capacity is the shape of the binding surface. With a rigid membrane the binding surface on the pore walls is predominantly concave in nature while with the Q type 2 membrane the gel network is akin to a network of rod-like structures within a macropore and hence the binding surface is predominantly convex in nature. The binding of large molecules on a concave surface would be lower than that on a convex surface having the same area due to greater steric restrictions with the former.

With currently available membranes, the low protein binding capacities relegate membrane chromatography to niche applications such as capture of proteins from dilute solutions or for removal of specific impurities such as endotoxins. The development of

high-capacity membranes such as those discussed in this chapter would enable the use of membrane chromatography for more mainstream bioseparation applications such as plasma protein fractionation and other similar separations.

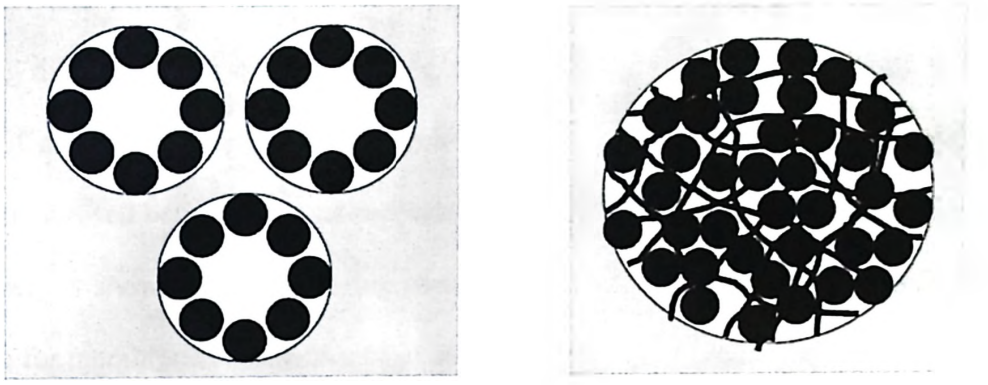

Figure 5.14 Comparison of protein binding on conventional rigid porous membrane with that on the macroporous gel-filled membrane

5.4.7 Performance comparison of membrane modules

Membrane module design is an important aspect of membrane chromatography. Feed flow distribution at the module inlet and effluent collection at the module outlet are critical for the efficient use of membrane binding capacity. Conventional module design has inlet and outlet in the form of a small circular channel with tapering at the end opening directly in to a space having significant larger circular cross-sections housing the stack of adsorptive membranes. In such design, the stack of adsorptive membranes is normally housed between porous supporting discs for certain degree of flow equalization. However, as shown in the following paragraph, such conventional module design is not enough for membrane chromatographic applications.

Figure 5.15 shows the performance comparison of a custom designed membrane module with that of the conventional module with Q type 1 membrane. The specifics of flow distribution at the inlet and outlet of custom designed module are discussed somewhere else [7]. In both modules, a stack of four Q type 1 membranes were housed in between three glass fiber prefilter discs on each side. These experiments were performed with 10 mM sodium phosphate having pH 6.5 as a binding buffer at flow rate 7 ml/min. The feed solution was 10 kg/m^3 HSA prepared in the binding buffer. It is quite evident from Figure 5.15 that the custom designed module gave much sharper breakthrough compared to conventional design. Table 5.4 shows the incipient and 1% breakthrough binding capacities in terms of membrane bed volume for both the modules. The new module design gave significant improvement in membrane binding capacity utilization

over conventional design. This can be attributed to more timely utilization of peripheral regions of the membrane with respect to central region of the membrane. It can be made possible by making solute flow path length within the new module design more uniform. Module design becomes more critical in scale up involving larger radial dimension compare to axial dimention.

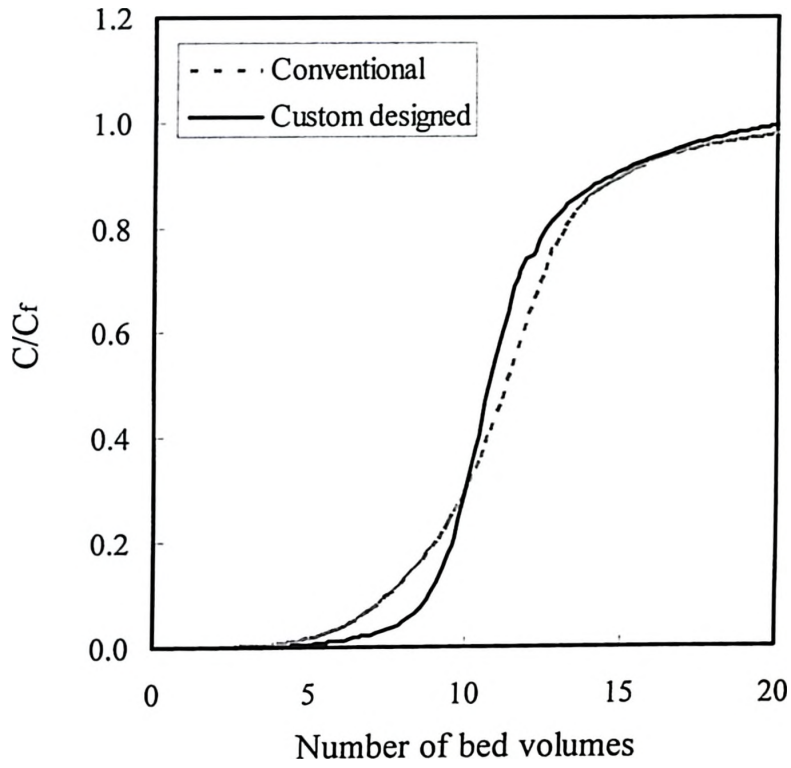

Figure 5.15 HSA breakthroughs on Q type I membrane with custom designed membrane module and the conventional module

Table 5.4 Performance comparison of custom designed membrane module with that of the conventional module

Module	Binding capacity (number of bed volumes)	
	Incipient breakthrough	1% breakthrough
Conventional design	2.8	4.5
Custom designed	4.6	5.8

5.4.8 Dynamic adsorption isotherm

Dynamic adsorption isotherm was studied in step input mode for Q type 2 membrane only. Since Q type 2 membrane showed very high HSA binding capacity, this study was carried out using a small membrane module with 10 mm effective membrane diameter. 10 mM sodium phosphate having pH 5.5 was used as a binding buffer. All the experiments in this study were carried out at 0.5 ml/min flow rate. In each experiment, feed protein solution (prepared in binding buffer) was passed through the membrane till the effluent concentration reached the feed concentration and remained stable. The saturation membrane binding capacity was then evaluated from the area under the UV curve of the eluted HSA peak based on appropriate calibration. Figure 5.16 shows the double reciprocal plot of bound HSA concentration (q) versus feed HSA concentration (C_f). The good linear data fit indicates that the adsorption of HSA on the membrane

follows a Langmuir type adsorption isotherm. From linear regression data of the double reciprocal plot, the maximum binding capacity at pH 5.5 is predicted to be 294 mg/ml.

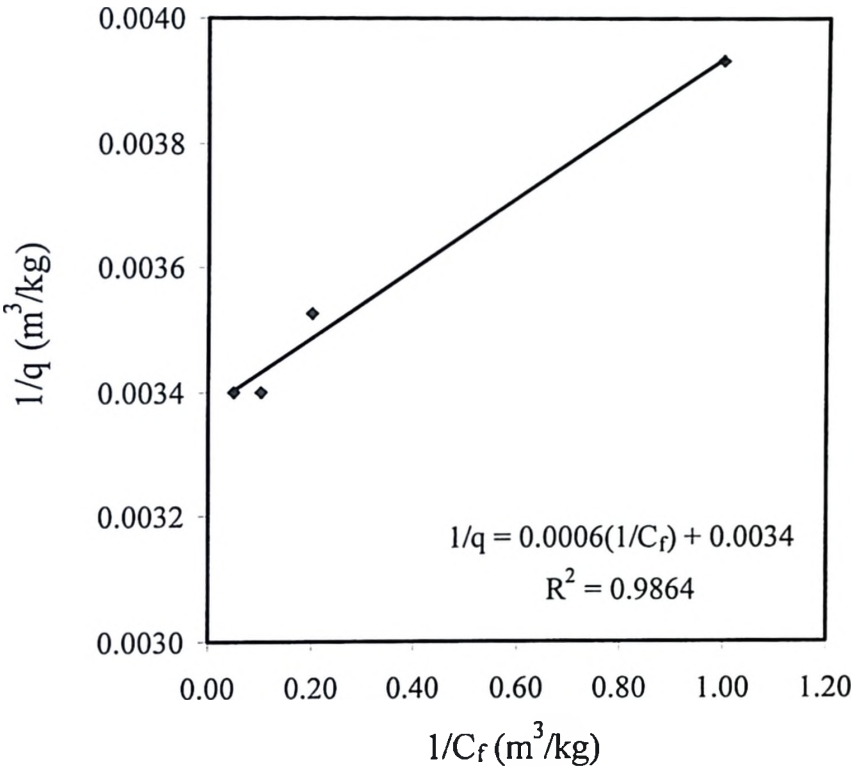

Figure 5.16 Double reciprocal plot of bound concentration versus feed concentration under saturating conditions. This plot demonstrates that HSA binding on the Q type 2 membrane follows Langmuir adsorption isotherm

5.4.9 Non-specific binding

Non-specific binding on both Q type 1 and Q type 2 membranes were studied by challenging the membranes with pulses of 10 kg/m^3 HIgG protein solutions prepared in 10 mM phosphate buffer having pH less than the pI of HIgG. Table 5.5 shows the amount of HIgG bound on both membranes at two pH values, both less than its pI. All the experiments were carried out at a fixed flow rate of 7 m/min with the pulse of 2 ml protein solution. It is evident from the Table 5.5 that both membranes bound some amount of HIgG at even pH 5.0 which is significantly less than its pI. At pH 5.0, HIgG is expected to carry net positive charge and hence should not bind to the membrane due to electrostatic interactions. Q type 1 membrane showed less amount of non-specific binding compared to Q type 2 membrane at both pH but then the binding capacity of Q type 1 membrane is significantly less than that of Q type 2 membrane. As pH of HIgG solution increased from 5.0 to 6.5, the amounts of HIgG bound to both membranes have also increased. This could be explained in terms of reduced net positive charge on HIgG at pH 6.5 compared to pH 5.0.

Table 5.5 Non-specific binding on gel-filled macroporous membranes

pH	Binding capacity (mg/ml)	
	Q type 1	Q type 2
5.0	0.47	3.90
6.5	2.30	9.60

5.4.10 HSA-HIgG separation

Figure 5.17 shows the separation of a simulated feed solution prepared by mixing 151.80 mg of HSA with 39.45 mg of HIgG in 15 ml of feed solution i.e. in nearly a 4:1 ratio, this being the actual ratio of these proteins in human plasma. A pH value of 5.5 has been identified by Gebauer et al. [15] as being suitable for plasma protein fractionation since at this pH HSA having a net negative charge would bind to an anion-exchange membrane while HIgG, the other major protein present in human plasma having a net positive charge would not bind to the same membrane. This pH was maintained using 10 mM sodium phosphate buffer since buffers with higher molarities result in lower HSA binding. A flow rate of 7 ml/min was selected for separation since it gave a high productivity at a reasonably low pressure drop. The primary flow-through peak which was obtained between 10 ml and 31 ml effluent volume was largely due to the unbound HIgG while secondary flow-through peak that was obtained between 36 ml to 70 ml effluent was due to the excess feed i.e. consisted of both HSA and HIgG. Feed, flow-through and eluted HSA samples were collected and analyzed by affinity chromatography and SDS-PAGE.

Figure 5.18 shows the affinity chromatograms obtained with the feed, flow-through (collected around 10 ml effluent volume) and the eluted HSA peak. The first peak on these chromatograms (corresponding to 1.2 minute) was due to HSA (which did not bind to the r-protein A column) while the second peak was due to HIgG. The feed solution contained 79.3% HSA while the eluted peak contained 97.3% HSA. Hence there

was significant enrichment of the albumin. The United States Pharmacopoeia specifies a purity requirement of >96% for therapeutic grade human albumin. The presence of some HIgG in the eluted peak indicates limited amount of non-specific protein (i.e. HIgG) binding. However, the extent of this was not enough to affect the HSA purity very significantly. The flow-through sample was largely free from albumin suggesting that high recovery rates were feasible.

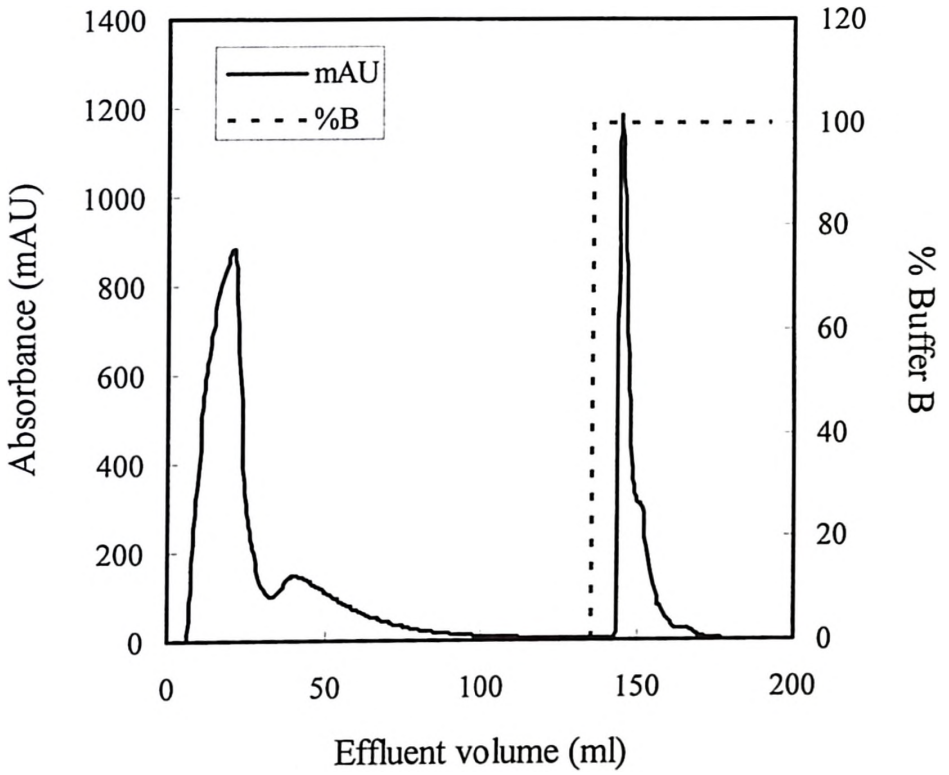

Figure 5.17 Separation of HSA and HIgG using Q type 2 membrane (flow rate: 7 ml/min; diameter of membrane disc: 42 mm; number of discs: 1; feed: 10.12 kg/m^3 HSA + 2.63 kg/m^3 HIgG; binding buffer: 10 mM sodium phosphate; pH5.5; eluting buffer: 1 M NaCl)

Figure 5.19 shows the stained SDS-PAGE results obtained with the feed, flow-through and the eluted peak samples. Two flow-through samples were collected in the separation experiment, the first around 10 ml effluent volume and the second around 40 ml effluent volume. The eluted peak showed one band indicating highly pure HSA. The first flow-through sample contained only HIgG while the second flow-through sample had a composition largely similar to that of the feed. In this separation experiment, the amount of HSA injected into the membrane module was in excess of its binding capacity. By the time the second flow-through sample was collected the HSA binding capacity of the membrane was saturated and excess HSA appeared in the flow-through. The separation results clearly indicate the suitability of using the Q type 2 membrane for plasma protein fractionation.

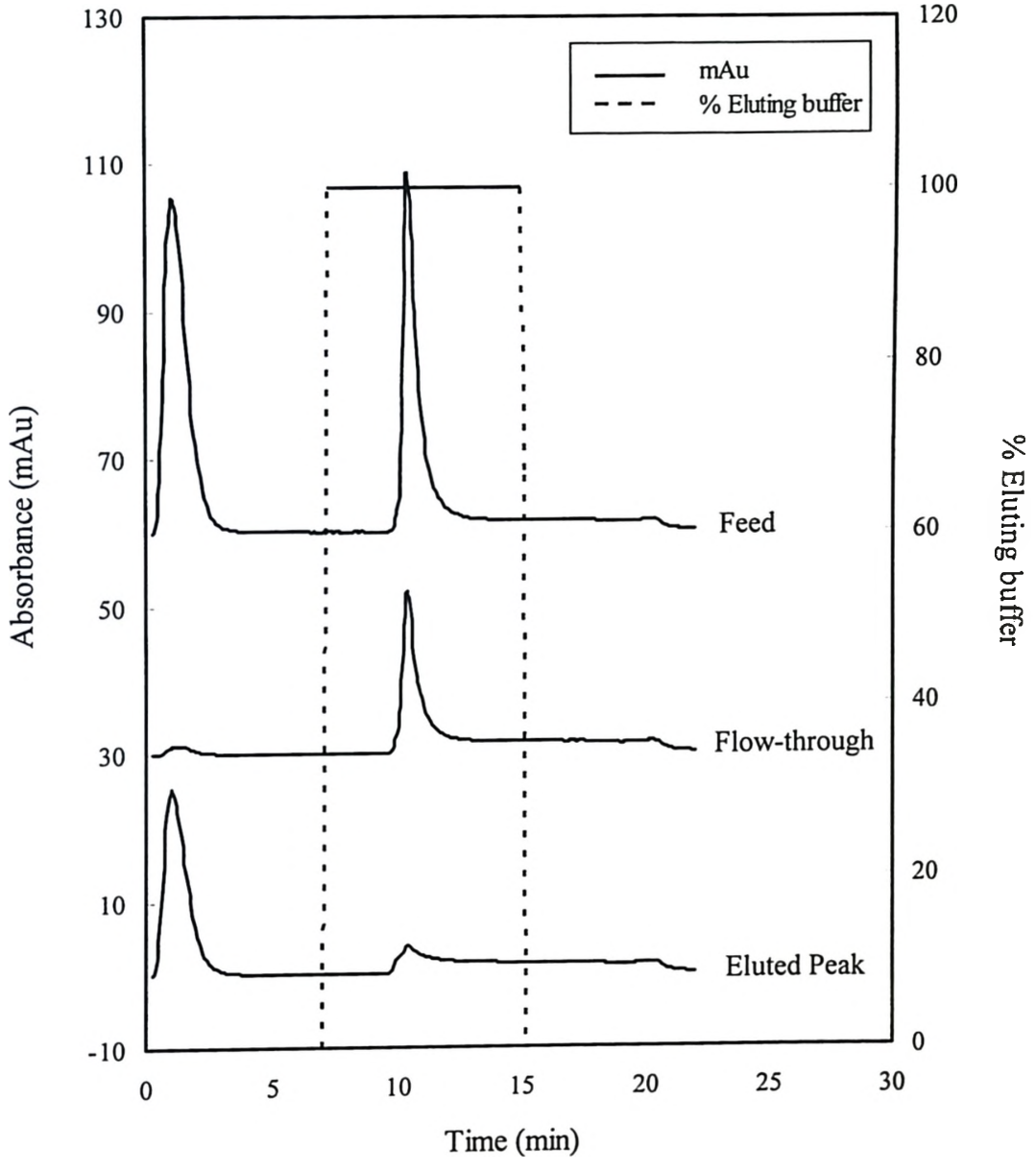

Figure 5.18 Affinity chromatograms obtained with feed, flow-through and eluted peak samples from HSA/HIgG separation using Q type 2 membrane (peak 1: HSA and peak 2: HIgG)

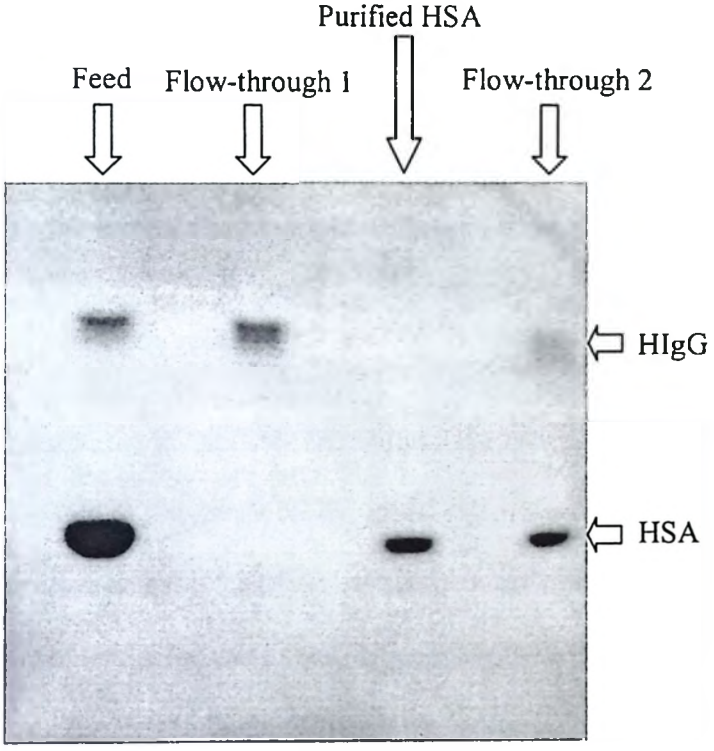

Figure 5.19 Non-reducing SDS-PAGE (10%) obtained with feed, flow through and purified HSA samples

5.5 Conclusions

The gel-filled anion-exchange membranes gave significantly higher HSA binding capacities (113 mg/ml for the Q type 1 and 299 mg/ml for the Q type 2 membrane, based on saturation binding capacities) when compared with commercial rigid adsorptive membranes as well as particulate chromatographic media. This was mainly due to the higher density of binding sites possible with the macroporous gel-filled membranes. Also

when compared with rigid adsorptive membranes, the gel-filled membrane had a higher proportion of convex binding surface. This resulted in less steric hindrance to HSA binding. Within the operating range, the binding capacities increased with increase in pH, this being due to the increase in net negative charge on the protein. The ionic strength of the binding buffer also had an effect on the binding capacity, the higher the ionic strength, the lower being the binding. This was due to the tendency of the buffer ions to competitively bind to the membrane. Tris buffer gave better binding capacities with both membranes compared to phosphate buffer. In the experimental ranges examined, the feed protein concentration and the feed flow rate did not have any effects on the amount of HSA bound. The potential for using the Q type-2 membrane for plasma fractionation was demonstrated by HSA/HIgG fractionation, these being the two major plasma proteins. Using the Q type 2 membrane the HSA concentration could be enriched from 79.3% to 97.3%. This demonstrated the suitability of using this membrane for plasma fractionation.

5.6 References

1. S. Brandt, R.A. Goffe, S.B. Kessler, J.L. O'Connor, S.E. Zale, Membrane-based affinity technology for commercial scale purifications, BioTechnology, 6 (1988) 779.
2. T.M. Przybycien, N.S. Pujar, L.M. Steele, Alternative bioseparation operations: life beyond packed-bed chromatography, Curr. Opin. Biotechnol., 15 (2004) 469.
3. R.V. Reis, A. Zydney, Membrane separations in biotechnology, Curr. Opin. Biotechnol., 12 (2001) 208.

4. W. Demmer, D. Nussbaumer, Large-scale membrane adsorbers, J. Chromatogr. A, 852 (1999) 73.
5. T.N. Warner, S. Nochumson, Re-thinking the economics of chromatography – new technologies and hidden costs, Biopharm Int., 16 (2003) 58.
6. R. Ghosh, Protein separation using membrane chromatography: opportunities and challenges, J. Chromatogr. A, 952 (2002) 13.
7. R. Ghosh, Membrane adsorption module, Canada Patent Application No. 2,463,386 (2004).
8. R. Ghosh, T. Wong, Effect of module design on the efficiency of membrane chromatographic separation processes, J. Membr. Sci., 281 (2005) 532.
9. I. Koguma, K. Sugita, K. Saito, T. Sugo, Multilayer binding of proteins on polymer chains grafted onto porous hollow-fiber membranes containing different anion-exchange groups, Biotechnol. Prog., 16 (2000) 456.
10. K. Tomomi, K. Saito, W. Lee, Protein binding to polymer brush based on ion-exchange, hydrophobic, and affinity interactions, J. Chromatogr. B, 790 (2003) 131.
11. M. Ulbricht, H. Yang, Porous polypropylene membranes with different carboxyl polymer brush layers for reversible protein binding via surface-initiated graft polymerization, Chem. Mater., 17 (2005) 2622.
12. R.F. Childs, A.M. Mika, J. Zhou, E. Komkova, T. Dey, R. Ghosh, C. Filipe, Composite materials comprising supported porous gels, US and PCT Patent Applications PCT/CA2004/000120 (2004).

13. M.M. Bradford, Rapid and sensitive method for quantitation of microgram quantities of proteins utilizing principle of protein-dye binding, Anal. Biochem., 72 (1976) 248.

14. D.E. Raymond, A. Manz, H.M. Widmer, Continuous separation of high molecular weight compounds using a microliter volume free-flow electrophoresis microstructure, Anal. Chem., 68 (1996) 2515.

15. K.H. Gebauer, J. Thommes, M.R. Kula, Plasma protein fractionation with advanced membrane adsorbents, Biotechnol. Bioengr., 54 (1997) 181.

16. K. Branovic, A. Buchacher, M. Barut, A. Strancar, D. Josic, Application of monoliths for downstream processing of clotting factor IX, J. Chromatogr. A, 903 (2000) 21.

17. A. Staby, I.H. Jensen, I. Mollerup, Comparison of chromatographic ion-exchange resins I. Strong anion-exchange resins, J. Chromatogr. A, 897 (2000) 99.

Chapter 6

Membrane Fouling during In-line Protein Microfiltration Processes

Part of this work will be submitted for publication tentatively titled 'Reversible and irreversible membrane fouling during in-line microfiltration of concentrated protein solution' to Journal of Membrane Science by Dharmesh M. Kanani, Xinghua Sun and Raja Ghosh.

6.1 Abstract

In-line microfiltration which is widely used for sterilization of therapeutic proteins prior to formulation is normally operated at constant flux by pumping purified protein solution through a membrane. Increase in trans-membrane pressure (TMP) due to

membrane fouling is a major problem in such processes. This study examines how resistance to filtration increases during in-line microfiltration processes. The TMP was found to increase in three distinct phases, each characterized by its own rate and extent of reversibility. A significant portion of TMP increase was found to be reversible upon front washing with buffer without any kind of physical or chemical cleaning. There was no evidence of concentration polarization in the process studied. Size exclusion chromatographic analysis of front wash sample suggested BSA monomer as the major foulant accountable for the reversible portion of fouling. Aggregate free protein solutions prepared by pre-filtration showed negligible membrane fouling. We hypothesize that trace amount of protein aggregates present in untreated feed solutions were responsible for initiating membrane fouling. However, the actual fouling was caused by the protein monomer which was sequestered on and within the membrane by association with the retained aggregates. The nature and location of the foulant on and within the membrane were examined by confocal microscopy. The deposition of the foulant was found to be restricted to a zone very close to the membrane surface. Effects of different parameters on membrane fouling were studied. Few intermittent protein filtration experiments were carried out in an effort to gain better insight in the membrane fouling process and to identify new strategies for conducting in-line microfiltration that would maximize the throughput.

6.2 Introduction

Microfiltration (MF) membranes are widely used in biopharmaceutical industry to carry out size based solid-liquid separations. They have found many applications in bioseparation of protein biopharmaceuticals ranging from clarification of suspensions to sterilization of final products [1-2]. MF membranes are used in the cross-flow mode for clarification type applications such as separation of cells or cell debris. Cross-flow or tangential flow reduces the build up of particulate matter near the membrane surface and thereby reduces resistance to flow through the membranes. In sterilization processes, however MF membranes are used in the dead-end mode to remove trace amounts of particulate matter such as bacterial or virus contaminations and protein aggregates formed in previous separation steps. Dead-end mode is preferred in the sterilization processes since the amount of particulate matter in the feed is very low. Cross-flow filtration can induce denaturation of proteins which may promote aggregation and hence loss of yield [3-4].

Syringe filters at laboratory scale and in-line filters at processing scale are commonly used for dead-end microfiltration of protein solutions. One of the major reasons for their popularity is their disposable nature which facilitates process validation and flexible manufacturing. They are normally operated at constant flux by pumping the feed solution at constant flow rate. In a constant flux process membrane fouling may cause the required transmembrane pressure (TMP) to increase significantly making it difficult to sustain the filtration process any further. Protein based membrane fouling is

caused by the deposition of proteins on the membrane surface or inside the membrane pores. This can happen even when the pore size is an order of magnitude greater than the size of protein molecule. Protein fouling is a complex phenomenon which is hard to model due to its dependence on a large number of parameters [2]. These parameters can be classified into three general categories: a) membrane material properties such as pore size, porosity, hydrophilicity, surface charge and surface topography, b) solution properties such as pH, salt concentration, amount of protein denaturation and aggregation and c) process parameters such as temperature, trans-membrane pressure and shear rate near the membrane surface. In the literature, both protein adsorption on membranes under static conditions [5-7] and protein deposition (or membrane fouling) under dynamic conditions [6-7] have been reported. Studies in static condition indicated that proteins were adsorbed as monolayer and this caused relatively small increases in membrane resistance while studies under dynamic conditions showed significantly greater increase in membrane resistance due to the deposition of proteins in the form of multi-layers. However, there is still a lack of agreement in the literature regarding the location of protein deposits and the rate of deposition during MF processes [7].

Protein fouling of MF membranes has been extensively studied and reported. However, there are relatively few systematic studies on protein fouling in the dead-end mode. Most of the earlier studies on fouling of MF membranes were carried out at constant pressure using stirred cell type devices which are fundamentally different from either syringe type or in-line filters [8-12]. In such processes, flux decreases over a period

of time due to fouling. In some of these studies the experimental data was modeled using either one of the four classical fouling models or combination of these: 1) complete pore blockage, 2) intermediate pore blockage, 3) pore constriction and 4) cake filtration. The complete pore blockage model assumes that each particle depositing on the membrane surface can perfectly plug one pore and there would be no flow through the blocked pore. The intermediate blocking model has similarities with the complete pore blockage model but it also accounts for the superimposition of particles. The pore constriction model assumes that the pore diameter could be reduced by the deposition of particles inside the pores. The cake filtration model assumes the deposition of particles on the membrane surface in the form of a growing permeable cake. Hlavacek and Bouchet [13] have developed mathematical formulations for different blocking laws for constant flux filtration processes and have checked their applicability to dead-end MF of protein solutions. They quantified the fouling through the use of a clogging coefficient (which characterize the physico-chemical conditions during an experiment) and the membrane porosity and found that the intermediate pore blockage model fit their data best. Whereas Bowen and Gan [6] explained the decreasing flux in constant pressure protein microfiltration using a standard blocking law. Many studies have clearly pointed out the inability of individual models in explaining the flux decline data for the full course of protein filtration experiments. To account for the change in fouling mechanism over the experimental range, some researchers have come up with combined models [14-16]. The combined model by Ho and Zydney [14] shows smooth transition from pore blockage to cake filtration and gives good fit with the flux decline data for BSA filtration through

polycarbonate track etched membranes. It can also accommodate the effects of membrane morphology but becomes numerically complex due to the use of four fitted parameters for homogeneous or composite membranes [17]. The combined models proposed by Bolton et al [15] are numerically simpler and easier to implement due to the use of two fitted parameters but physically less detailed. All these models provide better understanding of membrane fouling and serve as prediction tools for successful scale-up or scale-down of MF systems. However they do not tell anything about the severity of fouling or the extent of cleaning required to restore the flux.

This chapter discusses protein fouling of MF membranes in in-line filter holder at constant flux. It identifies three phases of membrane fouling, each characterized by its own rate constant and assesses the severity of fouling in terms of apparent reversible and irreversible fouling. The different mechanisms of protein fouling of microfiltration membranes are identified. The nature and location of the foulant is examined by size exclusion chromatography and confocal laser scanning microscopy. Effects of front washing and intermittent protein filtration on membrane performance are examined.

6.3 Experimental

6.3.1 Materials

Bovine serum albumin (BSA) (Catalog # A7906) was purchased from Sigma. BSA has molecular weight of 67 kDa, an iso-electric point (pI) of 4.8 and a stokes radius

of 3.48 nm. Alexa Fluor 488 conjugated BSA (Catalog # A13100) was purchased from Invitrogen Canada Inc. It contains 8 moles of dye per mole of BSA. Alexa 488 has fluorescence excitation and emission maxima 497 and 520 nm respectively. Fluorescence of the Alexa Fluor 488 fluorophore is independent of pH 4 to 10 and significantly brighter than fluorescein conjugates. Cellulose acetate membranes having pore size of 0.45 micron (Product # DS0210-4045) were brought from Nalgene Nunc International while 0.2 micron cellulose acetate membranes (Catalog # C020A047A) were purchased from Advantec MFS Inc. PVDF membranes with pore size of 0.22 micron (Catalog # GVWP 142 50) were brought from Millipore. All other laboratory chemicals were purchased from Sigma. 25 mM sodium phosphate buffer (pH 4.8) was used for preparing BSA solutions for fouling studies. Buffer and all other solutions used in this study were prepared using high quality water (18.2 MΩ) obtained from a NANOpure Diamond Life Science (UV/UF) Ultrapure water purification system (Barnstead). Buffers were microfiltered before use. 70 kg/m^3 BSA solution was prepared in 25 mM sodium phosphate buffer and its pH was adjusted to 4.8 using 0.1 M HCl while stirring. This solution was centrifuged at 2900 rpm for 20 minutes and its protein concentration was accurately determined spectrophotometrically after proper dilution. The BSA stock solution was stored at 6-8 °C and used within 3-4 days after appropriate dilution with 25 mM sodium phosphate buffer (pH 4.8).

6.3.2 Protein microfiltration experiments

Figure 6.1 shows the schematic diagram of the experimental set-up used in this study. All microfiltration experiments were carried out with 13 mm stainless steel syringe filter holder (1980-001, Whatman) which was integrated with an AKTAprime plus system (GE Healthcare Life Sciences) as shown in Figure 6.1. The membrane disc housed inside the syringe filter holder had 10 mm effective diameter. AKTAprime plus system is a compact unit with a pump, sample injector valve, UV flow cell, conductivity flow cell and pH flow cell with the electrode. The pressure at the upstream of membrane surface was continuously monitored using a pressure sensor (GBS-BTA, Vernier Software & Technology) connected to a computer through an interface. Downstream pressures (or back-pressure) at different flow rates were found out by doing dummy experiments with the same set-up but without a membrane disc inside the module. Absorbance-concentration calibration for BSA was created for the UV flow cell of AKTAprime plus system by pumping different concentration of BSA solution straight from sample injector valve to UV flow cell without any membrane module or column.

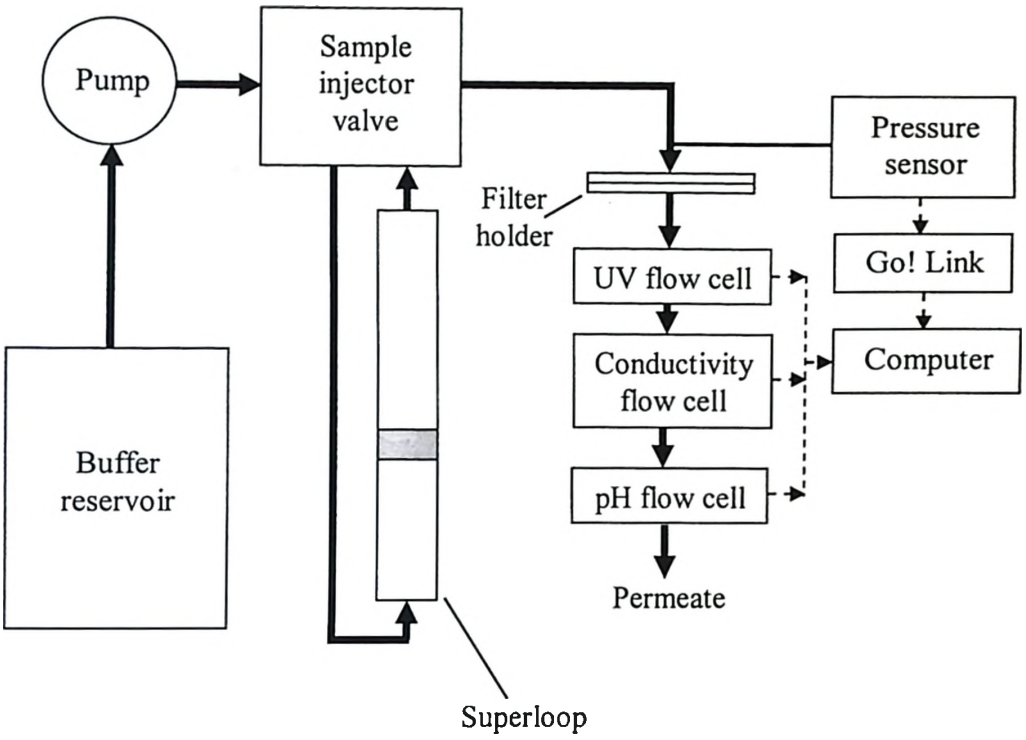

Figure 6.1 Schematic diagram of experimental set-up

Each experiment was carried out with a new membrane disc. The membrane disc was wetted by keeping it in deionized water for few minutes before placing inside the module. Thorough care was taken to avoid any air bubbles in the flow path or filter holder while integrating the syringe filter holder with AKTAprime plus system. Each experiment was started with buffer filtration at constant flux (8.49×10^{-4} m/s) for 10 ml to get the idea about the permeability of the new membrane disc and steady TMP baseline. The pump of AKTAprime plus system drove buffer from the reservoir to the filter holder through the sample injector valve. Protein filtration was carried out at constant flux

(8.49×10^{-4} m/s) by switching the sample injector valve from load to inject position thereby putting the superloop filled with protein solution (50 ml capacity) in the flow path. The superloop therefore served as a reservoir from which protein solution was delivered to the membrane module at constant flow rate. It should be noted that protein solution was pumped through the membrane directly from superloop without actually passing through the pump. After protein filtration, buffer filtration was again continued through the fouled membrane disc for 20 ml in the same flow direction to measure the permeability of fouled membrane disc. Therefore in each experiment (except one specific experiment), the buffer filtration-protein filtration-buffer filtration sequence was carried out in continuous manner without stopping the pump or dismantling the module. In this specific experiment, the aim was to collect the front wash (buffer filtration after protein filtration) sample for size exclusion chromatography (SEC) analysis. In this particular experiment, the pump was stopped after protein filtration and membrane module was dismantled to remove all the protein solution from the connecting lines as well as module. Before cleaning the module and all the connecting lines with 25 mM sodium phosphate buffer, membrane disc was taken out of the module along with the supporting disc. The membrane disc was dipped few times in water to remove the protein solution from the membrane surface and its supporting disc before mounting back into the module and carrying out buffer filtration (or front washing). This exercise was done to make sure that front wash sample contained only proteins dislodged from the membrane disc. Only initial approximately 0.7 ml of sample was collected during the front washing fearing the

possible dilution of sample upon further collection. All the experiments in this study were carried out at ambient temperature (23±2 °C).

In order to determine the location of deposited proteins on fouled membrane disc (whether internal or external), few protein filtration experiments were carried out using 10 kg/m^3 BSA solution spiked with 0.005 kg/m^3 Alexa Fluor 488 conjugated BSA using the above filtration protocol. Alexa Fluor 488 conjugated BSA solution was prepared in 25 mM sodium phosphate buffer just before the experiment. It was microcentrifuged before mixing with 10 kg/m^3 untagged BSA solution in order to remove any protein aggregate formed during the storage. After the filtration experiments, membrane discs were carefully taken out of the module and viewed under confocal scanning laser microscope.

6.3.3 SEC analysis of protein samples

The front wash, feed and permeate (or filtrate) samples were analyzed for the presence of BSA dimmers, and higher aggregates by SEC using an HPLC system (Varian Inc., Canada) with a high performance gel filtration column, Superdex 200 10/300 GL (GE Healthcare, USA). This column can separate globular proteins with size ranging from 10 kDa to 600 kDa (size equivalent to aggregate of 9 BSA monomers) with exclusion limit of 1300 kDa (size equivalent to aggregate of 20 BSA monomers). Its void volume was determined by Blue dextran with molecular weight of 2000 kDa. 50 mM

sodium phosphate buffer containing 150 mM NaCl with pH 6.9 was used as a mobile phase. All the samples were centrifuged at 10000 rpm for 10 minutes before loading into the column to remove bigger protein aggregates and particles which may otherwise clog the column. Protein concentration of each sample was measured spectrophotometrically at 280 nm both before and after centrifugation to keep the track of protein loss during centrifugation. 100 µl of centrifuged sample was injected for chromatographic analysis which was carried out at 0.2 ml/min mobile phase flow rate. The effluent was monitored at 280 nm wavelength.

6.3.4 Confocal laser scanning microscopy

A confocal microscope (Carl Zeiss LSM 510, Germany) was used to examine the membranes fouled with BSA solution spiked with Alexa 488 conjugated BSA. The fouled membrane discs were cut to the appropriate size and viewed in fluorescence mode from the upstream side with 488 nm laser wavelength using 50% glycerol as mounting medium. A stack of through-focus images were obtained by optical sectioning of the membrane and these images were then used to obtain the z-projection. Protein deposition both on the membrane surface and inside the membrane pores was also examined by viewing membrane cross-sections with the confocal microscope. Membrane cross-sections (5 µm wide) were obtained with a CM 3050S cryomicrotone (Leica, Austria) after coating the fouled membranes with tissue-tek O.C.T. (Sakura Finetek). The cross-sections were first viewed in reflection mode followed by fluorescence mode. These two images were then superimposed on each other to locate the deposition of proteins on the

membrane. In all cases, samples were magnified by a 63×objective, and zoom magnification was set at 2. The better-resolved confocal images of membranes were obtained by using high number of photons (scan speed - 8).

6.4 Results and discussion

Figure 6.2 shows TMP as a function of permeate volume during microfiltration of BSA solution at a constant volumetric permeate flux of 8.49×10^{-4} m/s. Steady TMP line during initial 10 ml of permeate volume corresponded to buffer filtration before protein filtration. It gave idea about the permeability of new membrane disc and confirmed the absence of any other foulant in buffer. Protein filtration was carried out from 10 to 26 ml of permeate volume after which buffer filtration was resumed and carried out for another 20 ml to estimate the permeability of fouled membrane disc. As can be seen from Figure 6.2, the TMP increased as soon as protein filtration was started and continued to increase over the entire course of protein filtration suggesting severe membrane fouling. The TMP increased in three distinct phases, each characterized by its own rate constant. The TMP increased slowly in phase I which lasted around 3-4 ml of permeate volume. The TMP then increased quite rapidly in phase II for another 2-3 ml after which in phase III the TMP increased at slower rate for the rest of protein filtration volume. Table 6.1 shows the fouling rate or rate of TMP increase during the three phases of protein microfiltration. Fouling rate was much higher in phase II compared to phase I and III. The rate of TMP increase was little less than double in Phase III compared to Phase I.

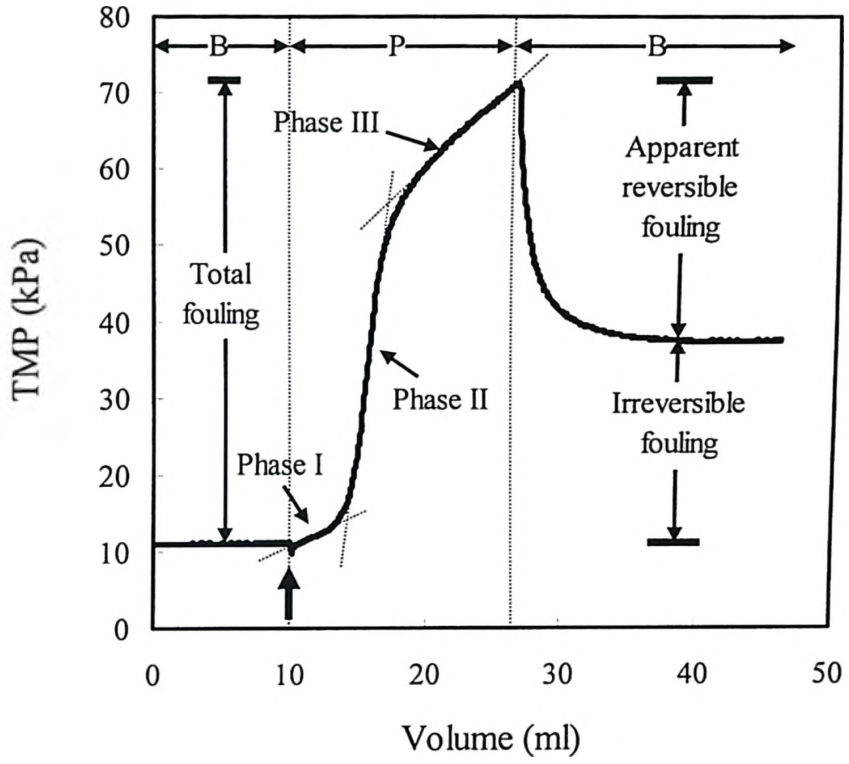

Figure 6.2 TMP as a function of permeate volume (BSA concentration: 10 kg/m^3; 0.45 micron cellulose acetate membrane; Flux: 8.49×10^{-4} m/s; volume of BSA solution: 16 ml); P – Protein filtration, B – Buffer filtration

The TMP-permeate volume data obtained during the protein microfiltration part of the experiment shown in Figure 6.2 was subjected to complete pore blockage, intermediate pore blockage and pore constriction law analysis using the linearized forms developed by Hlavacek and Bouchet [13]. Figure 6.3 shows the results thus obtained which also suggests that the membrane fouled in three phases during protein filtration.

None of the blocking laws could fit the entire protein filtration data (as would have been evident from a line over the whole data set) clearly pointing towards the predominance of different fouling mechanisms in different phases. However each blocking law gives linear segments having different slopes during the three phases. This analysis suggests that the membrane fouling mechanism changed from one phase to another. These results also suggest that TMP data on its own is not sufficient to predict the qualitative nature of membrane fouling in constant flux filtration process. What is also needed is thorough analysis of fouled membrane discs.

Table 6.1 Fouling rates during the three phases of TMP increase (BSA concentration: 10 kg/m^3; membrane: 0.45 micron cellulose acetate; flux: 8.49×10^{-4} m/s; volume of BSA solution filtered: 16 ml)

	Fouling rate (kPa/ml)
Phase I	0.97
Phase II	13.74
Phase III	1.80

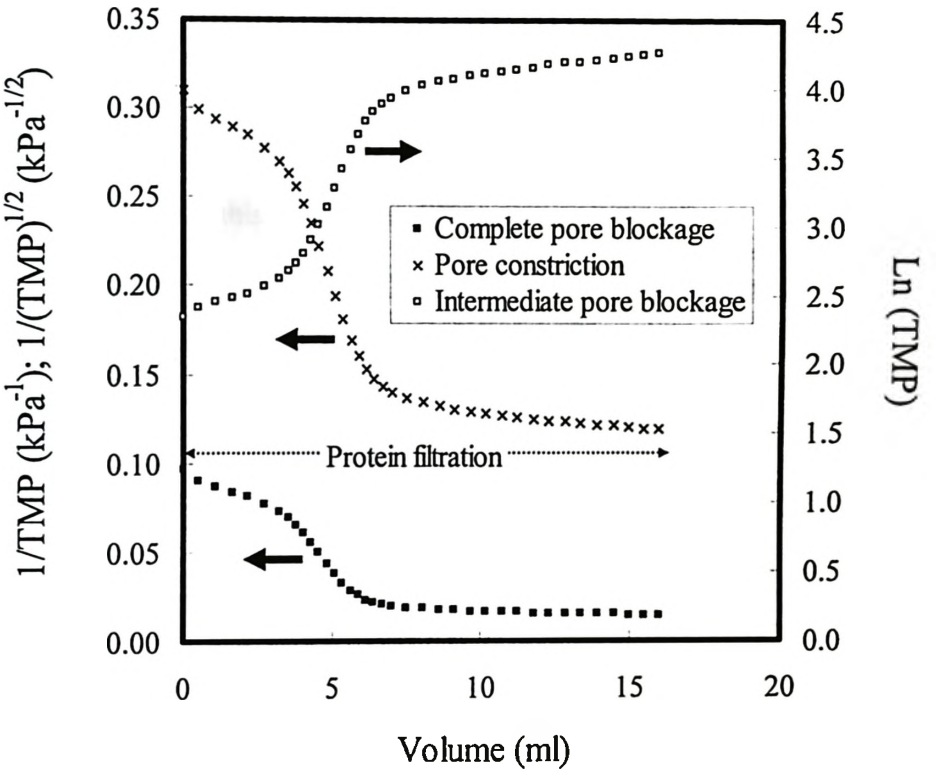

Figure 6.3 Complete pore blockage, intermediate pore blockage and pore constriction law analysis of BSA microfiltration in terms of their linearized form (BSA concentration: 10 kg/m^3; membrane: 0.45 micron cellulose acetate; flux: 8.49×10^{-4} m/s; volume of BSA solution filtered: 16 ml)

After protein filtration, when buffer filtration was continued in the same flow direction to measure the permeability of fouled membrane disc, TMP decreased rapidly as well as quite significantly. This clearly suggested that much of the increase in resistance during protein filtration was reversible in nature. Here, it should be noted that

buffer filtration was carried out immediately after protein filtration without dismantling the module or any kind of washing (either physical or chemical). Besides, the flow direction was same as protein filtration and hence it shouldn't be confused with backwashing. Therefore in this study, the difference between maximum TMP during protein filtration and stable TMP corresponding to buffer filtration after protein filtration (front washing) was termed as apparent reversible fouling. While the difference between stable TMP during buffer filtration before and after protein filtration was termed as irreversible fouling. The difference between maximum TMP during protein filtration and stable TMP corresponding to buffer filtration before protein filtration (pre-washing) was termed as total fouling.

In literature, enough careful attention has not been paid to the phenomenon of apparent reversible fouling during microfiltration process. In a few instances, concentration polarization has been assumed to be responsible for this [18-19]. Concentration polarization refers to the protein molecules accumulated near the membrane surface which are still in free form in the solution. They create osmotic back pressure and thereby indirectly increase the filtration resistance by reducing the effective TMP across the membrane. While membrane fouling refers to the protein molecules bound to the membrane surface. Concentration polarization phenomenon is noticed when protein transmission through membrane is less than 100%. To figure out the actual cause of the apparent reversible fouling, protein concentration was monitored in the permeate stream. Figure 6.4 shows the protein transmission profile for the above experiment. We

found it similar to the one obtained in a dummy experiment without any membrane present in the module. The protein transmission during the microfiltration process was therefore 100% and this effectively ruled out the possibility of any concentration polarization taking place. Similar fouling experiments were carried out using different concentration of BSA in the feed i.e. 5, 15 and 20 kg/m^3 and in all the these experiments, the protein transmission was found to be 100%. Therefore, osmotic back pressure resulting from concentration polarization cannot be justifiably attributed as one of the causes for increase in resistance during protein microfiltration. The absence of concentration polarization phenomenon in the protein microfiltration experiments reported in this work will be further justified by the data shown in Figure 6.7. The apparent reversible fouling was therefore most likely due to some reversibly adsorbed protein which was released during the front washing process. To test this hypothesis, the front wash sample was collected and analyzed for the presence of BSA monomer and aggregate by SEC using a high performance gel filtration column (Superdex 200 10/300 GL). Since front wash sample was already microfiltered, it should be free from larger protein aggregates which can otherwise clog the gel filtration column. Figure 6.5 shows the size exclusion chromatogram obtained where the peak at 68 minute retention time corresponds to BSA monomer. Dimers and lower order aggregates were absent in the front wash sample. The mobile phase retention time was determined using Blue dextran 2000 to be 39 minutes. Hence, the small bump observed around 33 minutes was due to some kind of disturbance. Therefore it can be concluded that BSA monomers are the major foulant species responsible for reversible fouling which comprises the significant

portion of total fouling. Kelly and Zydney [18] have suggested that BSA fouled membranes by chemical attachment to existing protein deposits via the formation of intermolecular disulfide linkages. Our results clearly indicate that native BSA monomer can also foul the membrane by physical and reversible attachment and can be removed by front washing.

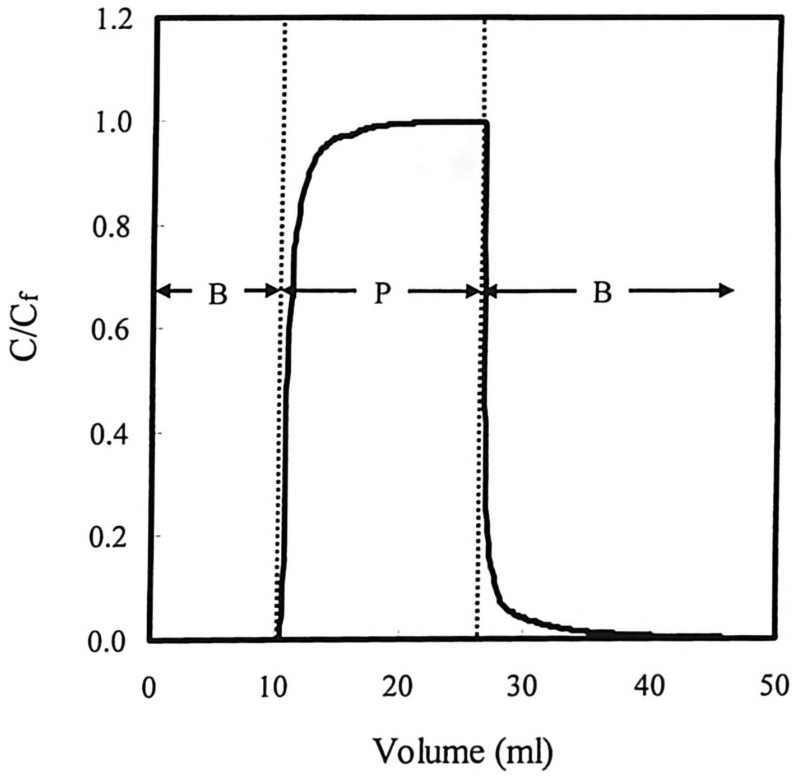

Figure 6.4 UV absorbance of permeate during BSA microfiltration (BSA concentration: 10 kg/m^3; 0.45 micron cellulose acetate membrane; Flux: 8.49×10^{-4} m/s; volume of BSA solution: 16 ml); P – Protein filtration, B – Buffer filtration

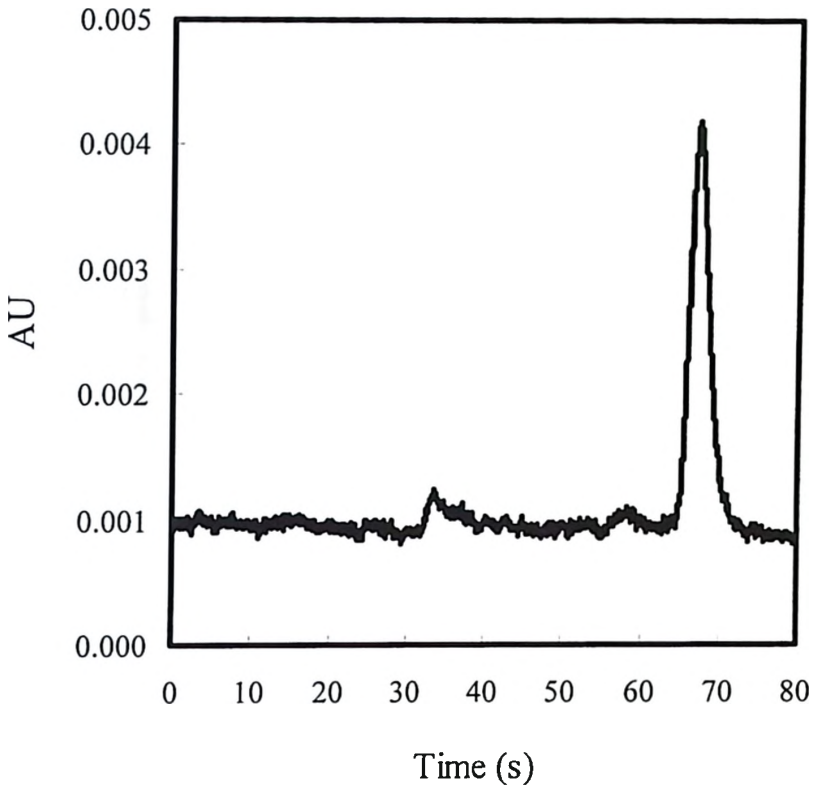

Figure 6.5 Chromatogram of front-wash sample obtained with high performance gel filtration column, Superdex 200 10/300 GL (flow rate: 0.2 ml/min)

Figure 6.6 shows the size exclusion chromatograms for the feed and permeate samples collected during an experiment similar to the one described in Figure 6.2. These showed that both feed and permeate contained mostly BSA and very small amounts of BSA dimer. The presence of BSA aggregates in the feed could not be confirmed from these SEC results, possibly be due to the extremely low concentration of these

aggregates. The chromatograms also indicate that the permeate sample contained a slightly lower percentage of dimer. The low concentration of BSA aggregates in the feed sample combined with small decrease in the percentage of BSA dimer in permeate clearly indicates that the most of the fouling was caused by BSA monomer. To figure out the role of very small amount of BSA aggregates in feed on membrane fouling, the BSA solution was filtered through two microfiltration membrane discs housed in separate filtration modules connected back to back in series. The TMP across each membrane module was monitored during this experiment (see Figure 6.7). These TMP profiles indicate severe fouling of the first membrane in the series with very little fouling observed with the second. By using the membrane in series, the aggregates present in the feed were retained by the first membrane and therefore the effective feed solution going into the second membrane module was virtually aggregate free. If protein aggregates did not play any significant role in membrane fouling then both membranes should have fouled to similar extents, which is clearly not the case here. Based on the results obtained so far, it may be inferred that BSA monomer was the principle foulant since front wash mainly contained BSA monomers and reversible fouling comprised a significant portion of total fouling. However, the BSA monomer could cause membrane fouling only when aggregates were present in the feed solution. Also, very small amounts of aggregate were sufficient for initiating fouling by BSA monomer. Kelly et al [20] have described fouling of MF membranes by BSA in a stirred cell module as a two-step process with initial deposition of conformationally altered BSA monomers and higher order aggregates serving as nucleation sites for the subsequent deposition of native BSA. Our results

obtained with the dead-end in-line microfiltration system lead us to a similar conclusion. TMP profiles in Figure 6.7 also confirm the absence of concentration polarization phenomenon in protein microfiltration reported in our work.

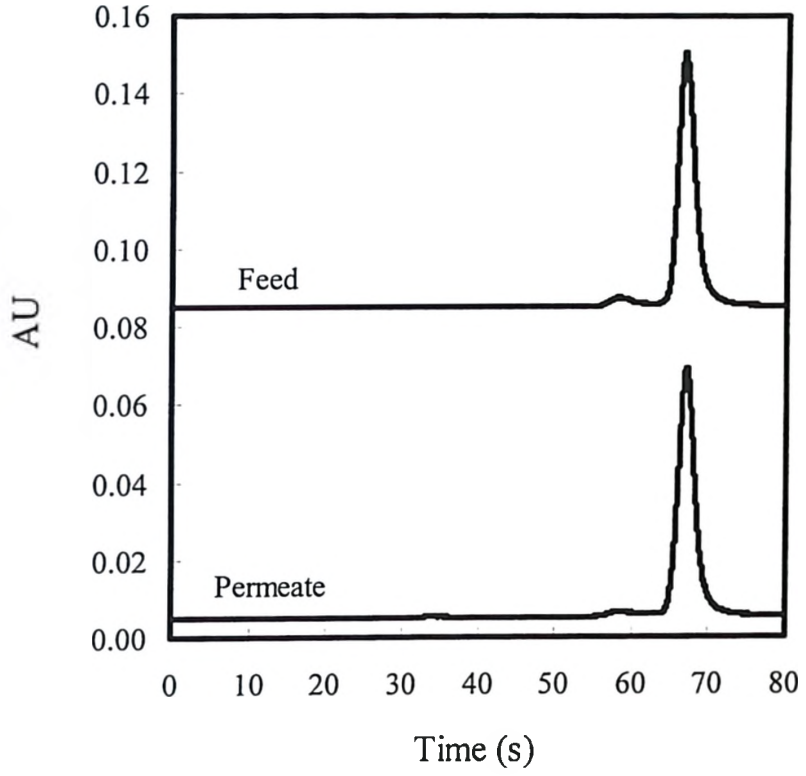

Figure 6.6 Chromatograms of feed and permeate samples obtained with high performance gel filtration column, Superdex 200 10/300 GL (flow rate: 0.2 ml/min)

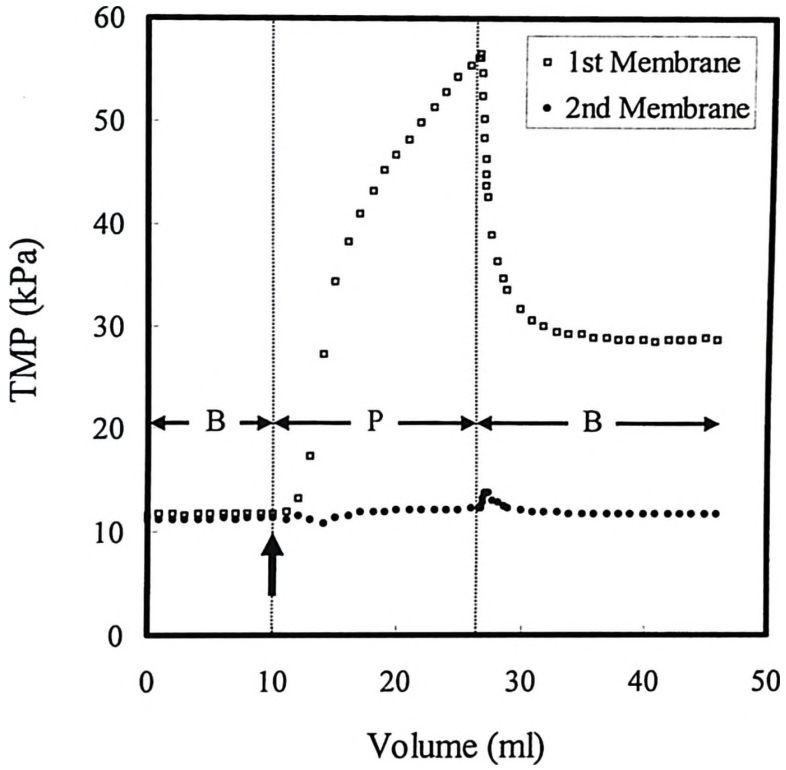

Figure 6.7 TMP profiles of two MF membranes housed in separate filtration module connected in series (BSA concentration: 10 kg/m^3; membrane: 0.45 micron cellulose acetate; flux: 8.49×10^{-4} m/s; volume of BSA solution filtered: 16 ml); P – Protein filtration, B – Buffer filtration

Figure 6.8 shows the effect of protein filtration volume on the reversibility of membrane fouling. New membrane disc was used in each of the experiment to filter different amount of protein solution. In all the experiments, stable TMP baseline at the

start of experiment corresponded to the buffer filtration. An arrow marks the start of the protein filtration step which was continued for different volumes in different experiments. In each experiment, protein filtration was followed by 20 ml of buffer filtration to measure the reversibility of flow resistance. With 4 ml of protein filtration, TMP increased only 3.3 kPa suggesting very little fouling which was almost irreversible in nature. With 16 ml of protein filtration, TMP increased quite significantly suggesting very severe fouling, but almost half of this TMP increase was reversible when buffer filtration was continued in the same direction. Table 6.2 shows increase in TMP due to apparent reversible fouling, irreversible fouling and total fouling along with the % apparent reversible fouling for the data shown in Figure 6.8. Table 6.2 clearly shows that initial membrane fouling was largely irreversible in nature. As more and more protein solution was filtered through the membrane, proportion of reversible fouling increased rapidly. At the end of phase II, reversible fouling accounted for more than 60% of total fouling. Once fouling reached to the third stage, the proportion of reversible fouling started decreasing slowly. At the end of 16 ml of protein filtration, reversible fouling still accounted for more than 55% of total fouling. Table 6.3 shows total fouling and its apparent reversible fouling component during different phases of membrane fouling. During phase I, membrane fouling was almost irreversible in nature. In phase II, reversible fouling initially increased slowly followed by rapid increase. From 4 to 6 ml of protein filtration, reversible fouling accounted for almost 40% of the total increase in fouling but from 6 to 8 ml of protein filtration, reversible fouling contributed for nearly 85% of the total increase in fouling. In total, reversible component accounted for around

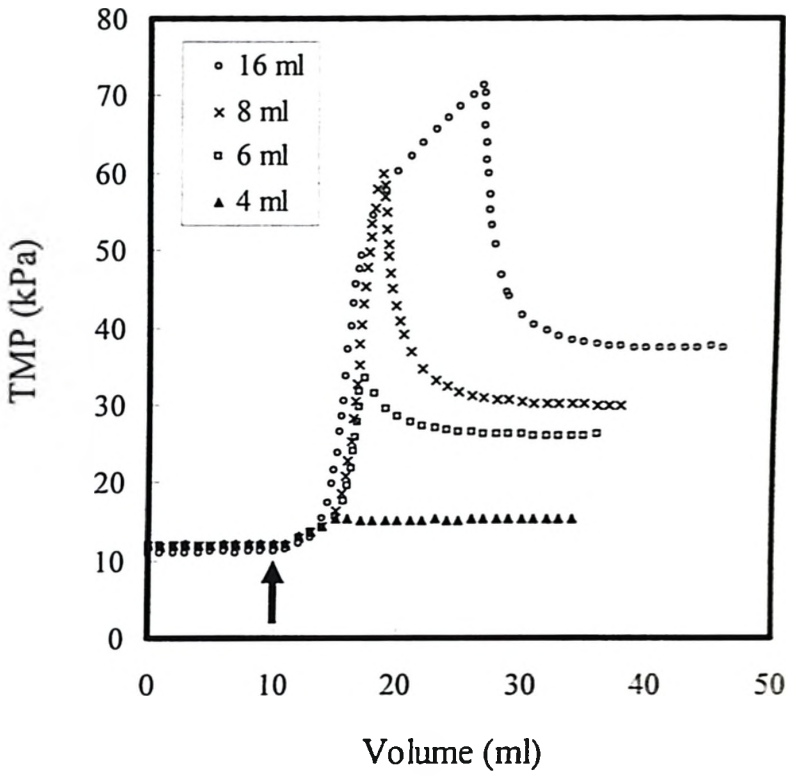

Figure 6.8 Effect of protein filtration volume on the reversibility of membrane fouling (BSA concentration: 10 kg/m^3; 0.45 micron cellulose acetate membrane; Flux: 8.49×10^{-4} m/s; volume of BSA solution filtered: 4, 6, 8 and 16 ml)

66% of total increase in TMP during phase II. From 8 to 16 ml of protein filtration (phase III) reversible increase in TMP (or fouling) accounted for one-third of total increase in TMP. This table clearly suggests that most of the contribution of reversible fouling came during the later part of phase II. While fouling in phase I was largely irreversible in

nature. The irreversible nature of fouling in phase I and largely reversible nature of fouling in phase II can be explained in terms of two step fouling process. Since membrane fouling is initiated by the deposition of trace amounts of protein aggregates, which could not be removed by front washing, fouling in phase I is irreversible in nature. But once fouling is initiated by the deposition of protein aggregates, these aggregates can serve as nuclei points for further deposition of protein monomers. Because of this loosely deposited protein monomers, significant portion of fouling in phase II and III is reversible in nature. Decrease in proportion of reversible fouling in phase III compared to phase II may be because of change in structure of already deposited protein mass due to further deposition on top of it.

Table 6.2 Effect of protein filtration volume on the reversibility of fouling (BSA concentration: 10 kg/m^3; membrane: 0.45 micron cellulose acetate; flux: 8.49×10^{-4} m/s)

Protein filtration volume (ml)	Total fouling (kPa)	Apparent reversible fouling (kPa)	Irreversible fouling (kPa)	% Apparent reversible fouling
4	3.30	0.10	3.20	3.03
6	21.75	7.45	14.30	34.25
8	48.20	29.95	18.25	62.14
16	60.35	33.95	26.40	56.26

Table 6.3 Contribution of apparent reversible fouling towards total fouling during each phase of membrane fouling (BSA concentration: 10 kg/m^3; membrane: 0.45 micron cellulose acetate; flux: 8.49×10^{-4} m/s)

Protein filtration volume (ml)	Total fouling (kPa)	Apparent reversible fouling (kPa)	% Apparent reversible fouling	% Apparent reversible fouling during three phases	Membrane fouling phase
0 to 4	3.30			3.03	I
4 to 6	18.45	7.35	39.84	66.48	II
6 to 8	26.45	22.50	85.07		
8 to 16	12.15	4.00	32.92	32.92	III

The possibility of solution viscosity influencing the apparent reversible fouling amount was examined. The viscosity of 10 kg/m^3 and 1 kg/m^3 BSA solutions were measured with a glass capillary Ubbelohde viscometer and were found to be around 1.05 MPa-s at the operating shear rate in the instrument. The shear rate in the membrane pores is expected to be in the 17000-22000 s^{-1} range which is higher than that in the viscometer. However, in the protein concentration range used in this work, shear dependent effects are likely to be negligible. Moreover, any viscosity contribution towards increase in pressure should have been apparent right from the start of each experiment. Since no such effects are observed any significant viscosity component in the reversible TMP increase during BSA microfiltration could be ruled out.

The use of confocal scanning laser microscopy for characterization of microfiltration membrane fouled by proteins has been reported by earlier workers [21]. Figure 6.9 shows fluorescent images of BSA fouled membrane cross-sections super-imposed on their respective reflection images. These membranes were fouled to different extent with 10 kg/m^3 BSA spiked with 0.005 kg/m^3 Alexa Fluor 488 labeled BSA. Figure 6.9a shows membrane disc fouled until TMP increased at phase I rate, Figure 6.9b shows membrane disc fouled until TMP increased at phase II rate while Figure 6.9c shows membrane disc fouled with 16 ml of protein solution. Quite clearly the protein fouling was largely restricted to a zone close to the membrane surface. The thickness of protein deposition zone increased with the extent of protein filtration: 2 μm at the end of phase I, around 5 μm at the end of phase II, and slightly more than 10 μm after 16 ml of protein filtration. These results support the hypothesis on the mechanism of membrane fouling described earlier. The extent of BSA monomer on the membrane material itself was clearly negligible. The aggregate present in the feed were retained by sieving, most likely due to surface filtration. The retained aggregates then formed the initiation points for attachment of monomer BSA. With increase in filtration volume, further aggregates are deposited and the BSA monomer attachment zone increases in dimension. Figure 6.10a-6.10b show the z-projection fluorescent images of membrane fouled with 16 ml of protein solution before and after front washing respectively. A comparison of the thickness of fluorescent zone confirms the effectiveness of front-washing in removing the reversibly deposited BSA monomer from the membrane.

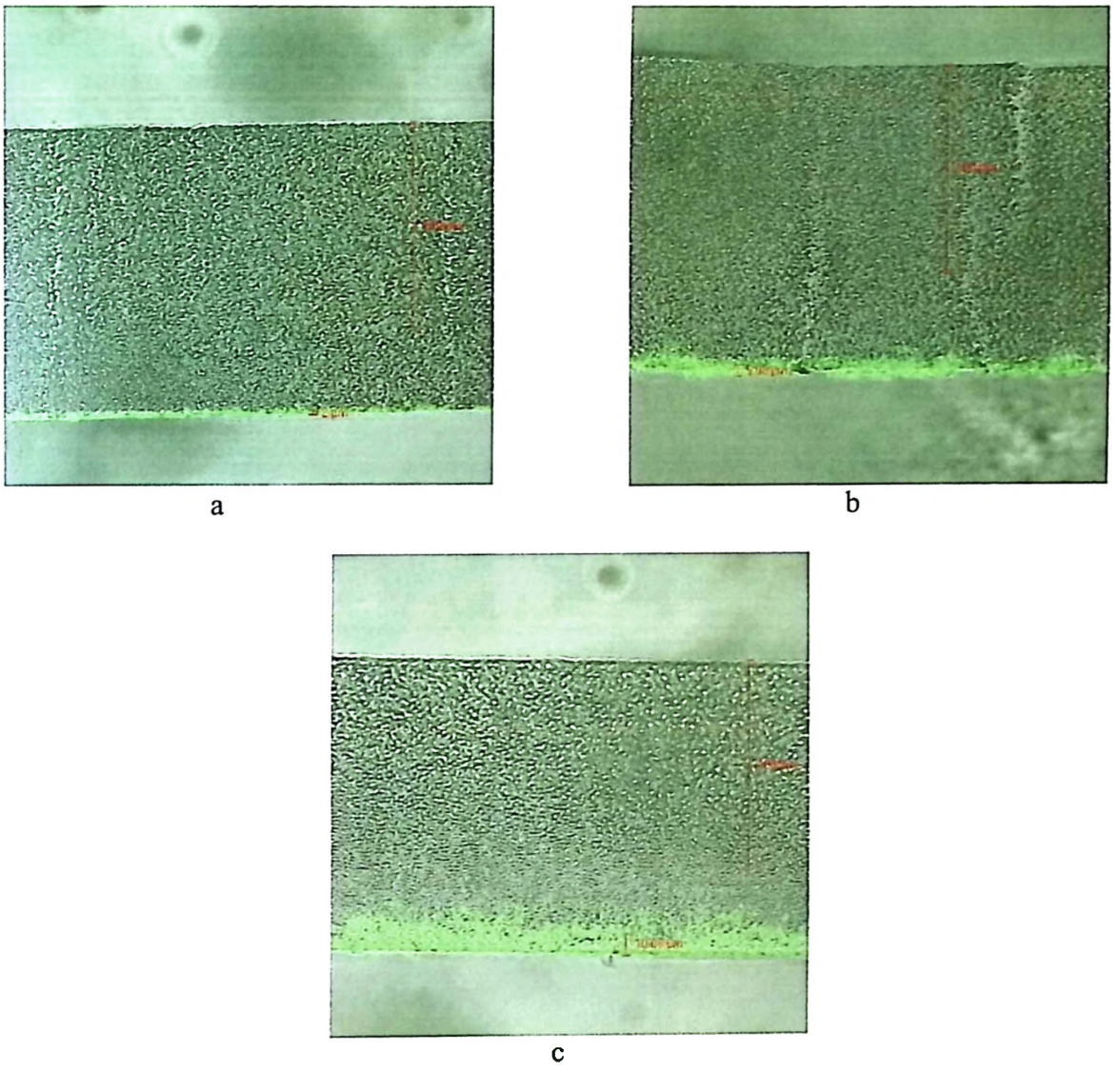

Figure 6.9 fluorescent images of membrane cross-sections super-imposed on their reflection images showing protein deposition at the end of (a) phase I, (b) phase II and (c) phase III (BSA concentration: 10 kg/m^3 + 0.005 kg/m^3 Alexa Fluor labeled BSA; membrane: 0.45 micron cellulose acetate; flux: 8.49×10^{-4} m/s)

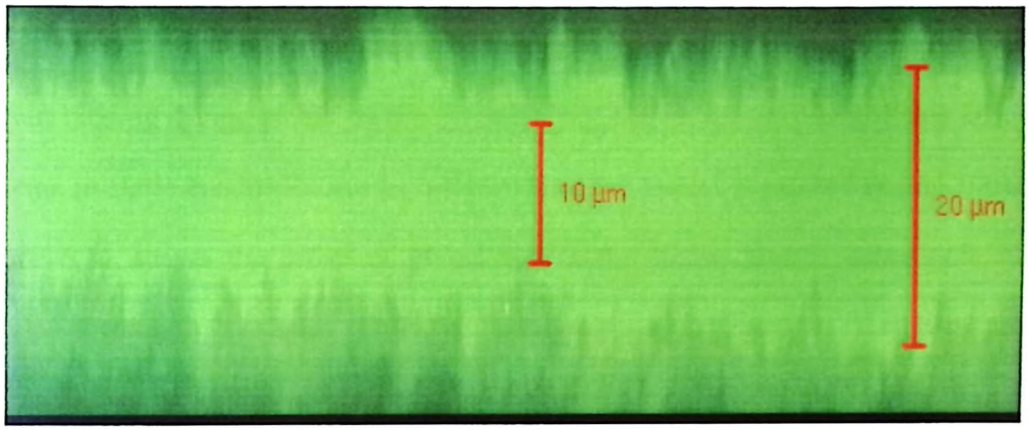

a

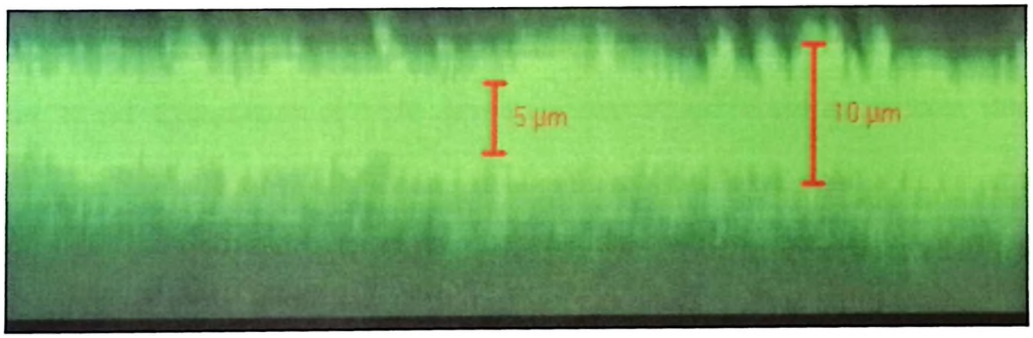

b

Figure 6.10 fluorescent images of z-projection of membranes fouled with 16 ml of protein (a) before front washing and (b) after front washing (BSA concentration: 10 kg/m^3 + 0.005 kg/m^3l Alexa Fluor labeled BSA; membrane: 0.45 micron cellulose acetate; flux: 8.49×10^{-4} m/s)

Earlier studies have used the term 'protein adsorption' for the protein binding on membrane during static condition while the term 'protein deposition' was used for the protein binding during actual protein filtration [7]. The structure of membrane adsorbed proteins in static conditions can be different than the protein deposited during filtration. Figure 6.11 shows the effect of pre-adsorption on further protein deposition during protein filtration. It shows TMP vs. permeate volume profiles for two protein microfiltration experiments carried out at similar operating conditions but one with fresh new membrane disc while the other with a membrane disc soaked in feed protein solution for 12 hrs. Both the experiments were carried out at 8.49×10^{-4} m/s flux with 10 g/l BSA as a feed protein solution. In both experiments, 10 ml of buffer filtration was followed by 24 ml of protein filtration after which buffer filtration was resumed and carried out for further 20 ml. Comparison of TMP during the first 10 ml of buffer filtration clearly shows negligible effect of protein adsorption on filtration resistance. As soon as protein filtration started, TMP increased rapidly and similarly in both the experiments indicating comparable protein deposition during protein filtration. Fouling rates were also very similar during all three phase of membrane fouling indicating negligible effect of prior protein adsorption on further protein deposition during filtration. These results support the earlier finding that protein adsorption plays very minor role in increase in flow resistance during protein filtration [7].

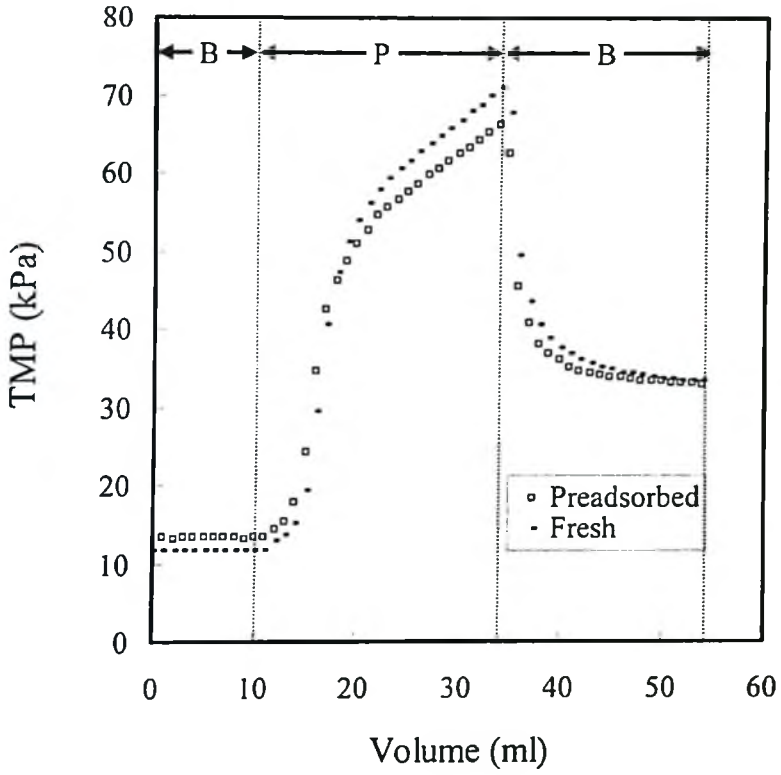

Figure 6.11 Effect of prior protein adsorption in static condition on protein deposition during protein filtration (BSA concentration: 10 kg/m^3; 0.45 micron cellulose acetate membrane; Flux: 8.49×10^{-4} m/s; volume of BSA solution: 24 ml); P – Protein filtration, B – Buffer filtration

Figure 6.12 shows effect of feed protein concentration on protein fouling of MF membranes. All three experiments were carried out at 8.49×10^{-4} m/s flux but with different concentration of feed protein solution. The dotted lines in the figure separate buffer filtration from protein filtration. At a given permeate volume during protein

filtration, TMP was higher at higher feed protein concentration indicating higher amount of fouling. Besides, the rate of TMP increase with respect to volume was higher at higher concentration than the corresponding ones at lower concentration during phase I, II and III. The volume of protein which could be filtered at a fouling rate characterizing the phase I behavior decreased with protein concentration.

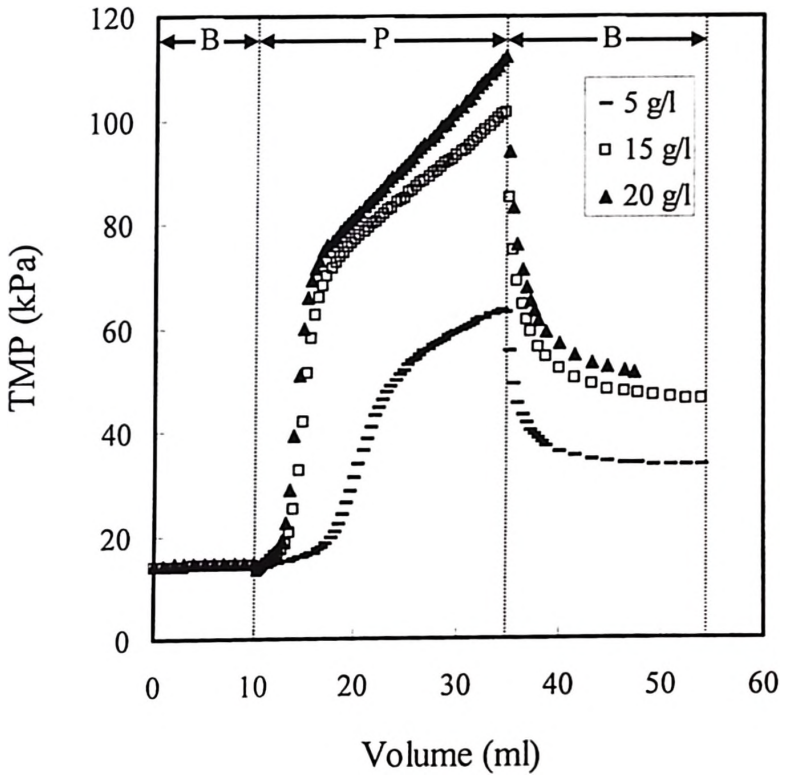

Figure 6.12 TMP vs. permeate volume profiles at different feed protein concentration (0.45 micron cellulose acetate membrane; Flux: 8.49×10^{-4} m/s; volume of BSA solution: 24 ml); P – Protein filtration, B – Buffer filtration

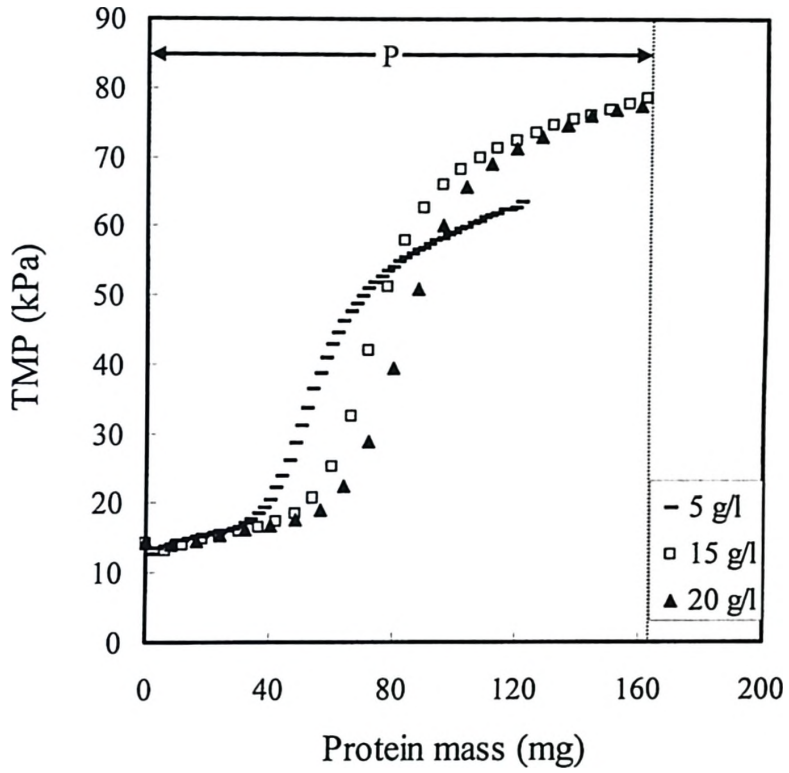

Figure 6.13 TMP vs. protein mass profiles at different feed protein concentration (0.45 micron cellulose acetate membrane; Flux: 8.49×10^{-4} m/s; volume of BSA solution: 24 ml); P – Protein filtration

Figure 6.13 shows the same TMP data as in Figure 6.12 but now plotted against protein mass filtered through the membrane. Interestingly, the feed protein concentration does not seem to affect fouling rates, now defined as the rate of TMP increase with respect to protein mass during phase I, II and III. In other words, the rate of TMP increase

with respect to protein mass filtered through the membrane seems to be independent of protein concentration during all three phases. Not only that, but the amount of protein mass which could be filtered through membrane during phase I, increased with protein concentration. Here, it should be noted that all three experiments were carried out at the same constant flux. These results seem to be quite interesting from the model development point of view.

Figure 6.14 shows TMP vs. volume profiles for four protein MF experiments carried out at different fluxes. All these experiments were carried out with 10 g/l BSA solution. The dotted lines in the figure separate buffer filtration from protein filtration. In all the experiments, buffer filtration after protein filtration (or front washing) was carried out at constant flux of 2.12×10^{-4} m/s, but the initial buffer filtration and protein filtration were carried out at different fluxes. It is evident from Figure 6.14 that flux did not affect the fouling rates (or rate of TMP increase) significantly during phase I, II and III. But, the volume of protein solution that could be filtered in phase I decreased with increasing flux. Besides, the transition from phase II to III was not smooth at lower fluxes (such as 2.12×10^{-4} and 4.24×10^{-4} m/s) compared to higher fluxes. At 2.12×10^{-4} m/s flux, TMP increased very rapidly in phase II, but then at the end of phase II, suddenly stopped increasing and started decreasing slowly for a while. After this very small period of decreasing TMP, it again started increasing but at much slower rate characterizing the phase III behavior. This strange transition from phase II to III at lower fluxes is quite reproducible but hard to explain based on the current knowledge. One possible reason for

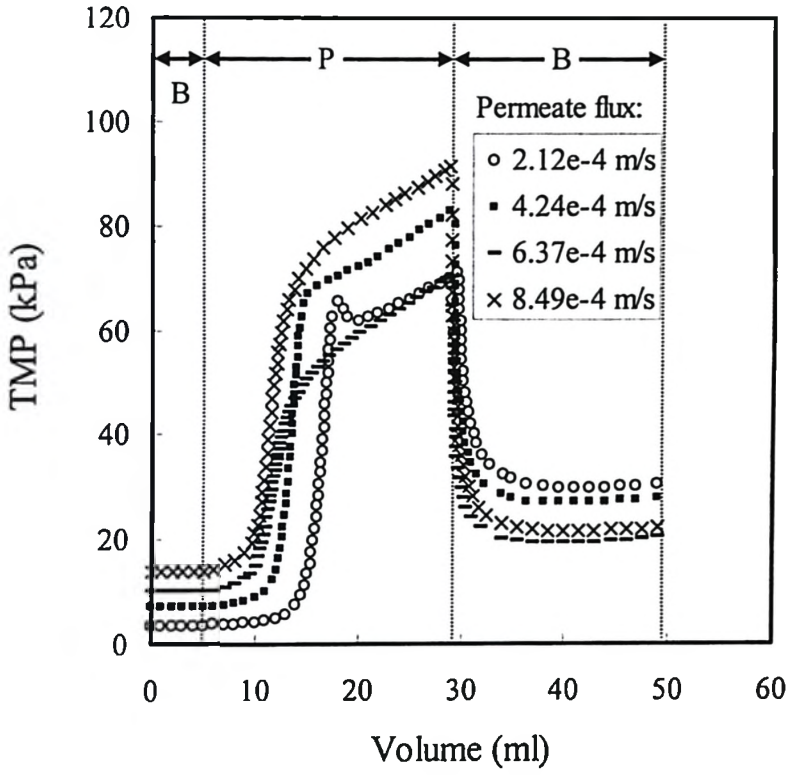

Figure 6.14 TMP vs. permeate volume profiles at different flux during protein filtration (BSA concentration: 10 kg/m^3; 0.45 micron cellulose acetate membrane; volume of BSA solution: 24 ml); P – Protein filtration, B – Buffer filtration

the drop in TMP during the transition from phase II to III could be the rearrangement of foulant layers due to rapid increase in TMP leading to a sudden change in permeability. It can be speculated that after certain pressure, protein deposit which is permeable to the flow could be compressed in radial direction leading to the temporary drop in TMP. After

momentary drop, TMP started increasing in phase III due to further continuous deposition. Figure 6.14 also points out higher amount of irreversible fouling at lower fluxes after front washing. Here, it should be noted that in all four experiments, front washing was carried out at same flux of 2.12×10^{-4} m/s while protein filtration were carried out at different fluxes. Higher amount of irreversible fouling at lower flux may be due to the longer time needed to filter the same amount of protein solution at lower flux. Over a period of time, initially loosely deposited protein mass may be getting permanently fixed to the membrane and hence contributing towards irreversible fouling.

Table 6.4 shows total resistances of membrane at the end of 24 ml of protein filtration along with membrane hydraulic resistance and fouling resistances at different fluxes. These values were calculated by using resistance in series model:

$$J_v = \frac{\Delta P}{R_m} \tag{6.1}$$

Where $R_m = R_m{}^0 + R_f$

This table suggests that total resistance during protein filtration at lower fluxes was higher compared to that at higher fluxes. Since membrane resistance is more or less constant in the flux range examined, higher total resistance means higher fouling resistance at lower fluxes.

Table 6.4 Fouling resistance and membrane hydraulic resistance at the end of protein filtration at different fluxes (BSA concentration: 10 kg/m^3; 0.45 micron cellulose acetate membrane; volume of BSA solution: 24 ml)

Flux (m/s)	TMP (kPa)	Resistance (kPas/m)		
		R_m	R_m^0	R_f
2.12×10^{-4}	70.8	3.34×10^{5}	1.61×10^{4}	31.7×10^{4}
4.24×10^{-4}	82.7	1.95×10^{5}	1.61×10^{4}	17.9×10^{4}
6.37×10^{-4}	70.2	1.10×10^{5}	1.61×10^{4}	9.41×10^{4}
8.49×10^{-4}	91.3	1.08×10^{5}	1.61×10^{4}	9.14×10^{4}

Figure 6.15 shows effect of front washing flow rate on the reversibility of membrane fouling. Two protein MF experiments designated as A and B were carried out with new membrane discs at similar operating conditions except front washing or buffer filtration after protein filtration. In both experiments, initial 10 ml of buffer filtration at 8.48×10^{-4} m/s was followed by 24 ml of protein filtration at the same flux. After protein filtration, buffer filtration was carried out in two steps, each of 20 ml. In experiment designated as A, front washing was first carried out at 2.12×10^{-4} m/s for 20 ml followed by another 20 ml at 8.48×10^{-4} m/s. While in experiment designated as B, front washing cycles were reversed, i.e. the first front washing was carried out at 8.48×10^{-4} m/s followed by the second one at 2.12×10^{-4} m/s. It is quite clear from this Figure that the first front washing at higher flux was relatively more effective compared to the second

one. TMP corresponding to both front washing steps in experiment B is lower than the corresponding ones at the same flux in experiment A. The difference in TMP corresponding to front washing is more pronounced at flux 8.48×10^{-4} m/s between both experiments. This data suggests that reversible component of fouling is gradually getting converted to the irreversible one with more permeate volume and the first front washing at higher flux is more effective since it can possibly remove more amount of deposited protein. Table 6.5 shows total membrane resistance and fouling resistance during front washing steps in experiment A and B. These values were calculated by using stable TMP at the end of each front washing step from equation 6.1. In each experiment, the total membrane resistance and fouling resistance were different at different front washing flux. This clearly points out the compressible nature of the deposited protein mass at different TMP/flux. Figure 6.15 also confirms that TMP became stable at the end of both front washing steps indicating no further removal of deposited protein mass or compression at constant TMP/flux. Since fouling resistance is lower at higher front washing flux in both experiments, it may be hypothesized that the deposited protein mass is more compressible along its thickness (or perpendicular to the convective permeate flow) rather than its surface (parallel to the convective permeate flow). Besides, effectiveness of the first front washing at higher flux is also evident from Table 6.5 upon the comparison of fouling resistances in both experiments at corresponding fluxes. In experiment A, when second front washing was carried out at relatively higher flux compared to the first one, TMP increased instantaneously (again due to increasing the

flux) and then decreased slowly for approximately 10 ml. This decrease in TMP indicates further washing of deposited protein at higher flux.

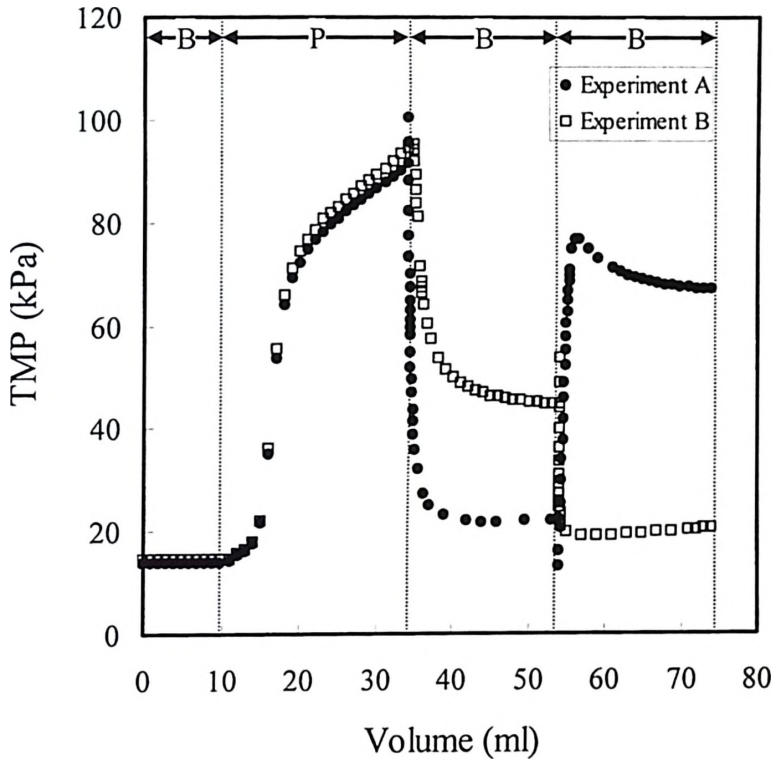

Figure 6.15 Effect of front washing flow rate on the reversibility of membrane fouling (BSA concentration: 10 kg/m^3; 0.45 micron cellulose acetate membrane; Flux: 8.49×10^{-4} m/s; volume of BSA solution: 24 ml); P – Protein filtration, B – Buffer filtration

Table 6.5 Total resistance and fouling resistance during the front wash steps in experiment A and B (BSA concentration: 10 kg/m^3; 0.45 micron cellulose acetate membrane; Flux: 8.49×10^{-4} m/s; volume of BSA solution: 24 ml). Experiment A – First front wash at 2.12×10^{-4} m/s for 20 ml followed by second front wash at 8.49×10^{-4} m/s for 20 ml; Experiment B – First front wash at 8.49×10^{-4} m/s for 20 ml followed by second front wash at 2.12×10^{-4} m/s for 20 ml

Experiment	Front washing Flux (m/s)	TMP (kPa)	Resistance (kPas/m)		
			R_m	R_m^0	R_f
A	2.12×10^{-4}	21.6	10.2×10^{4}	1.61×10^{4}	8.56×10^{4}
	8.49×10^{-4}	66.8	7.87×10^{4}	1.61×10^{4}	6.26×10^{4}
B	8.49×10^{-4}	44.6	5.25×10^{4}	1.61×10^{4}	3.64×10^{4}
	2.12×10^{-4}	19.5	9.19×10^{4}	1.61×10^{4}	7.58×10^{4}

Figure 6.16 shows TMP vs. volume profiles for 0.45 and 0.22 micron pore size CA membranes and Figure 6.17 shows the same for 0.22 micron pore size PVDF and CA membranes. All of these experiments were carried out at similar operating conditions. The dotted lines separate buffer filtration from protein filtration in both figures. It is quite evident from these figures that irrespective of the membrane pore size and material, MF membranes got fouled by protein in three phases in dead end mode and significant portion of fouling is reversible in nature. The fouling rate characterizing the individual phase and the proportion of reversible fouling is different for different membranes.

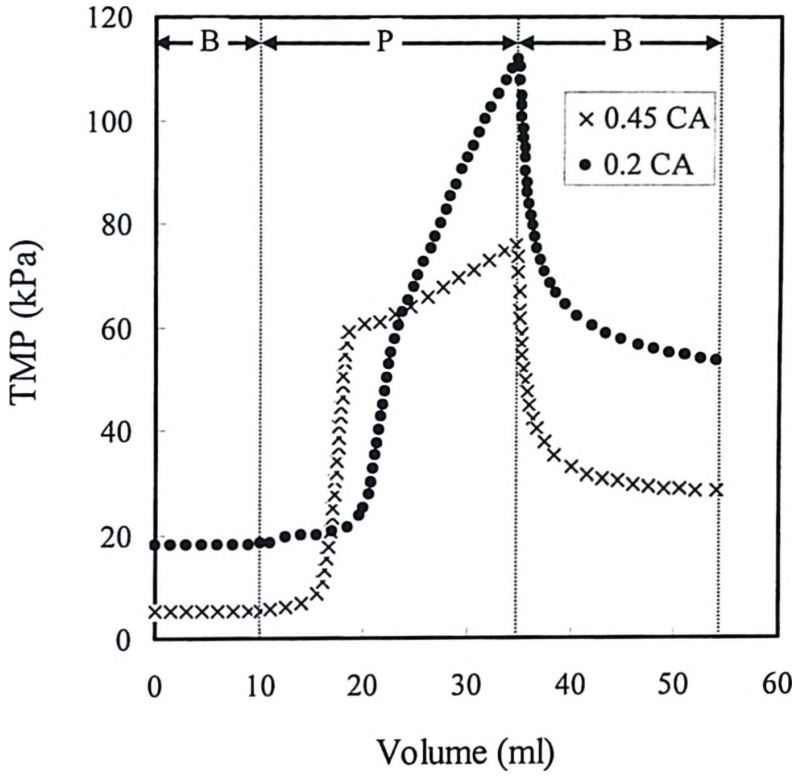

Figure 6.16 TMP profiles of 0.45 and 0.2 micron pore size cellulose acetate membranes (BSA concentration: 10 kg/m^3; Flux: 4.24×10^{-4} m/s; volume of BSA solution: 24 ml); P – Protein filtration, B – Buffer filtration

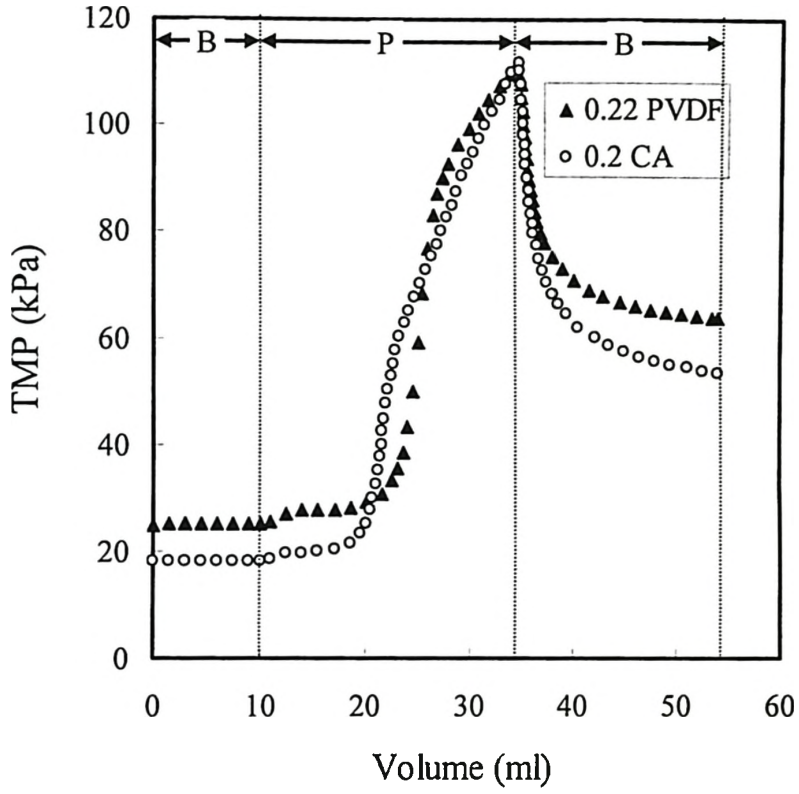

Figure 6.17 TMP profiles of 0.2 micron pore size cellulose acetate and 0.22 micron pore size PVDF membranes (BSA concentration: 10 kg/m^3; Flux: 4.24×10^{-4} m/s; volume of BSA solution: 24 ml); P – Protein filtration, B – Buffer filtration

Figure 6.18 shows the TMP as a function of permeate volume during BSA microfiltration carried out in two steps. After 10 ml of buffer filtration 8 ml of BSA solution was filtered. After a further 20 ml of buffer filtration 32 ml of protein solution was filtered as the second protein filtration step. The fouled membrane was then front washed with 20 ml of buffer. The first protein filtration step showed phase I and phase II

fouling behavior while in the earlier part of the second protein filtration step phase II fouling seems to have continued, albeit at a higher TMP increase rate than in the first step. The TMP then decreased a bit and then started rising again, however at a much slower rate suggesting that phase III fouling was taking place. The decrease in TMP at the transition between phase II and phase III fouling is hard to explain. A likely reason

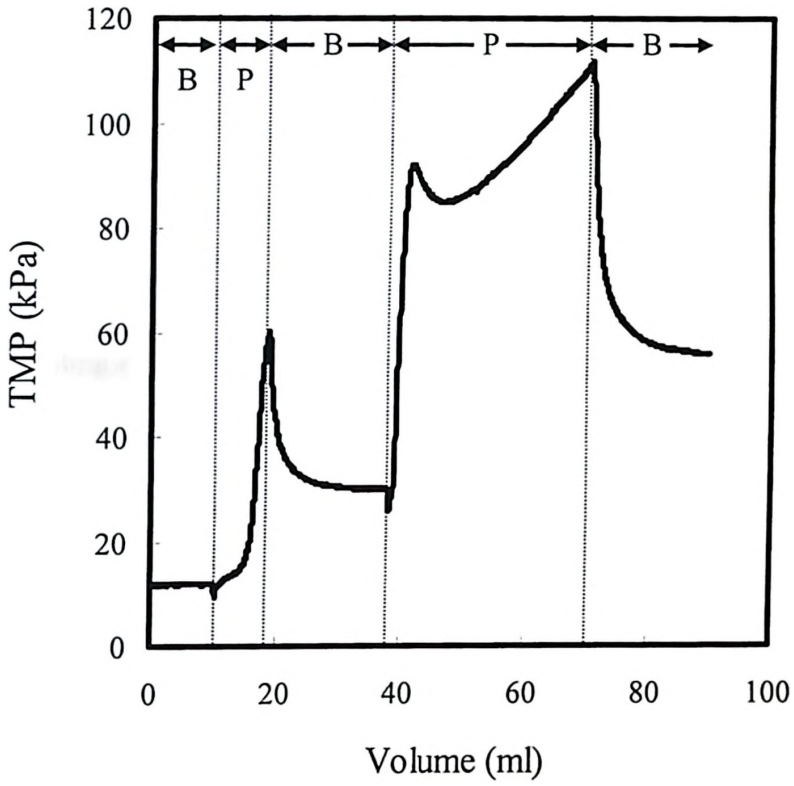

Figure 6.18 TMP as a function of permeate volume in two step protein filtration separated by buffer filtration (BSA concentration: 10 kg/m^3; 0.45 micron cellulose acetate membrane; flux: 8.49×10^{-4} m/s; volume of BSA solution: 8+32 ml); P – Protein filtration, B – Buffer filtration

could be a rearrangement of the foulant layer due to increased TMP leading to a sudden change in permeability. In each of the protein filtration steps, almost half of the respective TMP increase was reversible in nature. Table 6.6 shows the rates of TMP increase during the different fouling phases in the two step protein filtration process. The fouling rates during first two phases of the first protein filtration step are similar to those reported in Table 6.1 while the rate of phase III fouling was lower than the corresponding value in Table 6.1. Therefore, the pattern of protein fouling is sustained even after splitting up the protein filtration into steps with washing in between but the rates get altered.

Table 6.6 Fouling rates in two step intermittent protein filtration (BSA concentration: 10 kg/m^3; membrane: 0.45 micron cellulose acetate; flux: 8.49×10^{-4} m/s; total volume of BSA solution filtered: 8+32 ml)

	Fouling rate (kPa/ml)	
	Step 1	Step 2
Phase I	0.96	Absent
Phase II	15.72	37.19
Phase III	-	1.30

Figure 6.19 shows the TMP profile for a single microfiltration experiment in which 16 ml of BSA solution was filtered through the membrane in four equal steps. After each 4 ml of protein filtration, 20 ml of buffer was used to front wash the

membrane. During the first protein filtration step, the increase in TMP was low but almost totally irreversible in nature. In the second protein filtration step, the TMP increased in two phases and more than half of the total increase was reversible in nature.

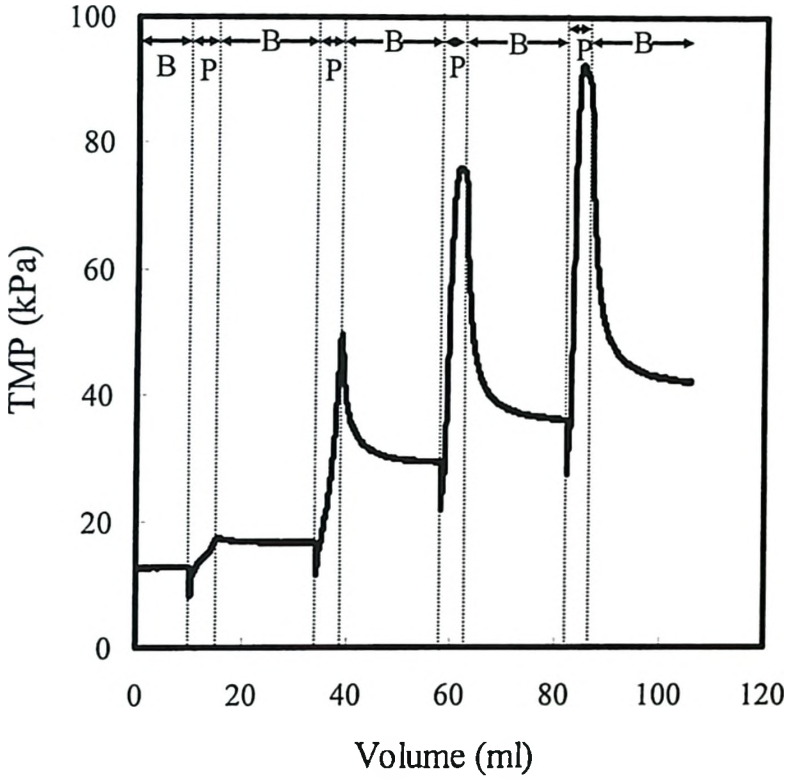

Figure 6.19 TMP as a function of permeate volume in four step protein filtration, each separated by 20 ml of buffer filtration (BSA concentration: 10 kg/m^3; 0.45 micron cellulose acetate membrane; flux: 8.49×10^{-4} m/s; volume of BSA solution: 4+4+4+4 ml); P – Protein filtration, B – Buffer filtration

In the third protein filtration step, the TMP increased quite rapidly initially but diminished towards the end, indicating the onset of phase III fouling. More than 85% of the increase in TMP during the third protein filtration step was reversible in nature. In the fourth protein filtration step, the initial TMP increase indicated phase II fouling. Quite clearly the front washing between the third and fourth protein filtration steps had moved the phase III fouling observed at the end of third step back to phase II fouling. However, towards the end of the fourth step a drop in TMP similar to that seen in Figure 6.18 indicated a re-start of phase III fouling. Again, almost 90% of the increase in TMP in the fourth step was reversible in nature. Table 6.7 shows rates of TMP increase in each of the four filtration steps.

Table 6.7 Fouling rates in four step intermittent protein filtration (BSA concentration: 10 kg/m^3; membrane: 0.45 micron cellulose acetate; flux: 8.49×10^{-4} m/s; total volume of BSA solution filtered: 4+4+4+4 ml)

	Fouling rate (kPa/ml)			
	Step 1	Step 2	Step 3	Step 4
Phase I	0.98	4.94	-	-
Phase II	-	13.27	27.83	38.31
Phase III	-	-	-	-

Figure 6.20 shows the TMP profiles for four different BSA microfiltration experiments, each carried out with a new membrane disc. In each of these experiments, a total of 8 ml of BSA solution was filtered through the membrane disc. In one of these, 8 ml of protein solution was filtered in one single step while in the others the 8 ml of protein solution was filtered in different step-wise combinations with 20 ml of buffer front washing following each step. When 8 ml of protein solution was filtered in three equal steps, there was almost no reversible fouling. The irreversible fouling at the end of the third step was slightly higher than the irreversible fouling observed with 8 ml of protein solution filtered as a single step. However, the total fouling in the single step protein filtration process was almost double than that due to the three equal steps. This is because of the presence of large amount of reversible fouling when 8 ml of protein solution was filtered in one step. Similar results were obtained when 8 ml of protein solution was filtered in three steps with first step comprising 4 ml of filtration and remaining two steps comprising 2 ml each. When 8 ml of protein solution was filtered in three steps with the first step consist of 6 ml of protein solution and remaining two steps comprising 1 ml each, both the total and irreversible fouling was higher than the one step filtration of 8 ml protein solution.

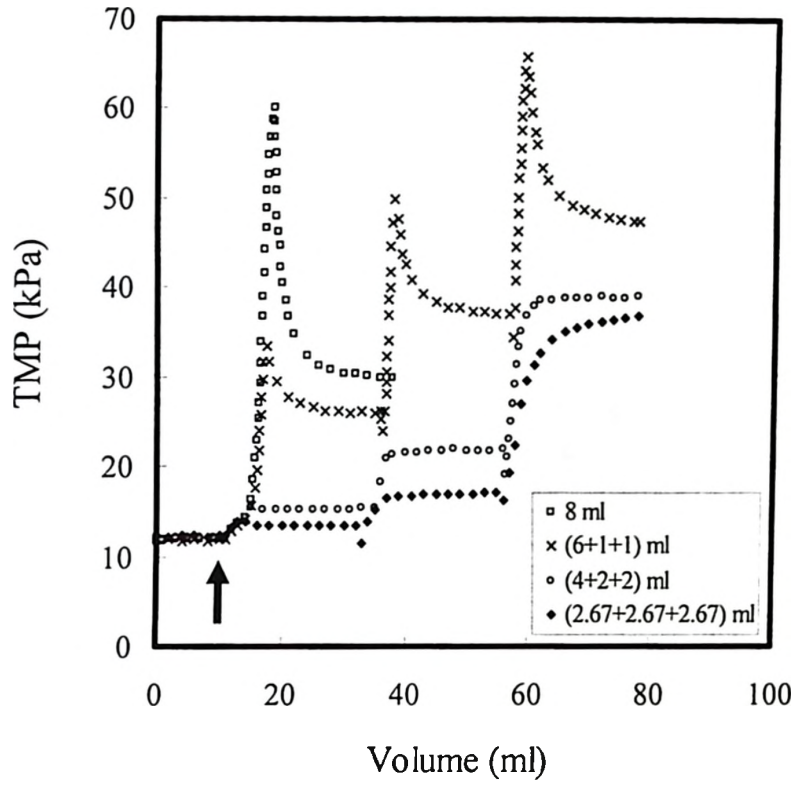

Figure 6.20 Continuous protein filtration vs intermittent protein filtration (BSA concentration: 10 kg/m^3; 0.45 micron cellulose acetate membrane; flux: 8.49×10^{-4} m/s; total volume of BSA solution: 8 ml)

Figure 6.21 shows the TMP profiles for another three BSA microfiltration experiments in which total 16 ml of protein solution was filtered through the membrane. In one of these, 16 ml of protein solution was filtered in one step while in the other two experiments, protein solution was filtered in two and four equal steps. Each protein

filtration step was followed by 20 ml of buffer front washing. The total membrane fouling was highest when protein solution was filtered in four equal steps of 4 ml and lowest when 16 ml of protein solution was filtered in one step. Comparison of the TMP profiles in Figure 6.20 and 6.21 suggest that if protein filtration is carried out intermittently in few steps, each one followed by few ml of buffer front washing rather

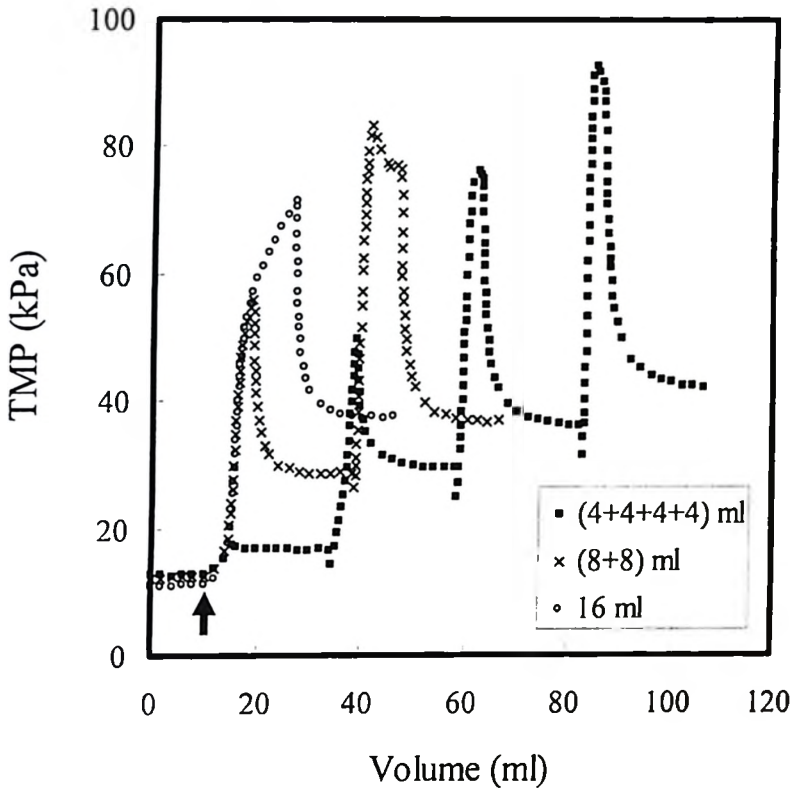

Figure 6.21 Continuous protein filtration vs intermittent protein filtration (BSA concentration: 10 kg/m^3; 0.45 micron cellulose acetate membrane; flux: 8.49×10^{-4} m/s; total volume of BSA solution: 16 ml)

than in one step, productivity of membrane either decreases or increases. If protein filtration is stopped in each step before the membrane fouling proceeds to phase II then productivity of membrane increases otherwise it decreases. It should be noted that with each protein filtration step, membrane fouling rate increases both for phase I and II. Since the fouling rate is much higher in phase II, membrane productivity can be increased by not allowing membrane fouling to reach phase II and carrying out the protein filtration by limiting the fouling to only phase I.

6.5 Conclusion

In constant permeate flux protein microfiltration processes carried out using in-line filters, the TMP increased in three distinct phases. Each phase could be characterized by its constant rate. The TMP increased much more rapidly in phase II when compared to phases I and III. A significant portion of TMP increase during protein filtration was reversible in nature despite almost 100% transmission of proteins through the membrane. The major increase in reversible fouling took place in phase II while the fouling during phase I was almost irreversible in nature. This apparent reversibility resulted from physical and reversible deposition of BSA monomers on protein aggregates retained on the membrane by sieving. The protein aggregates provided the initiation points for deposition of protein monomer. When aggregates were removed from the feed solution, fouling was negligible. The location of protein foulant was restricted to close to the membrane surface, clearly indicating the role of aggregates retained by sieving. This was

demonstrated by confocal laser scanning microscopy. Effect of different operating parameters such as feed protein concentration, permeate flux and washing flow rate and membrane properties such as pore size and membrane material on membrane fouling was studied. The protein deposit on membrane was found to be compressible in nature. Intermittent protein filtration experiments suggested that throughput of the membrane could be increased by preventing the fouling from proceeding to phase II.

6.6 References

1. L.J. Zeman and A.L. Zydney, Microfiltration and ultrafiltration: Principles and applications, Marcel Dekker, New York, 1996.
2. M. Cheryan, Ultrafiltration and microfiltration handbook, Technomic, Lancaster, 1998
3. A.S. Chandavarkar, C.L. Cooney, Mathematical modeling of flux decline caused by protein aggregation, ACS National Meeting, Washington DC, August 1990, cited from S.T. Kelly, W.S. Opong, A.L. Zydney, The influence of protein aggregates on the fouling of microfiltration membranes during stirred cell filtration, J. Membr. Sci., 80 (1993) 175.
4. M. Meireles, P. Aimar, V. Sanchez, Albumin denaturation during ultrafiltration: Effects of operating conditions and consequences on membrane fouling, Biotechnol. Bioeng., 38 (1991) 528.

5. W.S. Opong, A.L. Zydney, Hydraulic permeability of protein layers deposited during ultrafiltration, J. Colloid Interface Sci., 142 (1991) 41.
6. W.R. Bowen, Q. Gan, Properties of microfiltration membranes: Flux loss during constant pressure permeation of bovine serum albumin, Biotechnol. Bioeng., 38 (1991) 688.
7. A.D. Marshall, P.A. Munro, G. Tragardh, The effect of protein fouling in microfiltration and ultrafiltration on permeate flux, protein retention and selectivity: A literature review, Desalination, 91 (1993) 65.
8. E.M. Tracey, R.H. Davis, Protein fouling of track-etched polycarbonate microfiltration membranes, J Colloid Interface Sci., 167 (1994) 104.
9. C.C. Ho, A.L. Zydney, Effect of membrane morphology on system capacity during normal flow microfiltration, Biotechnol. Bioeng., 83 (2003) 537.
10. E. Iritani, Y. Mukai, Y. Tanaka, T. Murase, Flux decline behavior in dead-end microfiltration of protein solutions, J. Membr. Sci., 103 (1995) 181.
11. W.R. Bowen, J.I. Calvo, A. Hernandez, Steps of membrane blocking in flux decline during protein microfiltration, J. Membr. Sci., 101 (1995) 153.
12. J.S. Shiau, C.H. Tang, T.Y. Lin, D.M. Wang, A model for resistance growth during protein microfiltration, Sep. Sci. Technol., 38 (2003) 917.
13. M. Hlavacek, F. Bouchet, Constant flowrate blocking laws and an example of their application to dead-end microfiltration of protein solutions, J. Membr. Sci., 82 (1993) 285.

14. C.C. Ho, A.L. Zydney, A combined pore blockage and cake filtration model for protein fouling during microfiltration, J. Colloid Interface Sci., 232 (2000) 389.

15. G. Bolton, D. LaCasse, R. Kuriyel, Combined models of membrane fouling: Development and application to microfiltration and ultrafiltration of biological fluids, J. Membr. Sci., 277 (2006) 75.

16. C.D. Orsello, W. Li, C.C. Ho, A three mechanism model to describe fouling of microfiltration membranes, J. Membr. Sci., 280 (2006) 856.

17. C.C. Ho, A.L. Zydney, Theoretical Analysis of the effect of membrane morphology on fouling during microfiltration, Sep. Sci. Technol., 34 (1999) 2461.

18. S.T. Kelly, A.L. Zydney, Mechanisms for BSA fouling during microfiltration, J. Membr. Sci., 107 (1995) 115.

19. S.P. Palecek, S. Mochizuki, A.L. Zydney, Effect of ionic environment on BSA filtration and the properties of BSA deposits, Desalination, 90 (1993) 147.

20. S.T. Kelly, W.S. Opong, A.L. Zydney, The influence of protein aggregates on the fouling of microfiltration membranes during stirred cell filtration, J. Membr. Sci., 80 (1993) 175.

19. M. Ferrando, A. Rozek, M. Zator, F. Lopez, C. Guell, An approach to membrane fouling characterization by confocal scanning laser microscopy, J. Membr. Sci., 250 (2005) 283.

Chapter 7

Membrane Fouling Assessment Techniques

This chapter is organized based on the report submitted to 3M, Canada Company in **June 2006** by Dharmesh M Kanani and Raja Ghosh

7.1 Abstract

Traditional methods for studying fouling of MF membranes are very expensive and time consuming. This chapter reports three protocols to compare the protein fouling propensity of MF membranes. The first protocol is based on accelerated fouling in the dead end mode using pulsed injection technique. Apart from being very rapid, simple and cost-effective, it gives useful information about the membrane permeability, propensity of fouling and loss of membrane permeability due to both reversible and irreversible fouling. It also offers the flexibility of studying cleaning protocols simultaneously without dismantling the module. The two other protocols are based on critical flux

concept, one evaluated in dead end mode with syringe filter holder while the other with stirred cell module in the pseudo steady-state mode, both of these modes being widely used in the industry. The critical flux in dead end mode was much higher than the one in the pseudo steady state mode for a given membrane. The low critical flux with stirred cell module was attributed to the formation of relatively large protein aggregates in the bulk solution due to prolonged pumping.

7.2 Introduction

MF membranes are extensively used in downstream processing of protein solutions, e.g. for the separation of cell or cell debris from the proteinaceous media and sterile filtration of therapeutic grade proteins before final formulation. These membranes are either used in the dead-end mode in syringe type filter holders or in cross-flow in more specialized membrane modules, the mode depending on the types of application. Protein fouling is a major problem even though the pore sizes of the MF membranes are on average an order of magnitude larger than the sizes of the protein molecules. Fouling in constant pressure MF is reflected in a reduction in flux with time while in constant flux MF fouling leads to increase in TMP. Protein fouling of MF membranes is mainly attributed to the convection-induced protein deposition [1-2]. This protein deposition can either take place on membrane surface or inside the pores, the rate of which depends on the properties of membrane and protein solution as well as operating parameters such as temperature, TMP and shear rate near the membrane surface [3-5]. Fouling leads to the

time-dependent performance of the membrane processes i.e. productivity of the process decreases with time at constant operating conditions. Fouling also affects the quality of separation and necessitates frequent chemical cleaning of the membrane. This leads to the shorter life of the membrane and essentially contributes towards the processing cost. Fouling is still considered as the biggest obstacle for the wide-spread use of the membrane technology at commercial scale. Development of anti-fouling/fouling-resistant membranes can make membrane technology more attractive at commercial scale.

Membrane fouling is a complex phenomenon which requires very careful study. The study of membrane fouling has been extensively reported in the literature [6-19]. However, one of the major stumbling blocks in the study of membrane fouling has been the absence robust, reproducible membrane testing protocols which enjoy wide-spread acceptance. Traditionally, MF membranes are tested for their fouling propensity using flow decay method. This method involves the measurement of cumulative filtrate volume through a small membrane area until the flow rate drops to 10% or 20% of its initial value. The major disadvantage of this method is that a significant amount of protein solution is required to achieve the 80% or 90% reduction in flux. Proteins are expensive and hence extensive fouling assessment experiments such as flow decay method might not be the feasible option. Moreover, while developing new membranes, the sheer number of candidate membranes may make commercial scale fouling testing quite daunting not only in terms of cost but also the time. Hence, there is a requirement for

rapid, robust, reproducible, scaled-down fouling assessment techniques which provide processing conditions fairly representative of those in industrial scale processes.

The aims of our work are:

1) To design rapid, cost-effective and reliable protocols for testing membrane fouling by proteins in the dead-end and cross-flow modes

2) To compare the fouling propensity of different surface treated MF membranes developed at McMaster University with commercial membranes.

The specific goals are the development of the three types of protocols listed below:

1. Accelerated membrane fouling assessment in the dead-end mode using pulsed injection technique
2. Critical flux testing with syringe filter holder utilizing step input technique in the dead-end mode
3. Critical flux testing with stirred cell module in the pseudo steady-state mode

All three protocols are based on constant flux MF. In constant flux MF one has to monitor the TMP to track the fouling. This is relatively easy when compared to monitoring change in permeate flux which is required in constant pressure MF. Besides, it's relatively easy to run the filtration system at constant flux and all one need is just a good pump. Defrance and Jaffring have talked about the advantages of constant flux operation in more details [20].

7.3 Experimental

7.3.1 Materials

BSA (Catalog # A7906) was purchased from Sigma. Polyvinylidene fluoride (PVDF) membranes having pore size of 0.45 micron (Catalog # HVLP 142 50) were purchased from Millipore and cellulose acetate (CA) membranes having pore size of 0.45 micron (Catalog # DS0210-4045) were brought from Nalgene Nunc International. Polypropylene (designated as PP5) membranes having pore size of 0.45 micron were donated by 3M. Different surface treated membranes designated as E-4, PE-1, PE-3 and PE-4 were given by Prof. Ron Childs' group from Chemistry Department at McMaster University. These were prepared from PP5 membranes by some kind of surface treatment to render them hydrophilic and less prone to protein fouling. All other laboratory chemicals were purchased from Sigma.

7.3.2 Buffer and protein solution preparation

25 mM sodium phosphate buffer (pH 4.8) was used to prepare the protein solution. The rational behind choosing the solution pH 4.8 was the pI of BSA since proteins foul the membrane the most at their pI [1]. It was also used as the carrier phase in all the experiments in the first and second protocols. The buffer was prepared using 18.2 MΩ water obtained from a NANOpure Diamond Life Science (UV/UF) ultrapure water system and was microfiltered before use. 60 kg/m^3 BSA solution was used as the model foulant in the first protocol while 10 kg/m^3 BSA solution was used in the second

and third protocol. To prepare this test solution 80 kg/m^3 BSA was first prepared in 25 mM sodium phosphate buffer and the solution pH was adjusted to 4.8 using 0.1 M HCl. The protein solution was then centrifuged to remove any protein aggregate. The actual concentration of the protein in the solution was determined by measuring UV absorbance at 280 nm after appropriate dilution. This stock solution was then diluted to the required concentration using 25 mM sodium phosphate buffer, pH 4.8. The stock solution was stored at 4 – 6 °C temperature and used within 2 – 4 days of preparation.

7.3.3 Experimental set-up and methodology

Figure 7.1 shows the schematic diagram of the experimental set-up for the first protocol. A stainless steel syringe type filter holder (Whatman; 1980-001) having 13 mm nominal diameter was used as the membrane module. This could be fitted with membrane discs having effective diameter of 10 mm. Buffer was pumped at constant flow rate (4 ml/min) through the filter holder using a positive displacement pump (GE Healthcare; 19-1992-01). A constant permeate flux of 8.49×10^{-4} m/s through the membrane was maintained. The BSA solution was injected into the system in the form of a pulse using a sample injector valve (GE Healthcare; 19-7500-01) fitted with 5 ml sample loop (GE Healthcare; 18-1140-53). The pressure on the upstream side of the membrane was continuously monitored using a pressure sensor (Vernier Software & Technology; GBS-BTA) which was connected to a computer through an interface. The permeate was discharged to an open beaker at atmospheric pressure.

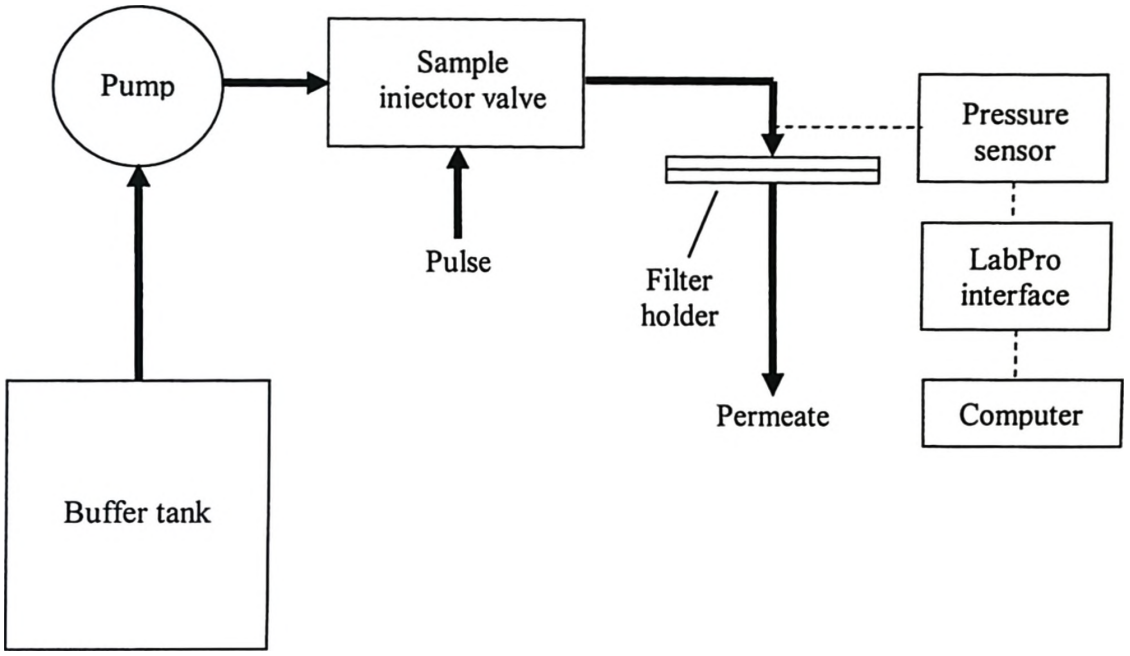

Figure 7.1 Experimental set-up for accelerated membrane fouling assessment in the dead-end mode

Each experiment in this study was carried out using a new membrane disc. The PP5 membrane is hydrophobic in nature and hard to wet with water. Therefore it was kept in ethanol for 30 minutes before use. This pre-treatment was not required for the other membranes discussed in this report. The protein solution was injected into the membrane module after 3 minutes of buffer flow through the membrane. The stable TMP before protein sample injection was used to determine the hydraulic permeability of the new membrane. A stable pressure also confirms the absence of any other foulant in the

carrier phase. After injecting the protein sample, buffer flow was maintained for another 6 minutes to wash the membrane disc. This removed any unbound or loosely held protein molecules. The stable pressure obtained after this washing was used to determine the hydraulic permeability of fouled membrane disc.

Figure 7.2 shows the schematic diagram of the experimental set-up for the second protocol. It is largely similar to the one used in the first protocol except the sample loop size. A 50 ml superloop was used for sample injection in this protocol. The BSA solution was injected into the system in the form of incremental flux steps using this superloop. The pressure on the upstream side of the membrane was continuously monitored using a pressure sensor. The permeate was discharged to an open beaker at atmospheric pressure.

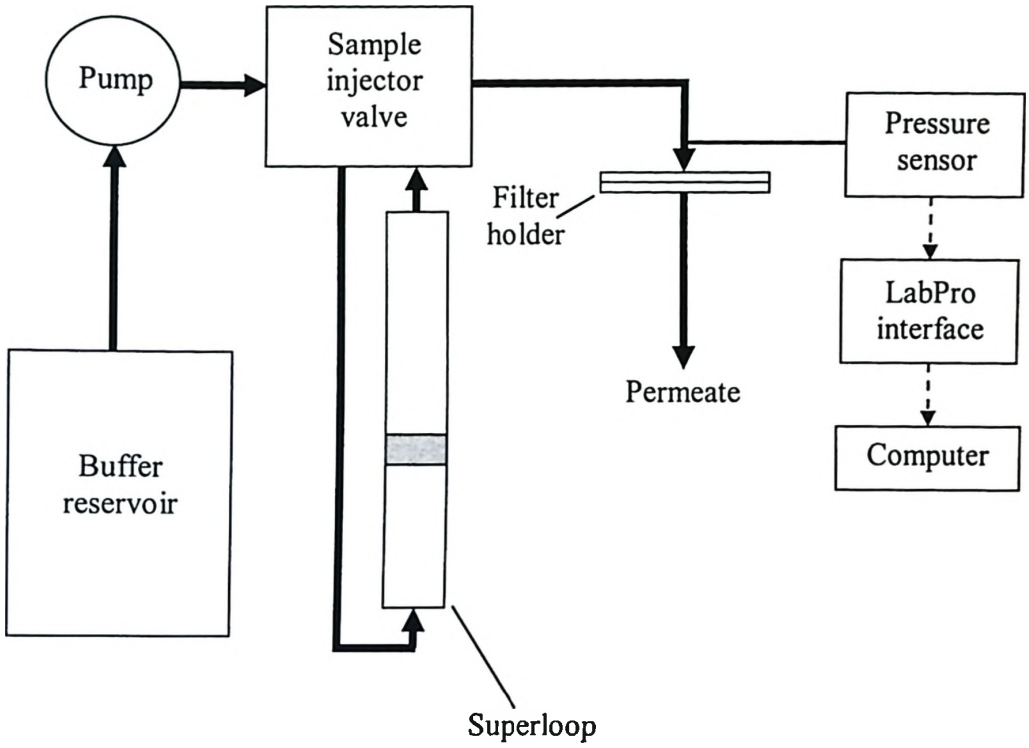

Figure 7.2 Experimental set-up for critical flux testing with syringe filter holder

Each experiment was carried out with a new membrane disc. Before protein sample injection, the membrane permeability was determined by passing buffer through the membrane at three different fluxes and measuring the corresponding TMP. The protein solution was filtered through the membrane at a flux of 2.12×10^{-4} m/s and the flux was increased in steps from $2.12\times10^{-4} \rightarrow 3.40\times10^{-4} \rightarrow 4.67\times10^{-4} \rightarrow 5.94\times10^{-4} \rightarrow 7.22\times10^{-4} \rightarrow 8.49\times10^{-4} \rightarrow 9.76\times10^{-4}$ m/s with each step size corresponded to 4 ml of

permeate volume. The stability of TMP during these steps was used to determine whether fouling had occurred. This method does not give an exact value of critical flux but is able to identify the range in which it takes place.

Figure 7.3 shows the schematic diagram of the experimental set-up for the third protocol. The stirred cell had working volume of 15.5 ml, and was fitted with membrane disc having effective diameter of 24 mm. The suspended bar impeller (diameter = 18.7 mm) inside the module was magnetically driven. Pump 'A' re-circulated the protein solution between feed tank and the stirred cell. The recirculation rate was monitored by flow meter '1'. Pump 'B' drove the permeate from stirred cell by suction at constant rate and this was directed back to the feed tank. The permeate flow was monitored by flow meter '2'. Both pumps were calibrated as instructed by the manufacturer. The TMP across the membrane was continuously monitored by a manometer which was connected to a computer for data logging. One leg of the manometer was connected to the upstream side of module while the other one was connected to the downstream side of module to give the TMP.

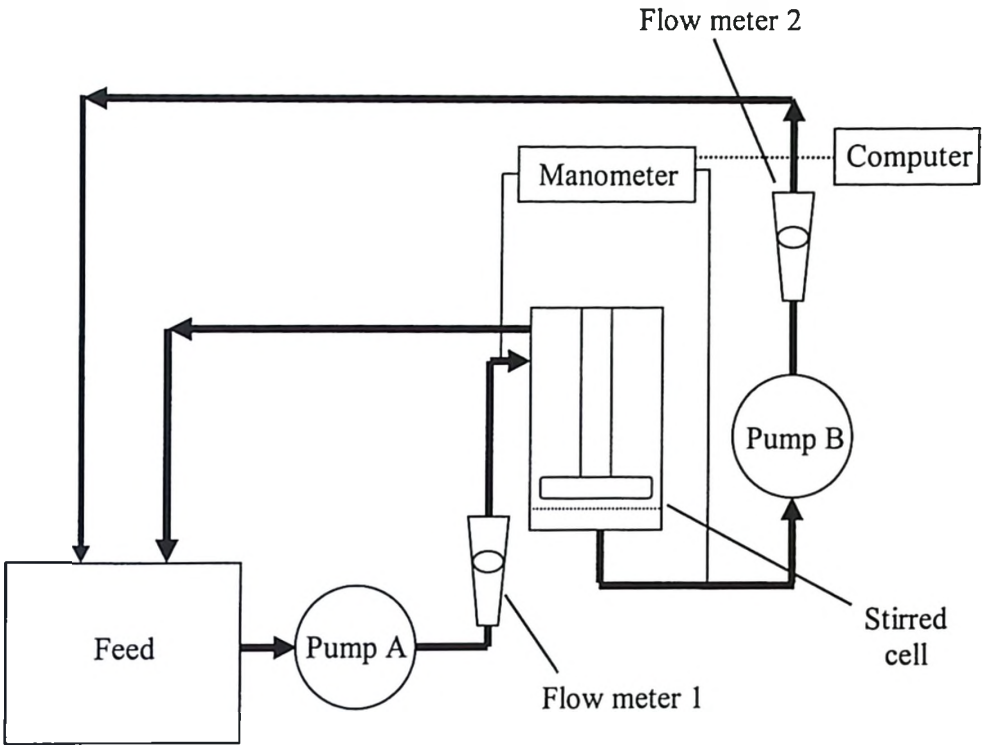

Figure 7.3 Experimental set-up for the stirred cell based protocol

Each experiment in this protocol was carried out with a new membrane disc. The stirred cell and feed tank were initially filled with phosphate buffer and the membrane permeability was determined by filtering buffer through the membrane at three different fluxes and measuring the corresponding TMP. The stirred cell and the connecting tubing were then emptied of the buffer and refilled with the BSA solution and connected to another feed tank containing additional BSA solution. In all the experiments the stirring

speed inside the module was kept constant at 950±50 rpm and the recirculation rate was set at 32.5 ml/min. All the experiments in this protocol were carried out using stepping flux method. Protein filtration was started at 8.35×10^{-6} m/s flux and was carried out until 10 ml of permeate volume was collected. Then flux was increased in steps from $8.35\times10^{-6} \rightarrow 16.70\times10^{-6} \rightarrow 25.05\times10^{-6} \rightarrow 33.39\times10^{-6} \rightarrow 41.74\times10^{-6} \rightarrow 50.09\times10^{-6} \rightarrow 58.44\times10^{-6} \rightarrow 66.79\times10^{-6} \rightarrow 75.14\times10^{-6} \rightarrow 83.48\times10^{-6}$ m/s with each step corresponded to 10 ml of permeate volume. The stability of TMP during the collection of 10 ml was exploited to detect the onset of critical flux.

7.4 Accelerated membrane fouling assessment in the dead-end mode using pulsed injection technique

Using this protocol, the fouling of MF membranes housed in a syringe type filter holder can be studied in the dead-end mode by the pulsed injection of a foulant (model protein) [21]. Dead-end MF is widely used for protein clarification and sterilization. In this protocol, MF membranes were subjected to very severe operating conditions for a very short period of time, the purpose being to simulate the fouling that would take place at a normal operating condition over an extended period of time. A few preliminary experiments were performed with 0.45 micron PVDF membrane to determine the amount of protein needed to substantially foul the membrane. The effects of feed protein concentration and the flux on membrane fouling were systematically studied. Based on these preliminary experiments, 60 kg/m^3 protein concentration was chosen in

combination with a 5 ml foulant sample volume. All the membranes were tested for their protein fouling propensity at 8.49×10^{-4} m/s flux. Figure 7.4 shows TMP vs. time profiles for six different MF membranes.

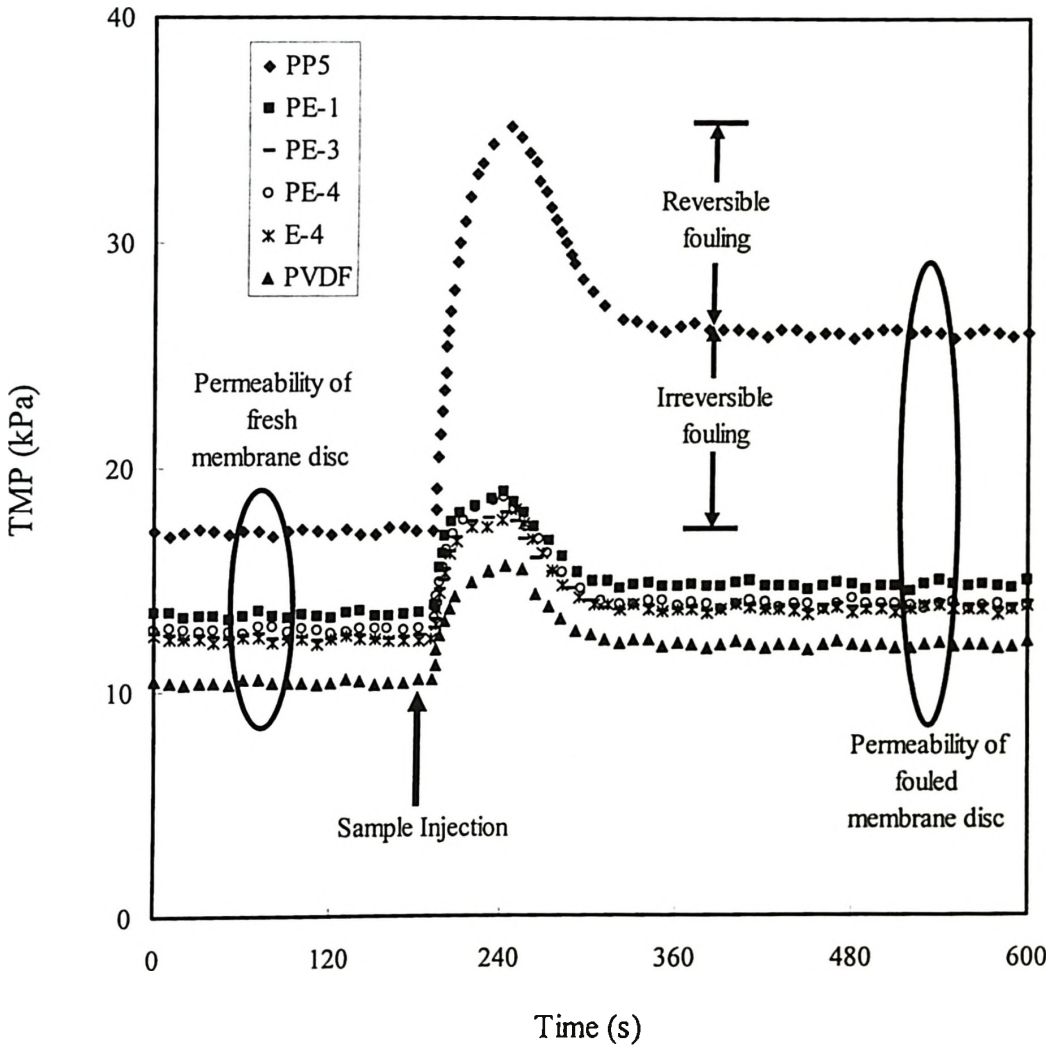

Figure 7.4 TMP vs. time profiles for six different MF membranes in the first protocol (BSA concentration: 60 kg/m^3; flux: 8.49×10^{-4} m/s and; pulse volume: 5 ml)

In Figure 7.4, the instant of introduction of the protein sample into the membrane module is marked by an arrow. The TMP started increasing as soon as the protein solution was injected into the module. Once the complete pulse of protein sample had passed through the membrane, the TMP decreased and stabilized at a certain value, this depending on the amount of irreversible protein fouling. In a given experiment, the difference between maximum TMP during protein filtration and steady TMP corresponding to buffer filtration after protein injection gives an idea about reversible fouling. The difference between TMP corresponding to buffer filtration before and after protein injection gives an idea about the loss of membrane permeability due to irreversible protein fouling. Preliminary experiments had indicated that both reversible and irreversible fouling resistance increased with the amount of protein solution filtered. Besides, a membrane which showed high irreversible fouling also showed higher reversible fouling. It is evident from Figure 7.4 that PP5 is the worst membrane both in terms of membrane permeability for buffer and the loss of membrane permeability due to protein fouling (both reversible and irreversible). PVDF membrane showed the highest permeability both before and after protein filtration. All the surface treated membranes had lower permeability both before and after protein filtration than the PVDF membrane.

A new parameter called "Performance Factor (Z)" is introduced to evaluate the performance of membrane in protein filtration quantitatively. A good membrane should have both higher permeability as well as better fouling resistance. Based on this rational,

Performance Factor (Z) is defined as a ratio of permeability of fouled membrane disc to the total TMP increase due to pulse injection.

$$Performance\ Factor\,(Z) = \frac{\xi_2}{[(P_3 - P_1) + (P_2 - P_3)]} = \frac{\xi_2}{P_2 - P_1} \qquad (7.1)$$

Where, ξ_2 = Permeability of fouled membrane disc

P_1 = TMP corresponding to buffer filtration through new membrane disc

P_2 = Maximum TMP during protein filtration or during the test

P_3 = TMP corresponding to buffer filtration through fouled membrane disc

$P_3 - P_1$ = TMP increase due to irreversible fouling

$P_2 - P_3$ = TMP increase due to reversible fouling

$P_2 - P_1$ = Total TMP increase due to fouling

This parameter takes into account both the permeability of fouled membrane disc and the total membrane fouling which is the sum of reversible and irreversible membrane fouling. A better membrane should have not only higher resistance towards membrane fouling (i.e. low increase in TMP due to fouling) but also higher ξ_2, final membrane permeability (i.e. low TMP corresponding to buffer filtration through the fouled membrane). Here, it should be noted that reversible fouling denotes the resistance to flow due to the factors other than irreversible deposition/adsorption of proteins on the membrane surface or within the pores of membrane. Some kind of cleaning is necessary to restore the loss of permeability due to irreversible fouling. Table 7.1 shows the comparison of different membranes in terms of their Performance Factors. The PP5 membrane is hydrophobic in nature and hence, it gave the worst performance as seen in

Figure 7.4. The poor effectiveness of PP5 membrane for protein filtration is also reflected in its very low Performance Factor. The PVDF membrane gave the highest Performance Factor among all the membranes tested. The high efficiency of PVDF membrane for protein filtration is quite evident from Figure 7.4 also. The Performance Factors for the surface treated membranes PE-1, PE-3, PE-4 and E-4 were much higher than their raw substrate PP5 membrane but still slightly lower than commercial PVDF membrane. This would suggest much better performance of surface treated membranes over their raw substrate PP5 for protein filtration. This is also quite evident from Figure 7.4. Thus, Performance Factor can be used as a good judge to compare the performance of MF membranes for protein filtration using this protocol.

Table 7.1 Membrane performance comparison via a newly defined parameter termed as 'Performance Factor' using the first protocol

Membrane	P_1 (kPa)	P_2 (kPa)	P_3 (kPa)	ζ_1 (m/kPas)	ζ_2 (m/kPas)	Performance Factor (Z), $\zeta_2/(P_2-P_1)$ (m/kPa^{2}s)
PVDF	10.42	15.50	12.02	81.5×10^{-6}	70.6×10^{-6}	13.9×10^{-6}
PP5	17.12	35.20	25.92	49.6×10^{-6}	32.8×10^{-6}	1.8×10^{-6}
E-4	12.35	18.00	13.60	68.7×10^{-6}	62.4×10^{-6}	11.0×10^{-6}
PE-1	13.43	18.80	14.68	63.2×10^{-6}	57.8×10^{-6}	10.8×10^{-6}
PE-3	12.43	18.00	13.73	68.3×10^{-6}	61.8×10^{-6}	11.1×10^{-6}
PE-4	12.77	18.60	13.79	66.5×10^{-6}	61.6×10^{-6}	10.6×10^{-6}

This protocol can also be used to rapidly study the efficiency of different types of cleaning solutions and the cleaning procedures to restore the performance of fouled membranes. In this work, we have used 25 mM sodium phosphate buffer having pH 4.8 for the front washing of the membrane after injecting the pulse of protein solution. But instead of it, any cleaning solution can be used for front washing the membrane to see its effectiveness. This protocol can also be slightly modified to include the backwashing by replacing the positive displacement pump with peristaltic pump (in which flow can be reversed) and connecting the outlet of the membrane module through a stopcoke 3-way valve with a beaker containing the cleaning solution and another container to collect the permeate.

7.5 Critical flux testing with syringe filter holder utilizing step input technique in the dead-end mode

Earlier studies indicated the existence of an identifiable critical flux in most MF and UF processes below which there is no or little membrane fouling [22-24]. Recently, Bacchin, Aimer and Field [25] have reviewed the concept of critical flux both from theoretical and experimental viewpoint. They compared the various methods reported in the literature to measure the critical flux in terms of their advantages and disadvantages along with their suitability for different types of application. They also explained the concept of sustainable flux and linked it with the concept of critical flux. Generally

speaking, critical flux is defined as the 'first' permeate flux at which fouling becomes noticeable. For a given feed solution the higher the critical flux the better is the membrane's performance in terms of fouling resistance and productivity. Critical flux of the membrane is usually measured at steady-state conditions in the cross-flow mode. This is both time and material consuming. We propose a protocol for rapidly determining the critical flux of MF membranes housed in syringe type filter holder in the dead-end mode. This protocol relies on the fact that protein transmission through MF membrane before it gets fouled severely is typically 100%.

Figure 7.5 shows the TMP and flux profiles plotted against the permeate volume for six different MF membranes. The protein filtration part is separated from the buffer filtration by dotted line. Relatively higher TMP for PP5 membrane during buffer filtration before protein injection indicates its lower permeability among all the membranes tested. The critical flux of PP5 membrane also seems to be lower than 2.12×10^{-4} m/s since TMP started increasing quite rapidly as soon as protein filtration started at 2.12×10^{-4} m/s. The remaining five membranes gave stable TMP at fluxes 2.12×10^{-4} m/s and 3.40×10^{-4} m/s. The PVDF membrane shows the highest permeability at all the fluxes tested. Figures 7.6 and 7.7 show the TMP and flux versus permeate volume profiles for the PVDF membrane and surface treated membranes respectively. The critical fluxes of these membranes seem to be in the same range.

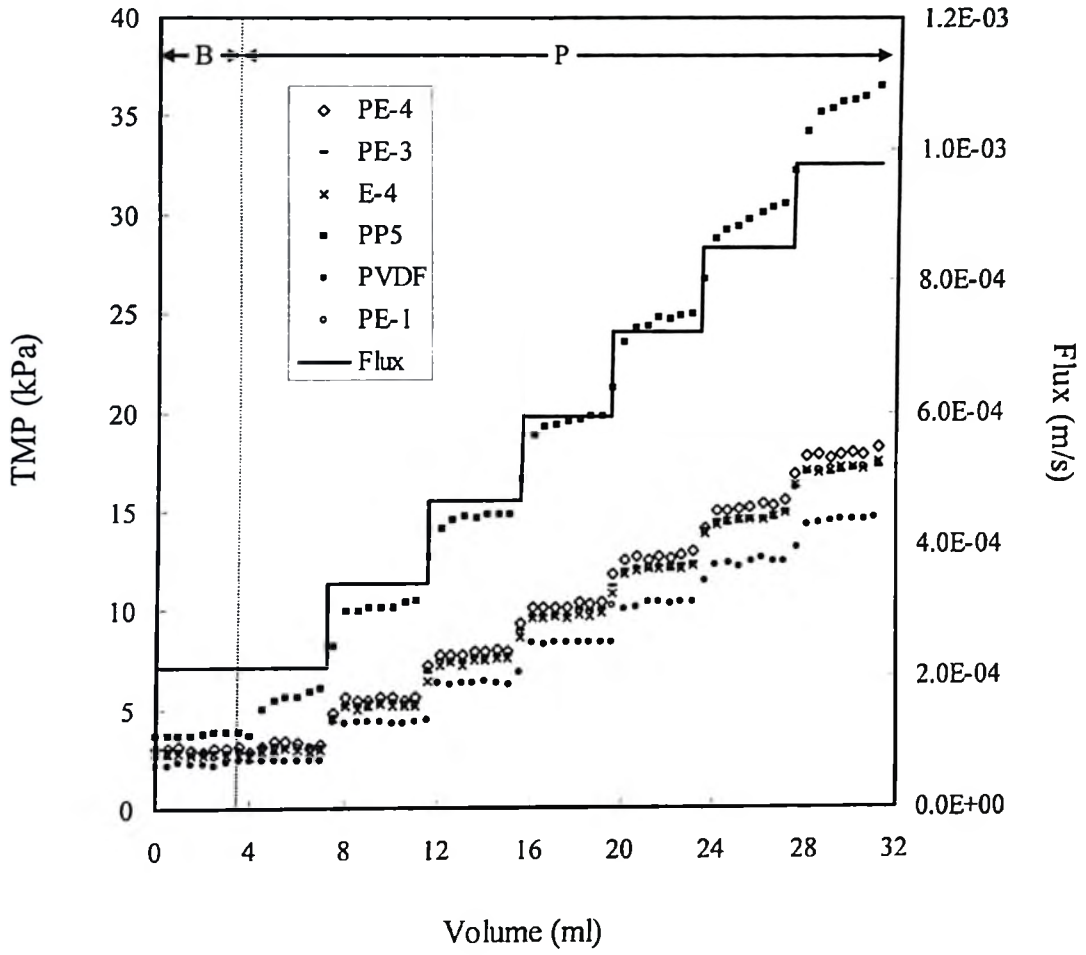

Figure 7.5 Critical flux study of different membranes in dead end mode: TMP and flux at different permeate volumes (BSA concentration: 10 kg/m^3; step size: 4 ml)

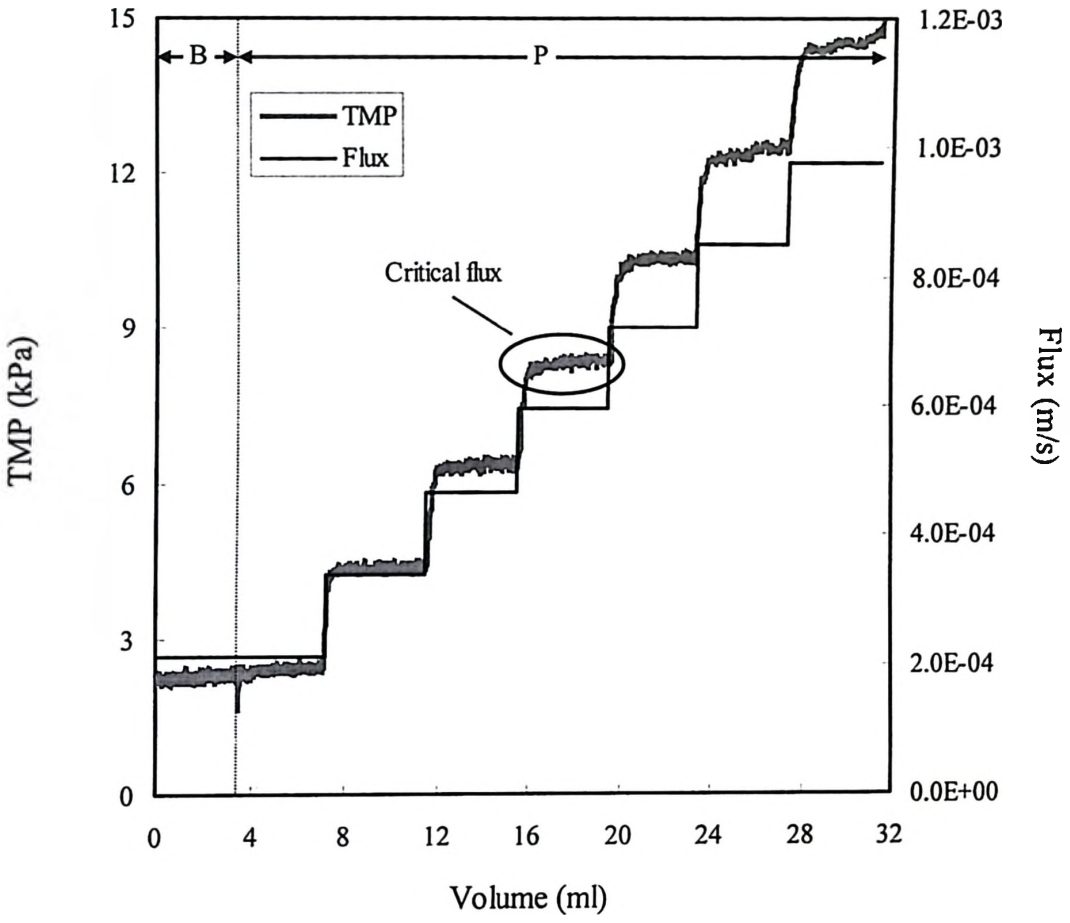

Figure 7.6 Critical flux of PVDF membrane (BSA concentration: 10 kg/m^3; step size: 4 ml)

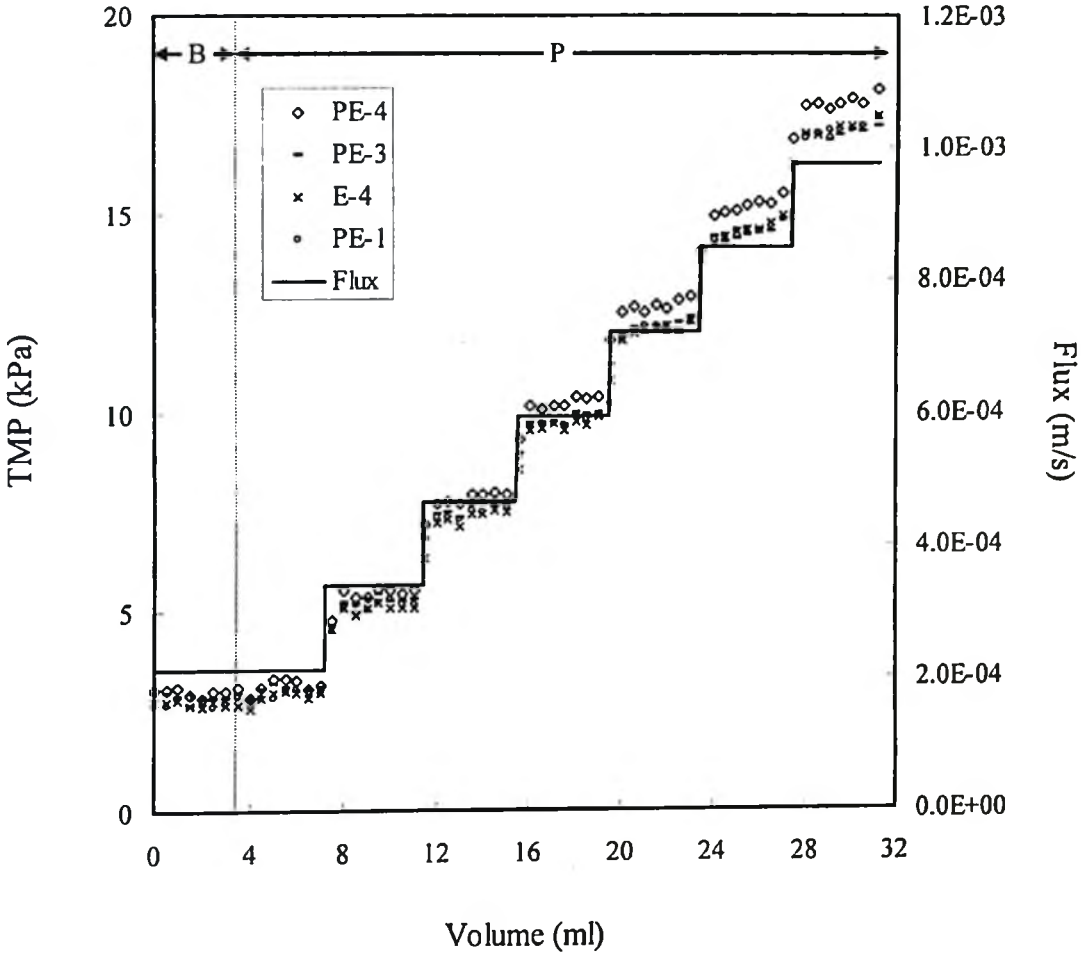

Figure 7.7 Critical flux of surface treated membranes (BSA concentration: 10 kg/m^3; step size: 4 ml)

Table 7.2 reports the slopes of the TMP vs. permeate volume profiles at different fluxes for six MF membranes. There are no reported standards characterizing the noticeable fouling rate, which can be used to define critical flux. This necessitates defining a fouling rate or slope of the TMP vs. permeate volume profile which can be used to identify the critical flux. In this protocol, the critical flux is defined as the flux at which TMP increases at a rate of 0.05 kPa/cm^{2}ml. Below this value, increase in TMP was found to be very slow and underutilized the potential throughput of membrane. At slopes higher than 0.05 kPa/cm^{2}ml, TMP increased quite rapidly in a short period of time and therefore lowering the total capacity of membrane.

Table 7.2 Slope of TMP vs. permeate volume data at different fluxes for all the membranes tested in the second protocol

	PP5	PVDF	E-4	PE-I	PE-3	PE-4
2.12×10^{-4} (m/s)	**0.2343**	*	*	*	*	*
3.40×10^{-4} (m/s)	0.1533	*	*	*	*	*
4.67×10^{-4} (m/s)	0.2139	*	**0.0615**	0.0477	0.0364	0.0400
5.94×10^{-4} (m/s)	0.3565	**0.0591**	0.0831	**0.0654**	**0.637**	**0.0829**
7.22×10^{-4} (m/s)	0.3731	0.0488	0.0975	0.0890	0.0761	0.0856
8.49×10^{-4} (m/s)	0.7588	0.1180	0.2131	0.1789	0.1528	0.1962

Based on the above critical flux definition, the critical flux of the PVDF membrane is in the range 4.67×10^{-4} – 5.94×10^{-4} m/s while that of PP5 is less than 2.12×10^{-4} m/s. PE1, PE3 and PE4 membranes have critical flux in between 4.67×10^{-4} – 5.94×10^{-4} m/s while that of E4 is in between 3.40×10^{-4} – 4.67×10^{-4} m/s.

7.6 Critical flux testing with stirred cell module in the pseudo steady-state mode

In this protocol, the critical flux of a membrane is measured using a stirred cell module. This test is representative of tangential flow MF. Figure 7.8 shows the TMP and flux at different permeate volumes for six different MF membranes. At very low flux, the TMP remains stable with respect to the permeate volume. Once the critical flux is reached for a particular membrane, the TMP starts increasing.

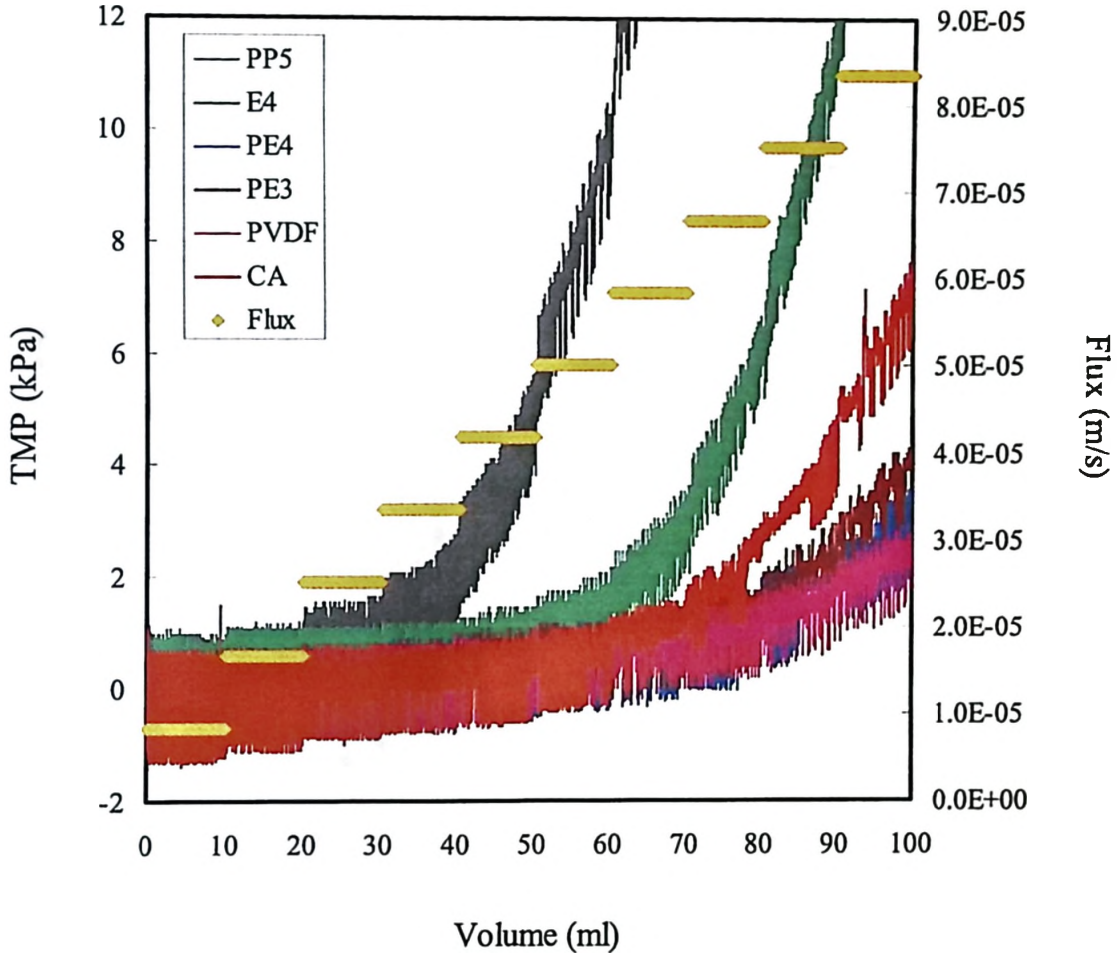

Figure 7.8 Critical flux of different MF membranes with the stirred cell protocol (BSA concentration: 10 kg/m^3; cross flowrate: 32.5 ml/min; stirring speed: 950±50 rpm; step size: 10 ml)

PP5 membrane showed a very low critical flux value and fouled severely above the critical flux while the PVDF membrane showed a much higher critical flux. The PVDF membrane also fouled less severely above the critical flux. The CA membrane gave a slightly inferior performance when compared with the PVDF membrane. PE-3 and PE-4 membranes gave better performance than the CA membrane. Table 7.3 summarizes the slopes of the TMP vs. permeate volume profiles at different fluxes for all the MF membranes. For this protocol, the critical flux is defined as the flux at which TMP increases at a rate of 0.009 kPa/ cm^2ml or higher. Below this value, the increase in TMP cane be regarded as negligible. Again, the value of fouling rate defining the critical flux was arbitrary chosen for this protocol keeping into mind the experimental methodology. It is quite possible that the same membrane can give different value of critical flux if the experimental methodology (such as step length, cross-flow etc) is changed slightly even with the same feed protein solution. Based on this definition, critical flux of the PVDF membrane was between 75.14×10^{-6} – 83.48×10^{-6} m/s, that of PP5 was in between 25.05×10^{-6} – 33.39×10^{-6} m/s and that of the CA membrane was between 58.44×10^{-6} – 66.79×10^{-6} m/s. All the surface treated membranes have critical flux higher than the PP5 membrane. Critical flux of E-4, PE-3 and PE-4 membranes were between 41.74×10^{-6} – 50.09×10^{-6}; 66.79×10^{-6} – 75.14×10^{-6} and 58.44×10^{-6} – 66.79×10^{-6} m/s respectively.

Table 7.3 Slope of TMP vs. permeate volume data at different fluxes for all the membranes tested in the third protocol

	PP5	PVDF	E-4	PE-3	PE-4	CA
8.35×10^{-6} (m/s)	*	*	*	*	*	*
16.70×10^{-6} (m/s)	0.0010	*	*	*	*	*
25.05×10^{-6} (m/s)	0.0043	*	*	*	*	*
33.39×10^{-6} (m/s)	**0.0165**	*	0.0016	*	*	*
41.74×10^{-6} (m/s)	0.0536	*	0.0029	0.0003	*	*
50.09×10^{-6} (m/s)	0.0860	0.0008	**0.0106**	0.0009	*	0.0071
58.44×10^{-6} (m/s)	0.1369	0.0034	0.0282	0.0024	*	0.0065
66.79×10^{-6} (m/s)	0.2128	0.0039	0.0625	0.0063	**0.0162**	**0.0261**
75.14×10^{-6} (m/s)	0.2864	0.0081	0.1191	**0.0167**	0.0161	0.0287
83.48×10^{-6} (m/s)	0.3185	**0.0140**	0.2064	0.0309	0.0180	0.0529

The critical fluxes of the membranes are highlighted in bold letters in Table 7.3. The data shown above clearly demonstrates the superiority of the surface treated membranes compared to the PP5 membrane in terms of their protein fouling resistance. PE-3 and PE-4 membranes have higher critical fluxes than the CA membrane. Indeed, the performance of PE-4 membrane was close to the PVDF membrane which regarded as a good commercial MF membrane.

Comparison of Table 7.2 and 7.3 clearly shows that the critical flux of respecti membrane was much lower in protocol 3 compared to protocol 2. This can be explained in terms of fouling by protein aggregates generated by shear denaturation of the proteins during repeated pumping in protocol 3. Chandavarkar and Cooney [26] have found that the rate of flux decline during cross-flow MF of BSA was strongly dependent on the characteristics of the pumps used to drive the protein solution through the module. They observed that prolonged pumping resulted in the formation of relatively large protein aggregates in the bulk solution, with the observed fouling behavior attributed to the deposition of these large aggregates on the membrane surface. Meireles et al. [27] have also reported the similar effects of pumping on protein aggregation in their study of BSA fouling of UF membranes. In protocol 2, membrane fouling was studied in dead end mode in which protein solution was not passed through the pump even once but it was directly injected from the superloop to the membrane module. Besides, protein solution was not recycled in protocol 2. While in protocol 3, membrane fouling was studied in cross-flow mode, in which total two pumps were used to drive the protein solution

through the module. Due to the closed system in protocol 3, prolonged pumping resulted in the formation of protein aggregates which caused lower critical flux. This was further verified by measuring the critical flux of PVDF membrane with experimental set up shown in Figure 7.3 but without cross flow pump and recycling of permeate back to the feed tank. This resulted in much higher critical flux, quite similar to the one in protocol 2.

7.7 Summary

In this chapter, three protocols which have been developed to assess the performance of MF membranes are discussed. The first protocol is based on accelerated fouling and rapidly gives information about the membrane permeability, propensity of fouling and loss of membrane permeability due to both irreversible and reversible fouling. Typical testing time is about 10 minutes. In addition to being a rapid technique, it is very easy to maintain sanitary conditions during the experiment. One of the attractive features of this protocol is the feasibility of studying cleaning protocol simultaneously without dismantling the module. The remaining two protocols are based on the critical flux concept, in which the objective is to identify the flux region where protein fouling is zero or negligible. The higher the critical flux of a membrane, the better is the productivity. The critical fluxes of membranes were measured both in dead-end mode and cross-flow mode, both modes being widely used in the industry. Normally, MF of protein solution is carried out in the dead-end mode in the polishing-up stages of a purification process for example to remove virus particles from finished products. MF in

the cross-flow mode is used in the early stages of a purification process for example to remove particulate material such as cells and cell debris from solutions. The MF membranes showed higher critical fluxes in the dead-end mode when compared to the cross-flow mode. This is counter intuitive and totally different from what is observed in MF of particulate material. This can be explained in terms of protein denaturation and hence aggregation of proteins over a period of time in cross-flow mode. In the dead-end mode, protein solution was used only once as there was no recirculation. Besides, there was no stirring and repeated pumping.

7.8 References

1. A.D. Marshall, P.A. Munro, G. Tragardh, The effect of protein fouling in microfiltration and ultrafiltration on permeate flux, protein retention and selectivity: A literature review, Desalination, 91 (1993) 65.
2. W.S. Opong, A.L. Zydney, Hydraulic permeability of protein layers deposited during ultrafiltration, J. Colloid Interface Sci., 142 (1991) 41.
3. L.J. Zeman and A.L. Zydney, Microfiltration and ultrafiltration: Principles and applications, Marcel Dekker, New York, 1996.
4. M. Cheryan, Ultrafiltration and microfiltration handbook, Technomic, Lancaster, 1998.
5. R. Ghosh, Protein bioseparation using ultrafiltration: Theory, applications and new developments, Imperial College Press, London, 2003.

6. W.R. Bowen, Q. Gan, Properties of microfiltration membranes: Flux loss during constant pressure permeation of bovine serum albumin, Biotechnol. Bioeng., 38 (1991) 688.
7. M. Hlavacek, F. Bouchet, Constant flowrate blocking laws and an example of their application to dead-end microfiltration of protein solutions, J. Membr. Sci., 82 (1993) 285.
8. E.M. Tracey, R.H. Davis, Protein fouling of track-etched polycarbonate microfiltration membranes, J Colloid Interface Sci., 167 (1994) 104.
9. A.L. Zydney, C.K. Colton, A concentration polarization model for the filtrate flux in cross-flow microfiltration of particulate suspensions, Chem. Eng. Commun., 47 (1986) 1.
10. E. Iritani, Y. Mukai, Y. Tanaka, T. Murase, Flux decline behavior in dead-end microfiltration of protein solutions, J. Membr. Sci., 103 (1995) 181.
11. W.R. Bowen, J.I. Calvo, A. Hernandez, Steps of membrane blocking in flux decline during protein microfiltration, J. Membr. Sci., 101 (1995) 153.
12. A. D. Marshall, P.A. Munro, G. Tragradh, Influence of permeate flux on fouling during the microfiltration of beta-lactoglobulin solutions under cross-flow conditions, J. Membr. Sci., 130 (1997) 23.
13. V. Chen, Performance of partially permeable microfiltration membranes under low fouling conditions, J. Membr. Sci., 147 (1998) 265.
14. C.C. Ho, A.L. Zydney, A combined pore blockage and cake filtration model for protein fouling during microfiltration, J. Colloid Interface Sci., 232 (2000) 389.

15. C.C. Ho, A.L. Zydney, Transmembrane pressure profiles during constant flux microfiltration of bovine serum albumin, J. Membr. Sci., 209 (2002) 363-377.

16. C.C. Ho, A.L. Zydney, Scale-up of microfiltration systems: fouling phenomena and V_{max} analysis, Desalination, 146 (2002) 75.

17. C.C. Ho, A.L. Zydney, Effect of membrane morphology on system capacity during normal flow microfiltration, Biotechnol. Bioeng., 83 (2003) 537.

18. M.E. Laska, R.P. Brooks, M. Gayton, N.S. Pujar, Robust scale-up of dead end filtration: Impact of filter fouling mechanisms and flow distribution, Biotechnol. Bioeng., 92 (2005) 308.

19. K. Young-June Choi, B.A. Dempsey, Bench-scale evaluation of critical flux and TMP in low-pressure membrane filtration, J. – Am. Water Works Assoc., 97 (2005) 134.

20. L. Defrance, M.Y. Jaffrin, Comparison between filtrations at fixed transmembrane pressure and fixed permeate flux: application to a membrane bioreactor used for wastewater treatment, J. Membr. Sci., 152 (1999) 203.

21. R. Ghosh, Study of membrane fouling by BSA using pulsed injection technique, J. Membr. Sci., 195 (2002) 115.

22. R.W. Field, D. Wu, J.A. Howell, B.B. Gupta, Critical flux concept for microfiltration fouling, J. Membr. Sci., 100 (1995) 259.

23. J.A. Howell, Sub-critical flux operation of microfiltration, J. Membr. Sci., 107 (1995) 165.

24. P. Bacchin, P. Aimer, V. Sanchez, Model for colloidal fouling of membranes, AIChE J., 41 (1995) 368.

25. P. Bacchin, P. Aimar, R.W. Field, Critical and sustainable fluxes: Theory, experiments and applications, J. Membr. Sci., 281 (2006) 42.

26. A.S. Chandavarkar, C.L. Cooney, Mathematical modeling of flux decline caused by protein aggregation, ACS National Meeting, Washington DC, August 1990, cited from S.T. Kelly, W.S. Opong, A.L. Zydney, The influence of protein aggregates on the fouling of microfiltration membranes during stirred cell filtration, J. Membr. Sci., 80 (1993) 175.

27. M. Meireles, P. Aimar, V. Sanchez, Albumin denaturation during ultrafiltration: Effects of operating conditions and consequences on membrane fouling, Biotechnol. Bioeng., 38 (1991) 528.

Chapter 8

Research Contributions and Recommendations for Future Work

8.1 Research contributions of thesis work

Protein bioseparation is a decisive factor in the successful commercialization of protein based biopharmaceuticals. It typically accounts for 50-80% of the total production cost. Due to the increased sales of approved protein biopharmaceuticals and increasing public opinion against rising drug costs, there is a need for economical bioseparation methods which combine high product throughput with high-resolution purification. Synthetic membrane based bioseparation techniques are promising in this respect. This thesis work has made significant contributions to the area of synthetic membrane based

processes ultrafiltration, membrane chromatography and microfiltration for protein bioseparation. The work in this thesis looks towards both the selectivity and throughput of membrane processes on the whole. The major research contributions of this thesis work are summarized in the following five subsections.

8.1.1 Protein bioseparation by ultrafiltration

Earlier researchers have mostly focused on manipulation of hydrodynamic volumes of proteins by optimizing the buffer conditions, protein-membrane interactions and control of concentration polarization to enhance/alter the selectivity of protein-protein separation by ultrafiltration. They have shown that good selectivity could be obtained in protein ultrafiltration by careful selection of buffer conditions and membrane, thereby exploiting the differences in charges on membrane and proteins. But protein-protein interactions have not been paid enough attention to manipulate the selectivity of separation. It has been widely perceived that presence of largely retained proteins near the membrane could hinder the passage of more favorably transmitted proteins. In this work, we have shown for the first time that selectivity could be changed quite dramatically or indeed a reversed selectivity could be obtained by simultaneously decreasing the sieving coefficient of preferentially transmitted protein and increasing the sieving coefficient of preferentially retained protein. This was made possible by exploiting the protein-protein interactions or more generally speaking the solute-solute interactions in the system. This work establishes the 'proof of concept' of dual-facilitating agent in protein fractionation by ultrafiltration. Our work demonstrates that

BSA can be used as a dual-facilitating agent to alter the selectivity of 30 kDa PES membrane for the fractionation of two model proteins myoglobin and lysozyme. Both model proteins have quite comparable molecular weight but pretty different pI. At selected physicochemical conditions and operating parameters, lysozyme transmitted preferentially over myoglobin through the membrane but in the presence of BSA at the same operating conditions, myoglobin transmission increased over that of lysozyme. The decrease in lysozyme transmission was due to electrostatic BSA-lysozyme interaction, while the simultaneous increase in myoglobin transmission was due to Donnan effect. Thus, dual-facilitating agent could be used to manipulate the transmission of myoglobin and lysozyme. This novel approach of using dual-facilitating agent is expected to add flexibility in carrying out protein fractionation using ultrafiltration.

8.1.2 Modeling of flux decline in ultrafiltration

Membrane fouling and concentration polarization have long been identified as the main sources for permeate flux decline in constant pressure protein ultrafiltration. Prior to the publication of this thesis work, most of the earlier work on modeling flux decline in ultrafiltration is based on the cumulative or simple additive effects of concentration polarization and membrane fouling. These models assumed that initial rapid flux decline at the start of process was due to the development of concentration polarization layer which remained more or less constant during the remaining period of filtration. While the more gradual decline in flux after rapid decrease was attributed to the membrane fouling at constant concentration polarization conditions. Thus these models completely ignored

the interplay between the concentration polarization and membrane fouling. Earlier, Gekas et al has used the interplay between concentration polarization and adsorption to account for the flux decline in ultrafiltration. But protein adsorption on membrane in static condition is quite different than membrane fouling by protein in filtration condition. In this work, we explained the first time the interplay between flux, concentration polarization and membrane fouling by assuming constant pressure ultrafiltration to be made up of a large number of sequential constant flux ultrafiltration steps. The model presented in this work demonstrates that the initial rapid flux decline is due to a combination of concentration polarization and membrane fouling and with the progress of filtration, the effect of concentration polarization becomes negligible. This model is conceptually much simpler and very useful to optimize the transmembrane pressure, and thereby identifying the trade off between productivity and working life of an ultrafiltration membrane.

8.1.3 Membrane chromatography

Membrane chromatography offers significant advantages over packed bed chromatography thanks to its convective driven transport phenomena. But due to lower binding capacities of commercially available membrane adsorbers, its commercial scale applications are still largely restricted to the removal of small amounts of target proteins and specific impurities such as endotoxins. The work on membrane chromatography in this thesis is mainly focused on the use of two novel high-capacity macroporous gel-filled membranes for ion-exchange chromatography of proteins. This study examines the

effects of different operating parameters such as pH, buffer ions, salt concentration, feed protein concentration and superficial velocity on HSA binding on both these membranes. The binding capacities of these membranes were calculated from the analysis of breakthrough curves. This thesis work demonstrates the suitability of one of the high binding capacity membranes for bind and elute type of applications by separating a simulated feed protein solution consisting of HSA and HIgG.

8.1.4 Protein fouling of MF membranes

In-line protein microfiltration processes are widely for sterilization of therapeutic grade proteins in the biopharmaceutical industry. They suffer from protein fouling even with the membranes having pore sizes an order of magnitude greater than the sizes of proteins. Many researchers have studied protein fouling of microfiltration membranes and used blocking laws to model their experimental data. Their studies definitely provide better understanding of membrane fouling and are useful for successful scale-up or scale-down of microfiltration systems. However, they do not tell anything about the severity of fouling or the extent of cleaning required to restore the flux. The work reported in the Chapter 6 of this thesis describes membrane fouling during in-line microfiltration of concentrated protein solution. It looks at the increase in filtration resistance during in-line protein microfiltration and the mechanism of membrane fouling. In this work, three phases of TMP increase were identified during constant flux BSA microfiltration: each characterized by its own rate constant and extent of reversibility. A significant portion of the increase in TMP during BSA microfiltration was reversible in nature despite almost

100% transmission of BSA and thereby nullifying the possibility of concentration polarization. BSA monomers are identified as the major foulant species responsible for the reversible portion of membrane fouling. In this study, it is hypothesized that membrane fouling is initiated by the presence of protein aggregates even at very minute level. This initial protein deposition can further trigger the membrane fouling by protein monomers. Confocal microscopy data suggested protein deposition restricted to a zone very close to the membrane surface. TMP increase was much more rapid in phase II compared to I and III. However, fouling in phase I was almost irreversible in nature while a significant portion of fouling in phase II was reversible. This study also reports the effects of intermittent protein filtration on the efficiency of microfiltration.

8.1.5 Fouling assessment techniques

Membrane fouling is a complex phenomenon. One of the major obstacles in the study of membrane fouling is the absence of robust and reproducible membrane testing protocols. Traditional fouling assessment techniques such as flow decay method are quite expensive and time consuming. Chapter 7 of this thesis describes three fouling assessment protocols.

The first protocol is based on accelerated membrane fouling in the dead end mode using pulsed injection technique. It is very simple, rapid, robust, reproducible and cost-effective. It gives the information about membrane permeability, propensity of fouling and loss of membrane permeability due to both irreversible and reversible fouling within just 10 minutes. It gives flexibility of studying the cleaning protocol simultaneously

without dismantling the module. The second and third protocols are based on the critical flux concept. The second protocol measures the critical flux in dead-end mode while the third one in cross-flow mode.

8.2 Recommendations for future research

8.2.1 Dual-facilitating agent in protein-protein separation

In this thesis work, we have used BSA as a dual-facilitating agent to alter the selectivity of separation of myoglobin and lysozyme in view of its molecular size which guarantied its total retention, and its charge (at the operating conditions used) which ensured the dual-facilitated effect. However, with actual protein bioseparation, BSA might not be the most appropriate dual-facilitated separating agent. In light of the current results, it is practical to see what other appropriately sized and charged macromolecules (such as dextrans and polyacrylic acid) or charged particles (e.g. latex) can be used as dual-facilitating agents. These charged polymers or charged particles should be well characterized and easily recoverable from the retentate after the experiments.

In this work, we have used compeletely retained negatively charged BSA to obtain the reversed selectivity, i.e. to increase the transmission of myoglobin through Donnan effect while simultaneously decreasing the transmission of lysozyme through BSA-lysozyme interaction. However, dual-facilitated separating agent can also be used to increase the selectivity. Therefore, to further support this concept, some other

macromolecules or particles which can be retained by the membrane and have net positive charge at the operating conditions should be used to increase the selectivity of separation of myoglobin and lysozyme. In this case, the role of dual-facilitating agent should be to further increase the transmission of lysozyme through Donnan effect and decrease the transmission of myoglobin through electrostatic attraction between myoglobin and dual-facilitating agent.

The detailed study on the concept of dual-facilitating agent in protein ultrafiltration can be undertaken with appropriately sized and charged macromolecules or particles which are well characterized. It should cover the effect of pH and ionic strength on the performance of dual-facilitating agent. The effect of permeate flux and system hydrodynamics should also be studied in order to understand the role of Donnan effect in greater detail. The effects of concentration and charge per mass of dual-facilitating agent on the separation should be further explored to obtain the enhanced performance. It will be useful to model the experimental data on dual-facilitated separation using Maxwell-Stefan equations combined with hydrodynamic model. This will facilitate the implementation of this novel approach to carry out the actual protein separation in the biopharmaceutical industry.

The work in this thesis explored the electrostatic interactions of dual-facilitating agent with one of the proteins that is being separated in combination with Donnan effect. But it may not be always possible to have the favorable charges both on a dual-

facilitating agent and the proteins that are being separated to induce the required electrostatic interactions in combination with Donnan effect. In such cases, the concept of dual-facilitating agent can be explored to combine affinity interactions with Donnan effect to alter the selectivity of separation, i.e. the dual-facilitating agent should be able to reversibly bind with one specific protein (being separated) through affinity interactions and at the same time affect the transmission of other protein through Donnan effect due to its charge properties. Indeed, any other solute-solute interactions apart from affinity and electrostatic interactions can be used as long as they are reversible to alter the selectivity of membrane for protein separation.

8.2.2 Ultrafiltration fouling

Chapter 4 describes a constant flux based mathematical model for predicting permeate flux decline in constant pressure ultrafiltration. The inspiration behind this model is the experimental observation that after the initial fouling phase, TMP increases at constant rate which in turn depends on the flux in constant flux protein ultrafiltration. Nevertheless, fouling in this work was studied at pH equal to pI of protein in both constant flux and constant pressure ultrafiltration. Therefore it is sensible to study the effects of different physicochemical parameters such as pH and salt concentration on the linearity of TMP increase after the initial rapid fouling phase in constant flux ultrafiltration for broader application of this model. Future work should also include the fouling study involving the mixture of proteins which are completely retained by the membrane. It should be noted that in this model, the compressibility of deposited protein

mass is entirely neglected. To understand the effect of compressibility of deposited protein, step-up and step-down protein ultrafiltration should be studied in greater details. Moreover it would be interesting to study the applicability of this model to the protein ultrafiltration with partial transmission of protein.

8.2.3 Microfiltration fouling

Chapter 6 describes membrane fouling during in-line protein microfiltration process rather qualitatively. So, the next step should be the modeling of experimental data to describe the membrane fouling quantitatively. This model can also serve as a useful tool in combination with the first fouling assessment protocol to compare the membrane performances in terms of their capacity in a very short time. Moreover, some TMP profiles during intermittent protein filtration are quite hard to explain. To further understand the protein fouling of microfiltration membranes, one should use more sophisticated online protein fouling characterization methods in addition to TMP profiles, which can locate the position of deposited proteins on membrane and give an insight about the morphology of deposited proteins.